Performance of Carbide and Coated Carbide Tipped Circular Sawblades

Xi-Yang Zhang

A thesis submitted in partial fulfilment of the
requirements of
Sheffield Hallam University
for the degree of Doctor of Philosophy

February 1995

Collaborating Establishment: Spear and Jackson Industrial Saws Limited

ACKNOWLEDGEMENTS

The author wishes to express his most sincere gratitude to his supervisors Professor M Sarwar, Dr. D Gillibrand and Dr. T Campbell for their guidance and helpful comments at the specific phases of this project.

Many thanks for Dr. S R Bradbury for his help at the early stage of this project.

Thanks are due to Mr. T Cockerham and D Eaton for their great help during the last stage of this project.

The author is extremely grateful to Mr. Keith Pascoe, the engineer of James Neill tools, for his co-operation and support in the early stage of this project.

Thanks are due to Mr. D Wilkinson and all other technicians for their help and co-operation in the experimental work.

Finally, to my wife, Dequin, and my son and daughter, Xun and Ling, for their moral support and understanding to my study and research.

ABSTRACT

Published work concerning the performance of coated and uncoated carbide tipped circular saw blades has been searched and reviewed. The search has shown that little similar experiments on the carbide tipped circular saw blades have been conducted. Furthermore the evidence shows that no work has been published on the application of coatings to the carbide tipped circular saw blades. Finite element analysis has been widely applied to the cutting process, but the application of finite element methods to the carbide tipped circular saw blade is still a new area of research.

In this investigation the performance and life of the carbide tool both uncoated and coated were quantified by rigorous measurement. The proposed carbide properties (composition, cobalt distribution, specific gravity, micro-structure and red hardness of carbide) have been experimentally tested. The failure modes for the carbide circular saw blades and carbide tipped saw segments have been established.

In this work a novel experimental approach was used, in which TiN and TiAlN coatings were applied to the carbide tipped circular saw. A feature of this approach is that a lower coating temperature is used and yet still retains the good bonding strength between the substrate and the coating.

The parameters obtained in this investigation were used as a basis in the development of a finite element model. This model was used to optimise tooth geometry and predict the failure mode with respect to temperatures and stresses.

Investigation has shown that TiN and TiAlN coatings have largely enhanced the tool life in the case of cutting proposed workpiece materials. The crater wear, flank wear and large chipping have been arrested or reduced.

Computer model and transverse rupture strength figure have been established. The results shows that the model used for qualitative analysis of a problem is possible and the examples conducted in the case of cutting mild steel is completely consistent with the failure modes obtained in the cutting tests.

CONTENTS

LIST OF FIGURES

LIST OF TABLES

CHAPTER ONE

INTRODUCTION

Machine processes require in many cases a workpiece which has to be cut to a suitable length capable of being processed later. Therefore, it can be asserted that the first process in a sequence of operations is often that of sawing to a suitable length from the raw bar.

Sawing being one of the most common cutting process has been the subject of many research investigations. Processes can be classified as, power hacksawing, bandsawing and circular sawing. All have their attendant advantages and disadvantages as outlined below. For example:

Power hacksawing has the slowest output rate because it is not a continuous cutting process. The blade does not cut on the return stroke and therefore the return time is unproductive. Both band saws and circular saws cut continuously, having no unproductive time.

Hacksaw machines are generally cheaper than either circular saw machines or bandsaw machines. Also the cost of circular saw blades is higher than for bandsaw and hacksaw blades. Some circular saws have replaceable segmental teeth which prolong the life of the blades.

Circular sawing has the highest output rate of the three processes, because the blade is the most rigid, and can therefore apply the highest cutting forces.

Kerf loss (width of cut) is greatest in circular sawing. The thickness of a circular saw blade determines the rigidity of the blade and is therefore thicker than band- and hacksaw blades. Bandsaw blades, being the least rigid, have the worst run-out. This is particularly severe when cutting a broad workpiece because the blade guides have to be positioned far apart.

Circular saws cut the most accurately, this is partly due to the rigidity of the blade, but it is also due to the close tolerances to which these blades are manufactured.

1.1 Circular Sawing

Circular sawing is a process employing a rotating, continuous cutting blade having teeth on its periphery to cut ferrous and nonferrous metals, plastics, and other materials to required length. With the workpiece clamped securely, the saw blade is either fed horizontally, vertically, or on an angle into the material.

The process is often called cold circular sawing to differentiate it from sawing of hot metal in steel mills and forge shops, which is beyond the scope of this thesis.

Cutting action in circular sawing is essentially the same as in milling, particularly slot milling. Each tooth removes a chip, which curls and is carried away from the cutting area in the tooth gullet, thus allowing continuous cutting.

Large circular sawing machines have been used for many years to cut off billets, forgings, extrusions, bars, tubes, and similar stock. Now, smaller machines are being increasingly applied for a wide variety of components. The process can be used to cut practically any material.

1.1.1 Advantages

Major benefits of circular sawing include high production capability and high accuracy. Rigid machines and blades permit high feed pressures. Many machine attachments and material handling systems are available to automate the process and thus reduce the non cutting portion of the cycle and decrease the labour costs. Also the changeover time for a

different-sized workpiece is fast, making the process economical for both small lot sizes and high production requirements.

Accuracy is inherent in circular sawing due to the rigidity of the machines and milling-type cutters. Length tolerance for most stock feed systems is ±0.10 mm (1,2)*. Virtually burr-free surface finishes are produced, often eliminating or reducing the need for secondary finishing operations. For blade sizes up to about 406 mm diameter, finishes typically range from 1.5 to 3.2 μm R_a. Surface finishes as smooth as 0.2 μm R_a have been produced in circular sawing aluminium, and finishes as smooth as 0.8 μm R_a in cutting steel. The harder the material being cut, the smoother the finish usually produced (1, 2).

Tooling costs are relatively low. It has been estimated that the tool cost for circular sawing of mild steels is less than 0.35 pence per square inch (6.45 cm^2) of material removed, making it one of the least expensive methods of sawing solid metals (1).

Because of its rigidity, there is no tendency for the blade to deflect, which would cause more wear on one side of the blade than on the other. With the resultant uniform wear rate, no loss of accuracy occurs as the blade dulls (1, 2).

Operating costs are low because the simple operation of circular saws lends itself to the unskilled labour. Blade speed selection is normally accomplished by push-button.

Changeover time for a modern machine to cut different types and sizes of material is only a few seconds. One blade will cut many materials and

*** Numbers in brackets are cited references listed at the end of the thesis.**

stock sizes within the capacity of the machine, and blade changing can be done quickly and easily.

Circular saws are relatively safe because of the low rotational speed of their blades. No need exists for the operator to have his hands in the cutting area, and many automatic machines have completely enclosed feeding and sawing areas.

1.1.2 Limitations

There are no real limitation to the use of circular saws. It is true that the initial investment is greater than for a hacksaw or bandsaw because a heavier, higher horsepower machine is required for comparable capacity. Increased productivity and accuracy, however, can result in rapid repayment of the capital cost of the machine if sufficient work is available to keep it operating efficiently. Circular saw blades are also more expensive initially than bandsaws or hacksaws, but they can be resharpened many more times and reground, if necessary, to cut different materials. Long blade life generally results in lower tool cost.

Greater loss of the material being cut, because of the increased kerf (width of cut), is often cited as a disadvantage of circular sawing, but this is often not the case. Circular saw blades as thin as 1.52 mm are available, but such thin tooling cannot withstand the high cutting forces and maintain the close tolerances for which circular sawing is noted. Most bar stock that is slugged into short lengths is 127 mm or less in diameter. In this range, circular saw blades normally have a thickness ranging from 2.44-3.00 mm. With the inherent accuracy of circular sawing and the short drop (waste) ends produced, generally 51 mm or less in length, material loss due to cutting width can be less than with other methods. Even when cutting very short lengths, it is often less expensive to produce a slightly

wider kerf with circular sawing than to remove material in a secondary operation to attain required accuracy (1, 2).

1.2 Circular Saw Machines

Circular sawing machines, having blades mounted on power-driven rotating spindles, are generally of four basic designs: Pivot-arm machines, vertical-column machines, horizontal-travel machines, and circular plate-sawing machines.

(1) Pivot-arm machine

Pivot-arm machines are used extensively for high-production slugging operations and cutoff of structural shapes. This design is generally considered the most universal within its capacity ranges.

Features of these machines include rapid cycle times; rigid construction; fast changeover; and automatic, semiautomatic, or computer numerical controlled (CNC) material handling systems.

Feed can be manually controlled, but air or hydraulic is used on most. The control system automatically adjusts the feed rate according to the mass of the material being cut.

(2) Vertical-column machines

Vertical-column machines, sometimes called vertical-feed sawing machines, are also widely used for both high production slugging and cutoff of structure shapes.

Features of this design include fast changeover and high productivity. With this design, the rotating blade moves down in a straight line to contact the workpiece. The feed motion of the blade is assisted by gravity.

Material is centred directly below the centre line of the saw blade and is cut with a high degree of accuracy.

(3) Horizontal travel machines

The essential feature of these machines are rapid cycling, fast changeover, and the automatic control system or computer numerical controlled (CNC) system.

For this type machine, the rotating blade is horizontally fed into the workpiece from the side.

(4) Circular plate sawing machines

These machines are a variation of horizontal-travel machines. They feature a long horizontal travel of the blade that provides capacity for cutting solid plates. The rotating blade travels on guide ways mounted either beneath or over the saw table.

These type of circular sawing machine is used extensively for cutting nonferrous material in lengths to 6m or more and 152 mm thick.

1.3 Circular Saw Blades

1.3.1 Blades

There are many brands of circular saw blades on the market. The types of blade available can be categorised as, solid circular saw blades, segmental blades, inserted tooth blades and carbide- tipped blades. Also the types of blade available can be categorised by the material from which they are made such as carbon tool steels, high speed steel (HSS) and carbides.

The most commonly used circular saw blades are high speed steel solid blades, high speed steel segmental blades and carbide tipped saw blades.

(1) High speed steel solid blades

These blades usually contain molybdenum. Often M2 or M42 steels are used for these blades.

The whole blade is hardened and tempered uniformly, and only a small portion of the blade around the pinholes and the central hole is softened.

(2) High speed steel segmental blades

These blades are manufactured with the segmental teeth formed from high speed steel, radially joined to a steel backing strip.

The teeth of the segment are fully hardened and tempered, whilst the backing strip is retained in a none heat-treatment condition.

Segmental blades are more widely used than solid blades because of their greater ability to absorb shock. Teeth on the segments can be designed to suit a specific requirement. Also, when individual segments are worn or broken, they can be removed, resharpened, and replaced a number of times, thus reducing blade cost. However, segmental blades generally have to be thicker than solid blades, and the surface finishes produced are not usually as smooth.

(3) Carbide tipped blades

Carbide tipped circular saw blades, available from 250-1829 mm diameter with kerf range between 4-10.29 mm, have a high- strength, low-alloy steel body, with carbide brazed to the tooth tops.

These blades have been used for many years to saw aluminium, brass, and some plastics. More recently, carbide-tipped blades have been increasingly used in cutting steel.

P40 carbide is widely used for carbide tipped blades to saw ferrous metals, and K20 or K30 carbide for carbide tipped blades to saw nonferrous materials.

1.3.2 Limitations and applications of the blades

Materials having high hardness, high strength, poor thermal conductivity, and high work hardening characteristics cause a lot of difficulties in machining. Therefore, the machining of these materials demands a cutting tool having a good thermal conductivity, high hot strength and high red hardness.

Table 1.1 presents the limitations and applications of HSS solid, HSS segmental and carbide tipped saw blades.

It can be seen that the high speed steel circular saw blades are not suitable for cutting "difficult to cut materials".

With the rapid development on the carbide tool materials, some attention has been paid on the development of the carbide tipped circular saw blades and some achievements have been made in the development of carbide circular saw blades. One of the most remarkable achievements was made by Henning and Maier, Germany in 1988 (3). The test was concerned about cutting piston pins, round bars and square bars as well as tubes for different batches. The results are shown in Figure 1.1.

In the investigation by Henning and Maier (3), they compared the cutting rates for both high speed steel saw blades and carbide tipped saw blades. These values show that in the case of cutting difficult to cut materials the

performance of the carbide tipped saw blades is much better than that of high speed steel saw blades.

According to their investigation, carbide-tipped saw blades are more expensive than HSS-saw blades, but these carbide saw blades also have noticeably higher tool life.

The examples of the applications show that carbide-tipped saw blades are noticeably superior to the HSS-saw blades with respect to the cutting rate as well as the blade service life. With these positive characteristics carbide circular saw blades have reached a strong position among the circular saw blades. However, comparing with the current position for HSS circular saw blades, the carbide circular saw blades have not been given enough attention and most of the successful applications only deal with machining of wooden, plastic and nonferrous materials.

1.3.3 Tooth geometry

(1) Triple-chip tooth design

The most common type of tooth geometry is the triple-chip or high-low pattern illustrated in Figure 1.2. This design essentially provides a milling-type cutter with each pair of teeth producing three chips.

The first tooth in each pair, called the roughing tooth, is higher and chamfered 45°C on each side so that one-third of its width remain flat and removes a single chip from the centre of the cut with each pass.

The second tooth in each pair, called the finishing tooth, is lower (an amount equal to 0.02 times the pitch) and flat and removes two chips per pass, one from each side of the slot produced by the preceding roughing tooth.

Tooth widths on the circular saw blades must be wider than the body to prevent jamming in the cut.

Triple-chip tooth geometry is recommended for most ferrous cutting applications, particularly for sawing solid stock and thick section, because it can withstand high loads and is capable of rapid stock removal rates.

(2) Straight-tooth design

Another geometry commonly used for sawing brass and aluminium is the straight-tooth design.

With this design, the teeth are not bevelled and they are all the same height.

1.4 Previous Work

There is a dearth of research work published on the cutting process of circular saws. In general work is still in the incipient stages, especially that undertaken on the coated and uncoated carbide tipped circular saws. Among the few publications (3, 4 and 5), the only one on the performance of the carbide tipped circular saw was published by Henning and Maier (3). The work published in (3) does not specify exactly the nature of the failure modes for carbide tipped circular saws , and also omits the influence of the mechanical properties such as red hardness and bending strength on the performance. In (6, 7, 8 and 9) the failure modes for the carbide tools are considered but it is limited to other carbide tools.

The above published work does not fully explain several points which are considered below. Namely, normal failure behaviour and its associated failure modes. The effect of carbide grain size, composition and

carbide porosity and mechanical properties such as red hardness, on the performance of carbide circular saws are also not explained.

The work published by Bradbury , Keenan and Sarwar (4) demonstrates how a method was developed to assess the cutting performance of high speed steel circular saw, focussing on a segment instead of a full saw blade.

In the present investigation, the method of (4) was used for imitation cutting tests to assess the cutting performance of a carbide tipped circular saw. Also the method was extended where a new and modified special test rig was designed to meet the requirements of performance evaluation. An aspect of this investigation therefore is to study the variation in tool geometry such as rake angle and clearance on the performance of the saw. This is given particular attention for cutting of hard materials such as stainless steel and nimonic alloys.

Advanced surface engineering technologies have been successfully applied to high speed steel and carbide cutting tool inserts (10 - 13), and the potential benefits in terms of both performance and longer tool life , are now well established. However, contemporary published work is confined to coated high speed steel cutting tools, and coated carbide cutting tool inserts. To the author's knowledge, there is no published work pertaining to the application of coatings on the carbide tipped cutting tools.

Finite element methods have been widely applied (14 -17) in many fields of metal cutting for example, Bradbury and Sarwar (14) considered a graphical approach to computer-aided analysis in the design of bandsaw teeth. They developed a yield map to predict the behaviour of bandsaw teeth.

1.5 Objectives

The aim of the present investigation is to formulate an objective approach which will enable the performance of the coated and uncoated carbide tipped circular saw segments to be evaluated.

The objectives can be summarised as follows:

(1) Identification of the failure modes on both full product circular saw blades with carbide teeth and on carbide saw segments.

(2) Optimisation of the proposed carbide substrate tool materials. This is intended to optimise the carbides used in the saw blades.

(3) Development of a simulation process for the cutting behaviour of full circular saws, achieved by testing and experimenting.

(4) Design of a carbide tipped saw segment suitable for simulating cutting test and application of coating.

(5) measurement and quantification of performance and life of carbide saw segments.

(6) Development of a experimental approach used for the application of coating techniques to the saw segments.

(7) Assessment and comparison of the performance of coated and uncoated segments.

(8) The parameter obtained in the investigations of items (3)-(5) will be used as a basis in development of a Finite Element model. A graphical approach to computer aided stress analysis to predict the possible tooth failure mode with respect to temperatures and stresses will be used. This can be used to optimise tooth geometry, tool materials, and the application of the coatings.

CHAPTER TWO

WEAR MECHANISMS AND FAILURE MODES OF CARBIDE CIRCULAR SAW BLADES

2.1 Introduction

Tool failure is characterised by significant wear mechanisms. These mechanisms can be classified as, adhesive wear, abrasive wear, diffusion wear, plastic deformation wear and premature fracture (thermal crack or thermal fatigue and mechanical fatigue).

In the case of carbide tipped circular saw, the failure mode can be a combination of all the above failure mechanisms or due to a single incidence failure attributed to one particular wear mechanism.

Despite the complex nature of wear, there is in general one or two mechanisms which are dominant. The workpiece material, the tool geometry and the machining conditions are the factors that are prominent in the wear mechanism, whilst the extent of wear is determined by the properties of the cutting tool material.

In this chapter, the variable wear mechanisms of carbide tools were studied. The specific failure modes of carbide tipped circular saws were investigated to contribute to the further investigation of performance of the carbide tipped circular saws.

2.2 Wear Mechanisms Of Cemented Carbide Tools

The mechanisms pertaining to wear and its variables have been researching for years. Consequently, many modes of failure have been proposed to occur by one or more mechanisms acting at the same time, and some, on the same region of the tool face.

The five most common wear mechanisms of carbide cutting tools are discussed below:

2.2.1 Adhesive wear (Attrition wear)

The adhesive wear is a process that a whole grain, part of grain or a mass of grains in the tool material are moved away little by little due to shearing or pulling action, which is occurs at chip-tool interface. The adhesive wear has a relationship with the following factors:

(a) Surface condition

The worse the surface finish of tool, the higher the wear rate. The micro-strength (micro-cracking and residual stress) has effect on the adhesive wear (6).

(b) The adhesion between the tool and workpiece material

The adhesive aspect between carbide and workpiece is related to the temperature and composition of the materials in contact. For example, within the regular limitation of cobalt (Co) content, the adhesive temperature for the tungsten carbide and titanium carbide combination (WC+TiC) will be 150°C higher than that for WC grade. This is due to the formation of TiO_2 at high temperatures (12,18). This hard particle will make the uneven surface formed if the particle project from the surface of tool.

(c) The grain size of carbide.

The relationship between the grain size of carbide and adhesive wear, the finer the grain, the lower the adhesive wear (18).

2.2.2 Abrasive Wear

Because of the high hardness of cemented carbide, abrasive wear is much less likely to be a significant wear process with cemented carbides than with high speed steel. (18).

To resist abrasive wear, a low percentage of cobalt in the cemented carbide is the most essential feature, and a fine grain size also is beneficial.

2.2.3 Diffusion Wear

In the cutting process, a high temperature is generated, resulting in an intimate contact between the tool face and new machined surface of the workpiece. A highly active chemical activity is manifest during this process. This results in a relatively large difference in the surface energy of the metal. The energy transforms the machined surface and chip into an austenitic structure. This provides a favourable condition for the intimate diffusion between the workpiece and tool face.

The characteristics of diffusion wear are as follows:

(a) micro-wear surface is relatively even. Even if the surface is examined with microscope, there are still no obvious pits formed.

(b) A remarkable increase in the diffusion speed will occur as the increase in cutting temperature.

(c) The speed of the diffusion will be variable with the different composition of tool materials.

In the case of cutting steel with carbide tools, the cutting temperature will reach 1070~1270K (18). Resulting in the diffusion wear being the main wear mechanism to the cemented carbide. From the cutting temperature of 1070K, the process of diffusion for carbide tools will be as follows:

Tungsten (W), cobalt (Co) and carbon (C) of cemented carbide are diffused into the bottom layer of the chip. Iron (Fe) of steel workpiece is diffused into the cemented carbide, resulting in a lower hardness and brittle phase on the surface of the cemented carbide (18).

There is strong evidence that crater wear by diffusion occurs only at relatively high rates of metal removal (6, 21).

2.2.4 Plastic deformation wear

The metal removal rate is often limited by deformation of the tool under compressive stress on the rake face. Carbide tools can withstand only limited deformation, even at elevated temperature. These cracks lead to sudden fracture.

Failure due to deformation is more probable at high feed rate, and when cutting materials of high hardness. The maximum deformation is seen to be at the cutting edge, and this a common feature when cutting steel and iron. A tool with a sharp cutting edge, or a very small cutting edge radius, starts to deform at the cutting edge and fails, for this reason, at much lower speed than when a large cutting edge radius is used. In many cutting operations the precise form of the cutting edge radius may be critical for the performance of the tool.

When cutting steel at high speed and feed rate, a crater is formed on the rake face of tungsten carbide-cobalt tools, with an unworn flat at the tool edge.

2.2.5 Premature fractures

Circular sawing is an intermittent cutting operation. During cutting, the cutting tools are subject to repeated impacts and thermal cycling. As a result, cracks are generated in interrupted cutting tools (19). Erratic tool

life is often caused by the fracture before the tool is much worn. This type of tool failure is called premature fracture.

2.2.5.1 Thermal Crack (Thermal Fatigue)

Where cutting is interrupted very frequently, as in circular sawing, numerous short cracks often occur in the tool.

These cracks are caused by the alternative expansion and contraction of the surface layers of the tool as they are heated during cutting, and cooled by conduction into the body of the tool during the intervals between cuts.

The cracks are usually initiated at the hottest position on the rake face, some distance from the edge, then spread across the edge and down to the flank (19, 20 and 21). If cracks become very numerous, they may join and cause small fragments of the tool edge to break away. Also they may act as stress-raisers through which fracture can be initiated. Many carbide manufacturers have therefore selected the composition and structure least sensitive to thermal fatigue as the basis for grades recommended for milling and sawing (22).

2.2.5.2 Mechanical Fatigue

As the cutting speed is reduced and feed is increased, tool stresses increase thereby increasing the risk of tool failure by mechanical fatigue. Consequently, the tool tip is subjected to high compressive stresses resulting in tool failure. Thermal effects in such cases, however, are not predominant. Nevertheless, when a combination of high speed with moderate to high feed is selected, both thermal and mechanical stresses contribute to tool failure. Tool stresses in intermittent cutting are noticed to be relatively higher as compared to regular cutting. This is attributed to the sticking on the interface between the tool and workpiece. The possibility of stress amplification in intermittent cutting, due to adhesion of a portion of chip,

had been reported and discussed by Takeyama (11). The increase in normal stress results in a rather small value of the coefficient of friction. Apparently, high normal stress together with adhesion can help in accelerating the wear rates in intermittent cutting.

During the intermittent cutting, saw blades are also subjected to repeated impacts and friction between the interface of the work piece and tool face. As a result, some types of the chipping and cracking will occur. Some research reports indicate that the interaction between repeated mechanical impacts and thermal cycling as regards the failure of tools in intermittent cutting is not well understood. Zorev contends that impact is of minor importance when compared to the role thermal fatigue in determining tool life (23). Okushima and Hoshi attribute chipping at low speeds to mechanical impact. At high speeds, chipping is due to cracks parallel to the cutting edge on the flank and rake face (24). The cause of these parallel cracks is not attributed to thermal fatigue and what role impact might play on their formation is not considered. However, at high speeds, the thermal crack is the most frequently observed type of crack in the chip/tool contact area.

2.3 Failure Modes Of Carbide Circular Saws

Despite the intensive investigations that have dealt with tool wear and failure modes in their various forms, little work on failure modes of the carbide circular saw has been done by now. For this reason, failure modes of carbide circular saw segments and full blades were identified using a stereo microscope with photographic facilities and a scanning electron microscope.

In the investigation of failure modes of carbide circular saws, it has been found that there are two categories of principal failure modes, unacceptable premature failure and acceptable normal wear (Figure 2.1), for both

full carbide circular saw blades and saw segments. It was also found that the failure modes for full saw blades are consistent with those of saw blade segments.

2.3.1 Premature failure modes

Premature fractures are the most common failure modes for carbide circular saw blades. These are due to the brittleness and low thermal conductivity of the carbides, and result in greatly reduced tool life and increased tool costs.

The following figures show failure modes due to premature failure:

The bevel chipping on the tooth corner of the blade as shown in Figure 2.2. This is often attributed to the unreasonable tool geometry design.

Figure 2.3 shows breakage and stripping occurred on the tooth tip when sawing MS at high feed and cutting speed. This is due to poor tool material leading to tool deformation.

Figure 2.4 shows a failure mode that tooth is removed, caused by destruction of the brazed joint between carbide tip and shank of the blade. The tooth and its backing material are stripped off (Figure 2.5).

It should be indicated that for premature failure modes, the coatings can not arrest these types of failure modes. The only way to arrest these types of failure modes is to optimise the tool materials or modify the geometry of the tool.

2.3.2 Acceptable failure modes

In addition, there are some other normal wear modes such as flank wear, crater wear, cutting edge chipping and deformation, that have occurred

when sawing with carbide tools. The acceptable wear modes of carbide tools described briefly as follows:

2.3.2.1 Flank wear

The type of wear which occurs on the flank face of a tool is usually called flank wear, but some times it is referred to as the clearance wear (Figure 2.6).

Flank wear is the most widely used criterion for evaluating tool life, and is often used in metal cutting research to assess different aspects of tool wear. This occurs where the cutting edge of the tip is in rubbing contact with the workpieces, resulting in the surface finish to deteriorate. The wear mechanism is one of abrasion combined with diffusion wear in a ratio which is a function of cutting speed, diffusion wear being increasingly important at higher cutting speeds. Workpieces containing abrasive particles, such as entrapped sand from casting or hard inter-metallic particles, can cause very rapid wear. In general, the solution is to use a tool that combines high hardness and crater wear resistance without sacrificing edge strength.

When sawing aluminium, mild steel and stainless steels and nimonic alloy, long chips and built-up edge (Figures 2.7 and 4.22) occur more readily. These cause the development of flank wear or crater wear on the rake face of the blades by abrasive wear due to unstable built-up edge break down and long chips clogging in the gullet between the teeth.

2.3.2.2 Crater wear

When cutting steel at high speed and feed rate, a crater is formed on the rake face of tungsten carbide-cobalt tools, with an unworn flat at the tool edge (Figures 2.6 and 2.8).

There is convincing evidence that the wear process in crater of WC-Co tools is one in which the metal and carbon atoms of the tool diffuse into the work material seized to the surface and are then carried away in the chip. Crater wear by diffusion occurs only at relatively high rates of metal removal or high cutting temperature. When cutting nimonic alloy or stainless steels, the cutting temperatures will be as high as 750-1000 °C (25, page 238). Due to poor thermal conductivity, the cobalt in the carbide will diffuse into the workpiece at high temperature. With the binding element removed a layer of low shear strength material exists on the surface of the tooth. This is transported from the tool by the underside of the chip, and a crater is formed on the rake face.

2.3.2.3 Edge chipping and deformation

When cutting steel, under conditions where a built-up edge is formed, the edge of a WC-Co carbide tool may be destroyed rapidly by attrition. As with high-speed steel tools, fragments of the tool material of microscopic size are torn from the tool edge, but whereas this is a slow wear mechanism with steel tools, it causes rapid wear on carbide tools. If the built-up edge is firmly bonded to the tool and is broken away as a whole, as frequently happens where cutting is interrupted, relatively large fragments of the tool edge may be torn away as shown in Figure 2.9.

To improve tool life where attrition is dominant, attention should be given to reducing vibration, increasing rigidity and providing adequate clearance angle on the tools.

Circular sawing is an intermittent cutting operation where cyclic mechanical and thermal stresses are applied to the cutting edge. This results in fine cracks generated on the rake face, spread across the cutting edge, and then down to the flank of the tool (Figure 2.10). Plastic deformation

of the cutting edge, particularly on the tool corner (Figure 2.11), is caused by high stresses. It usually occurs at heavy feeds.

The limit to the rate of metal removal as cutting speed or feed are raised, is often caused by deformation of the tool under compressive stress on the rake face. Carbide tools can withstand only limited deformation, even at elevated temperatures, and cracks form which lead to sudden fracture. Figure 2.12 shows such a crack in the top of a tool, this surface being stressed in tension as the edge is depressed.

Failure due to deformation is more probable at high feed rates, and when cutting materials of high hardness. The maximum deformation is seen to be at the cutting edge, and this a common feature when cutting steel and cast iron. A tool with a sharp cutting edge, or a very small cutting edge radius, starts to deform at the cutting edge and fails, for this reason, at much lower speed,then a large cutting edge radius is used. In many cutting operations the precise form of the cutting edge radius may be critical for the performance of the tool.

CHAPTER THREE

CHARACTERISTICS OF CARBIDE SUBSTRATE MATERIALS

3.1. Introduction

With the progress of science and technology, great demands are being placed on material performance. The newer materials such as nickel based materials and stainless steels are more difficult to cut-off. Some of the characteristics presented by these materials are high hardness, high yield strength, greater work-hardening and in some cases poor thermal conductivity. The combination of characteristics present considerable difficulties when using cold sawing as a cutting off process. So, sawing of these materials demands relevant cutting tools possessing good thermal conductivity, high red hardness, very good toughness and yield resistance so that there is sufficient wear-resistance in machining high hardness materials and sufficient impact-resistance in machining high strength materials.

In order to investigate the present circular saw blade materials and to solve the problem of sawing difficult to cut materials such as nickel based alloys and stainless steel, this chapter presents a description of the characteristics of carbide substrate materials.

The characteristics of the proposed carbide substrate materials such as the carbide grades SP35, SP45, S4 and MK20, have been investigated by scanning electron microscope, chemical composition analysis, Vickers hardness (red hardness), gravity measurement, porosity analysis, image analysis using DIGIS-CAN/FDC software and Mean Linear Intercept. These carbide substrate materials were selected for investigation because

they are traditionally used for the tool materials of carbide tipped circular saw blades.

In this chapter, a new approach for testing the red hardness of carbides was developed.

The purpose of the investigation was to select the best carbide grades used for the tool materials of the circular saw blades among the proposed carbide grades.

3.2 Composition Of The Carbides

The composition of the carbide grades were analysed using an x- ray fluorescence spectrometer. The compositions are given in Table 3.1.

According to the investigation, grades SP35, S4 and SP45 belong to Tungsten-Titanium-Tantalum carbide type which if it was not for the development of coated carbides, would be the most popular class of hard metals. MK20 is Tungsten carbide (WC/Co) which was the first commercially available cemented carbide consisting of fine, angular particles of tungsten carbide bonded with metallic cobalt.

3.3 Red Hardness Of The Carbides

Red hardness (hot hardness) is one of the most important factors used to assess the properties of the hard metals.

Red hardness tests were undertaken by connecting a thermocouple to a carbide tip specimen, This assembly was then inserted into a silicon vacuum tube to avoid oxidisation during heating, which was very important approach for measurement of carbide high temperature as the carbides will be oxidised at above 400°C as shown in Figure 3.1. The tube was then put into an electronically controlled oven and heated at the required temperature for 5 minutes. After this period of time, the speci-

men was removed from the oven and silicon tube onto the test plate of a Vickers hardness machine, the red hardness of the carbide tip was then measured using the standard V.H indentation (10 kg load) in the surface region adjacent to the thermocouple which was being used to monitor the specimen temperature, as shown in Figure 3.2.

Values of red hardness for the carbide grades under investigation are compared in Figure 3.3 and figure 3.4 shows the cooling curve during the carbide specimen taken out from the oven.

It can be seen from Figure 3.3 that at a temperature of 600 to 700 °C, the MK20 and SP45 carbides lose their hardness completely, while S4 and P35 retain high hardness at these elevated temperatures owing to their higher contents of titanium and tantalum (9, page 34), as shown in Table 3.1.

3.4 Specific Gravity Of The Carbides

Carbide density is extremely sensitive to composition and the degree of porosity. The gravity of the carbides were investigated by the conventional method (22) and the results are listed in Table 3.2.

Comparing to figure 3.5 and Table 3.1, the estimated values of Ti and Co are roughly similar to the results obtained by x-ray fluorescence spectrometer, using the facilities in the Materials Research Institute, SHU.

3.5 Metallographic Determination Of Porosity

The proposed carbide samples were examined and assessed by scanning the surface of the test-piece section at a magnification of either 100 or 200 times as shown in Figures 3.6, 3.7, 3.8 and 3.9. According to "British Standard BS 5600: part 4: section 4.14: 1980" (26), for pores up to 10 μm , the porosity level shall be designated as A02, A04, A06 or

A08 (A02 designation represents the finest porosity level and A08 designation is the coarsest porosity level). Pores within the range 10 to 25 μm, the porosity level shall be designated as B02, B04, B06 or B08 (B02 designation represents the finest porosity level and B08 designation is the coarsest porosity). The results are given below:

The porosity level of MK20 is A06 and the total volume of porosity in the carbide is about 0.2%; The porosity level of SP35 is B06 and the total volume of porosity in the carbide is about 0.2%; The porosity level of SP45 is A06 and the total volume of porosity in the carbide is about 0.2%; The porosity level of S4 is B08 and the total volume of porosity in the carbide is about 0.6%.

3.6 Grain Size

According to "British Standard : section 4.13: 1980" (27), the micro structure of the carbides was examined using scanning electron micro-scope and from the micro-graphics in Figures 3.10, 3.11, 3.12 and 3.13, it can be clearly seen that the grain sizes of MK20 is much finer than that of S4, SP45 and SP35 grades.

The grain size of the proposed carbides was also calculated by the linear intercept method and given in Table 3.3. It can be seen that the true mean diameters of MK20 and SP45 are smaller than the other carbide grades. MK20 and SP45 are fine-grain size carbide, and S4 and SP35 are medium-grain size carbides.

3.7 Image Analysis

Since the hardness and toughness can be influenced to some extent by the size, distribution, and homogeneity of the cobalt, the distribution and proportion of cobalt is a very important property for carbides.

The proposed carbide samples were examined by a JXA-840A electron probe micro analyser, and analysed using DIGIS-CAN/FDC software. The results are shown in Figure 3.14. It can be seen that the total percentages of cobalt in the proposed carbides are similar to those obtained from composition analysis (Table 3.1).

The distributions of cobalt in S4 is very similar to those in SP35. The coarsest distributions of cobalt and the lowest cobalt content are within MK20 and the finest distributions of cobalt and highest cobalt content are within SP45 (mainly arranged within 0 to 1.5 microns).

According to the test results of red hardness of these carbide grades (Figure 3.3), it can be obviously seen that the amount of cobalt content and the distributions of cobalt have no influence on the red hardness of carbides.

3.8 Discussion

From the investigation, the carbide grades S4 belongs to WC-TiC-TaC-Co alloys which have a good crater wear resistance and retains the highest hardness at elevated temperatures, 600 to 700 °C attributable to their higher content of titanium as shown in Table 3.1.

The carbide grade MK20 is Tungsten carbide (WC/Co) which was the first commercially available cemented carbide consisting of angular particles of tungsten carbide bonded with metallic cobalt.

The porosity level of MK20 is A06 and the total volume of porosity in the carbide is about 0.2% and the grain size is the finest among the proposed carbide substrate.

According to the comprised characteristics of the carbide substrates, the carbide grades S4 and MK20 were chosen as the best tool materials.

CHAPTER FOUR

PERFORMANCE TEST OF UNCOATED CARBIDE TIPPED CIRCULAR SAW SEGMENTS

At present there exists no standard for the performance of carbide tipped circular saw blade, this chapter attempts to formulate an assessment for test procedures. In this way it may be possible to define a new performance method.

4.1 Test objectives

A test procedure was developed with the following six objectives:

1. To develop an experimental approach to simulate the cutting behaviour. This involves the design of carbide tipped circular saw segments, and devise a test rig for single teeth cutting test.

2. To assess the performance of the proposed carbide substrate materials.

3. To identify the main failure modes for the proposed carbide circular saw segments.

4. To assess the performance and life of saw segments with different carbide substrates and tool geometries.

5 To provide necessary information for application of coatings to the segments in order to arrest the tool failure and enhance the tool life.

6. To determine the cutting data for a computer model to calculate stresses due to cutting.

4.2 Performance assessment method

4.2.1 Introduction

Full blade cutting tests are both time consuming and costly. Owing to complexities in assessing multi-point tools, it was necessary to develop an alternative, economical way to assess the performance and wear characteristics of carbide circular saws.

A single point testing method has been successfully developed by Bradbury, Keenan and Sarwar in the evaluation of high speed steel circular saws (4). These tests show how the cutting behaviour of individual teeth and of pairs of teeth have been identified. This has allowed the characterisation of specific teeth rather than averaging all the teeth on the periphery of the blade. It has enabled the distribution of work between rough and finish teeth to be appraised, demonstrating the effects of changes in tooth geometry on individual teeth. This facility will be of considerable benefit when evaluating new tooth design for high speed steel circular saw.

In the present work, the single point testing method has been developed on the base of the method developed by Sarwar and Keenan. The modification of the method is explained in the following sections.

4.2.2 Specific cutting energy

As a parameter, Specific Cutting Energy, is introduced in the following assessment of cutting performance of carbide tipped circular saw, it is necessary to explain the parameter.

Specific cutting energy (Esp) is a parameter which gives an indication of process efficiency.

The relationship between specific cutting energy, the cutting power and the metal removal rate is taken from (28)

$$Esp\ (for\ a\ pair\ of\ teeth) = \frac{Cutting\ Power}{Metal\ Removal\ Rate} \quad (J/mm^3\ or\ GJ/m^3)$$

$$Cutting\ Power = Cutting\ force\ x\ Cutting\ speed$$

$$= N\ x\ V \qquad (N\ x\ m/s = J/s)\ \text{(watts)}$$

$$Cutting\ speed = Spindle\ speed\ x\ \Pi\ x\ Saw\ diameter \quad \text{(m/s)}$$

$$Material\ removal\ rate = Kerf\ x\ Cut\ Length\ x\ In\ feed\ rate \quad \left(\frac{mm^3}{s}\right)$$

$$\frac{In\ feed\ rate}{pair\ of\ teeth} = \frac{In\ feed\ rate}{Spindle\ speed\ x\ No.\ pairs\ of\ teeth\ per\ blade} \quad (mm/rev.)$$

In multi-point metal cutting applications, results tend to adhere to a similar form, which is represented by the general curve shown in Figure 4.1. It consists of three distinctive areas:

At the left hand side, at low feed / pair of teeth, the cutting efficiency is low and Esp high. This is due to "size effect." At right hand side of the curve, at large feed / pair of teeth, the specific cutting energy starts to rise again. This is due to the gullet being too small to accommodate the large volume of material removed. Energy is wasted deforming the chip, and since the chip is less likely to be ejected before the next cut, severe clogging can occur resulting in very high cutting forces.

An improvement in performance would be implied by a "lowering" of the curve indicating that less energy is consumed removing a given amount of workpiece material.

4.2.3 Data process

Figure 4.2 shows the diagram of the data acquisition system. The transient forces generated by the cutting action were measured and recorded by a digital oscilloscope. The digitised values were input to the microcomputer, and then the test force data was analysed to determine the specific cutting energy (Esp).

The data was displayed graphically relating Esp vs feed per pair of teeth or cutting force and thrust force vs feed per pair of teeth as a performance curve. The data was graphically displayed Esp vs surface contact area cut as a life curve.

4.2.4 The wear criterion used for tool life cutting tests

As performance tests assume wear is not significant, i.e. the tool is essentially unworn, the following criterion is only used for tool life tests.

For the acceptable tool wear such as flank wear, the measurements of tool wear were carried out by using the techniques recommended by ISO 3685 - 1977, page 10 shown in Figure 4.3 (29). As the flank wear is not regularly worn in zone B, the value of 0.6 mm on the width of the flank wear was used as a criterion of assessment of tool life when cutting mild steel. Because the flank wear is regular in zone B when cutting stainless steel and nimonic alloy, the value of 0.3 mm on the width of the flank wear was used as a criterion of assessment of tool life in the case of cutting these workpiece materials. The width of flank wear was measured with a tool room microscope.

For crater wear, the depth of the crater is given a value of 0.18 mm as a criterion of assessment of tool life in case of cutting mild steel. The depth of crater wear was measured with a ruler and eye-attach lens.

The amount of chipping is evaluated by the maximum width of the flank wear land. A value of 0.6 mm is recommenced as a criterion of assessment of tool life.

4.2.5 The test rig

A Dean Smith and Grace lathe fitted with a variable speed controller was used to provide the relative motion of the tool and workpiece (Figure 4.4). The carbide segment was securely clamped to a purposely designed fixture that fitted into the three jaw chuck. The segment teeth were at a radius of 125 mm with the same effective geometry as the full blade.

As considering the influence of gullet and pitch on the cutting performance, the tools used for cutting tests were a single point tooth with a back pair of teeth and two gullets taken from a full segment. This ensures that the cutting behaviour is more like that of a full saw blade rather than a single tooth with a front pair of teeth.

As the pitch between the teeth is 30 mm, the workpiece material was designed as a cross section of 30mm x 50 mm. This enables a full cut for each tooth to be taken.

The workpiece was securely mounted on a fixture which was bolted to the top of a three force component dynamometer. The dynamometer in turn was bolted to the cross-slide of the lathe (Figure 4.5).

During a cut, a proportional electric charge was set up in the dynamometers for each of the force components measured. These charges were fed into a charge amplifier where they were converted into proportional voltages. Only two force components were measured, representing the cutting force and thrust force.

The equipment used to quantify the forces generated during the tests and data processing included the following:

Kistler 3-Axis load dynamometer

Kistler charge amplifier

Gould 20MHz digital storage oscilloscope

Microcomputer linked to an Epson printer

4.2.6 Cutting test procedure

The cutting tests were divided into two steps. One is performance cutting test and the other is life cutting test or wear test.

4.2.6.1 Single point tooth performance test procedure

Performance tests were undertaken to determine the optimum cutting feed and speed for each work piece material and each carbide grade and establish the optimised cutting conditions to be used in the tool life cutting tests.

For each type of segment and workpiece material, the following test procedure was carried out before and during the performance cutting tests:

4.2.6.1.1 Inspection of the geometry of the proposed saw segments

In order to meet the requirements of the single point tooth testing, a carbide circular segmental saw that was assembled with segments was specially designed (Figure 4.6). The segments were designed with the same gullet and pitch, but with different rake angle, cutting edge radius and clearance angle. Each segment is composed of two pairs of teeth (rougher tooth and finisher tooth) as shown in Figure 4.7.

Each segment was viewed under a microscope and checked for uniformity of geometry. Figure 4.8 shows the new carbide circular saw segment. Prior to cutting test, the geometrical features of the segments were inspected using a shadow graph. Measurements were carried out to determine the tooth edge radius, rake angle, clearance angle and tooth tip to gullet base height. Details and each feature of the carbide saw segments are shown in Figure 4.9. The segment types, carbide grades, geometrical dimensions and workpiece materials to be cut are listed in Table 4.1.

4.2.6.1.2 Cutting conditions for performance cutting tests

The proposed cutting conditions for the performance cutting tests are shown in Table 4.2.

4.2.6.1.3 Workpiece materials

The composition and hardness of four types of workpiece materials, mild steel, 302S25 stainless steel, nimonic alloy and LM4 aluminium were investigated. All workpiece materials have the same cross-sectional area (30 x 50mm). Hardness and composition were investigated and the results are given in Tables 4.3, 4.4 and 4.5.

4.2.6.1.4 Performance cutting test

Six types of carbide tipped circular saw segments were used for cutting four kinds of workpiece materials. The details of each type is given in Table 4.1.

The lathe was set to a specified cutting speed for each type of the saw segments (Table 4.2). A lowest feed rate for a specified segment and workpiece material was selected (Table 4.2). When the tooth had progressed into the workpiece a distance which ensured that a "full" cut was taken, the data acquisition commenced. The cutting and thrust force

components were recorded for every fourth cut. After the forces generated during fifty cuts had been captured the test was terminated and the data processed. The width of the slot cut was measured using the tool makers microscope and recorded. The process was then repeated for large feed of pair of teeth (such as for cutting mild steel, 0.037, 0.0416, 0.0581, 0.066, 0.0825, 0.1188, 0.161, 0.1848, 0.2343, 0.264, 0.33, 0.4158, 0.4686, 0.594, 0.66 millimetres per pair of teeth).

At the end of the test three data files had been produced for each type of segment and workpiece material tested. Three data files were then displayed graphically relating Esp vs feed per pair of teeth. Superimposition of these three curves enabled the optimised cutting condition for a segment form to be determined in relation to a "lowering" of the curve. This curve indicates that less energy is consumed removing a given amount of 50 cuts of workpiece material such as shown in Figure 4.10.

4.2.6.2 Single tooth wear test procedure

The purpose of the wear test is to assess the tool life and determine the main failure mode for each type segment.

The aims are to study failure characteristics for the different types of carbide saw segments and determine the main failure modes when cutting the workpiece materials.

A series of sections was cut by a saw segment at the optimum cutting speed and feed. These optimum cutting speed and feed were determined in the previous performance cutting tests.

The workpiece materials used in the life cutting tests were the same as those used in performance cutting tests.

Three segments for each type were used in cutting each type of workpiece material.

The data obtained in the tests were input to the microcomputer, and the force data were analysed and calculated to determine the specific cutting energy. The data were then displayed graphically relating Esp to cumulative area cut for a specific segment at an optimised cutting conditions. The teeth of the segments were examined and photographs were taken to evaluate the wear behaviour.

4.3 Cutting test results

Results and failure modes from the performance and wear tests are displayed in Figures 4.10 to 4.42.

4.3.1 Performance test results

The performance of metal-cutting tools is often stated in terms of specific cutting energy, which is the cutting energy required to remove a unit volume of workpiece material. The performances of single teeth have been measured by relating the cutting force to the feed per pair of teeth. The data was then displayed graphically relating Esp vs feed per pair of teeth or cutting force and thrust force vs feed per pair of teeth as a performance curve.

4.3.1.1 Cutting mild steel

Performance test results for segments A1 and A2 are presented as graphs of feed per pair of teeth versus specific cutting energy in Figures 4.10 and 4.11.

Figures 4.10 and 4.11 show the performance of segment types A1 and A2 cutting a 50 x 30 mm mild steel bar workpiece at various feeds and three different cutting speeds. At the left hand side, at low feed of pair of teeth, the cutting efficiency is low and specific cutting energy is high. This is due to "size effect" or "ploughing forces" (18). In the central region

of the curve, the feed of pair of teeth is large comparing to the edge radius of the tool. The ploughing forces become less significant as a factor of the total cutting and thrust forces. The efficient cutting occurs and performance is improved until the flow of the chip is restricted, as in right hand region of the curves. At right hand region of the curve, at large feed of pair of teeth, the specific cutting energy starts to rise again. This is due to the gullet being too small to accommodate the large volume of material removed. Energy is wasted deforming the chip, and since the chip is less likely to be ejected before the next cut, severe clogging can occur resulting in very high cutting forces or high Esp.

An improvement in performance would be implied by a "lowering" of the curve (central region of the curve) indicating that less energy is consumed removing a given amount of workpiece material.

This allows a direct comparison of performance for the same segment type at three different cutting speeds, enabling the optimised cutting condition to be determined. Optimised curves for both types of segments are shown in Figure 4.12 and 4.13.

4.3.1.2 Cutting 302S25 stainless steel

Performance test results for segment types A1, A2, B1 and B2 are presented as graphs of feed per pair of teeth versus specific cutting energy in figures 4.14, 4.15, 4.16 and 4.17.

Figures 4.14, 4.15, 4.16 and 4.17 show the performance of the A1, A2, B1 and B2 segments cutting 50 x 30 mm 302S25 stainless steel bar workpieces at various feeds and three different cutting speeds.

Performance curves cutting at the optimised cutting speed for segment types A1, A2, B1 and B2 segments sawing 302S25 are shown in Figures 4.18, 4.19, 4.20 and 4.21.

4.3.1.3 Cutting LM4 aluminium

Clogging of the gullet of segment types C1 and C2 segments occurred when cutting aluminium at feeds greater than 0.033 mm/rev. , and cutting speeds of 670, 1000 and 1400 m/min. This is due to extensive plastic deformation occurring prior to fracture, which clogs the gullet between the teeth (Figures 4.22 and 4.23). Modified design of tools is required for cutting aluminium.

4.3.1.4 Cutting C25 nimonic alloy

Performance test results for segment types A2 and B2 are presented as graphs of feed per pair of teeth versus specific cutting energy in figures 4.24 and 4.25.

Figures 4.24 and 4.25 show the performance of A2, and B2 segments cutting a 50 x 30 mm C25 nimonic alloy bar workpiece at various feeds and three different cutting speed.

Performance curves cutting at the optimised cutting speed for segment types A1, A2, B1 and B2 segments sawing 302S25 are shown in Figures 4.26 and 4.27.

4.3.1.5 Optimised cutting conditions

As mentioned above, an improvement in performance would be implied by a "lowering" of the curve (central region of the curve) indicating that less energy is consumed removing a given amount of workpiece material. This allows a direct comparison of performance for the same segment type at three different cutting speeds, enabling the optimised cutting condition to be determined. Optimised curves in the case of cutting the proposed workpiece materials are shown in Figures 4.12, 4.13, 4.18, 4.19, 4.20, 4.21, 4.26 and 4.27.

The optimised cutting conditions for wear tests are listed in Table 4.6.

4.3.2 Wear test results

Wear tests for each workpiece material and segments were carried out to evaluate the rate of performance deterioration. Details are given of the segments cutting mild steel, nimonic alloy and stain less steel at optimised cutting speed and feed rates determined from the initial performance cutting tests.

Once the tooth had progressed into the workpiece material a distance such that a full cut was taken, the data acquisition commenced. The force components were captured by a Kistler 3-Axis load dynamometer for every tenth cut.

The digitised data was input to the microcomputer, and the force data was analysed and calculated to determine the specific cutting energy. The data was then displayed graphically relating Esp to cumulative area cut for a specific segment at an optimised cutting conditions. The teeth of the segments were examined and photographs were taken to evaluate the wear behaviour.

4.3.2.1 Cutting mild steel

Figure 4.28 shows Specific cutting energy (Esp) versus cumulative area cut. The specific cutting energy of uncoated segment type A1 is much smaller than uncoated segment A2 and B1. Comparing to their life, the segment A1 has the longest tool life and the segment B1 obtains a much longer tool life than that of A2 segment under the same cutting conditions. It should be indicated that both segment A1 and B1 have negative rake angle.

Figure 4.29 shows tool flank wear versus the area cut. The wear of segment type A1 is far smaller than that of segment type A2.

Figures 4.30 to 4.32 show the configuration of wear of segment A1, A2 and B1. For segment type A1, failure was mainly due to the crater wear and flank wear on the rougher tooth and breakage on the finish tooth, shown in Figures 4.30 and 4.31. With segment type A2, the main failure modes were crater wear and edge chipping on the rougher tooth, figure 4.32(a). The large edge chipping is produced on the roughing tooth of segment B1, figure 4.32(b).

4.3.2.2 Cutting 302S25 stainless steel

Wear test results for segment types A1, A2, B1 and B2 are presented as graphs of cumulative area of material cut versus specific cutting energy, Figures 4.33 and 4.34. It can be seen in Figures 4.33 and 4.34 that the specific cutting energy of uncoated segment type A2 is much smaller than that of uncoated segment A1. The specific cutting energy of B2 segment is much smaller than that of B1 segment. Comparing to tool life, the segment B2 obtains the longest tool life among these segments under the same cutting conditions.

Figure 4.35 shows tool flank wear versus the area cut. The wear of segment type B2 is far smaller than that of the other segments.

Figures 4.36 - 4.39 show the configuration of wear of segment A1 and A2.

The failure of segment types A1 and A2 were due to the edge chipping and bevel chipping as shown in Figure 4.36 and 4.37. However, for the segment type B1, failure was caused by the large chipping on the top of rougher tooth, shown in Figure 4.38. The failure for B2 segment was due to the edge chipping as shown in Figure 4.39.

4.3.2.3 Cutting C25 nimonic alloy

Wear test results for segment types A1, A2, B1 and B2 are presented as graphs of cumulative area of material cut versus specific cutting energy, as shown in Figure 4.40. It can be seen that the specific cutting energy of uncoated segment type A2 is little lower than that of segment B2. The tool life for A2 segment is little longer than B2 segment.

Figures 4.41 and 4.42 show the configuration of wear of segment B2 and A2.

The failures of segment types B2 and A2 were due to the edge chipping and flank wear as shown in Figures 4.41 and 4.42.

4.4 Discussion

Table 4.7 shows the performances and normal feature of the uncoated segments. It can be simply summarised as follows:

(1) In case of cutting mild steel, the segments with negative rake angle give better performance than those with positive rake angle. The performances for A1 and B1 are better than A2 and B2, figure 4.29. Comparing the tool materials, the carbide grade S4 used for segment types A1 and A2 were more suitable for cutting mild steel than carbide grade MK20.

(2) In case of cutting 302S25 stainless steel, the segments with positive rake angle performed much better than those with negative rake angle. The performances for B2 and A2 segments were better than A1 and B1, figures 4.33, 4.34 and 4.35. Comparing the tool materials, the carbide grades MK20 used for segment types B1 and B2 were more suitable for cutting stainless steel.

(3)The edge chipping, crater wear and flank wear were often occurred in case of cutting the proposed workpiece materials. For this reason, TiN

and TiAlN coatings will be applied to the segments to arrest or reduce the above failure modes. These types of coatings possess a high resistance to those wear.

CHAPTER FIVE

APPLICATION OF PHYSICAL VAPOUR DEPOSITION TECHNIQUES TO CARBIDE TIPPED CIRCULAR SAW SEGMENTS

The aim of this chapter is to describe how advanced surface coatings (TiN and TiAlN) may be applied to carbide tipped circular saw segments. Testing and analysis of these coatings are carried out to identify the performance of TiAlN and TiN coatings.

5.1 Introduction

A significant contribution to the development of cemented carbide tools is the application of hard coatings. A substantial improvement in the cutting tool performance and productivity is achieved by the combination of a wear-resistant coating with a hard and tough substrate (30-32). This outstanding improvement is imparted by a thin hard coating typically 3-10 μm thick (33).

For the brazed carbide tools, application of coatings is still a very new research area.

In the case of the carbide tipped circular saws two main difficulties are experienced in the application of coatings to the brazed carbide tools. Firstly the limitation of saw blade size, normally the full saw size is larger than the volume of the coating chamber. Secondly the high coating temperature will melt and destroy the brazed joint. This high temperature will soften the steel shanks of brazed tools. The melting points for braze materials are normally between 600° - 650°C, and normal working temperature for PVD coating process is between 400° - 600°C (34). The melting points for braze materials are normally between 600 and 650°C, however the braze material begins to loose its strength at temperature

above 400°C which is within the normal PVD coating temperature range of 400 - 600°C. High temperatures can also deform the coated saw blades. Then the blade has to be reground to size for accuracy. Thus the coatings will be destroyed. For this reason, the application of coating to the brazed carbide tipped circular saw will be a significant technical break-through in the application of coating techniques.

5.2 Selection of a suitable coating technique and its advantages

5.2.1 Introduction

A new brazing material with higher melting point (about 710° - 810 °C) has been found in the market, but it is too expensive to be suitable for commercial production. The cost for this new brazing material is two times that of normal brazing material. The most common brazing material used in the carbide circular saw production is Easy-flo No.3 that has a melting point about 600°C. Therefore, it is necessary to find a suitable coating technique and establish an appropriate coating method, which will not weaken the braze.

The most commonly used coating techniques for coating cutting tools use vapour deposition and may be broadly classified into two categories: physical vapour deposition (PVD) and chemical vapour deposition (CVD). Within these two general categories there are many coating techniques, based on the principles of mass transfer. Some techniques combine certain characteristics of two or more basic techniques, thus allowing greater versatility in the process or product.

5.2.2 Physical vapour deposition (PVD)

Physical vapour deposition (PVD) is an expression covering a wide range of coating processes such as sputtering techniques (glow discharge deposition, planar magnetron sputtering and ion beam sputtering), arc

deposition and plasma assisted physical vapour deposition. The common feature is that they are all carried out under a partial vacuum condition in which at least one of the depositing species is atomised from solid within the chamber. The process may be assisted by the action of a glow discharge, sputtering or plasma, in which case it is called Plasma Assisted PVD. Figure 5.1 shows the typical schematic PVD system.

The PVD process allows the deposition of metal, alloy and ceramic coatings onto a wide rage of substrates. The interface between the coating and substrate can be modified and characteristics of the coating (i.e., thickness, structure and composition) can be controlled. This also permits the formation of coatings at comparatively low temperature, (i.e. <450°C for plasma assisted physical vapour deposition) (34).

5.2.2.1 Advantage of PVD coating

PVD coatings have the following advantages:

(1) Coatings have good adhesive strength, which is attributed to the high arrival energy of the coating material and the possibility to "sputter-clean" the surface by argon ion bombardment prior to deposition.

(2) Coatings usually require no finish machining, as they replicate the original surface finish.

(3) Deposition temperature can be low 400° to 500°C.

(4) Thickness is very uniform - attributed to gas scattering effects and the ability to rotate and reciprocate items relative to the source.

(5) The coating structure can be controlled.

(6) A very wide range of coating and substrate materials can be used.

(7) There are usually no effluents or pollutants produced.

(8) Deposits have high purity.

(9) The "hydrogen embrittlement" problems, sometimes experienced with electroplating, can be avoided.

(10) The coating systems readily lend themselves to automated batch manufacture.

5.2.2.2 Limitations of PVD coatings

PVD coatings have the following limitations:

(1) The process has to be carried out under a partial vacuum condition.

(2) Coatings on substrates of complex shapes can not be deposited.

(3) No thick boundary layer at the substrate surface is formed. Thus the bonding strength between the coating and substrate is very weak.

(4) Grain size is more coarse than that deposited by CVD.

(5) PVD coatings are significantly thinner than CVD coatings. This reduced thickness is disadvantageous when abrasive wear resistance is the primary requirement.

5.2.3 Chemical vapour deposition (CVD)

5.2.3.1 Conventional CVD

Chemical vapour deposition may be defined as a technique in which a mixture of gases interacts with the surface of a substrate at a relatively high temperature. This results in the decomposition of some of the

constituents of the gas mixture and the formation of a solid film or coating on the substrate.

In its most fundamental form, CVD requires a source of precursor gases, a heated reaction chamber, and a system for the treatment and disposal of exhaust gases. The precursor gases include inert gases such as nitrogen and argon, reducing gases such as hydrogen, and a variety of reactive gases such as methane, carbon dioxide, water vapour, ammonia, chlorine, and others.

The gas mixture is carried into a reaction chamber heated to the desired temperature. The various techniques of heating include resistance heating using silicon carbide or graphite heating elements, or induction. In some cases, the substrate may be directly heated by passing an electric current through it. In induction heating the part may be directly heated when it acts as a susceptor. In these two cases, the walls of the reactor are at a relative low temperature, and therefore these techniques are described as cold-wall CVD. When the external heat source is used to heat the walls of the reaction chamber from which heat is radiated to the substrate, the technique is called as hot-wall CVD. The various heating techniques are schematically illustrated in Figure 5.2 (34). As CVD is not suitable simply because of the high working temperature (about 700°-1000°C), it is not necessary to describe the process in detail.

In addition to the conventional CVD the newly emerging techniques of Plasma CVD (PCVD) and Laser CVD (LCVD) will be discussed briefly.

5.2.3.2 Plasma-assisted chemical vapour deposition

This technique has recently come into prominence because it allows deposition to take place at reduced substrate temperature, typically below about 600°C (34).During this process, the kinetic energy of electrons in

the plasma is utilised to activate the chemical reactions in the vapour phase (Figure 5.3).

A major difference between conventional CVD and plasma CVD is that the thermo-dynamic principles of chemical reactions which govern the former do not apply to plasma CVD, which enables the PCVD to work at a lower temperature than CVD.

5.2.3.2.1 Advantages of PCVD

(1) In plasma-assisted CVD, the activation barrier to the chemical reaction is overcome by the dissociation of the reactive gases in the plasma, this is attributed to the impact of the high-energy electrons. This allows the reaction gas temperature to be lowered considerably, which is a very important consideration in many applications.

(2) Broad excitation energy distribution.

(3) Large reaction volume.

(4) Gas phase reaction are possible.

(5) Optical properties are not important.

(6) Low deposition temperature.

5.2.3.2.2 Limitation of PCVD

(1) Can cause contamination from chamber walls.

(2) Limited (low) pressure range.

(3) Irradiation damage in insulating films is possible.

(4) It is not economical and popular technique.

5.2.3.3 Laser chemical vapour deposition coatings

Laser chemical vapour deposition (LCVD) is a newly emerging technology in which the conventional CVD processes are enhanced by laser activation (Figure 5.4). In that sense, laser CVD is similar to plasma CVD processes. However, there are some major differences between these two techniques. The energy distribution of electrons in a plasma discharge, for example, is much broader than that of the photons emitted from a laser (34).

5.2.3.3.1 Advantage of LCVD

(1) Well-defined and controllable reaction volume.

(2) Highly directional light source allows precise localisation of deposition.

(3) Can be carry out at any pressure.

(4) Irradiation damage is considerably reduced.

(5) Low deposition temperature.

5.2.3.3.2 Limitation of LCVD

(1) Narrow excitation energy distribution.

(2) Gas phase reactions are reduced.

(3) Optical properties of gases and substrate are important in photolytic LCVD.

(4) For this new technique , it is not widely applied to the cutting tools because of this technique cost high.

5.2.4 Determination of the suitable coating technique

As mentioned above, the low deposition temperature is the most important factor for selection of coating technique. PVD, PCVD and LCVD are suitable for coating brazed carbide tools at low temperature because of the low deposition temperature. However, LCVD and PCVD methods are very expensive and not widely applied in the production of hard coatings. For this reason, PVD is the best choice for coating brazed-carbide tip circular saw.

5.3 Experimental procedure for the application coatings to the carbide segments and characteristics of coatings

Since coating the carbide tipped circular saw does not have a clearly defined standard, it is necessary to develop a new experimental approach.

The experimental procedure is simply given in Figure 5.5.

The test results and the testing approach for each step are discussed in the following sections.

5.4 Segment heating resistance test:

5.4.1 The purpose of the heating resistance test

Although PVD technique can provide a low working temperature at 400° to 600°, the problem is whether the brazed carbide saw segments can be coated without deformation occurring between the tips and steel shank. For this purpose, the heating resistance test should be carried out before coating the segments.

In this test, the segments were heated at 400° to 600° and kept for two hours. These working conditions are similar to those of PVD. This

enables the most suitable coating temperature to be determined without any shape changed between the carbide tip and steel shank.

5.4.2 Deformation

Deformation between the carbide tip and steel shank may take place in two directions (X and Y directions as shown in Figure 5.6). However, the deformation in X direction was much smaller than that in Y direction attributed to the restraints on the front side and back side of the tip as shown in Figure 5.6 (view A). For this reason the deformation in X direction was negligible. If a deformation occurred, the large deformation should be developed in Y direction because any deformation will develop in a direction with a low stresses.

In this test, the deformation in Y direction was measured in terms of cross deviation (absolute value). The cross deviation is given by:

$$\text{Cross Deviation error on rough tooth} = \frac{H_i - H_{i*}}{Hi*} \times 100\ \%$$

Where H_i - Value of H1, H2, H3 and H4 on the heated teeth.

H_i* - Value of H1*, H2*, H3* and H4* on the new teeth.

5.4.3 The equipment for the test

Heating test: Carbolet furnace SW2, Figure 5.7.

Geometry measurement of saw segments: MU-214B Societe Genevoise (Figure 5.8).

5.4.4 The test procedure and test results

Firstly the new uncoated carbide tipped circular saw segments were put into the SW2 Carbolet furnace which automatically controlled the heating

temperature. The heating tests were carried out at a temperature of 500°C and the segments were kept at this temperature for two and half hours which were the proposed highest working temperature and the longest working time.

After cooling, the geometries of the heated segments and new segments were both examined with MU-214B Societe Genevoise measurement equipment. The results measured for both types of segments (unheated and heated segments) were compared with each other to find out weather there is any deformation occurred on the cutting edge after heating.

Secondly both heated and unheated segments with the same geometries were measured with MU-214B optical measure machine to determine the cross deviation from the base line on the equipment as shown in Figure 5.6.

The testing results are shown in Table 5.1. It can be seen that the largest cross deviation error between the teeth is 0.157% occurred on the A1 segment.

The heated segment is shown in Figure 5.9.

Thirdly the cutting tests were carried out with A1 segment to compare the performance for both heated and unheated segments.

Comparison of performance curves for unheated and heated segments are shown in Figure 5.10. The two performance curves are almost on the same position. Thus it can be sure that the heated segments with the cross deviation error of less than 0.157% give the same performance as new segment.

5.5 Determination of coating condition and equipment

5.5.1 Determination of coater

In order to reduce the cost for this research project, the best choice should be in the University.

For these reasons, HTC 1000-4 ABS system was chosen as coater that can provide working temperature at about 350°-600°C.

5.5.2 Determination of coating temperature

The coating temperature is a very important factor which will influence the properties of the coatings. Normally, the high coating temperature will be beneficial for enhancing the bonding strength between the substrate and coating. However, as mentioned above, the coating temperature can not be too high to avoid the deformation of the segments.

For this reason, three batches of the carbide tips (not carbide segments) were coated with TiN at the temperatures of 350°, 400° and 450°C. The coatings on the tips were examined by VANOX-T optical microscope and the cross structures of the coatings were examined by JEO 8410 electron microscope. From the testing results, it had been found that bonding strength between the substrate and coating was very poor at coating temperature of 350°C as shown in Figures 5.11(a),5.11(b) and 5.11(c). At coating temperature of 450°C, a very good bonding condition was obtained as shown in Figures 5.12(a),5.12(b) and 5.24. Therefore the temperature of 450°C was chosen as the best working temperature.

5.5.3 Determination of working conditions

The working conditions were established as follows:

1) Preheating temperature: TSP=350 °C.

2) Target clean: Target power Pt=7kw; Coil current Ic=0; Substrate voltage Ub=0; Argon flow fAr=15; Working time (5 minutes).

3) Ion etch: Substrate bias UB=1200V; Target current It=100A.

4) Coating material: TiN and TiAlN were chosen as coating materials to arrest the most common failure modes such as crater wear, flank wear and edge chipping.

5) Coating temperatures: 450°C.

6) Working time for the coating process: 120 minutes.

5.6 Application of coatings to the segments

5.6.1 Experimental equipment

Coating equipment: HTC 1000-4 ABS system which has four targets and was used for coating cutting tools (Figure 5.13).

5.6.2 Substrate holder

The design of the substrate holder has a very substantial effect on the practical operation of a PVD hard-coater.

As HTC 1000-4 ABS system, smaller pieces such as carbide tipped saw segments go through a triple planetary rotation during the coating process. Figures 5.14 and 5.15 show the substrate holder. The holder is mounted on a turntable bonded in the system. The segments are mounted vertically on either six or twelve rotating satellites. During the coating process the satellites are moved through the chamber, rotating on the cathodes, which themselves are also vertically oriented, Figures 5.14 and 5.15.

In order to make sure that the tools are adequately coated all over, during the coating process the substrates continued to be rotated by driving mechanisms.

5.6.3 System control and process sequence

The HTC 1000-4 ABS system is equipped with and monitored by a Mitsubishi SPC control unit. All operation functions are controlled by SPS control system (Figure 5.16).

The typical process sequence for this system is summarised in Figure 5.17.

5.6.4 Application of coatings to the segments

Before the segments were taken into the chamber, the segments were carefully cleaned to avoid the contamination of the coatings and weakening the bonding strength. The cleaning process was carried out in the vapour cleaning container (Figure 5.18). The segments were put into a vibrational container with a 60°C temperature cleaning liquid and kept for 20 minutes. Then the segments were moved into an other container with clean water for 10 minutes. After this process, the segments were vapoured and dried in the third container.

Pumping down is followed by a process step that essentially results in heating of the segments. This may be a glow discharge process, or it can use built-in heating elements available on special order.

The coating process is preceded by pretreatment with ion etching. An etching step in an inert gas such as argon can be incorporated as a matter of course.

Deposition of the hard coating takes place during the unbalance- magnetron sputtering procedure. The typical dynamical coating rate is 2.5 to

3μm/h. The negative voltage is -50 V, and the bias current density is adjustable between 0.5 and 5 mA/cm^2. The total cycle time (working time) was arranged within 2 hours.

Titanium nitride coatings were deposited onto a range of substrates by arc bond sputtering as shown in Figures 5.19 and 5.20.

All coatings were normally 5μm and single layer coating.

5.7 Geometry measurement of the segments

5.7.1 The purpose of the test

Although the best coating temperature was determined before coating the segments, the coated segments still needed to be carefully examined to determine whether any deformation occurred during the coating process.

5.7.2 The equipment for the test

Geometry measurement of saw segments: MU-214B Societe Genevoise (Figure 5.8).

5.7.3 The test procedure and results

The geometries of the coated segments were examined by the same method used during the heating resistance test to assess the geometry after coating.

According to the investigation in section 5.4, the cross deviation error (Figure 5.6 and Table 5.1) must be within the tolerance of less than 0.157% to avoid the tooth deformation.

The geometries of both coated and uncoated segments were measured with MU-214B optical measure machine to determine the cross deviation

from the centre line of the tooth. The testing results are shown in Table 5.2. It can be seen that the largest cross deviation error is 0.078%.

5.8 Characteristics of coatings

In order to characterise the coatings, the scratch adhesion test, micro hardness test and scanning the micro structures of segments were carried out to find out the differences of the coatings.

5.8.1 Scratch adhesion test

There are many different tests to measure the adhesion of a coating to a substrate such as pull tests, bend tests, scratch tests, etc. Hard coatings on hard substrate (such as carbides) have very high adhesion strength (35, 36). Because of this high adhesion strength, there is only one practical test for measuring the adhesion of hard coatings. It is the scratch test.

5.8.1.1 The test equipment

Scratching test: MEGATECH ST-200 Scratch Adhesion Tester (Figure 5.21).

5.8.1.2 The test procedure

In the scratch test, a diamond indenter with a known load pulled over the surface of the coating. The load is increased until the coating becomes damaged, either through a cohesive or adhesive failure. The load at which this failure occurs is known as the critical load usually given in units of kilograms force or Newtons.

Scratch adhesion test was performed using MEGATECH ST-200 scratch adhesion tester fitted with a Rockwell C diamond stylus. Scratches were performed using a range of fixed loads for a traverse length of 5 mm.

Initial scratches were performed at a load of 10 N and table speed of 5mm/min at which some stripping of the coating was observed.

5.8.1.3 The test results

The scratch test results for the coatings tested are shown in Figure 5.22. The critical load for the coating failure decreased in the following order: TiAlN TiN. It can be seen from these results that TiAlN coatings had better adhesion strength than that of TiN coatings. The multi-component coatings (TiAlN) showed the higher loads for coating removal, comparing to the TiN coating.

Figures 5.23 and 5.24 show the scanning electron micrographs of selected scratch channels. For TiN coating, the extensive cracking and spallation of the coating were observed outside the scratch channel. This reflected the poor adhesion characteristics of this coating, as shown in Figure 5.23. In contrast, the scratch channel for TiAlN (Figure 5.24) shows no signs of coating spallation along the its scratch length.

5.8.2 Micro-indentation hardness testing

5.8.2.1 The test equipment

Micro-hardness test: Microhardness Tester (Figure 5.25)

5.8.2.2 The test procedure

To measure the hardness of a hard, thin coating, it is necessary to use light loads on an indentation test. The two common types of indentation tests that are used are the Vickers test and the Knoop test. The difference between the two is the shape of the indenter. The Vickers test uses a diamond pyramid whereas the Knoop indenter uses a diamond indenter that is elongated along one axis. The Vickers makes a deeper penetration than the Knoop one does, and this difference can be important to avoid

substrate effects. In hard coatings, it is often very difficult to determine the end of the elongated knoop indentation, but this problem is not present with the Vickers test. Hence the Vickers indenter is usually used to measure the hardness of hard coatings (37, 38).

As the load is decreased in these micro hardness tests, it is very common to find an apparent hardness increase. Since the coating was thin (5 μm), a 15 gram load was used with a Vickers indenter.

5.8.2.3 The test results

The hardness for the coatings and their substrates are graphically represented in Figure 5.26. Some observations can be made, from the results that all coatings were harder, comparing to the substrates, decreasing in the following order: TiN TiAlN S4 SP35 MK20 SP4.

5.8.3 Micro-structure of the coatings

There are three available microscopy techniques used to look at the structure of the hard coatings. They are optical, scanning electron microscope such as Phillips 500 SEM and JEOL 8410, and transmission electron(TEM) microscopy.

5.8.3.1 The test equipment

Micro structure of coating: JEOL 8410 Electron Microscope.

5.8.3.2 The test results

The morphologies of the cross section of the nitride based coatings (TiAlN, TiN), using JEOL 8410 Electron Microscope, are respectively shown in Figures 5.27 and 5.28. For TiN coating, a columnar structure was observed (Figure 5.27), and no columnar structure for TiAlN coating (Figure 5.28).

5.9 Cutting test

Metal cutting tests are very important for assessment of the performance of the coatings. The cutting tests were carried out at the same cutting conditions as those used for uncoated segments.

The performances for coated segments were carried out to compare the performance for both coated and uncoated segments.

The failure modes for coated segments, in case of cutting mild steel, stainless steel and nimonic alloy, were established to compare the wear behaviour for both coated and uncoated segments.

5.9.1 The test equipment

Cutting test: Dean Smith & Grace lathe with specially designed test ring (Figures 4.4).

General view of segment: a Phillips 500 SEM Scanning Electron Microscope (Figure 5.29).

5.9.2 Cutting Tools

The tools were coated with TiN and TiAlN coatings as shown in Figures 5.19 and 5.20. There were six types of segments coated using two kinds of coatings with coating thickness 5 μm (Table 5.3). The coatings were produced using the HTC 1000-4 ABS system which has four targets and was specially used for coating cutting tools.

The tool geometries and the substrate materials are the same as those of the uncoated segments as shown in Table 4.2.

5.9.3 Workpiece materials

The cross section 30x50 mm of mild steel, 302S25 stainless steel and C25 nimonic alloy were used as workpiece materials.

The hardness and composition of the workpiece materials are shown in Tables 4.3, 4.4 and 4.5.

5.9.4 Cutting conditions

The optimised cutting conditions for the cutting tests are shown in Table 4.6. These optimised cutting conditions were determined from the previous performance cutting tests for the uncoated segments.

All cutting tests were carried out under dry cutting conditions.

5.9.5 Wear measurements

The testing was carried out by using the techniques for wear measurements recommended by ISO 3685-1977 (29, page 10). The value of 0.6 mm for the flank wear was used as a criterion for the tool life in case of cutting mild steel (Figure 4.3). The value of 0.3 mm for the flank wear was used as a criterion for the tool life in case of cutting stainless steel and nimonic alloy, figure 4.3. The width of the flank wear land was measured with a tool room microscope.

5.9.6 Cutting test results and discussion

Six types of the coated (TiAlN, TiN) segments were used for the cutting test (Table 5.3).

The performances of TiN and TiAlN coated tools were evaluated in terms of the wear resistance of the coated layer and the bonding strength between the coatings and different substrate materials.

Results for the life tests are presented as the graphs of Esp versus cumulative area cut and width of flank wear (VB) versus cumulative area cut.

5.9.6.1 Cutting mild steel

The cutting conditions used for cutting the mild steel with the coated segments are shown in Table 4.6.

Figure 5.30 shows a comparison of the flank wear versus area cut for the TiAlN coated and the uncoated segments at the same cutting condition. As compared with wear behaviour of the segments, the wear of the TiAlN coated A1 and B1 segments are much smaller than the uncoated segments. The TiAlN coated A1 segment shows the greatest wear resistance and the longest tool life.

Figure 5.31 shows a comparison of the specific cutting energy (Esp) versus area cut for the TiAlN coated and the uncoated segments at the same cutting condition. It can be seen that the coated segments have the lower cutting energy than the uncoated segments while with the same area cut. The TiAlN coated A1 segment has the lowest cutting energy with the surface area cut of 0.3 m^2 and the longest tool life.

Figure 5.32(a) to 5.32(e) show the configuration of wear for the TiAlN coated A1 and B1 segments when cutting mild steel.

As indicated in Chapter four, for the uncoated segment type A1, the failures were due to the crater wear on the rake face and the large chipping produced on the finish tooth after the area cut of 0.23 m^2, figure 4.32(b). In the contrary for the TiAlN coated A1 segment, the coating on both rake face and flank face of the roughing tooth was almost undamaged after 0.3 m^2 area cut, figures 5.32(a) and 5.32(b). The main failure reason for the

TiAlN coated A1 segment was attributed to the chipping of the bevelling after 0.56 m^2 area cut (Figure 5.32(c)).

Figure 5.32(d) shows the tool wear on both rake face and flank face of TiAlN coated segment B1. The wear for coated B1 segment was smaller than the uncoated segment B1 (Figure 4.31) even after 0.2 m^2 area cut. The failure for the TiAlN coated segment B1 was mainly due to the chipping on the bevelling of finish tooth after the area cut of 0.3 m^2, figure 5.32(e).

The crater wear for the TiAlN coated segments A1 and B1 seems to be arrested.

Figure 5.33 shows a comparison of the specific cutting energy (Esp) versus area cut for the TiN coated and uncoated A1 and A2 segments when cutting mild steel. The TiN coated A1 segment consumed the lowest cutting energy while with the same area cut and obtained the longest tool life. The TiN coated segment shows a greater cutting energy increased after 0.1 m^2.

Figures 5.34(a) and 5.34(c) show the configuration of wear of TiN coated A1 and A2 segments.

Figure 5.34(a) shows the cutting edge on the rough tooth of TiN coated A1 segment after the area cut of 0.42 m^2, comparing to the crater wear on the uncoated A1 segment after the area cut of 0.23 m^2, figure 4.30, the crater wear has been arrested. The failure for the TiN coated A1 segment was due to the flank wear after 0.42 m^2 area cut, figure 5.34(b). For the TiN coated A2 segment, the failure was mainly attributed to the crater wear on the rough tooth after 0.16 m^2 area cut, figure 5.34(c). However, as compared with the large crater wear on the rough tooth of uncoated

A2 segment after 0.07 m^2 area cut, figure 4.32, the crater wear on the rake face of the TiN coated A2 segment has been reduced and the tool life was increased. Figure 5.35 shows the comparison of the performance of the TiN and TiAlN coated segments when cutting the mild steel. As compared to them, the TiN and TiAlN coated A1 segments consumed the lowest cutting energy after 0.26 m^2 area cut. The TiAlN coated A1 segment has the longest tool life.

5.9.6.2 Cutting 302S25 stainless steel

The cutting conditions used for cutting the stainless steel with the coated segments are shown in Table 4.6.

Figure 5.36 shows a comparison of the flank wear versus area cut for the TiAlN coated and the uncoated segments (the types of A2, B1 and B2 segments) at the same cutting condition. The wears for the TiAlN coated B2 and A2 segments are much smaller than the other segments while with the same area cut, showing the greatest wear resistance. The TiAlN coated B2 segment has the longest tool life.

Figure 5.37 shows comparison of the specific cutting energy versus area cut for the TiAlN coated and uncoated B1 and B2 segment. It can be seen that the TiAlN coated B2 segment has the lowest cutting energy while with the same area cut and the longest tool life. The TiAlN coated B1 segment has no much improvement on the performance.

Figures 5.38(a) to 5.38(d) show the configuration of wear of the TiAlN coated B1 and B2 when cutting 302S25 stainless steel.

Figure 5.38(a) shows, comparing to the failure mode of the uncoated segment B2 after 0.0092 m^2 (figure 4.39), the cutting edge chipping on the rough tooth has been arrested after 0.016 m^2 area cut. The coated

layers on both rake and flank faces are broken quite smaller. The amount of edge chipping is quite smaller even after 0.026 m^2 area cut, figure 5.38(b).

Figure 5.38(c) shows, comparing to the failure mode of uncoated segment B1 after the area cut 0.002 m^2 (Figure 4.38), the large chipping on the cutting edge of the roughing tooth has been arrested. However, the chipping on the bevelling of the finish tooth still remains a very large area after 0.009 m^2 as shown in Figure 5.38(d).

Figure 5.39 shows the performance for the TiAlN, TiN coated and uncoated A1 and A2 segments. The TiN coated segment A2 gives a better performance than uncoated and coated A1 segments. However, comparing to the tool life and the consumed cutting energy of the segments, the TiAlN coated A2 segment gives the lowest cutting energy and the longest tool life. The TiN coated segment A1 has little improvement in performance.

It can be seen that the TiAlN coatings perform much better than TiN coatings, in the case of cutting stainless steel. This is attributed to the fine grain size and high temperature oxidation resistance of the TiAlN coatings. For the TiAlN coatings, the reaction with hot air is at 800°C and for the TiN coatings it oxidises with hot air at 550°C (42).

Figures 5.40(a) to 5.40(d) show the configuration of wear of the coated A1 and A2 in case of cutting 302S25 stainless steel.

Comparing to the failure mode of uncoated A2 segment after the area cut of 0.0043 m^2 (figure 4.37(a)), figure 5.40(a) shows that the chipping on the bevelling of the finishing tooth of the TiAlN coated A2 segment has been reduced after 0.022 m^2 area cut. The wear and the chipping on the

roughing tooth of the TiAlN coated A2 segment are smaller, figure 5.40(b).

Figure 5.40(c) shows the wear on the finish tooth of the TiN coated segment A1. It can be seen that the TiN coating on the cutting edge is completely destroyed, and large chipping has occurred on the tooth.

Figure 5.40(d) shows the breakage and the edge chipping on the rough tooth of the TiAlN coated segment A1. Comparing to the failure mode of the uncoated segment A1, the chipping on the rough tooth is not arrested by the coatings. This is attributed to the unsuitable tool material (carbide S4 grade) and too large negative rake angle when cutting stainless steel. Figure 5.41 shows the comparison of the performance of the TiN and the TiAlN coated segments. The TiAlN coated B2 segment has the lowest cutting energy with the same area cut and the longest tool life. Also it can be seen that the TiAlN coated segment A2 has the second longer tool life. However, the cutting energy is rapidly increased after 0.009 m^2 area cut, so the cutting force increased.

5.9.6.3 Cutting nimonic alloy

The cutting conditions used for cutting the nimonic alloy with the coated segments are shown in Table 4.6.

In Figure 5.42 the coated A2 and B2 segments have a lower cutting energy and a longer tool life than the uncoated segments. However, comparing to the tool life and the cutting energy, the TiAlN coated A2 segment have the longest tool life and the lowest cutting energy, but not the TiN coated B2 segment.

Figures 5.43(a) to 5.43(b) show the wear configuration for TiAlN coated segments in the case of cutting C25 nimonic alloy.

The main failures of the segments are attributed to chipping and built-up edge, figures 5.43(a) and 5.43(b).

5.10 Discussion

Both TiN and TiAlN coatings have been successfully applied to the carbide tipped circular saw segments.

The results have indicated both TiAlN and TiN coatings have enhanced the performance of the carbide tipped circular saw when cutting the proposed workpiece materials.

The results have identified TiAlN to be the better coating when cutting stainless steel and mild steel.

The maximum cutting forces and thrust forces developed by both TiN and TiAlN coated and uncoated A1 and B2 segments cutting mild steel and stainless steel have been plotted against feed rate per pair of teeth, figures 5.44, 5.45, 5.46 and 5.47. The cutting forces and thrust forces for coated segments are much smaller than those of uncoated segments. Also the results show that the forces produced with the TiAlN coated segments have identified to be lower than those of the TiN coated segments.

CHAPTER SIX

FINITE ELEMENT ANALYSIS

6.1 Introduction

The development and application of mathematical models to simulate and control the metal cutting process has occurred over a number of decades. However, the basic finite element technology originated only in the early 1960s. With the availability of inexpensive computational power, the number of numerical investigations of cutting has been increasing rapidly for a variety of tasks, including: off-line model and process design, prediction of tool failure modes and tool geometry design etc. With in creased demands from customers, a better understanding of the wear behaviour of the related carbide tipped circular saws has been given much attention by the saw producers. This is now considered to be a key point towards the improvement of the saw quality. In this project a completely new model was established to predict the failure behaviour of carbide tipped circular saws; evaluate and compare the stress distributions with the different carbide circular saw failure configurations; optimise the geometries of saw blades; and provide basic information for the application of a coating to a sawblade.

Because the basic mechanical properties of cemented carbides are high hardness and low toughness, having only slight ability to deform plastically without fracture at room temperature, the modelling for the carbide tipped circular sawing only involves a linear problem.

Nowadays, a number of FE packages such as ABAQUS, P3/PATRAN, ANSYS, DYNA, MARC and I-DEAS have been used in metal cutting . In this study, the I-DEAS programme was used as a preliminary application of the finite element technique to the cutting of mild steel. For the

further modification of the model, P3/PATRAN was used for pre-processing and post-processing.

6.2 Mathematical model

6.2.1 Displacement of a point within element

The displacement of a node is given by,

$$\Delta X i = N\ I\ (x\ j)\ \Delta d\ I\ i \qquad (1)$$

Where $\Delta X\ i$ - Displacement increment at a point in element.

$\Delta d\ I\ i$ - Displacement increment of a node.

$N\ I\ (x\ j)$ - Interpolation function (shape function).

6.2.2 Relationship between stress and strain

According to the Generalised Hook's Law ,

$$\sigma = [D]\ \varepsilon \qquad (2)$$

Where σ - Stress tensor.

ε - Strain tensor.

[D] - material elasticity matrix or material property matrix (constant for a given material).

For a 3D stress strain system,

$$[D] = \frac{E}{1-\nu}\begin{bmatrix} \frac{1-\nu}{1-2\nu} & \frac{\nu}{1-2\nu} & \frac{\nu}{1-2\nu} & 0 & 0 & 0 \\ \frac{\nu}{1-2\nu} & \frac{1-\nu}{1-2\nu} & \frac{\nu}{1-2\nu} & 0 & 0 & 0 \\ \frac{\nu}{1-2\nu} & \frac{\nu}{1-2\nu} & \frac{1-\nu}{1-2\nu} & 0 & 0 & 0 \\ 0 & 0 & 0 & \frac{1}{2} & 0 & 0 \\ 0 & 0 & 0 & 0 & \frac{1}{2} & 0 \\ 0 & 0 & 0 & 0 & 0 & \frac{1}{2} \end{bmatrix}$$

Where E - Young's modulus.

ν - Poisson's ratio.

6.2.3 Relation between strain and displacement

Symbolically the strain-displacement relationships (39) are,

$$\varepsilon = [B]\, d \qquad (3)$$

Where ε - Strain tensor.

d - Displacement tensor.

$[B]$ - Strain and displacement gradient matrix. [B] will be determined by the characteristics of element and shape function.

6.2.4 Relation between nodal displacement and force

The following relationship exists between nodal displacement and nodal force (39),

$$f = [K]\, \boldsymbol{d} \qquad (4)$$

Where f - Nodal force vector.

d - Nodal displacement vector.

$[K]$ - Element stiffness matrix.

$$[K] = \int_v [B]^T [D][B] dV \qquad (5)$$

Where $[B]^T$ - Strain and displacement gradient matrix $[B]$ transposed, T - transpose.

$[B]$ and $[D]$ was defined in the sections 6.2.2 and 6.2.3.

dV - differential element of volume.

6.2.5 Equivalent stress and equivalent strain

In order to simplify analysis of a problem, it is necessary to find out a stress and strain to represent this complex stress and strain state. According to mechanics of elasticity (39), the equivalent stress and equivalent strain are

$$\sigma_{eq} = \frac{1}{\sqrt{2}} \sqrt{(\sigma_1 - \sigma_2)^2 + (\sigma_2 - \sigma_3)^2 + (\sigma_3 - \sigma_1)^2 + 6(\sigma_{12}^2 + \sigma_{23}^2 + \sigma_{31}^2)}$$

$$\varepsilon_{eq} = \sqrt{\frac{2}{9}[(\varepsilon_1 - \varepsilon_2)^2 + (\varepsilon_2 - \varepsilon_3)^2 + (\varepsilon_3^2 - \varepsilon_1)^2 + 6(\varepsilon_{12}^{2+} \varepsilon_{23}^2 + \varepsilon_{31}^2)]}$$

Where σ_{eq} - Equivalent stress

ε_{eq} - Equivalent strain

σ_1 , σ_2 and σ_3 - Principal stress

ε_1 , ε_2 and ε_3 - Strain

σ_{12} , σ_{23} and σ_{31} - Shear stress

6.3 Preliminary application of finite element technique to carbide tipped saw blade

6.3.1 Introduction

The finite-element method is a powerful numerical procedure for solving the mathematical problems of engineering. Its application ranges from stress analysis, fluid and thermal flow to diffusion and electro-magnetism (14, 15 and 16).

In order to investigate the problem associated with further development of the model, a single tooth computer model for preliminary analysis was set up.

This section presents a fundamental analysis of stress, strain and displacement of a single tooth model of carbide tipped circular saw through a practical example. For the preliminary analysis a single tooth model cutting mild steel was set up, in order to investigate the problems associated with the further development of the model.

6.3.2 Principal features of the single tooth finite element model

6.3.2.1 Tooth geometry and dimension of the single tooth model

The initial work described in this chapter only concerns the roughing tooth of type A1 segment with negative rake angle 18° and clearance angle 8° (Table 4.2).

The dimensions and geometry of the single tooth model are shown in Figure 6.1.

6.3.2.2 Blade materials

Segment type A1 material was modelled and material elasticity matrix was established.

The material properties used for the single tooth model are listed in Table 6.1. If required, additional sets of material properties could be defined in the weld region for a more accurate description of the tooth medium.

6.3.3 Finite element modelling of the single tooth

The stress and strain behaviour within the carbide tipped circular saw tooth developed during the cutting tests was simulated by computer model using the finite element method. The I-DEAS finite element package was used to prepare a 2D single tooth finite element model. The model constructed contained 299 nodes and 246 elements (quadratic elements), as shown in Figure 6.2. Plane stress conditions were assumed for each element within the model. Since the analysis of the tooth gullet forms an important feature of the current work, the blade structure surrounding the central gullet was represented by a finer mesh. Since a high stress gradient was likely to be present in the region of the flank, an increased density of elements was used to present the structure in this area.

6.3.4 Imposition of boundary conditions

The nodes along boundary A-B were restrained in both of x and y directions while the nodes along the boundary A-C and C-D were restrained in the y direction, as shown in Figure 6.2.

6.3.5 Distribution of load

Applying the cutting and thrust force quantified through the cut simulation test, the model was loaded along the rake face over the chip/tool

contact length. According to the distributed loading criterion (6), under higher loading condition such as sawing with carbide tipped circular saws, contact between tool and work surface is so nearly complete over a large part of the total area of the interface, that sliding at the interface is impossible under most cutting conditions. For this reason, the cutting force and thrust were simply divided into two sub-boundary force components (figure 6.2) homogeneously acting on the nodes of the interface between the rake face and workpiece surface.

The measured contact length between the tool and workpiece material at feed/tooth of 0.355 mm is about 1 mm.

The maximum forces in the case of tooth failure are given as follows:

Cutting force F_c = 1520 N (each component cutting force = 760N) Thrust force F_t = 500 N (each component thrust force = 250N)

In this case, the cutting force and thrust force were discretized and homogeneously applied on two nodes along the rake face as previously described, figure 6.2.

6.3.6 Model solution and output

The model was considered to behave elastically under the static loading condition. Under this loading condition the tooth structure was stressed according to the linear relationship derived from the elastic modules. Analysis of the elastic solution determined whether the transverse rupture strength of the material has been exceeded at any point within the tooth structure. This was achieved by comparing the transverse rupture strength (1.85 KN/mm^2 for carbide MK20) of the constituent tooth materials with the equivalent stress values determined within the model solution, derived using von Mises yield criterion (39).

The described model has been used to simulate the elastic material behaviour. Data were calculated and analysed by the I-DEAS finite element package, and then the output from the model was displayed graphically relating distributions of stress σ_y and σ_x, equivalent stress and equivalent strain.

Figure 6.3 shows the equivalent stress distribution. Distributions of stresses σ_x and σ_y are shown in Figures 6.4 and 6.5. Figure 6.6 shows the equivalent strain distribution. The analysis indicated that the maximum equivalent stress (332 N/mm^2) did not exceed the transverse rupture strength of the materials within the tooth structure.

6.3.7 Discussion

An initial finite element model, featuring one tooth and using elastic finite element analysis has been obtained. However, the results from this basic finite element model appeared not to be satisfactory. After having considered the preliminary finite element analysis strategy and activities, mentioned in section 6.3, the following aspects were either incorrect, or required clarification in the further model:

(1) The maximum equivalent stress (332 N/mm^2) is far smaller than the transverse rupture strength (1850N/mm^2) of the materials within the tooth structure. This does not reflect the actual stress distribution on the cutting edge in the case of the tool failure. The maximum equivalent stress on some area of the cutting edge should exceed or equal the transverse rupture strength if the tooth is to fail.

(2) The total cutting and thrust forces acquired from the simulation cutting tests should be uniformly discretized and homogeneously distributed over the chip/tool contact area in line with generally accepted load distributions.

(3) As the gullet size and shape significantly affect blade performance, the single tooth model could not truly reflect the stress distribution in the full segment (Figure 6.1). A satisfactory geometric model should include gullets with roughing tooth and finishing tooth as shown in Figure 4.8.
(4) Restraints and loads should be applied radially and tangentially to the circular saw instead of in the X and Y directions (Figure 6.7).

(5) No indication is given as to how the predicted stress values correlated with the strength of the carbides and what happens to the teeth during the simulation tests.

6.4 Further modification of computer model

In order to modify the initial model, a new modelling strategy was established as shown in Figure 6.8.

6.4.1 Assumptions of model

Figure 6.9 shows a 3D view of the carbide tipped circular saw segment with its co-ordinate axes. The segment was 60 mm x 32 mm x 5 mm, and a 0.2 mm cutting edge radius.

In order to simplify the problem, it is necessary to make a number of assumptions about the cutting process. Through these assumptions it was possible to simplify a complex 3D problem to a 2D problem and therefore keep the model within the computing capacity of the computer system.

The most important assumptions are given below:

(1) Since the values of length and width of the segment were much larger than that of thickness as shown in Figure 6.9, a plane condition (plane stress) was assumed for each element within the model. Under this condition, the stress along the direction of thickness (σ_z) is equalled to zero (40).

(2) The temperature and stress distributions on chip/tool cross area were uniform in z direction.

(3) For an unworn tooth the thrust force (radial force) was smaller than the cutting force apart from when the tool worn.

(4) The cutting edge radius was small in relation to the depth of cut (0.2 mm for the cutting edge radius and 0.355 mm for the depth of cut).

(5) The model used was elastic.

6.4.2. Improved geometric mode

The second geometric model featured one roughing tooth, one finishing tooth and two gullets as shown in Figure 6.7. The first tooth is roughing tooth and the other one is the finishing tooth. This is consistent with the geometry of the segment used in the imitation cutting test. As full carbide tipped circular saws are composed of the same size segments, a single segment model will be more realistic than the single tooth model to reflect the stress state on the saw blade.

In order to obtain a more accurate geometric model, the dimensions were processed and coordinates established through a series of software packages such as AUTO-CAD and COSMOS. The coordinate data acquired from these software were input to the preprocessor P3/PATRAN. Figure 6.10 shows the geometric model input to P3/PATRAN (input data see Appendix 1).

6.4.3 Coordinates of the new model and boundary restraints

Figures 4.6 and 6.7 show that the segments are radially composed of a full circular saw. Figure 6.7 indicates that both side boundaries (A-B, C-D) and bottom side (B-D) of the segment are radially related to the centre of the saw. The restraints applied to the previous model in X and

Y directions were unsuitable. For this reason, the X-Y-Z coordinate system was changed into a cylindrical coordinate. For 2D problem, it was a tangent and radial (T-R) system) as shown in Figure 6.7.

The nodes along boundary A-B and C-D were restrained in the tangential direction (nodes in the radial direction are free) while the nodes along the boundary B-D was restrained in both T (tangential) and R (radial) directions, as shown in Figure 6.11.

6.4.4 Tool/chip contact area

In order to apply the chip/tool contact length to the F.E. model it was necessary to measure chip/tool contact length. This method was used by M.Sarwar in 1982 (41).

Prior to starting the cut, the face of the segment was coated with blue felt tip ink. The cutting speeds is low and, hence, the low temperature, did not affect the ink coating used.

In addition to measuring the depth of cut and recording the cutting force components, on completion of each cut the chip/tool contact length was measured using a ruler and eye-attach lens.

Figure 6.12 shows the results of tests on cutting mild steel using A1 and A2 segments. The variation of chip/tool contact length with increase in depth of cut is shown.

6.4.5 Application of measured forces to the model

The cutting forces and thrust forces were quantified through the simulation cutting tests.

The cutting forces (tangential forces) were uniformly divided into three cutting force components and homogeneously applied to three nodes along the rake face over the tooth-chip contact length, figure 6.11.

The contact length between the tool surface and workpiece was determined in the section 6.4.4, figure 6.12. In the case of cutting mild steel at a feed rate of 0.355 mm per pair of teeth, the chip/tool contact length was about 1 mm.

The concentrated thrust force was loaded on the cutting edge of the tooth. The thrust force component should not be applied to the clearance face as no metal to metal contact occurs in this region apart from when the tool is worn.

The forces applied to the roughing tooth and finishing tooth were given as follows:

Roughing Tooth

Cutting force F_c = 1520N, each component cutting force = 507N. Thrust force F_t = 500N.

The cutting component forces were homogeneously applied to the first, the third and the fifth nodes for the model as shown in Figure 6.11.

Finishing Tooth

Cutting force F_c = 1230N, each component cutting force = 416.7N. Thrust force F_t = 400N.

The total thrust forces were homogeneously applied to the nodes on the cutting edge for the model as shown in Figure 6.11.

This loading condition was the same as that when cutting mild steel with type A1 segment after 500 cuts.

6.4.6 Application of measured temperatures to the model

6.4.6.1 Measurement of temperature on the cutting edge

The temperatures on the cutting edge were measured and processed with a Cyclops T135 SM Thermal Imager, as part of a system, for creating thermal images and measuring temperature in a wide variety of applications, by combining the scanner unit (Figure 6.13) with The Land Image Processing System (L.I.P.S.) and monitor (Figure 6.14).

The thermal signals were captured at a rate of five per second. Measurements on mild steel at a cutting speed of 203 m/min and feed rate of 0.355 mm/per tooth were taken. The captured data were processed by The Land Image Processing System (L.I.P.S.), allowing an IBM-AT compatible personal computer to be used to store and manipulate the thermal images obtained from the Cyclops T135 SM Thermal Imager.

Figures 6.15 show the images of cutting temperature obtained at a cutting speed of 203 m/min and a feed rate of 0.23 mm/rev. for mild steel. The highest cutting temperature was about 750°C and at a distance of 0.1 - 1 mm from the cutting edge.

6.4.6.2 Application of measured temperatures to the model

The shape of the temperature distribution on the chip/tool interface can not be determined by The Cyclops T135 SM Thermal Imager. It is necessary to investigate a suitable method for the determination of the shape of temperature distribution on the chip/tool interface. The shape of the temperature distribution at the chip/tool interface has been investigated by Trigger (1961), Usui (1984) and Dearnly (1983) (42, 43 and 44).

Among the investigations, the most reasonable suggestions were made by Dearnly and Usui. They suggest that the temperature distribution along the tool rake face is more uniform than that proposed by Trigger as shown in Figure 6.16(a). It can be seen that the distributions proposed by Usui and Dearnly (43, 44) have a very similar general shape. These results were obtained by direct measurement at chip/tool contact interface at a feed rate of 0.25mm/rev for cutting mild steel. In the region of 0.1 to 1 mm close to the cutting edge they have very similar and uniform values. It was decided to choose a uniform distribution on the chip/tool contact length. The temperature of 750°C was homogeneously imposed to the two elements adjacent to the cutting edge for the F.E. model, figure 6.16(b).

6.4.7 Meshing of the model

The model was constructed with a quadrilateral element with four nodes.

In order to save the computing time for calculation, the model was constructed with different sizes of elements. For this purpose, the "Mesh seed" function in Patron was used for the generation of the elements in the model. This selection allows user to specify the number of elements and their varying size along an edge of an entity. The symbol L2/L1 represents the ratio of the length of the last element to that of the first element along the edge (45).

A mesh seed of 0.3 was chosen in the chip/tool contact region. It was found to be rather reasonable when a short contact length, required such as 1 mm in length was required, The mesh seed was chosen so that the fine elements were generated and the cutting force could be spread over four or five elements. Also a value of 0.3 mesh seed was chosen in the clearance face and the gullet regions because high values of stress were generated in these regions.

In order to reduce the computing time for calculation, a value of 0.8 mesh seed was applied to the other region on the model. This enables the large size element to be generated in the model.

Because of different size of elements applied to a model, the aspect ratio of some element was exceeded a value of 15:1 in the areas as shown in figure 6.11 (Area A, B, C and D), resulting in grossly distorted elements. However, as these regions are far from the cutting edge, there is not much influence in the stress distribution of the model (Figure 6.11).

The model was constructed using 751 nodes to form a structure containing 655 quadrilateral elements featuring four nodes on each element (figure 6.11).

All geometric structure and meshes were established and generated in a cylindrical coordinate system.

6.4.8 Imposed the material properties to the model

The properties of the tool materials for the new model are shown in Table 6.2.

6.4.9 Model solution and output

6.4.9.1 Introduction

In the following section the mechanical and thermal stress behaviour within the tooth structure of a type A1 segment with negative rake angle was analysed when cutting mild steel.

It should be indicated that although the boundary restraints applied to the model were in a cylindrical coordinate, the output results in ABAQUS were automatically transferred into results in X-Y coordinate system. All stress values are in an unit of N/mm^2.

Data were calculated and analysed by the ABAQUS finite element package and then displayed graphically relating distributions of equivalent stress σ_{eq}, stress σ_{xx}, stress σ_{yy}, equivalent thermal stress, displacement and deformation.

In order to predict the behaviour of carbide tipped circular saw teeth over the range of prevalent cutting conditions, a graphical approach (Transverse rupture strength figure) was developed, which can be used to compare the yielding characteristics of the models with the failure modes of the cutting tools. This enables an assessment of the strength and weakness of the tooth profile and provide reliable information for the modification of the saw tooth profiles.

6.4.9.2 Result

Figure 6.17 shows the equivalent stress distribution on the model. It can be seen that the maximum equivalent stress of 2.3kN/mm^2 occurred on the rake face adjacent to the cutting edge for the roughing tooth. However, on the finishing tooth, the highest equivalent stresses are distributed on the flank face. These phenomenon are similar to the tool failure modes obtained during the cutting tests, the crater wear occurred on the roughing tooth and edge chipping occurred on the finishing tooth, as shown in Figures 4.30 and 4.31.

The maximum shear stress distribution are given in Figure 6.18. The maximum values of the shear stresses of -0.469kN/mm^2 occurred at the rake faces adjacent to the cutting edge of both roughing and finishing teeth. On the junction between the tip and backing material of the finishing tooth, the shear stress is very large. Also it can be seen that the stresses on the roughing tooth and its backing material are basically negative value and the positive value stresses are on the finishing tooth. The distribution of stress σ_{xx} is given in Figure 6.19. The highest positive

value is on the flank face of the finishing tooth, and the maximum compressive value is on the rake face adjacent to the cutting edge for the roughing tooth.

The distribution of stress σ_{yy} is given in Figure 6.20. The highest stress values are on rake face and flank face adjacent to the cutting edge.

The distribution of displacement and the equivalent strain ε_{eq} are given in Figure 6.21. For the equivalent strain distribution, it can be seen that the maximum value of the equivalent strain is mainly concentrated in three areas; the area on the rake face and flank face adjacent to the cutting edge for the finishing tooth, the flank face of the roughing tooth and the bottom area of the first gullet. However, the maximum strain distribution area for the finishing tooth is much larger than that of the roughing tooth. The displacements of the elements are represent by the arrangement of the arrows. The large displacement is in the area adjacent to the cutting edges on both roughing and finishing teeth.

Figure 6.22 shows the equivalent thermal stress distribution at the cutting temperature of 750 °C. The highest equivalent thermal stresses are concentrated on both roughing tooth and the finishing tooth. However, the finishing tooth is suffers the much higher thermal stress than the roughing tooth.

6.4.10 Assessment of strength characteristics of the model

An extensive stress data file is created for each model solution that documents the behaviour at each node within each element of the mesh. Consequently for a structure that contains many elements, the stress data file is huge and the interpretation time consuming. The magnitude of the problem is compounded when considering the number of model solutions required to predict a possible failure mode of a proposed saw segment.

For this reason, it is necessary to establish transverse rupture strength figures to simplify the assessment for the strength and weakness of the saw tooth.

6.4.10.1 Strategic stress

The strategic stress means the stress that dominates the wear behaviour of a cutting tool. Through the investigation in section 6.4.9, the equivalent stress, σ_{xx} stress, σ_{yy} stress and shear stress σ_{xy} belong to the strategic stress.

In order to develop the transverse rupture strength figure, the strategic stresses were selected from a region within the scope of a distance of 2.5 mm from the cutting edge on either rake face or flank face. This distance is larger than the chip/tool contact length (1 mm). Consequently the stress behaviour within the chip/tool contact area can be covered.

6.4.10.2 Transverse rupture strength figure

The stress behaviour on either rake or flank face for each load case applied to the model was already determined in the section 6.4.9. The approximate values of the stresses within a region of 2.5 mm from the cutting edge were measured by a ruler from the above figures directly. A comparison between these stress values and the transverse rupture strength of the constituent tooth material determined whether the stress levels had reached the onset of transverse rupture strength. Furthermore, the position in which the strategic stress values exceeded the transverse rupture strength on either rake or flank face was determined. Then, each type of stress value against the distance from the cutting edge on rake face or flank face of a tooth can be displayed graphically, as shown in the following figures 6.23 - 6.27.

Figure 6.23 shows the transverse rupture strength figure for the equivalent stress related to the cutting force and thrust force on the roughing tooth.

Figure 6.24 shows the transverse rupture strength figure for the σ_{xx} stress related to the cutting force and thrust force on the roughing tooth.

Figure 6.25 shows the transverse rupture strength figure for the σ_{yy} stress related to the cutting force and thrust force on the roughing tooth.

Figure 6.26 shows the transverse rupture strength figure for the shear stress σ_{xy} related to the cutting force and thrust force on the roughing tooth.

Superimposition of the above transverse rupture strength figures for the strategic stresses on rake face of the roughing tooth of the model enables the yielding characteristics of the tooth form to be determined in relation to the applied cutting and thrust forces over a full range of loading conditions, as shown in Figure 6.27.

6.4.10.3 Discussion

Using the method demonstrated in section 6.4.10.2. the transverse rupture figures for rake face and flank face of the roughing tooth or finishing tooth of the model can be established.

An example of carbide tipped circular saw type A1 segment in the case of cutting mild steel was used to demonstrate how the computer model can predict the failure modes through the establishment of transverse rupture strength figure.

Figure 6.27 shows the stress values against the distance from the cutting edge on the rake face of a roughing tooth related to the applied cutting and thrust force of 2000 N and 1541 N when cutting with type A1 segment. Stress σ_{xx}, stress σ_{yy}, shear stress σ_{xy} and equivalent stress

σ_{eq} were found to increase with distance from the cutting edge and reached its maximum at a distance of about 0.5 mm from the cutting edge. The region over which the equivalent stress was equalled to or larger than the transverse rupture strength (Transverse rupture strength: 1.85 KN/mm^2) of the element material was at the distances of 0.4 to 0.6 mm from the cutting edge.

By analysing the stress distributions and comparing the transverse rupture strength figure with the failure modes, it can be judged whether the model is consistent with the failure modes obtained during the imitation cutting tests. It can be seen that the maximum equivalent stresses on the rake face of the roughing tooth are distributed at the distance of 4 to 6 mm from the cutting edge (Figure 6.27) which is consistent with the crater wear which occurred during cutting mild steel, as shown in Figure 5.34.

Figure 6.28 shows combined mechanical and thermal stresses on the flank face of roughing tooth. The normal stress σ_{yy} and equivalent stress were a maximum at the cutting edge and decreased almost linearly to zero at the distance of 2.4 mm from cutting edge. Stress σ_{xx} was found to increase with distance from the cutting edge and reached its maximum at a distance of about 0.5 mm from the cutting edge.

Figure 6.29 shows the strategic stress values against the distance from the cutting edge on the rake face of the finishing tooth related to the applied cutting and thrust forces of 1800N and 500N for the case of cutting with type A1 segment. Stress σ_{xx}, shear stress σ_{xy} and equivalent stress σ_{eq} were found to increase with distance from the cutting edge and reached its maximum at a distance of about 0.5 mm from the cutting edge.

No region over which the equivalent stress was equalled to or larger than the transverse rupture strength (Transverse rupture strength: 1.85 KN/mm^2) of the element material was found at the rake face of the model.

The normal stress σ_{yy} was maximum at the cutting edge and decreased almost linearly to zero at the distance of 2.4 mm from cutting edge.

Figure 6.30 shows the stresses acting on the flank face of the finishing tooth against the distance from the cutting edge. Stress σ_{yy} and equivalent stress σ_{eq} were maximum values at the cutting edge. The region over which the equivalent stress was equalled to or larger than the transverse rupture strength (Transverse rupture strength: 1.85 KN/mm^2) of the element material was at the cutting edge. This is just consistent with the failure mode, edge chipping on the finishing tooth (Figure 5.33), in the case of cutting mild steel.

It was also found that the thermal stresses on both rake and flank faces of the model were much smaller than the other stresses and therefore has no dominant influence in the strength and weakness of the saw segment. In order to investigate the relationship among the loads, stress distributions and failure modes, the models with three different loading conditions (Table 6.3) and the same boundary conditions had been studied.

The difference among the models are shown in Figure 6.31. It can be seen that as the loads are increased, the area of the maximum stress distribution on the roughing tooth is enlarged and gradually extended towards the cutting edge, which is completely consistent with the crater wear which occurred during the cutting of mild steel, as shown in Figures 6.32(a), 6.32(b) and 6.32(c).

In general, a comparison between these values and the transverse rupture strength of the constituent tooth materials shows that transverse rupture strength has been exceeded on the rake face of the roughing tooth and flank face of the finishing tooth. This is completely consistent with the failure modes obtained during the cutting of mild steel (flank wear on finishing tooth and crater wear on roughing tooth).

The models with different rake angle and the same flank clearance at the same loading condition and boundary condition were also investigated. Figure 6.33 shows the testing results. It can be seen that as the rake angle is decreased, the values of maximum equivalent stresses on the rake face of the roughing tooth are reduced, but values of the stress σ_{yy} on the flank face of the roughing tooth are increased and the high equivalent stress distribution area is moved towards to the cutting edge. It means that the tendency for flank wear on the roughing tooth is increased and the tendency for crater wear is decreased. This phenomenon is completely consistent with the failure modes obtained when cutting mild steel with segment types A1and A2. As mentioned in chapter 5, the failure of the segment A1 with negative rake 18° on the roughing tooth was mainly attributed to the edge chipping on finishing tooth in spite of the crater wear on the roughing tooth. The failure for segment A2 with a rake angle of 0° was due to the edge chipping on both teeth in the case of cutting mild steel. However, the life for segment A1 is much higher than that of segment A2 when cutting mild steel. For this reason, it can be seen that the segment with negative rake gives much better performance than the segment with positive rake. However, if the rake angle is too large, the equivalent stress will be increased greatly which will cause carbide breakage.

CHAPTER SEVEN

CONCLUSION AND FURTHER WORK

There is no evidence that similar experiments on the application of coatings to the carbide tipped circular saw have been conducted. In this work a novel experimental approach was used, in which TiN and TiAlN coatings were successfully applied to the carbide tipped circular saw segments. A feature of this approach is that a lower coating temperature is used and yet still retains the good bonding strength between the substrate and the coating.

The parameters obtained in this investigation were used as a basis in the development of a Finite Element model. This model has been used to predict the failure mode with respect to temperature and stress.

7.1 Conclusion

(1) The main failure modes of the carbide tipped circular saws have been identified (Chapter 2). These failure modes have been used in the assessment of the saw segment performance and provided the necessary information for the application of coatings.

The investigation has indicated that the edge chipping, crater wear and flank wear are main failure modes when cutting the proposed workpiece materials. For this reason, TiN and TiAlN coatings were applied to the segments to arrest or reduce the above failure modes. These types of coatings possess a high resistance to the kinds of failures described in chapter 2 &Chapter 4.

(2) The characteristics of the proposed carbide substrate tool materials have been investigated. The tests dealt with were red hardness (hot hardness), composition analysis, grain size, cobalt content and porosity

level of the proposed carbide grades. From the investigation, the carbide grades S4 and MK20 possessed the best combination of characteristics and were chosen as the substrate materials for the saw segments. Among them, the carbide grade S4 has the highest red hardness and the grade MK20 has the finest grain size (Chapter 3).

(3) A method of assessing the performance and life of the proposed carbide saw segments was established. Cutting tests using a specially designed test rig were carried out and the performance and life of the cutting tools were quantified and a picture library of the failure modes was established (Chapter 4).

(4) Limited experimental work as part of the programme has shown that, when cutting mild steel at the optimum cutting conditions, the A1 and B1 segments with negative rake angle cut more efficiently than the A2 and B2 segments with positive rake angle. Comparing with the performance of the B1segments, the A1 segments had a better performance than the B1 segments, which was attributed to the properties of the tool materials. The carbide grade S4 used for A1 segments possesses a higher red hardness than the carbide grade MK20 used for B1, B2 segments (Chapter 3 & 4).

(5) When cutting 302S25 stainless steel with the uncoated segments, the segments with positive rake angle performed much better than those with negative rake angle. For example the B2 and A2 segments gave a better performance than A1 and B1 (Chapter 4). Concerning the performances of the different tool materials, the B2 segments made with the carbide grade MK20 cut more efficiently than the other carbide tipped saw segments. This is due to the carbide grade MK20 having the finer grain size among the proposed carbides (Chapter 3 & 4).

(6) A new experimental method for the application of coating techniques to the segments has been developed. Both TiN and TiAlN coatings have been successfully applied to the carbide tipped circular saw segments.

In this work a novel experimental approach is used to apply coatings to the carbide tipped circular saw. A feature of this approach is that a lower coating temperature is used. However, good bonding strength between the substrate and the coating is still remained (Chapter 5).

(7) The coating characteristics were investigated experimentally. These characteristics include grain structure, micro hardness, and bonding strength of coatings. The experimental work has shown that the TiAlN coating has finer grain size and better bonding strength than the TiN coating (Chapter 5).

(8) The cutting test results have shown that both TiAlN and TiN coatings have enhanced the performance and tool life when cutting the proposed workpiece materials.

The results have identified TiAlN to be a better coating than TiN coating when cutting stainless steel and mild steel. For example, TiAlN coated A1 segments cut more efficiently than TiN coated A1 segments. When cutting stainless steel, TiAlN coated B2 segments cut more efficiently than TiN coated B2 segments (Chapter 5).

(9) The experimental work has shown that, when cutting mild steel and stainless steel, the cutting forces and thrust forces for coated segments are much smaller than those of uncoated segments. Also the results shows that the forces produced with the TiAlN coated segments are lower than those of the TiN coated segments (Chapter 5).

(10) Experimental work has shown that, when cutting the nimonic alloy, the performances of both TiAlN and TiN coated segments were not much

better than the uncoated segments. This is due to the high strength and low thermal conductivity of the workpiece material (nimonic alloy) and the present carbide tool materials could not meet the requirement for cutting such workpiece material (Chapter 5).

(11) A two dimensional thermal and mechanical problem has been studied using an elastic finite element analysis.

The example of carbide tipped circular saw type A1 segment when cutting mild steel was used to demonstrate how the computer model can predict the failure modes through the establishment of a transverse rupture strength figure (Chapter 6).

(12) By analysing the stress distributions and comparing the transverse rupture strength figure with the failure modes for the case of cutting mild steel, it can be seen that the maximum equivalent stresses on the rake face of the roughing tooth are distributed at a distance of 0.5 mm from the cutting edge which is consistent with the crater wear that occurred on the roughing tooth of the A1 segments when cutting mild steel (Chapter 4 & 6).

(13) The model shows the maximum σ_{yy} stress and equivalent stress on the flank face of the finishing tooth are at the flank face adjacent to the cutting edge, which is consistent with the failure mode of edge chipping on the finishing tooth when cutting mild steel (Chapter 4 & 6).

(14) It was also found that the thermal stresses on both rake and flank faces of the model were less than $200MN/m^2$ and had no dominant influence on the strength of the saw segment (Chapter 6).

(15) Models with three different loading conditions have been studied. The models have shown that when the loads are increased, the area of the maximum equivalent stress distribution on the roughing tooth is enlarged

and gradually extended towards the cutting edge, which is completely consistent with the development of the crater wear that occurred on the roughing tooth when cutting mild steel (Chapter 6).

(16) Models with different rake angle and the same flank clearance at the same loading condition and boundary condition were also investigated. The model shows that as the rake angle decreased, the values of maximum equivalent stresses on the rake face of the roughing tooth are reduced, but values of the stress σ_{yy} on the flank face of the roughing tooth are increased and the high equivalent stress distribution area is moved towards to the cutting edge. It means that the tendency for flank wear on the roughing tooth is increased and the tendency for crater wear is decreased. This phenomenon is completely consistent with the failure modes obtained when cutting mild steel with the A1 and A2 segments. As mentioned in chapter 5, the failure for the A1 segment with negative rake 18° on the roughing tooth was mainly attributed to the edge chipping on finishing tooth in spite of the crater wear on the roughing tooth. The failure for the A2 segment with rake angle 0° was due to the edge chipping on roughing tooth when cutting mild steel.

7.2 Suggestions for further work

(1) Limitations of the present work

The work presented in the present thesis has a number of limitations which could be rectified by some further work. Firstly the load distribution on the rake face has been assumed to be homogeneous, in reality this is not exactly true and an improvement in the model could be made by making a suitable allowance for the load variation on the rake face. Secondly the assumption made of plane stress could be further investigated by incorporating into the model a stress value in the Z direction to

examine whether the effect on the stresses predicted is significant. This could lead to a change of assumption to plane stress for the model.

(2) Carbide tipped circular saw segments

The performance of the segments with the other types of tooth/gullet geometry should be investigated on the single tooth test rig. The data collected could be used to determine the optimum tooth/gullet geometry. The scale of these investigations would be immense, but the information could be useful for optimisation of carbide tipped circular saw tooth and gullet in a commercial production.

(3) Tool materials

Investigation has shown using the proposed tool materials that, when cutting the very difficult-to-cut materials such as nimonic alloys and other heat-resisting alloys, the performances of the proposed tools were not good enough. For this reason, the new tool materials such as super-fine carbides with high strength, high red hardness and good thermal conductivity should be used as tool materials when cutting these materials.

(4) Multi-layer coatings

Multi-layer coatings should be applied to the carbide tipped circular saw segments to enhance the wear resistance. Multi-layer coated segment could cut more efficiently than a single layer coated segment when cutting the difficult-to-cut materials.

REFERENCE

1 Charles H. Priefer, "Circular Sawing", Merryweather Machinery Co, Chapter6, P36-45, 1973.

2 Charles H. Prifer, "Circular Sawing", Kling Bros, Engineering Works, 1976.

3 K Henning And H Maier, "“Circular Sawing With Carbide- Tipped Sawblades - A Way Of Production With Technical And Economical Advantages”", Industrial & Production Engineering, 12 (1988) 2.

4 S R Bradbury, M.P. Keenan And M. Sarwar, "The Development Of A Simulation Technique To Evaluate The Performance And Life Of High-speed Steel Circular Saw Blades" Sheffield Hallam University, 1993.

5 Trent, E M. “Wear Of Metal Cutting Tools”, Treaties On Material Science And Technology, Vol. 1.3 “wear”, D Scott Ed: Academic Press, London, 1979, 443-489.

6 H Chandrasekaran "On the Nature of Micro-Chipping of HSS Saw teeth During Power Hack Sawing", Annals of the CIRP Vol. 33/1/1984.

7 H Chandrasekaran, "Tooth Chipping During Power Hack Sawing and The Role of Saw Material Characteristics

8 J Pekienik "An investigation of Cutoff Bar and Pipes by Horizontal Band Sawing", TFR University of Rijeka/Yugoslavia, Annals of the CIRP Vol. 31/1/1982, P53-58.

9 Kenneth J. Brookes A, “World Directory And Handbook Of Hardmetals”, Second Edition, An Engineer’s Digest Publication.

10 M. Sarwar, D. Gillibrand and S.R. Bradbury, “Forces, surface finish and friction characteristics in surface engineered single- and multiple-point cutting edges” Surface and Coating Technology, 49 (1991) 443-450

11 H. Takeyama, "Surface Integrity Of Cemented Carbide Tool And Its Brittle Fracture", Annual Of The Cirp Vol.31/1/1982.

12 M R James, "Coated Cemented Carbide Cutting Tools", The Metallurgist and Material Technologist, 9, 1977, P483-486.

13 A Matthews, "Surface Engineering In Cutting Technology", J. Vac. Sci. Technol.,A6, 2754,1989.

14 S R Bradbury and M Sarwar, "A Graphical Approach To Computer-aided Stress Analysis In The Design Of Bandsaw Teeth", Proceedings of the Fourth International Conference on Production Research, Sheffield, 9, 1988.

15 P D Muraka Et Al,"Influence Of The Process Variable On The Temperature Distribution In Orthogonal Machining Using The Finite Element Method", Int. J. Mach. Sci. Vol. 21, 1979, P445-456.

16 Katsuhiro Maekawa Et Al,"Finite Element Analysis Of Temperature And Stresses Within An Internally Cooled Cutting Tool", Bull. Japan Soc. Of Prec. Eng. Vol. 23, No. 3, 1989, P243-246.

17 D A Stephenson,"Tool Temperatures In Interrupted Metal Cutting", Journal Of Engineering For Industry, May 1992, Vol. 114/127.

18 E M Trent, "Metal Cutting", ISBN 0 408 10603 4.

19 D S Dugdals (1977), "Fracture Of Cemented Carbide Tools In Face Milling", Proc. 18th Int. Mtdr Conf., P.523.

20 G S Andreev (1974), "Thermal State Of Tool Cutting Edge In Intermittent Cutting", Russian Eng. J. , 54, P56.

21 Okishima, K. And T. Hoshi, "Thermal Crack In Carbide Face Milling Cutter-i", Bulletin Of Jsme, Vol. 5, 1962, P151- 160.

22 Xi-yang Zhang, M Sarwar "The Influence Of Hot Hardness On Life Of Carbide Tipped Circular Saws When Sawing Ms And Stainless Steel", Proceedings of the AMPT'93, Vol. 3, P1945, Aug.,1993.

23 N.N Zorev (1963), "Machining Steel With A Carbide Tipped Tool In Interrupted Cut With Continuous Cycles", Annals of CIRP, 18, p.555.

24 Okishima, K. and T. Hoshi, "Thermal Crack In Carbide Face Milling Cutter-i", Bulletin of JSME, Vol. 5, 1962, pp. 151-160.

25 Yong RongFu, "Fundamental of Mechanical Cutting", ISBN 7-111-00366-7/TG.114, Mechanical Engineering Publisher, in China.

26 BS 4490:1989, Section 4.14 "Metallographic Determination Of Porosity And Uncombined Carbon"

27 BS 4490:1989, Section 4.13 "Metallographic Determination Of Microstructure"

28 P M Archer, M. Sarwar "Evaluation Of Performance And Wear Characteristics Of Bandsaw Blades", Proceedings of the fifth national conference on production research, September, 1989.

29 BS 5623:1979, "Tool-life Testing With Single-point Tools"

30 M R James, "Coated Cemented Carbide Cutting Tools", Page 483-486, The Metallurgist And Materials Technology.

31 D. P Upton, "The Performance Of New PVD Coating On Cutting Tools", Department Of Mechanical & Production Engineering, Aston University.

32 O. Knotek, T. Leyendecker, "Industrial Deposition Of Binary, Ternary, And Quaternary Nitrides Of Titanium, Zirconium, And Aluminium" J. Vac. Sci. Technol. A 5(4), July/aug 1987

33 E. Posti,"Coating Thickness Effects On The Life Of Titanium Nitride PVD Coated Tools", Materials & Manufacturing Processes, 4(2), 239-252 (1989).

34 T S Sudarshan, "Surface modification technologies- An engineer's guide", ISBN 0-8247.8009-4

35 S J Bull "Failure Modes In Scratch Adhesion Testing", Surface And Coating Technology, 50 (1991) 25-32.

36 P R Chalker, "A Review Of The Methods For The Evaluation Of Coating-substrate Adhesion", Material Science And Engineering, A140 (1991) 583-592.

37 S. J. Bull "New Developments In The Modelling Of The Hardness And Scratch Adhesion Of Thin Film", AEA Industrial Technology, Harwell Laboratory, Didcot, Oxfordshire.

38 D S Stone, "Hardness And Elastic Modulus Of Tin Based On Continuous Indentation Technique And New Correlation", J. Vac. Sci. Technol. A9 (4), Jul./aug 1991.

39 G M Hu, "Finite Element Analysis Method", Si Dai Publication, China, Jan., 1977.

40 Hong Shen "Mechanical Engineering Manual", Vol. 8, Machinery industrial publisher in China in 1982.

41 M Sarwar, "The effect of tooth geometry on blade performance in power hacksawing", Proceedings of first conference Irish Manufacturing Committee, 1984.

42 K J Trigger, American Machinist, Vol.110, No.15 (1961), p.101.

43 E Usui, Wear, Vol.100 (1984), pp 129-151.

44 F Dearnly, Trans. J.I.M. Vol.18, (1983), pp 222-243.

45 "Introduction to PATRAN 3-Exercise Workbook", Release 1.1B, P/N 903015, 1993.

Bibliography:

(1) Xi-yang Zhang, M Sarwar "Characteristics of carbide circular saws", Proceedings of the AMPT'93, Vol. 3, P1915, Aug.,1993.

(2) Xi-yang Zhang, D Gillibrand, M Sarwar, "Performance of titanium nitride coated carbide tipped circular saws when cutting stainless steel and mild steel", School of Engineering, Sheffield Hallam University, Feb., 1995.

(3) Xi-yang Zhang, D Gillibrand, M Sarwar, "Performance of titanium aluminium nitride coated carbide tipped circular saws", School of Engineering, Sheffield Hallam University, Feb., 1995.

(4) Xi-yang Zhang, T Campbell, G Cockham, M Sarwar, " Prediction of failure of carbide tiped circular saws by FE modell", School of Engineering, Sheffield Hallam University, Feb., 1995.

(5) Trent, E M. "Wear of metal cutting tools", Treaties on Material Science and Technology, Vol. 1.3 "Wear", D Scott Ed: Academic Press, London, 1979, 443-489.

(6) W.F. Hastings & P.L.B. Oxley , The University of New South Wales,Australia "Predicting Tool Life from Fundamental Work Material Properties and Cutting Conditions", Annals of the CIRP Vol.25/1/1976.

(7) N. Alberti, S. Noto La Diega, "The Effects of the Fracture, Chipping and Wear of Cemented carbide tools on the Determination of the optimum Metal- Cutting Conditions" Annals of the CIRP Vol. 30/1/1981.

(8) O. Knotek, T. Leyendecker, "Industrial deposition of binary, ternary, and quaternary nitrides of titanium, zirconium, and aluminium" J. Vac. Sci. Technol. A 5(4), July/Aug 1987

(9) W F Hastings & P.l.b. Oxley , The University Of New South Wales, Australia "Predicting Tool Life From Fundamental Work Material Properties And Cutting Conditions", Annals Of The Cirp Vol.25/1/1976.

(10) Geoffrey Boothroyd, " Fundamentals of Metal Machining and Machine Tools", ISBN 0-07-085057-7.

(11) P.E. Liu, "Discussion about the force and power parameters of hot saw", J. of heavy machinery in China, 1987.

(12) P.E. Liu, "Calculation and analysis of tooth profile of hot sawblade", J. of heavy machinery in China, 1985.

(13) P.E. Liu, "Test report of tooth profile of hot saw (1)", J. of heavy machinery in China, 1985.

(14) P.E. Liu, "Test report of tooth profile of hot saw (2)", J. of heavy machinery in China, 1985.

(15) Shaw, M.C. "The Assessment of Machinability", Machinability, Prof Conf. on Machinability, Iron and Steel Inst., London, 1967, 1-9

(16) Mills and Redford, AH. "Machinability of Engineering Materials", Applied Science Publishers, London, 1983

(17) B M Kramer and P K Judd, J. Vac. Sci. Technol. A3, 2439, 1985.

(18) B M Kramer, J. Vac> Sci. Technol., A4, 2870, 1986.

(19) N. Alberti, S. Noto La Diega, "The Effects Of The Fracture, Chipping And Wear Of Cemented Carbide Tools On The Determinations Of The Optimum Metal- Cutting Conditions" Annals Of The Cirp Vol. 30/1/1981.

(20) Pekelharling, "Predicting Tool Life From Fundamental Work Material Properties And Cutting Conditions", Annals Of The Cirp Vol. 25/1/1976.

(21) L.P Ward, "Observations on the structure, hardness and adhesion properties of a selection of multi-component refractory element nitride coatings"

(22) D. Klaphaak, "TiN coatings can extend your tool life", Machine & Tool Blue Book, Aug 1989, Vol.84 pp46-49.

(23) N A Kudrya,"Current Development Trends Of Cemented Carbides For Cutting Tools", Stankii Instrument, Vol. 57, Issued 6, 1986, P22-23.

(24) Metals Handbook 8th Edition, Vol.3 Machining, American Society For Metals.

(25) A E Focke, "Deformation Of Tungsten Carbide Tools When Cutting Inconel 718", Annals Of The Cirp Vol. 32/1/1989.

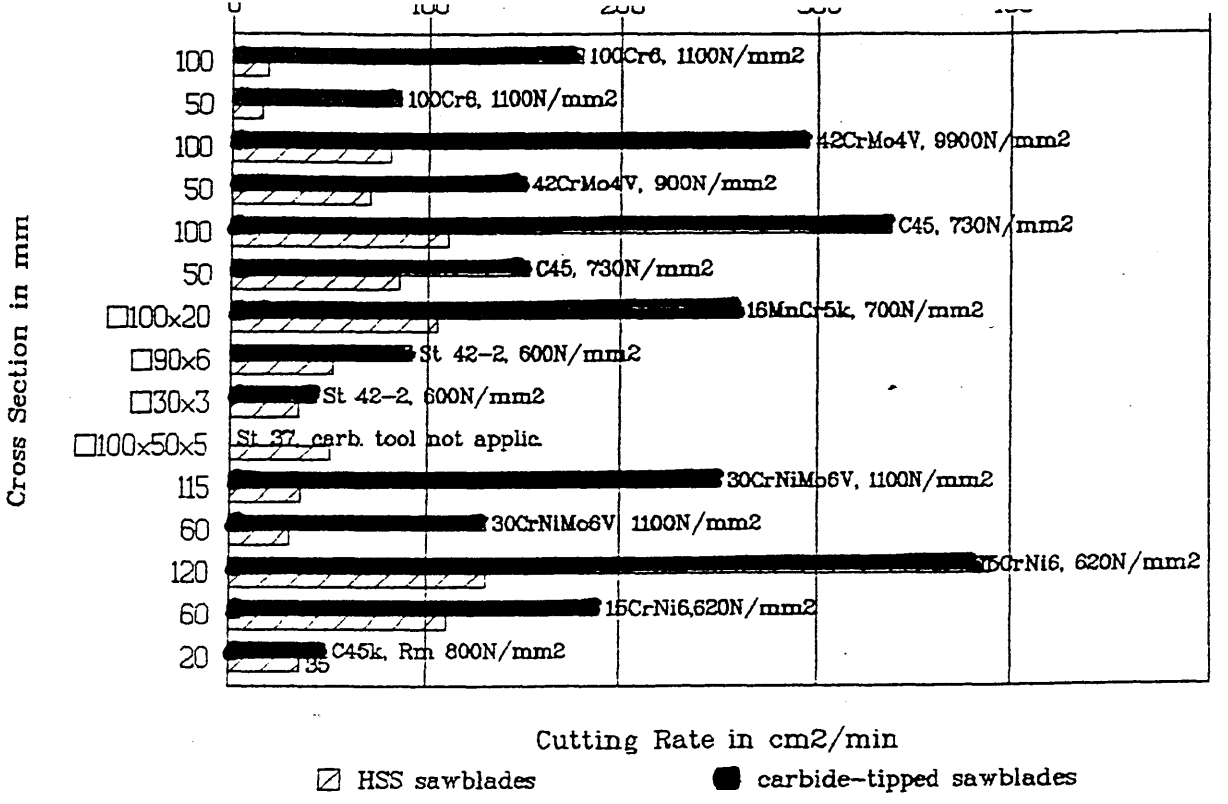

Figure 1.1 Cutting rate with HSS-sawblades and carbide-tipped sawblades

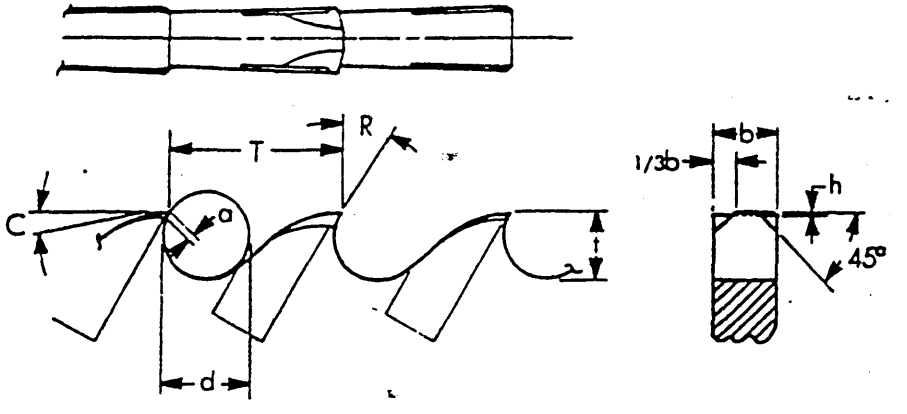

C= Clearance angle 8°
R= Rake angle 18°
T= Pitch
a= .0.05 × T
d= 0.5 × T
t = 0.4 × T
h= 0.02 × T
b = Width of blade
1/3b= Chamfer of tooth

Figure 1.2 Geometry of a circular saw segment

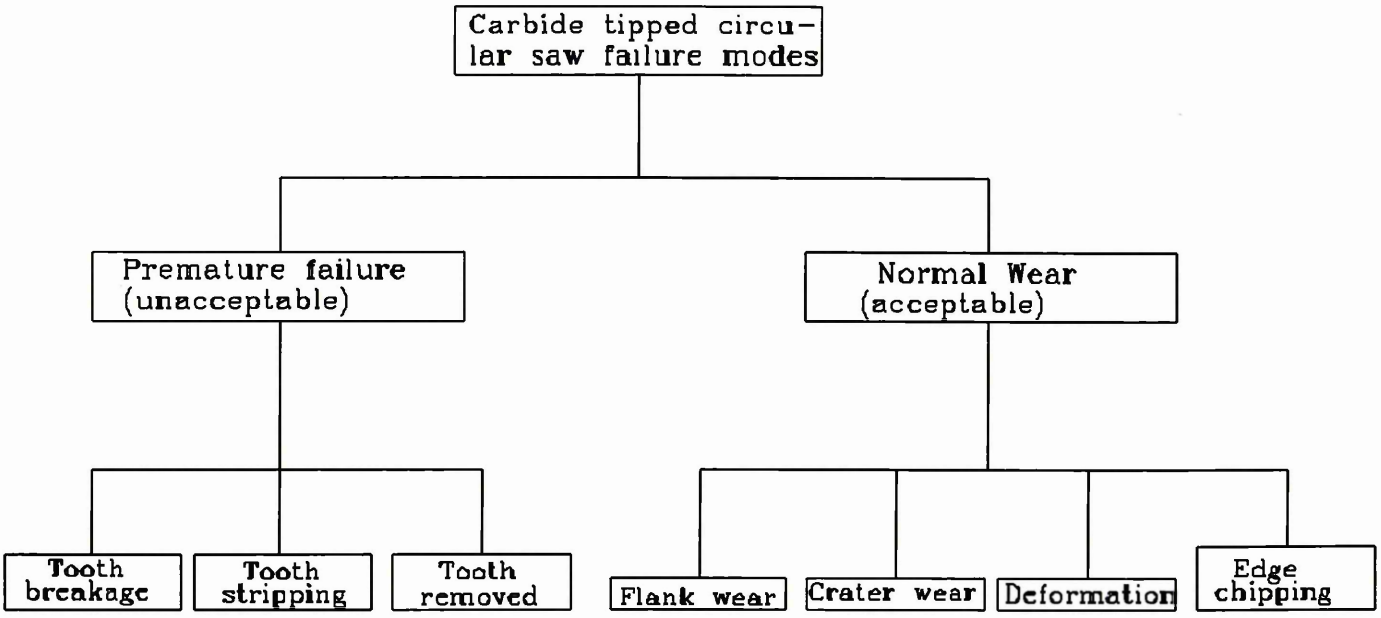

Figure 2.1 Premature failure and acceptable failure modes

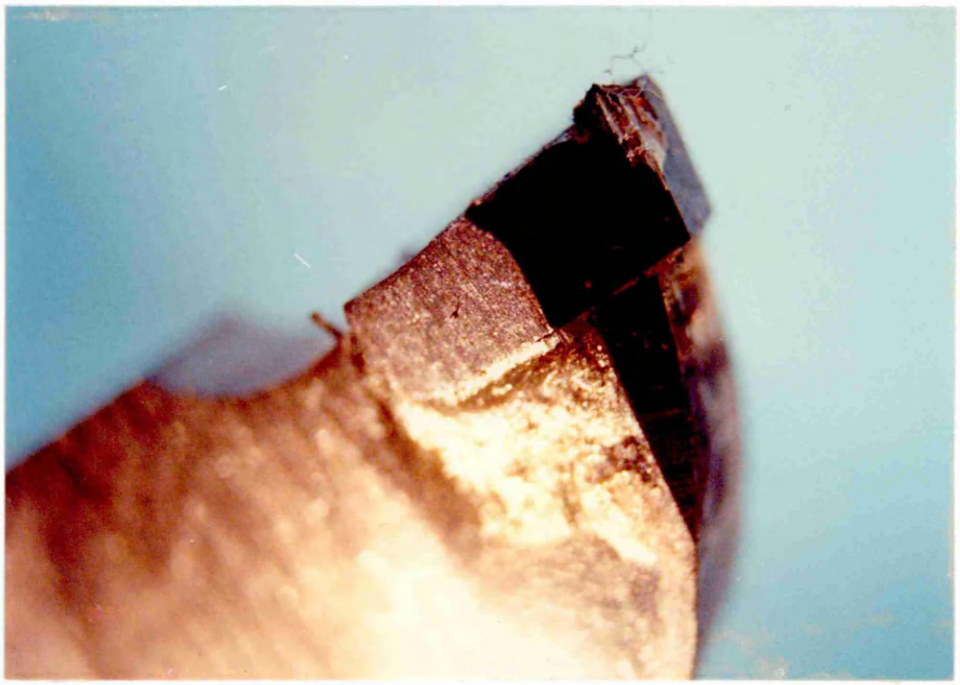

Figure 2.2 The bevel chipping on the tooth corner

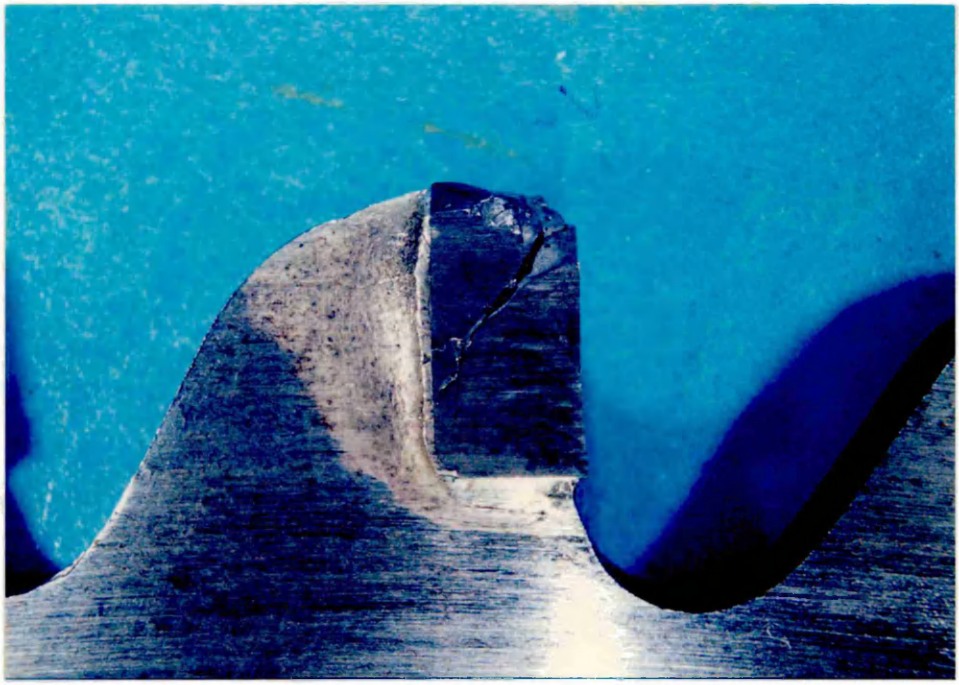

Figure 2.3 shows breakage and stripping occurred on the tooth tip

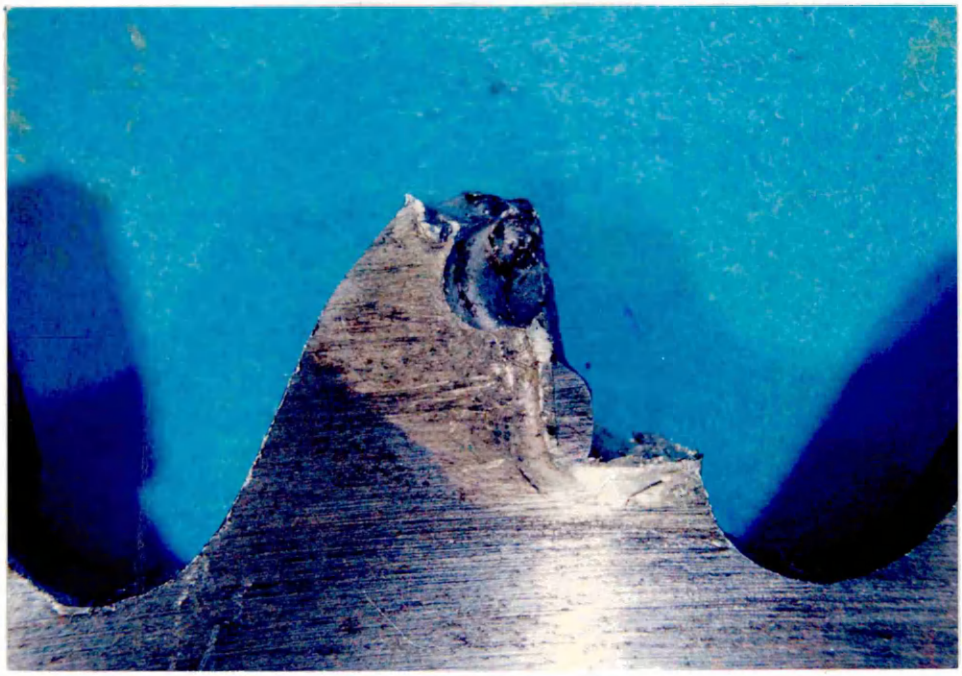

Figure 2.4 The tooth is removed caused by destroying the brazed joint between carbide tip and shank of the blade.

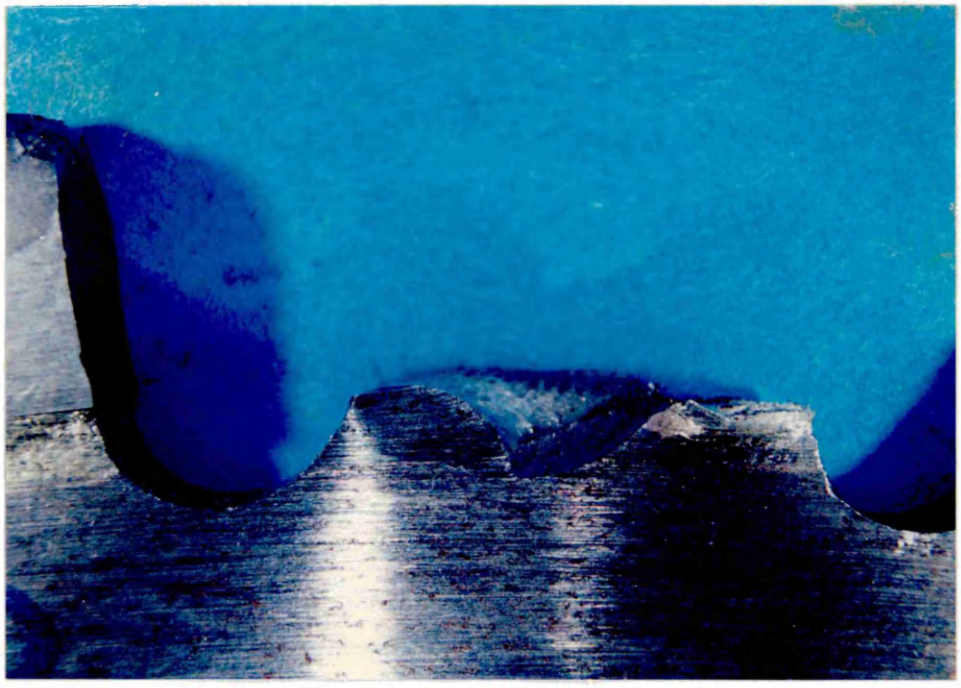

Figure 2.5 The large chipping and breakage of the tooth

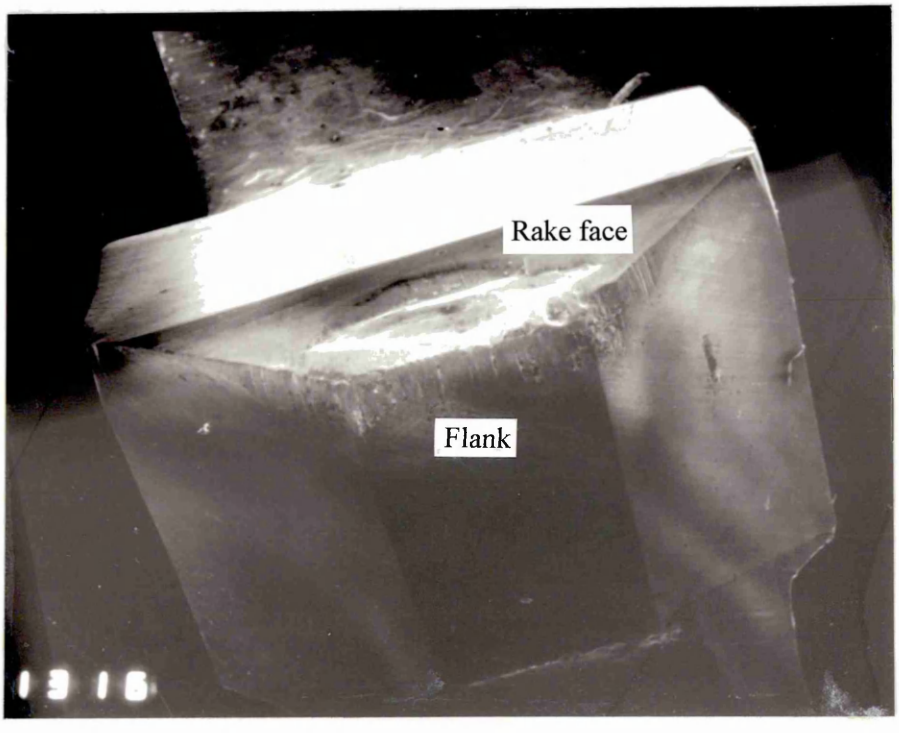

Figure 2.6 The flank wear of the tooth when sawing stainless steel

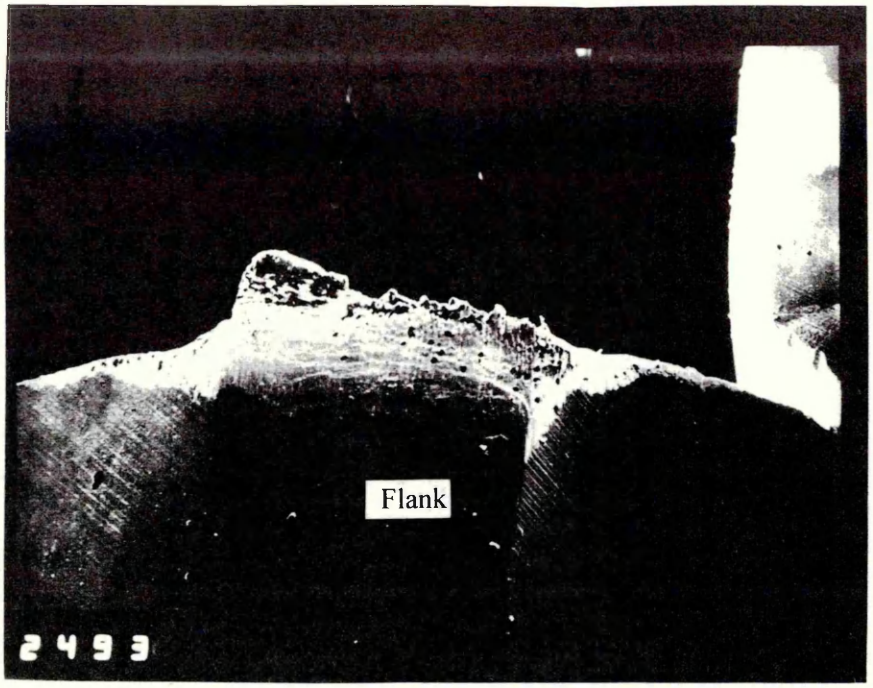

Figure 2.7 Built-up edge occurred When sawing nimonic alloy

Figure 2.8 The crater wear produced When cutting mild steel at high speed and feed rate

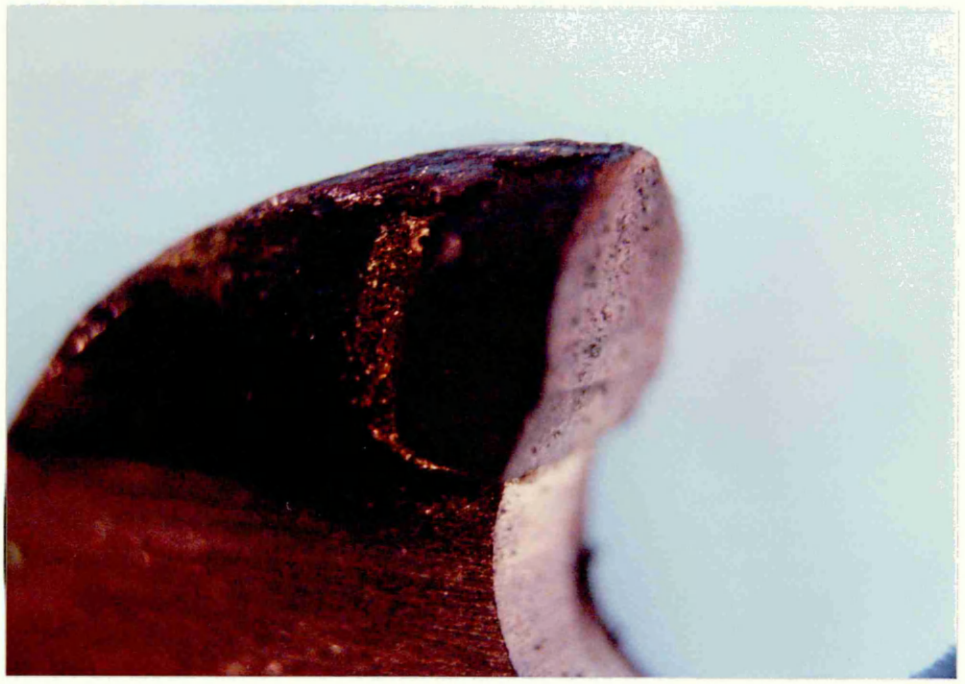

Figure 2.9 Large chipping occurred on the cutting edge

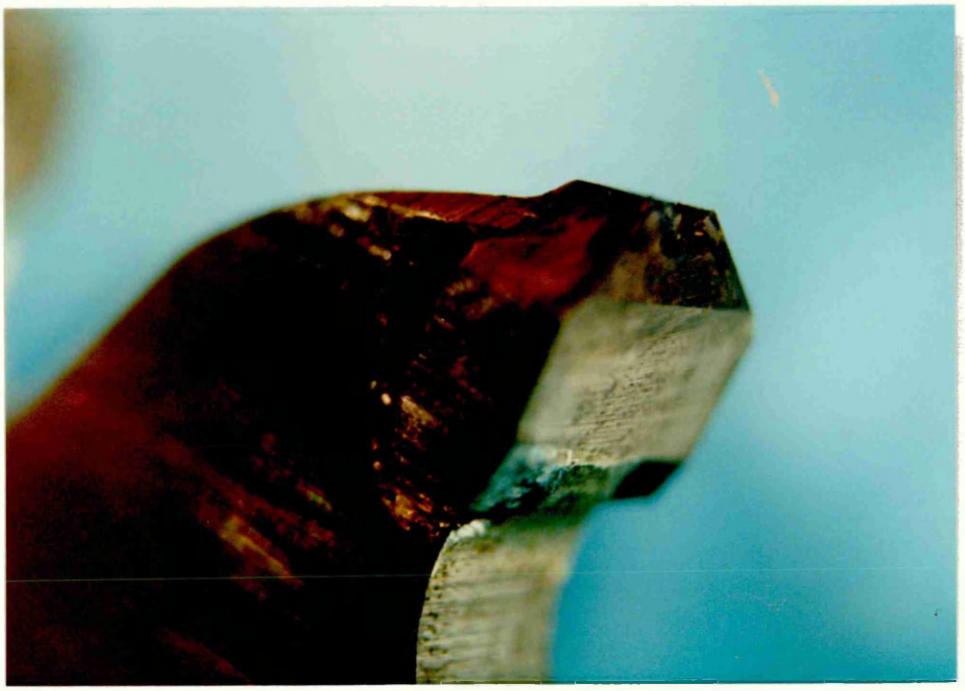

Figure 2.10 The cracks generated on the rake face, spread across the cutting edge

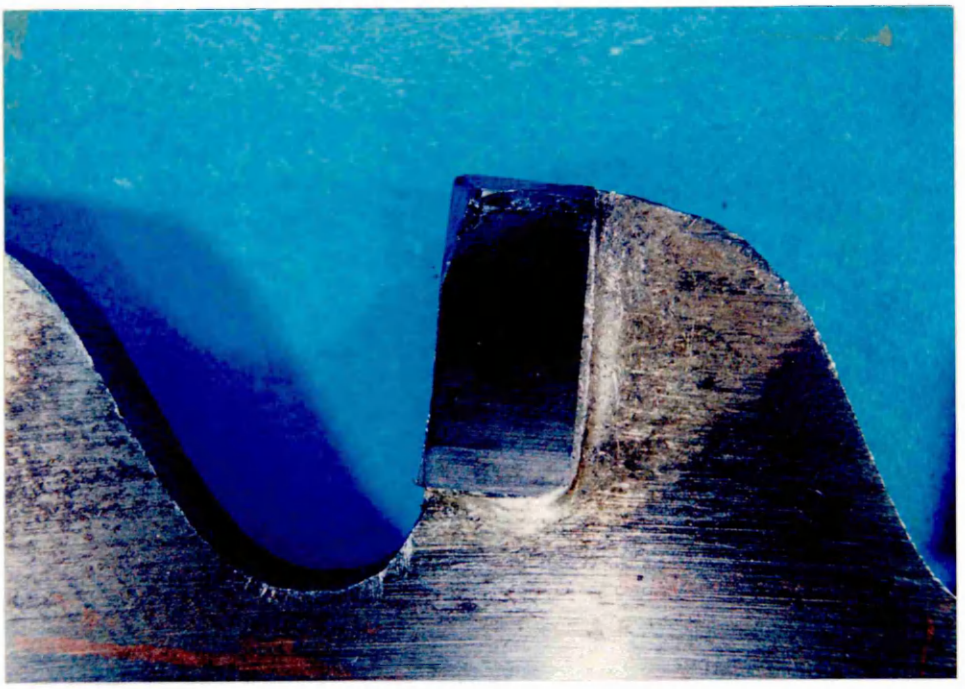

Figure 2.11 The deformation of the cutting edge, particularly on the tool corner caused by high temperatures and stresses

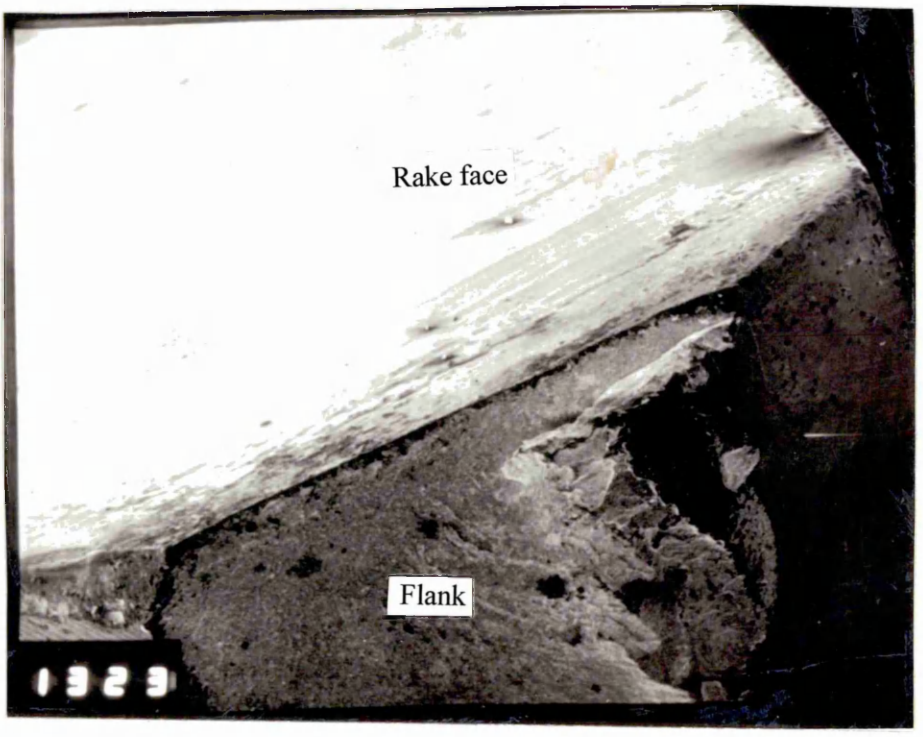

Figure 2.12 The fracture suddenly produced at high compressive stress leading to the edge depressed

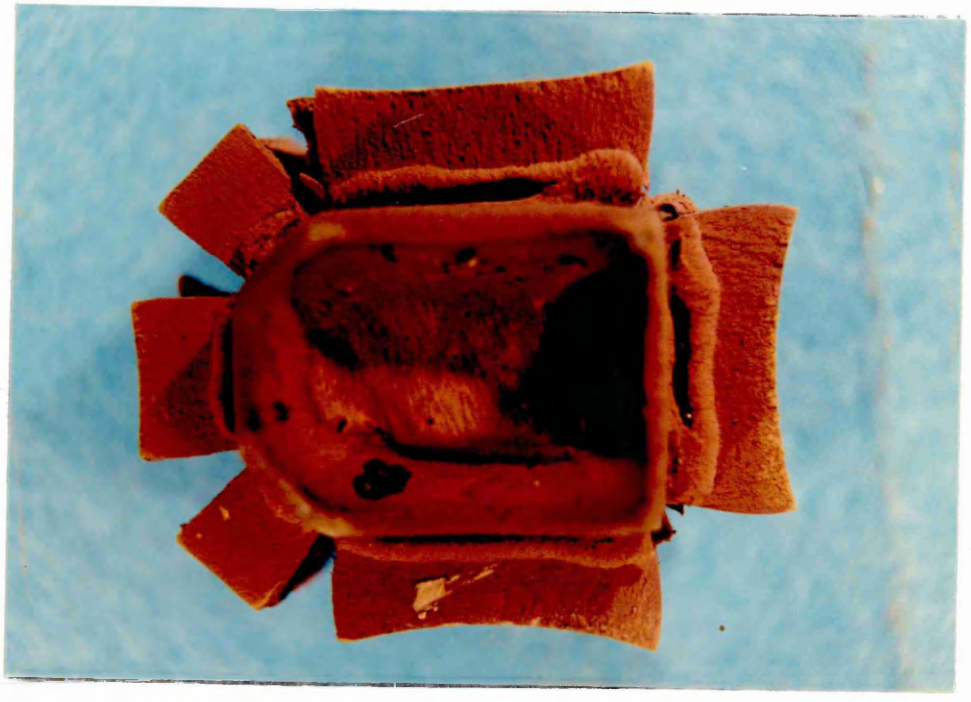

Figure 3.1 The carbide tip oxidised at 400 degree C

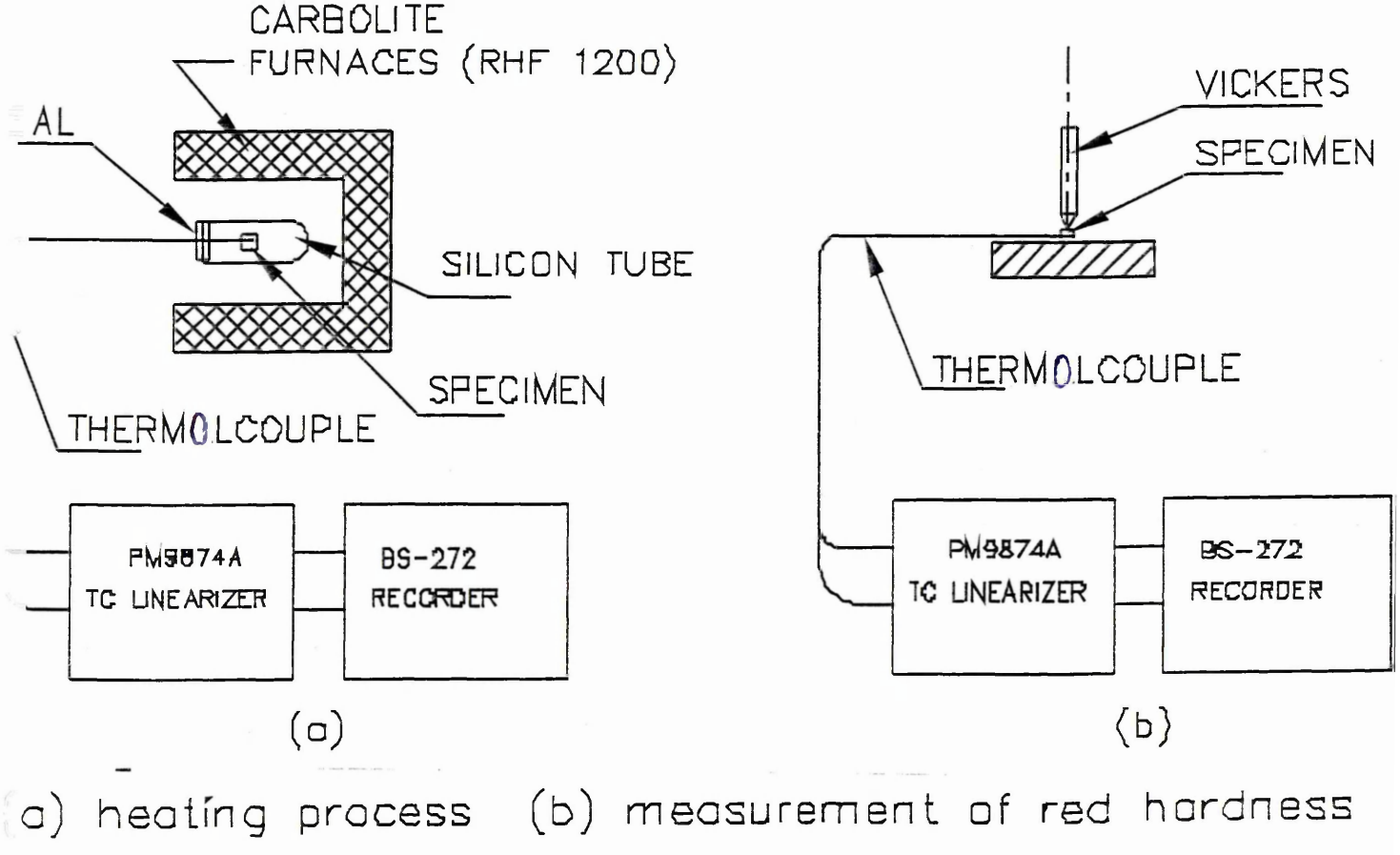

a) heating process (b) measurement of red hardness

Figure 3.2 Flowchart of red hardness test process

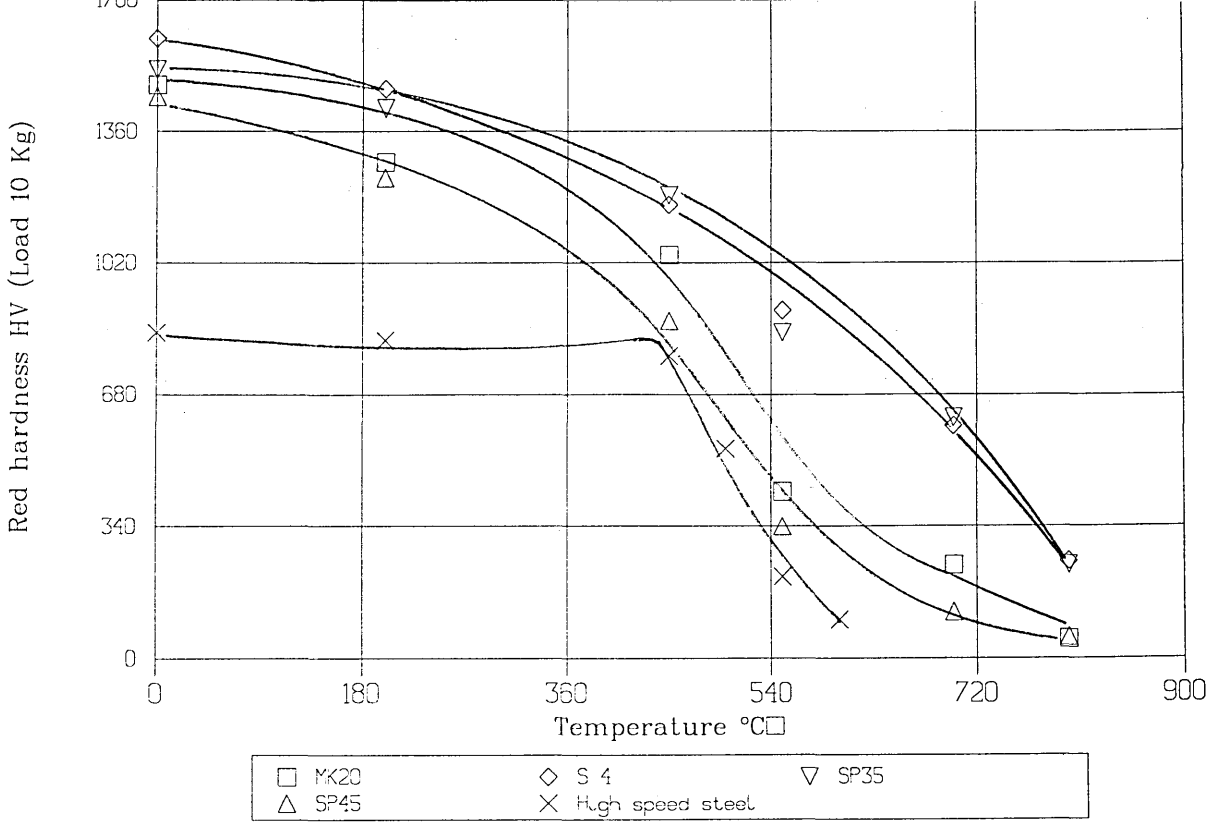

Figure 3.3 Comparison of the red hardness of different carbide grades

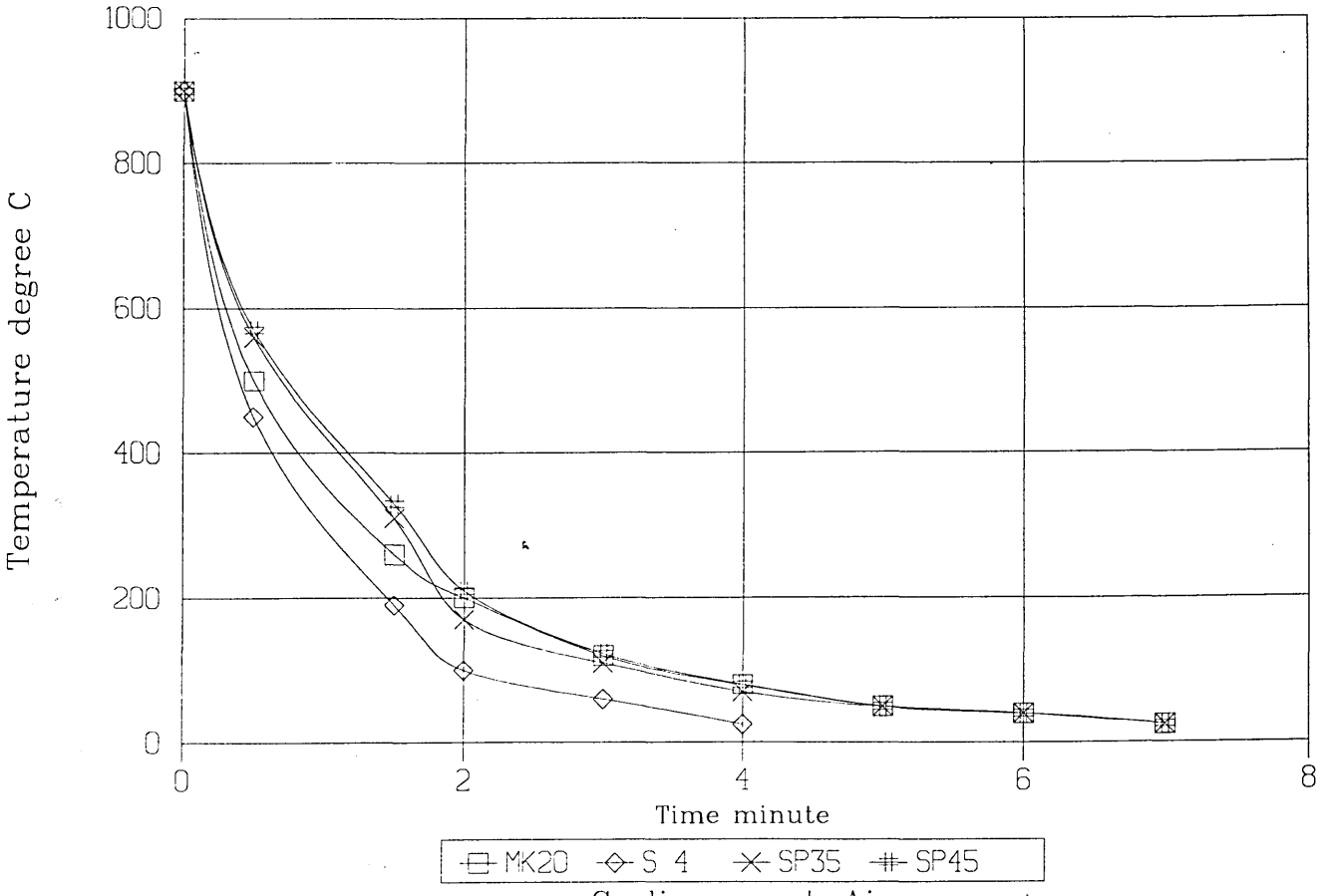

Cooling agent: Air

Figure 3.4 Cooling curve of the carbides

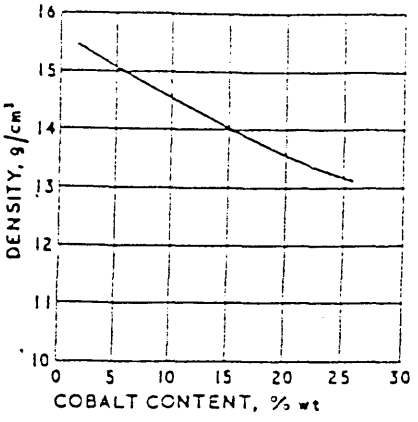

Figure (1) (left) Density of typical WC/Co grades; variation with cobalt content.

Figure (2) (right) Density of WC/TiC/Co and WC/TiC/Ta(Nb)C/Co grades; variation with TiC content (calculated figures, assuming zero porosity). Practical values are typically 0.1 to 0.2 g/cm³ lower.

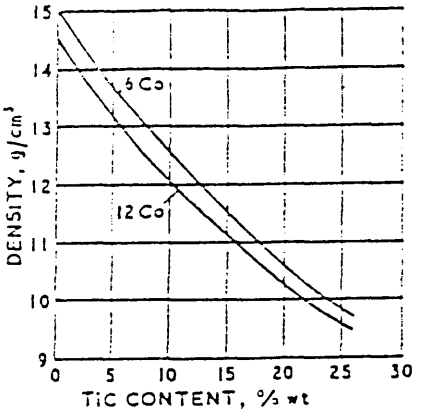

Figure 3.5 Density of the carbide grades; Variation with cobalt content, from World Directory and Handbook of Hardmetals, p35.

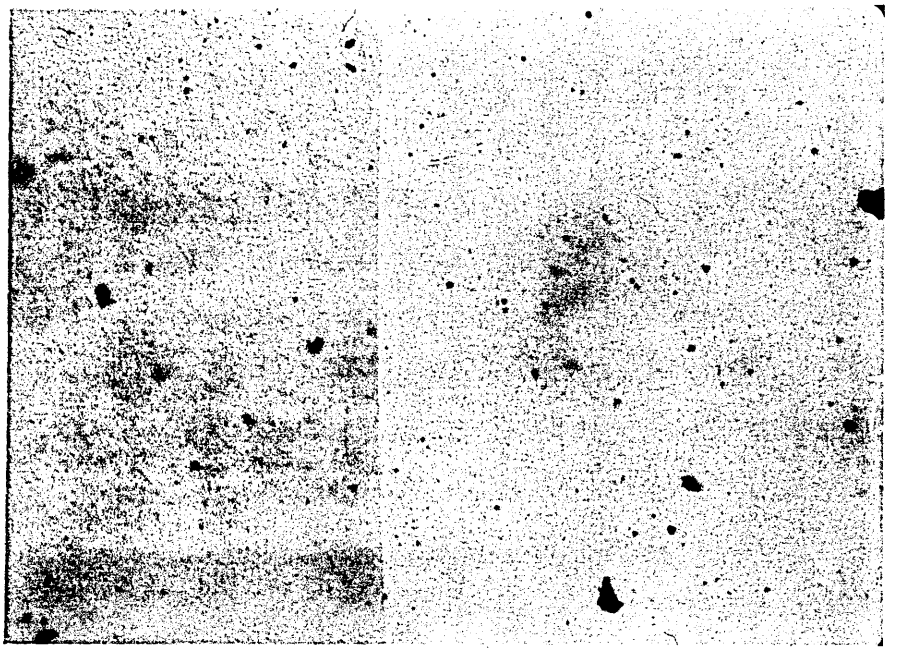

Figure 3.6 Porosity and pores of S4 carbide X200

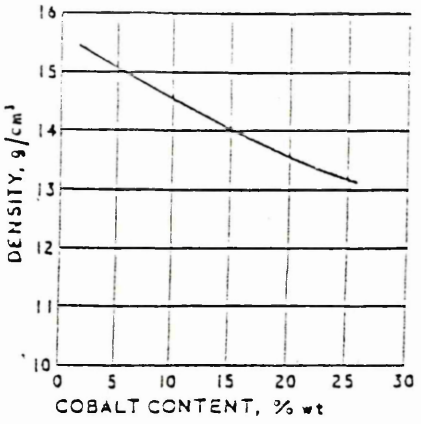

Figure (1) (left) Density of typical WC/Co grades; variation with cobalt content.

Figure (2) (right) Density of WC/TiC/Co and WC/TiC/Ta(Nb)C/Co grades; variation with TiC content (calculated figures, assuming zero porosity). Practical values are typically 0.1 to 0.2 g/cm³ lower.

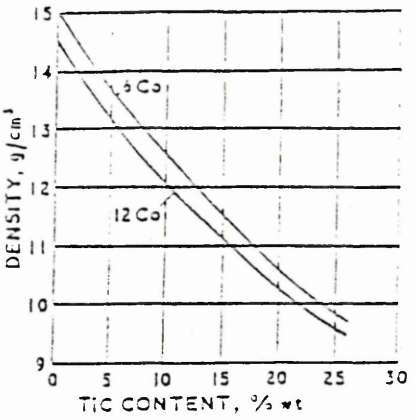

Figure 3.5 Density of the carbide grades; Variation with cobalt content, from World Directory and Handbook of Hardmetals, p35.

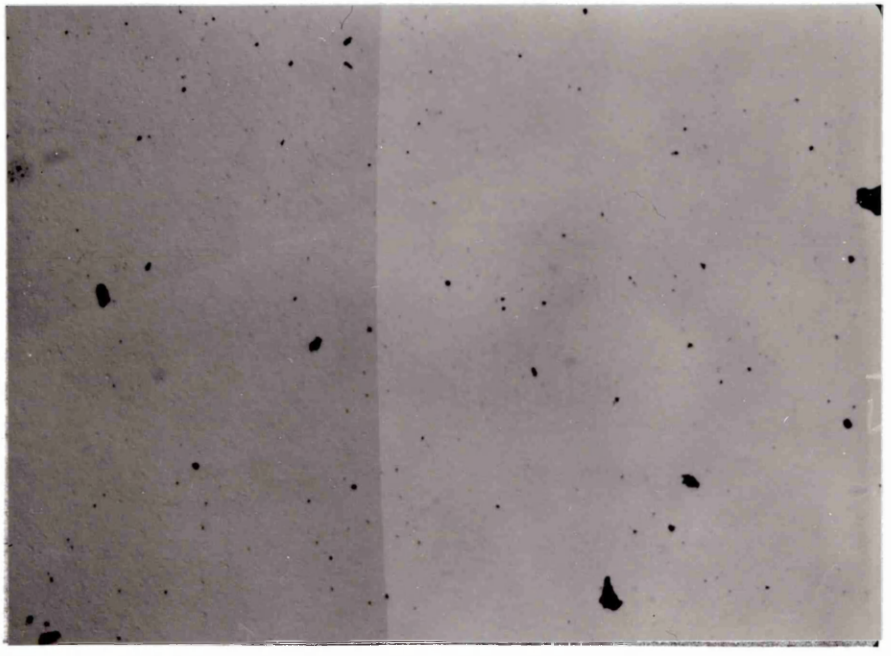

Figure 3.6 Porosity and pores of S4 carbide X200

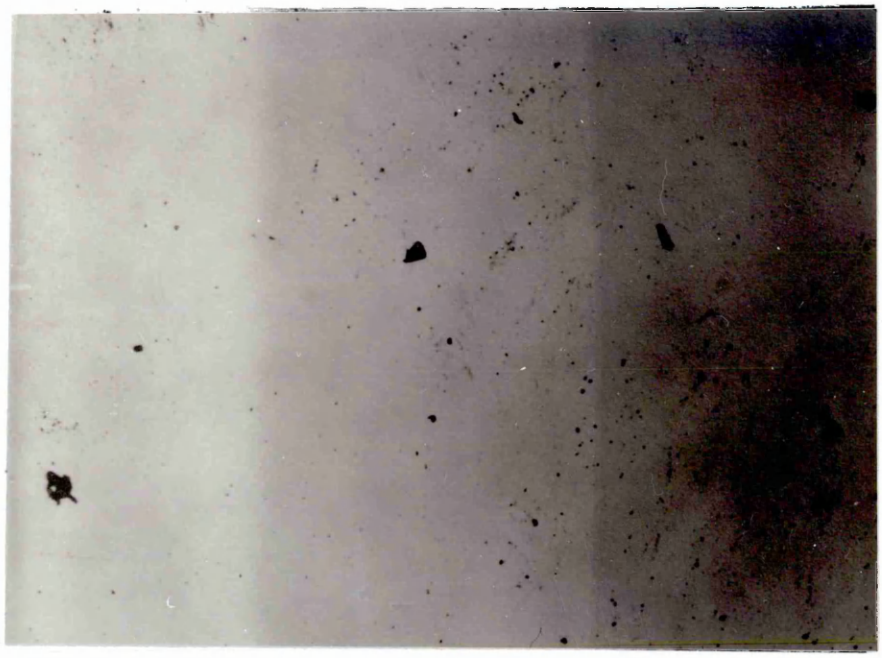

Figure 3.7 Porosity and pores of SP45 carbide X200

Figure 3.8 Porosity and pores of SP35 carbide X200

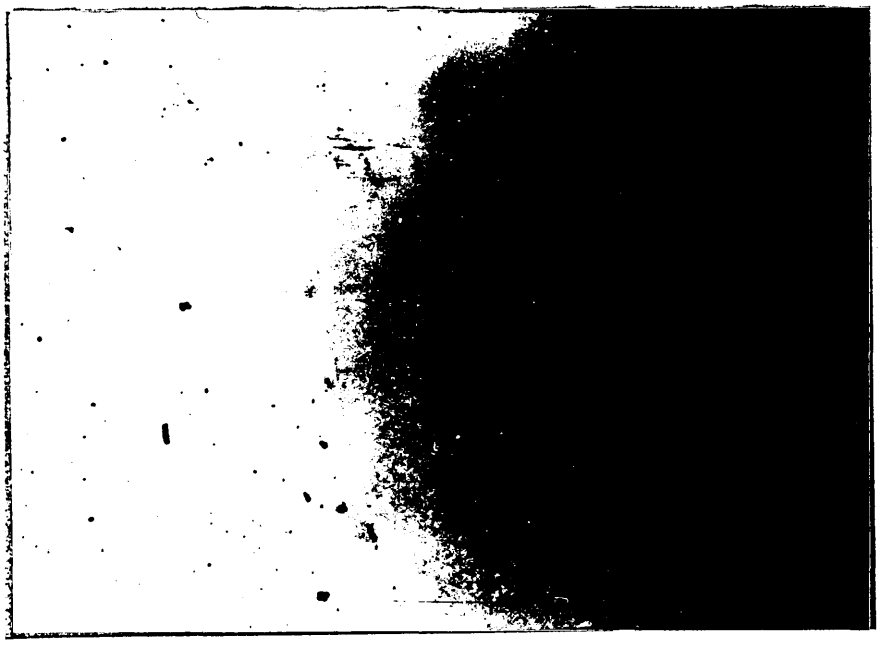

Figure 3.9 Porosity and pores of MK20 carbide X200

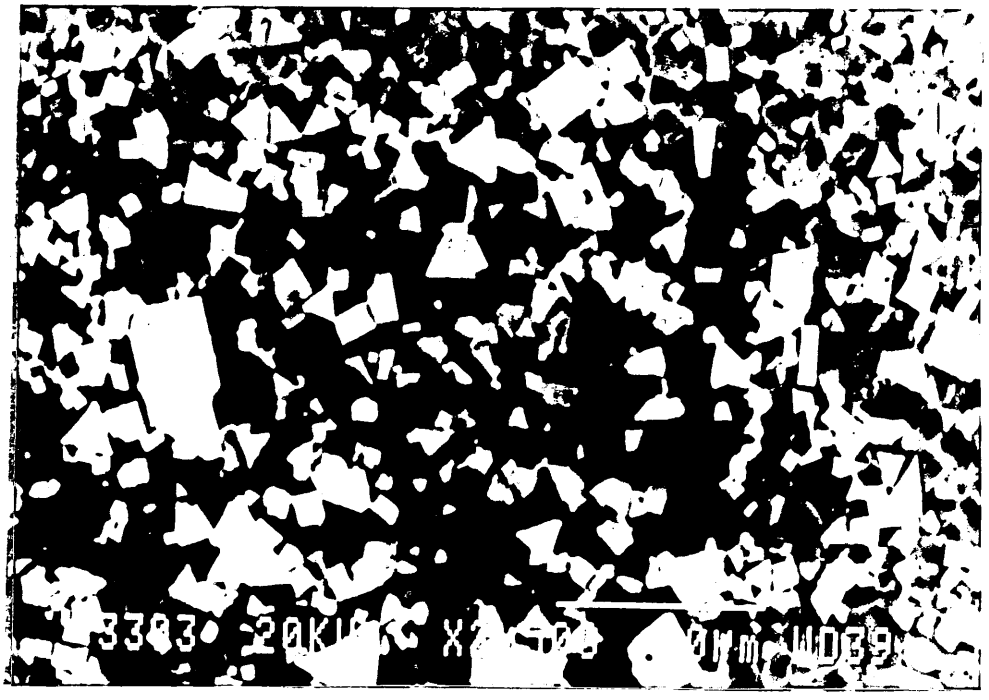

Figure 3.10 Micro structure of SP35 carbide (WC/Co/Ta/Ti) X2500

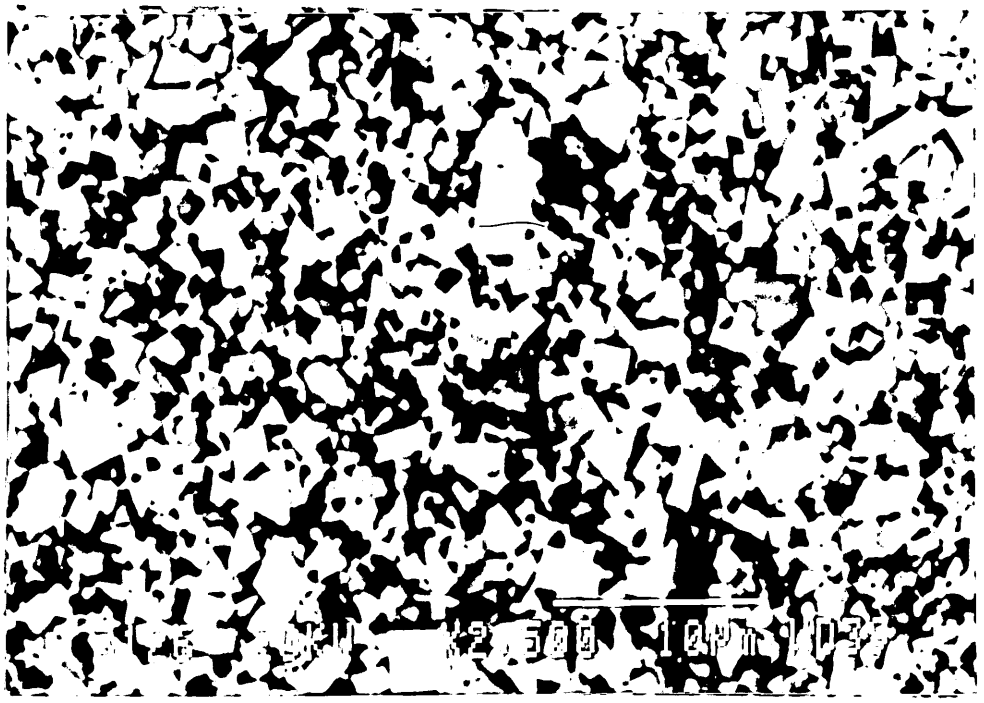

Figure 3.11 Micro structure of SP45 carbide (WC/Co/Ta/Ti) X2500

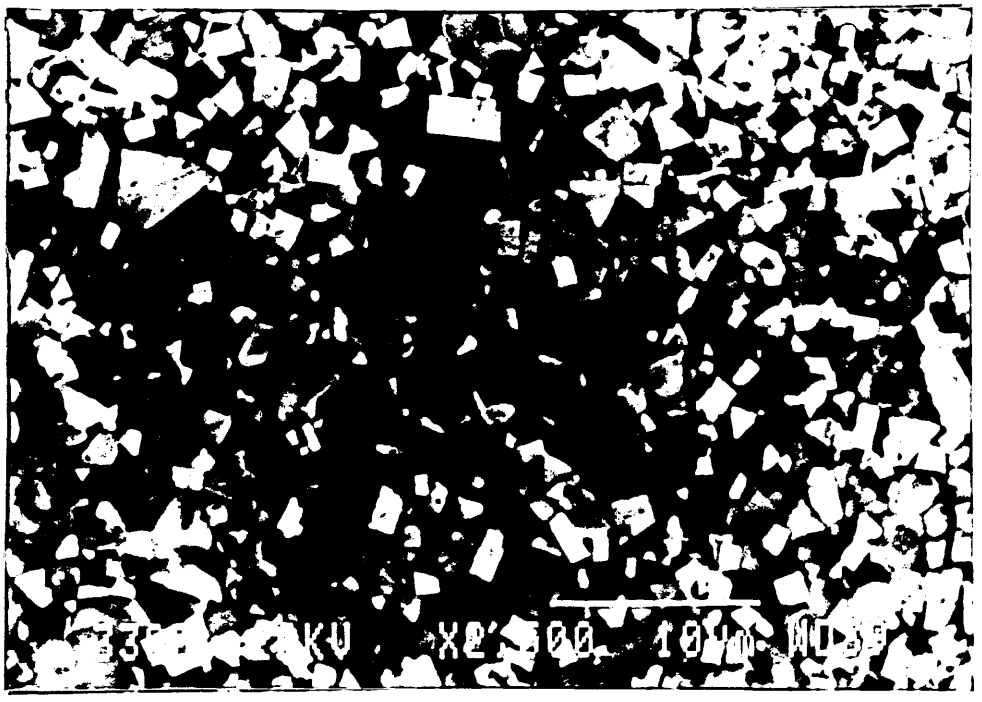

Figure 3.12 Micro structure of S4 carbide (WC/Co/Ta/Ti) X2500

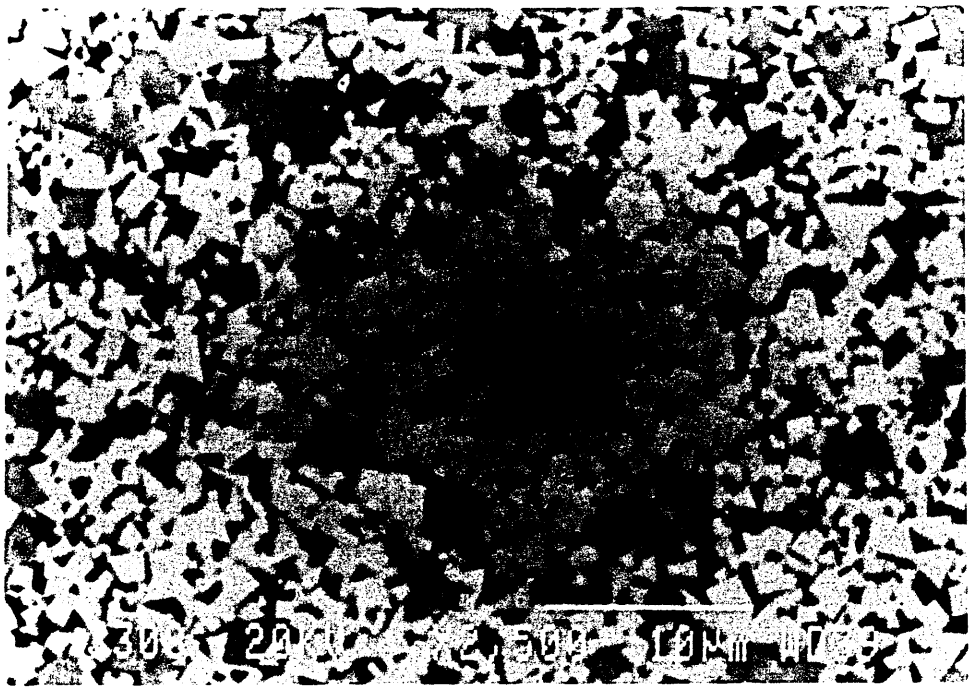

Figure 3.13 Micro structure of MK20 carbide (WC/Co/Ta/Ti) X2500

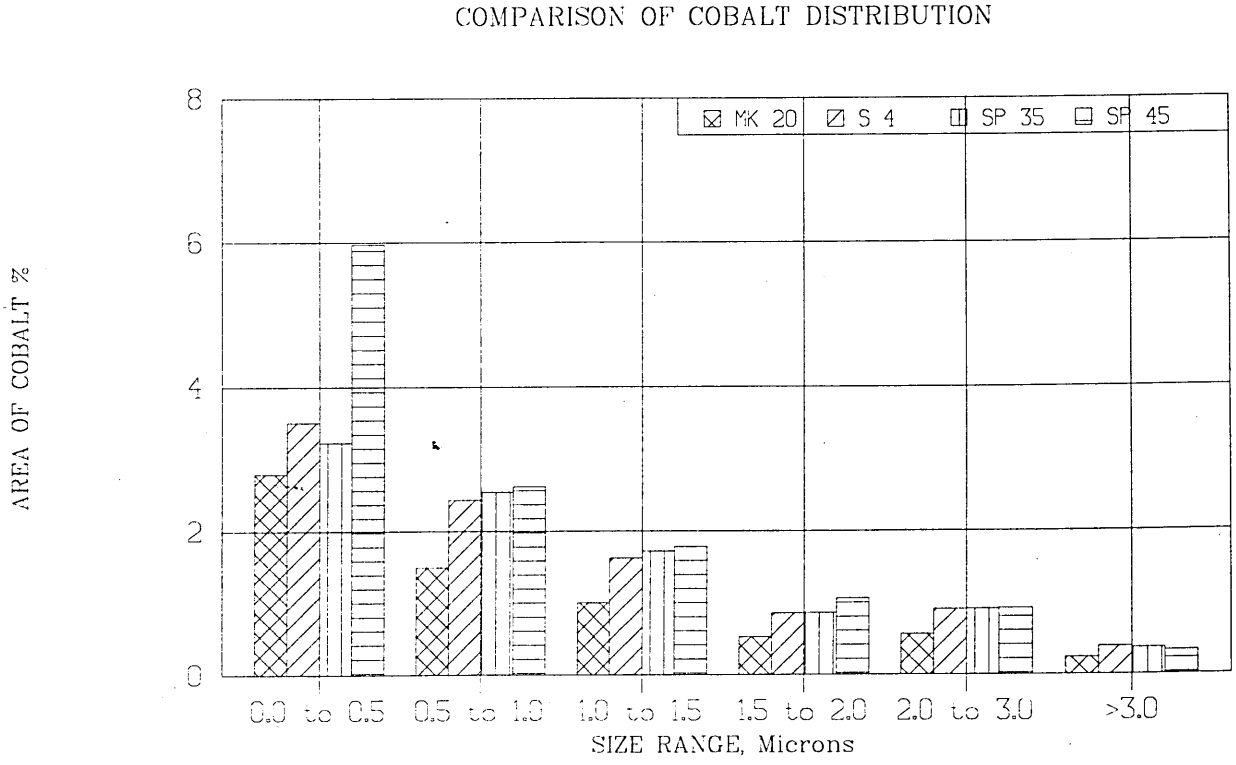

Figure 3.14 Comparison of Co distribution of the carbide substrate materials

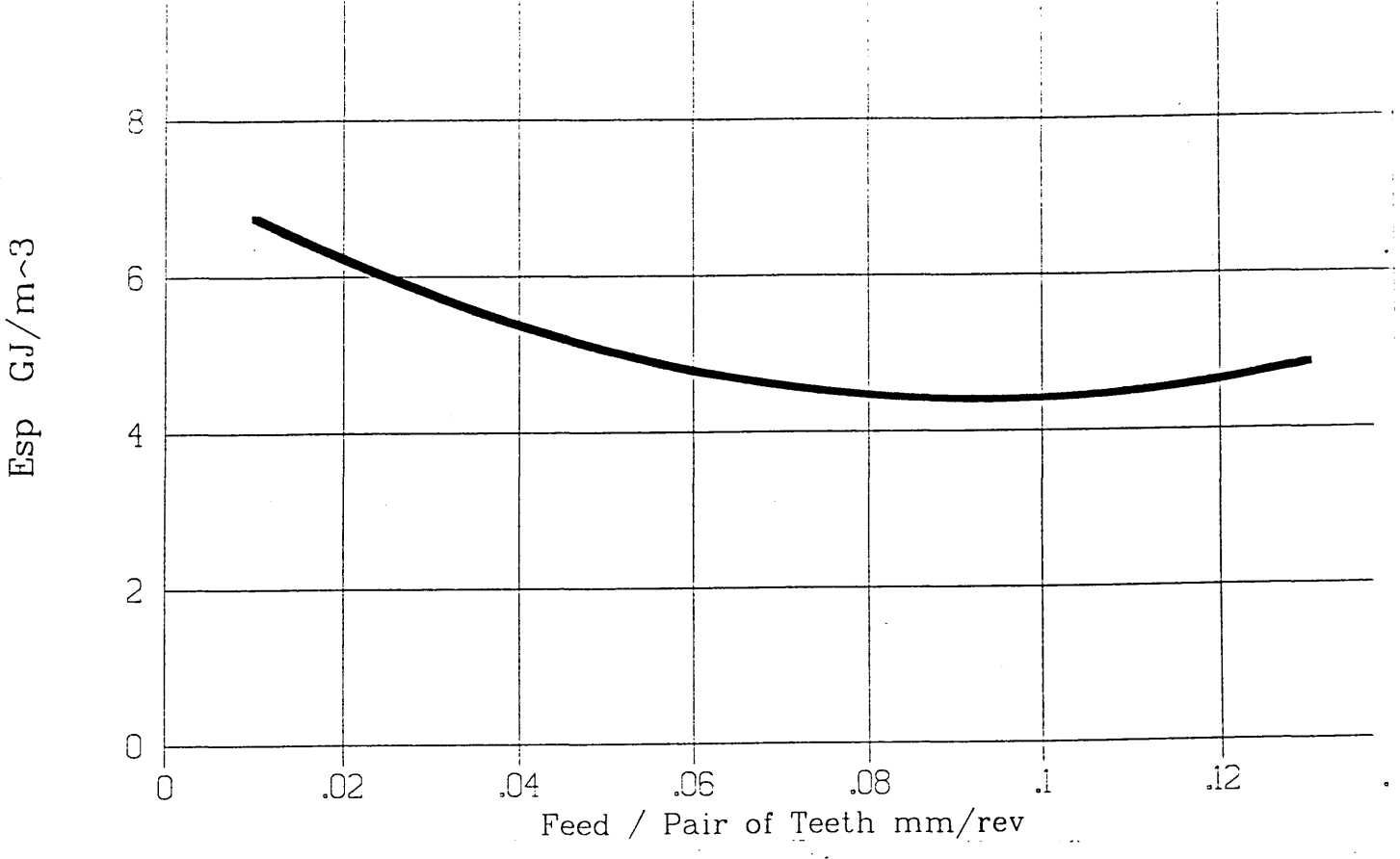

Figure 4.1 General curve of specific cutting energy against feed rate

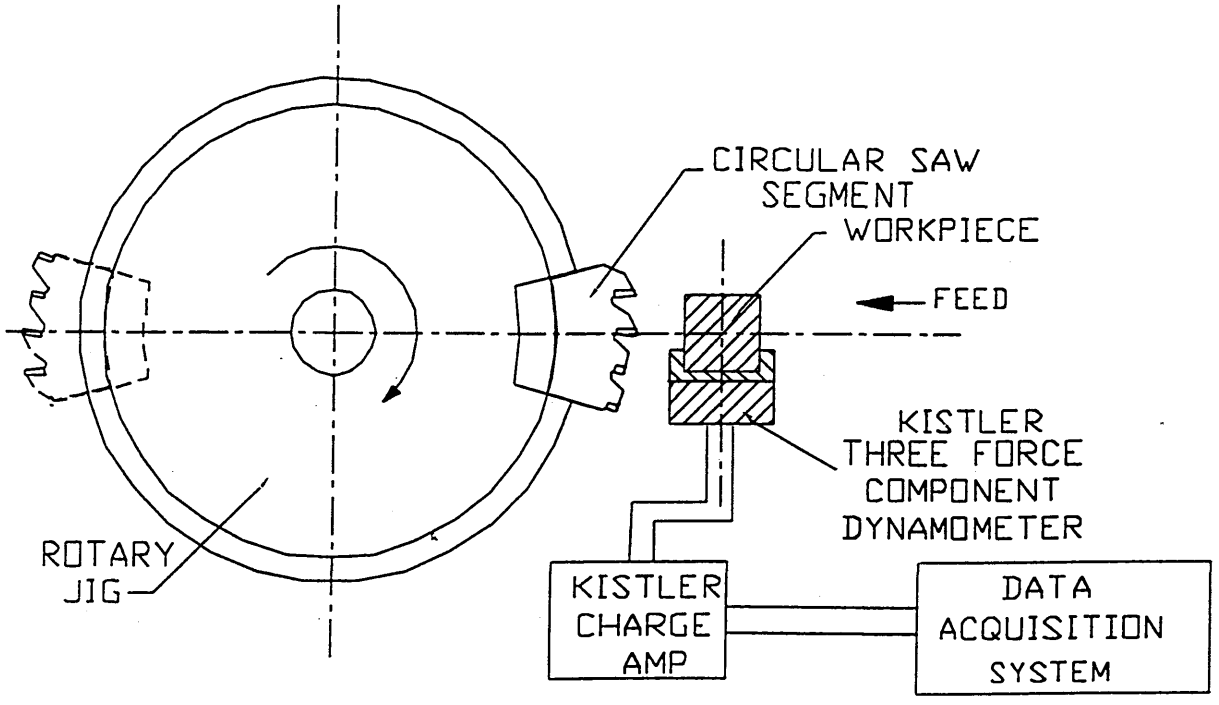

Figure 4.2 Diagram of test rig and saw segment

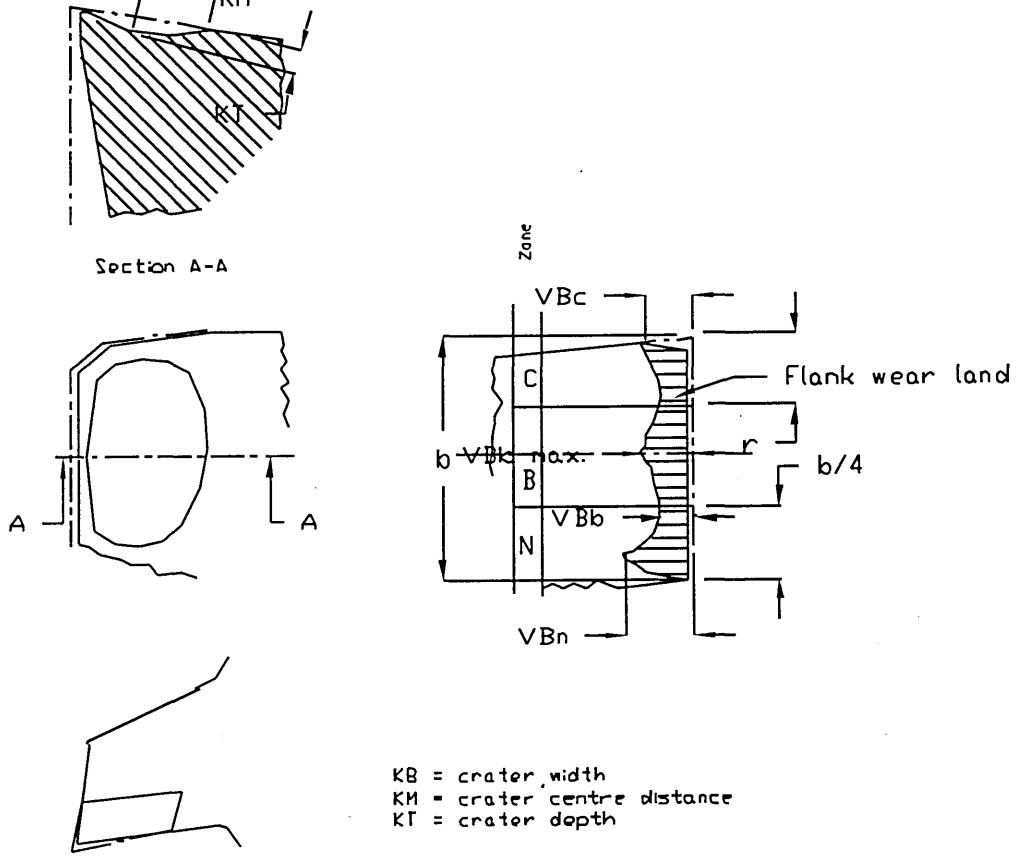

Figure 4.3 Some types of wear on turning tools as recommended in ISO 3685-1997, page 10.

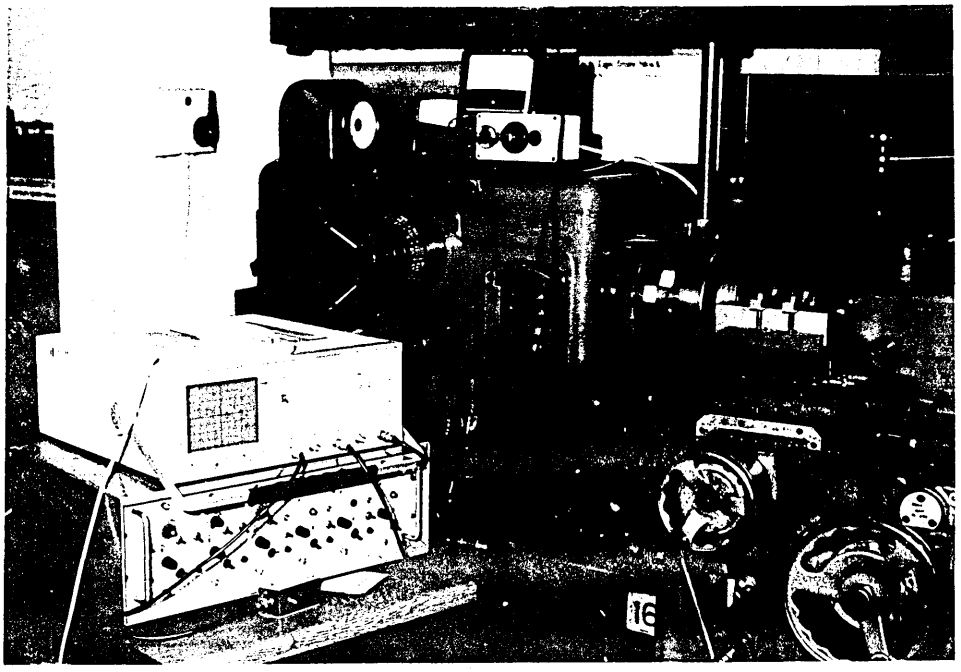

Figure 4.4 The test rig for the single point cutting test using with carbide circular saw segment

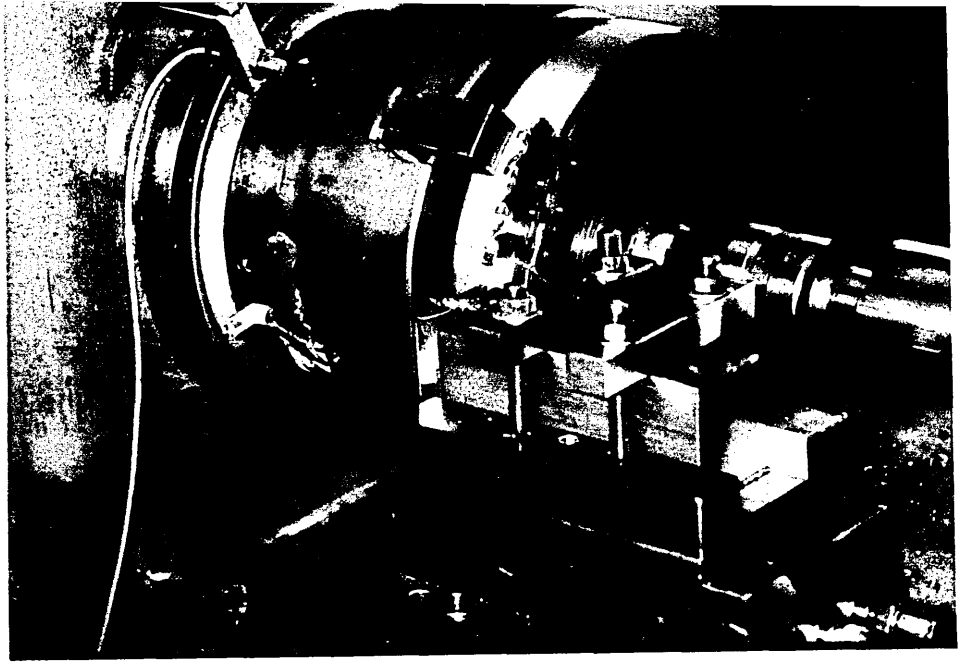

Figure 4.5 The location of workpiece and dynamometer of the test rig

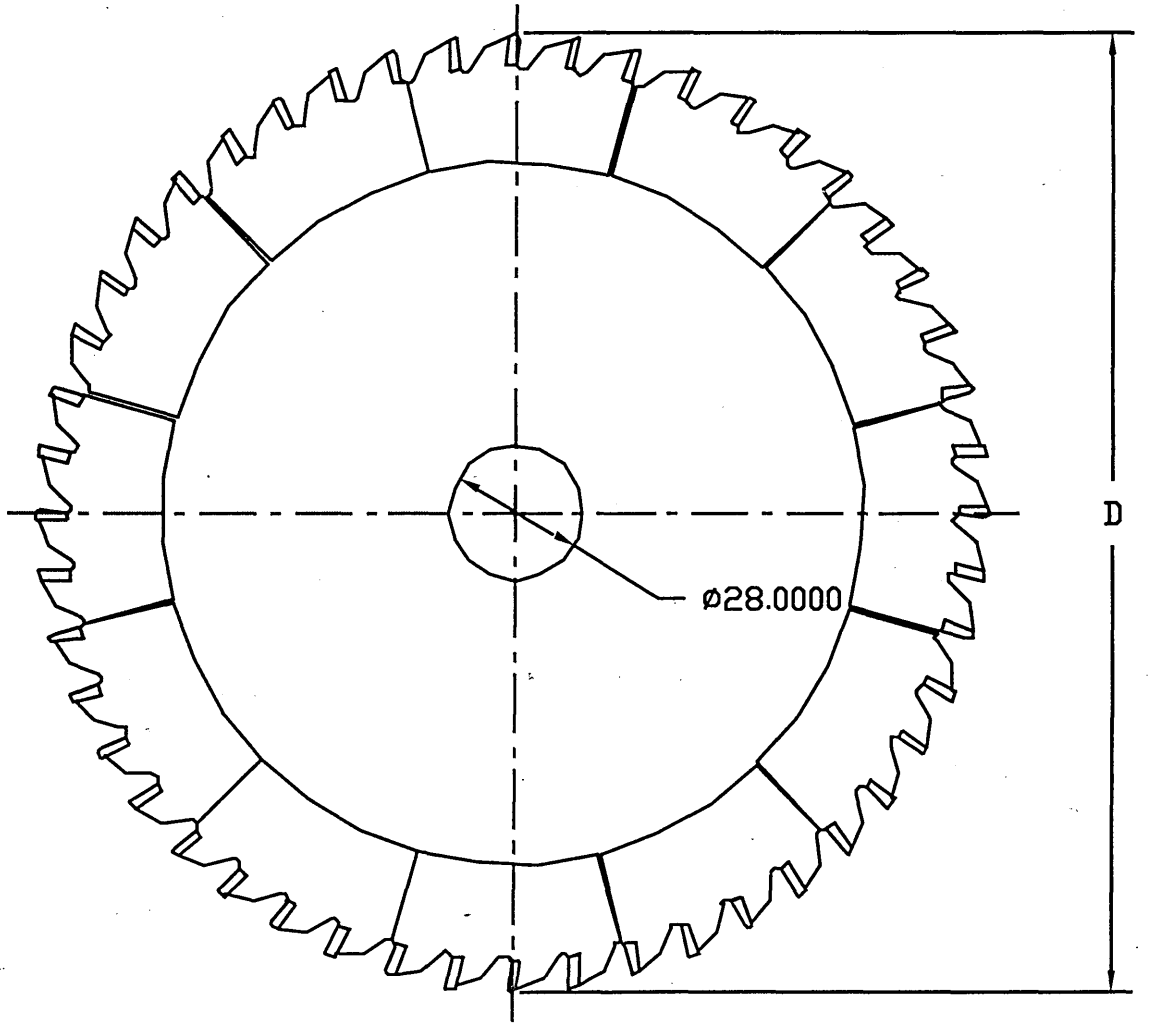

Figure 4.6 Carbide tipped circular segmental saw

Figure 4.7 The newly designed uncoated segment of carbide tipped circular segmental saw

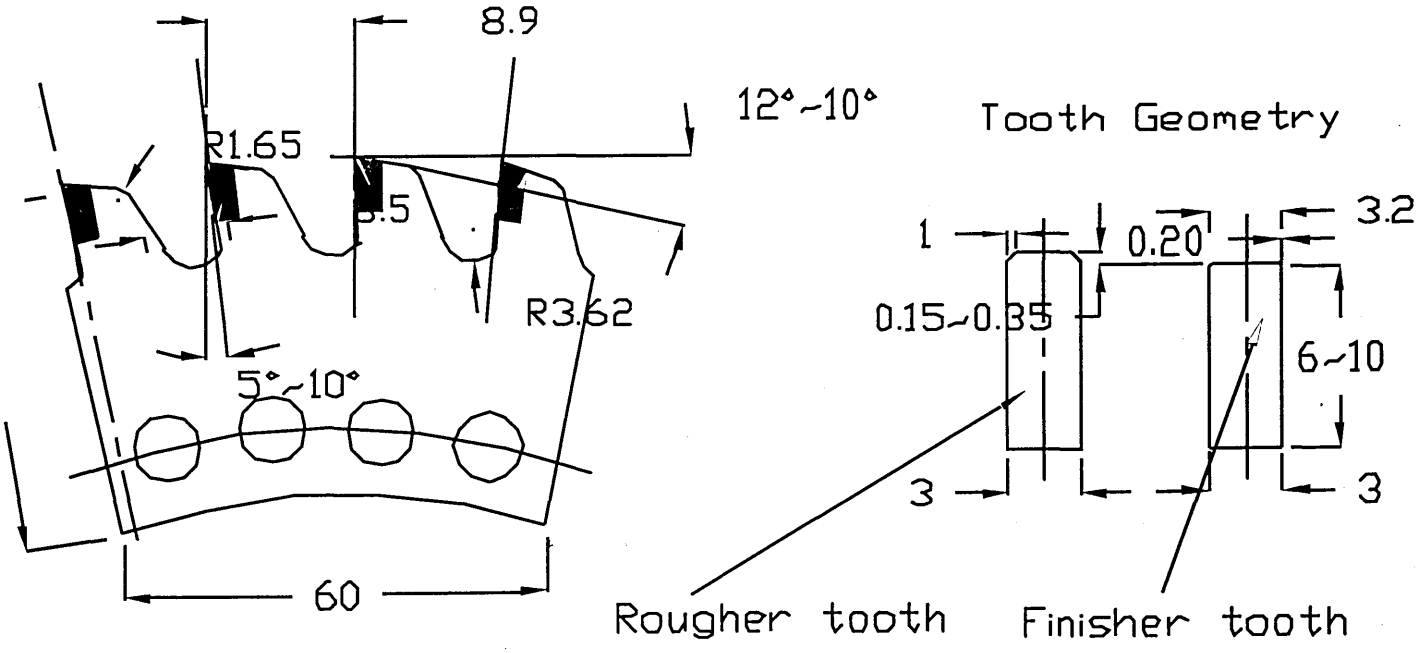

Figure 4.8 The roughing and finishing teeth of the segment

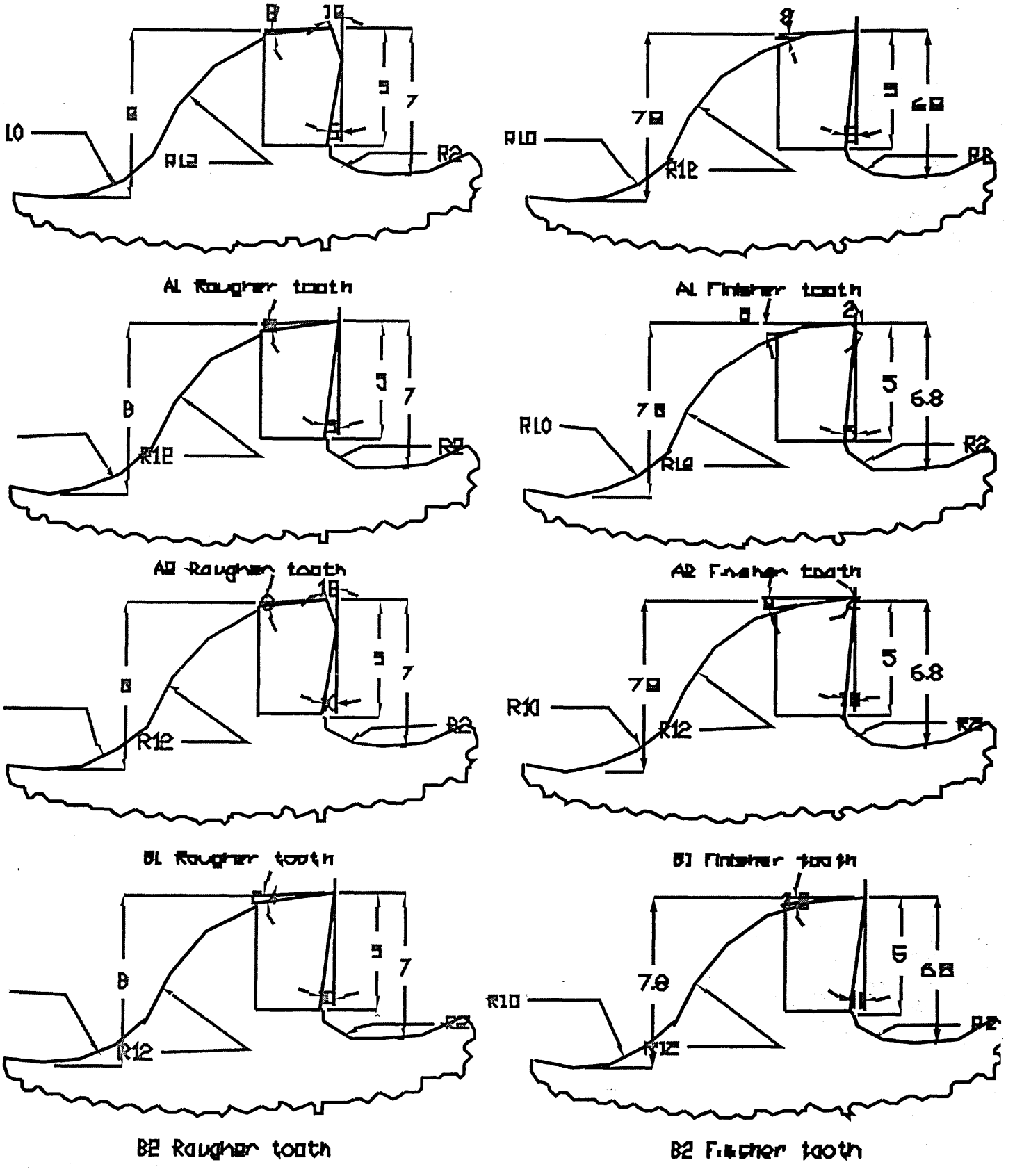

Figure 4.9 Geometry and dimension of carbide circular saw segments

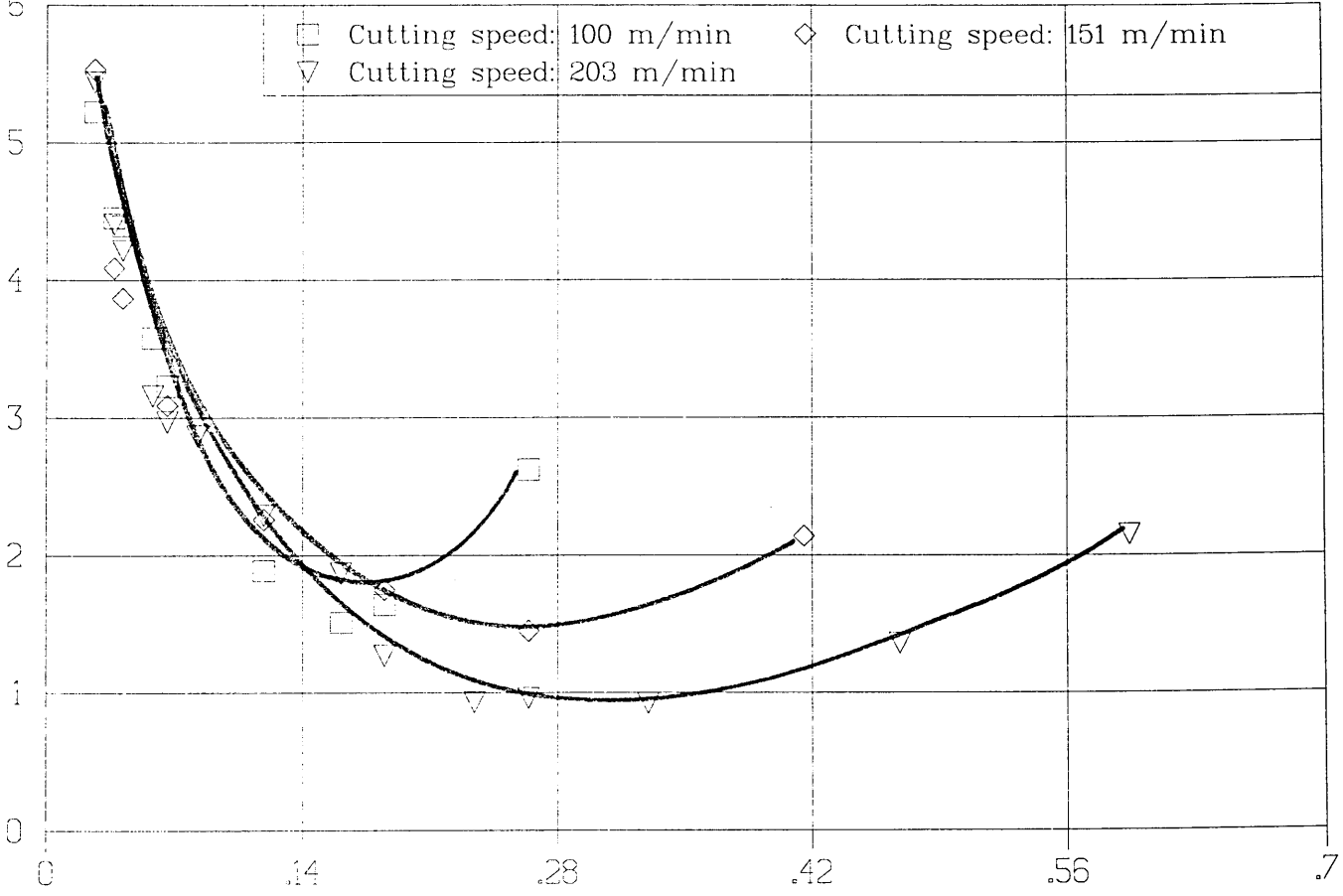

Figure 4.10 Performance of A1 segment when sawing MS

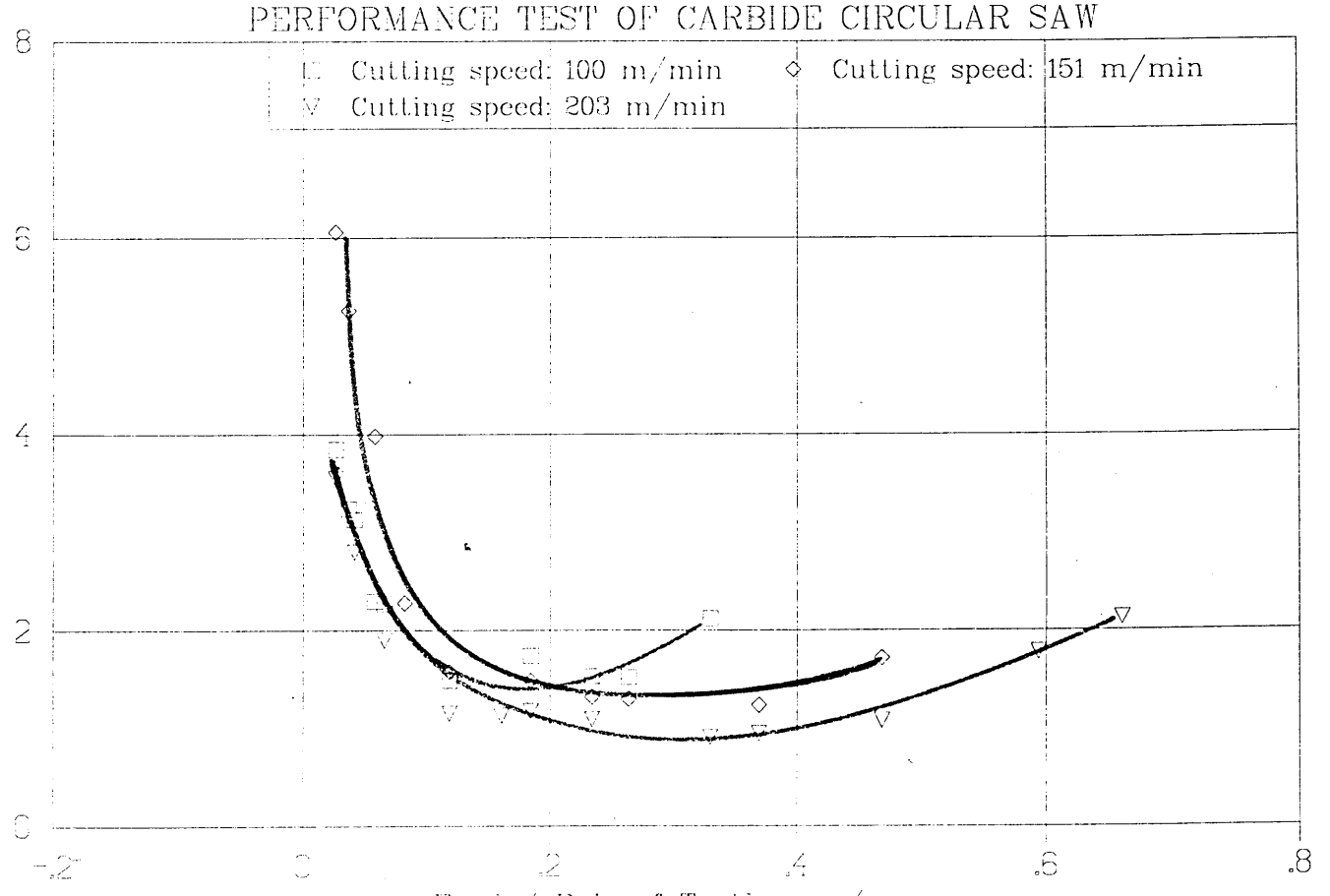

Figure 4.11 Performance of A2. 5/-/8 carbide circular saw when sawing MS

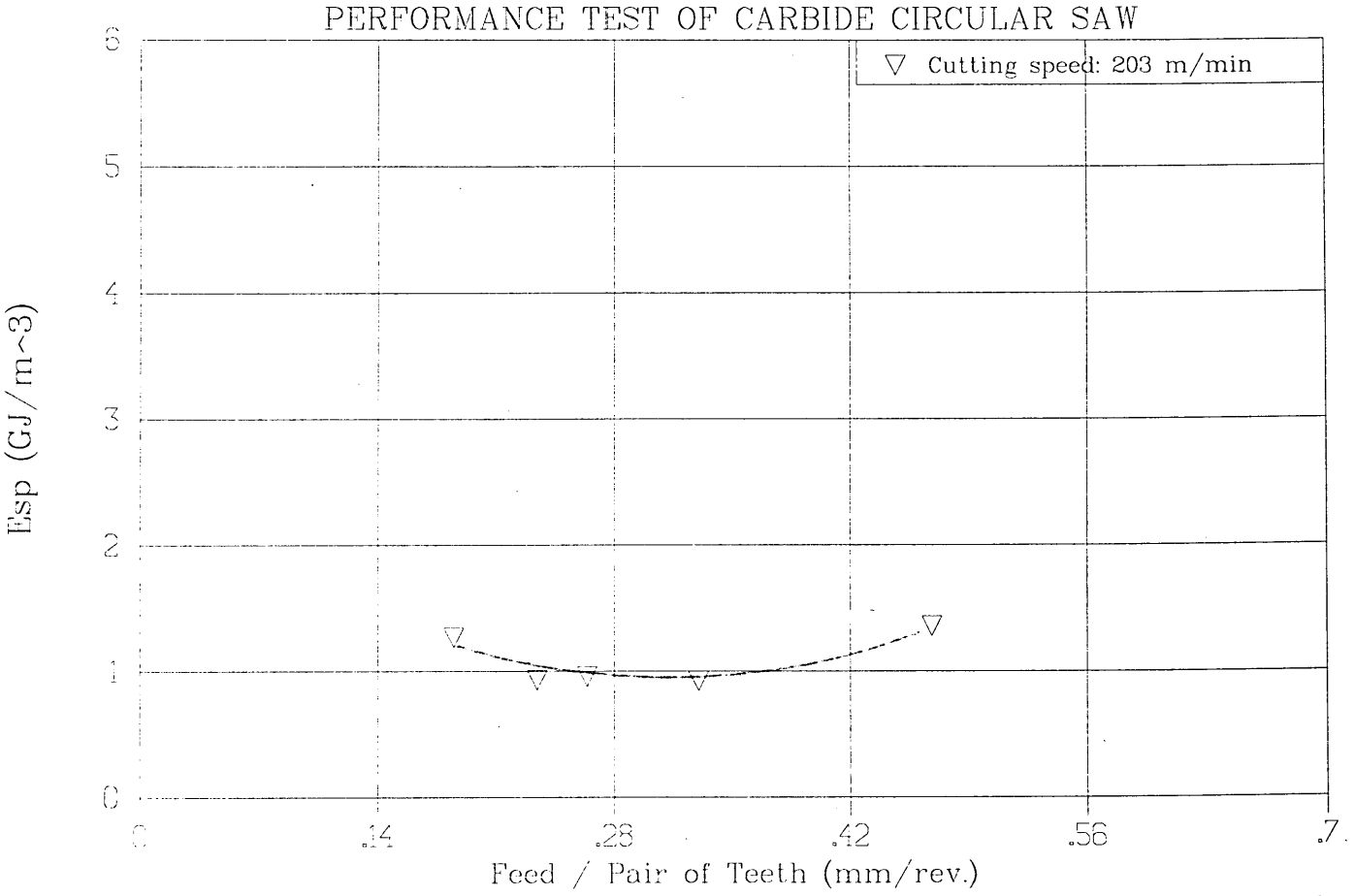

Figure 4.12 Performance of A1. 5/18/8 carbide circular saw when sawing MS

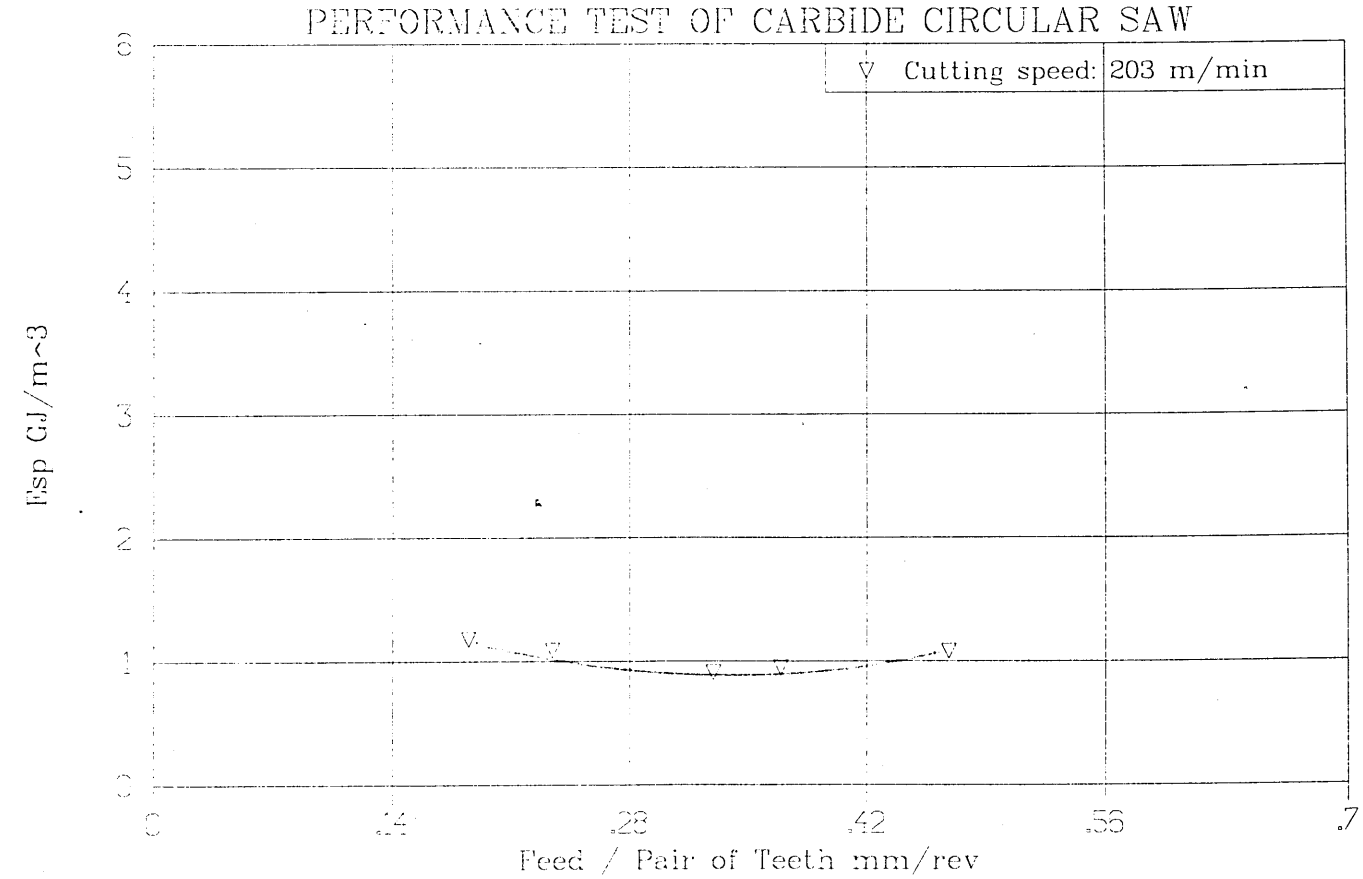

Figure 4.13 Performance of A2. 5/–/8 carbide circular saw when sawing MS

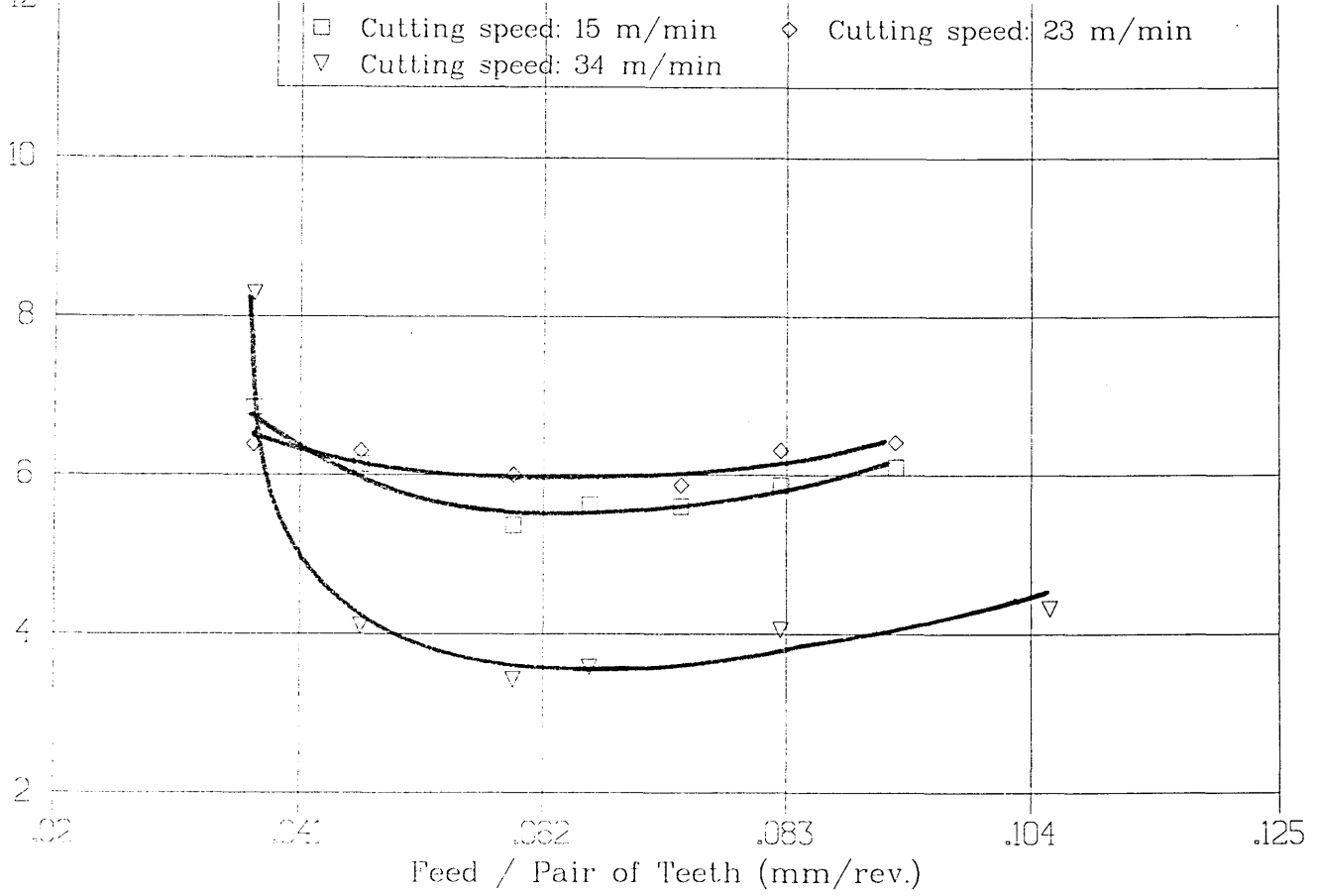

Figure 4.14 Performance curve of A1. 5/18/8 carbide circular saw when sawing 302S25 stainless steel

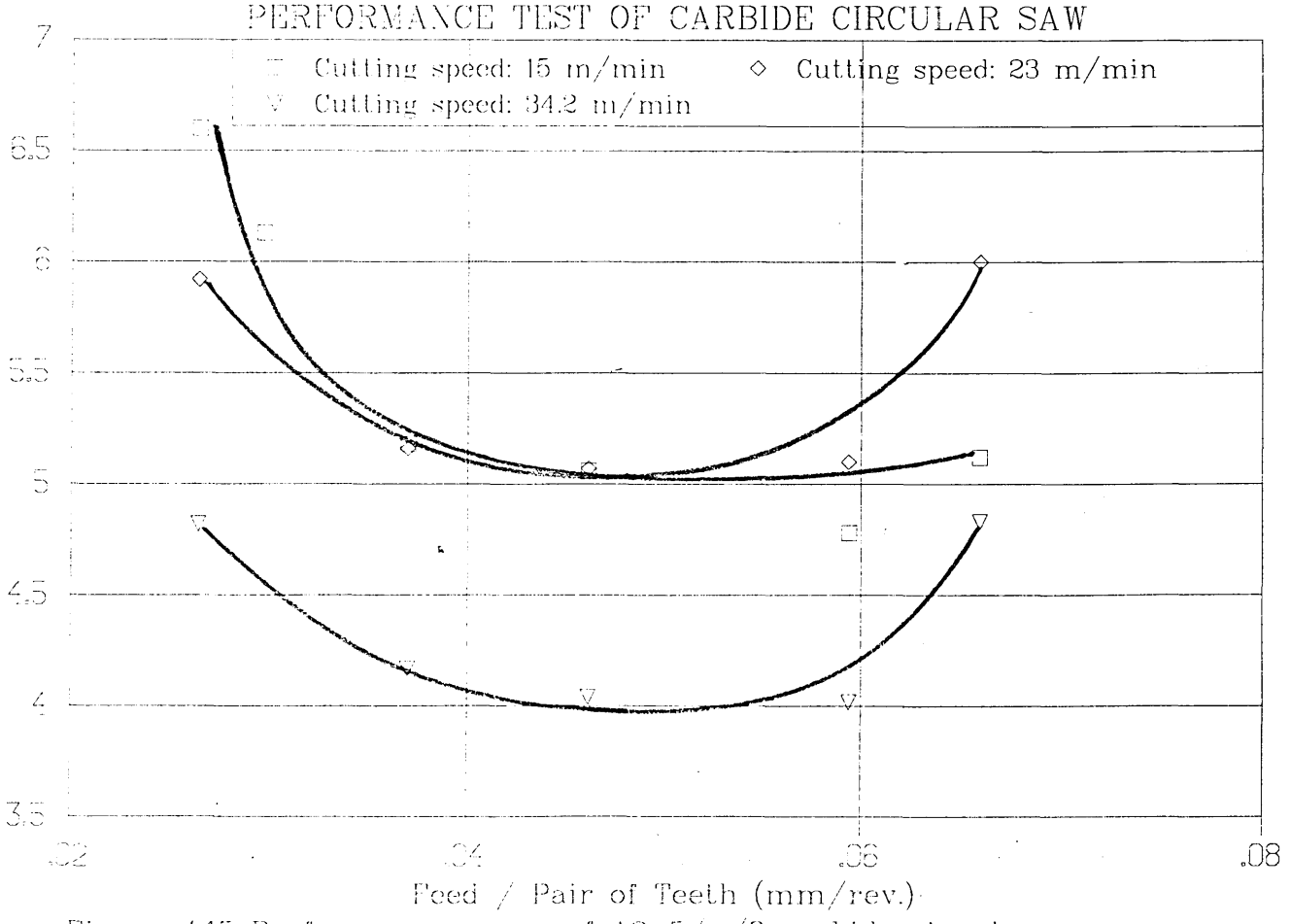

Figure 4.15 Performance curve of A2. 5/--/8 carbide circular saw when sawing 302S25 stainless steel

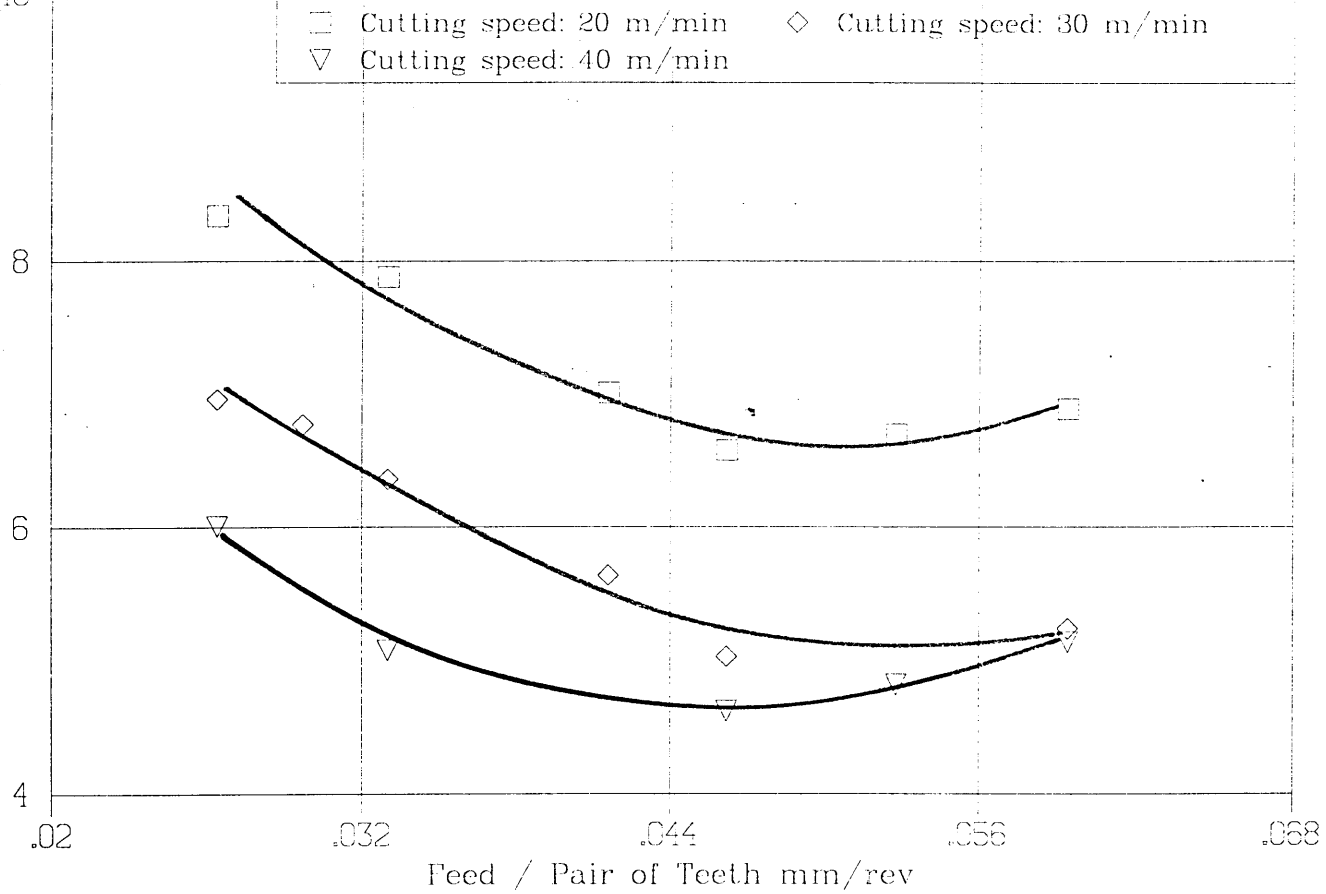

Figure 4.16 Performance curve of Bl. 10/18/8 carbide circular saw when sawing 302 S25 stainless steel

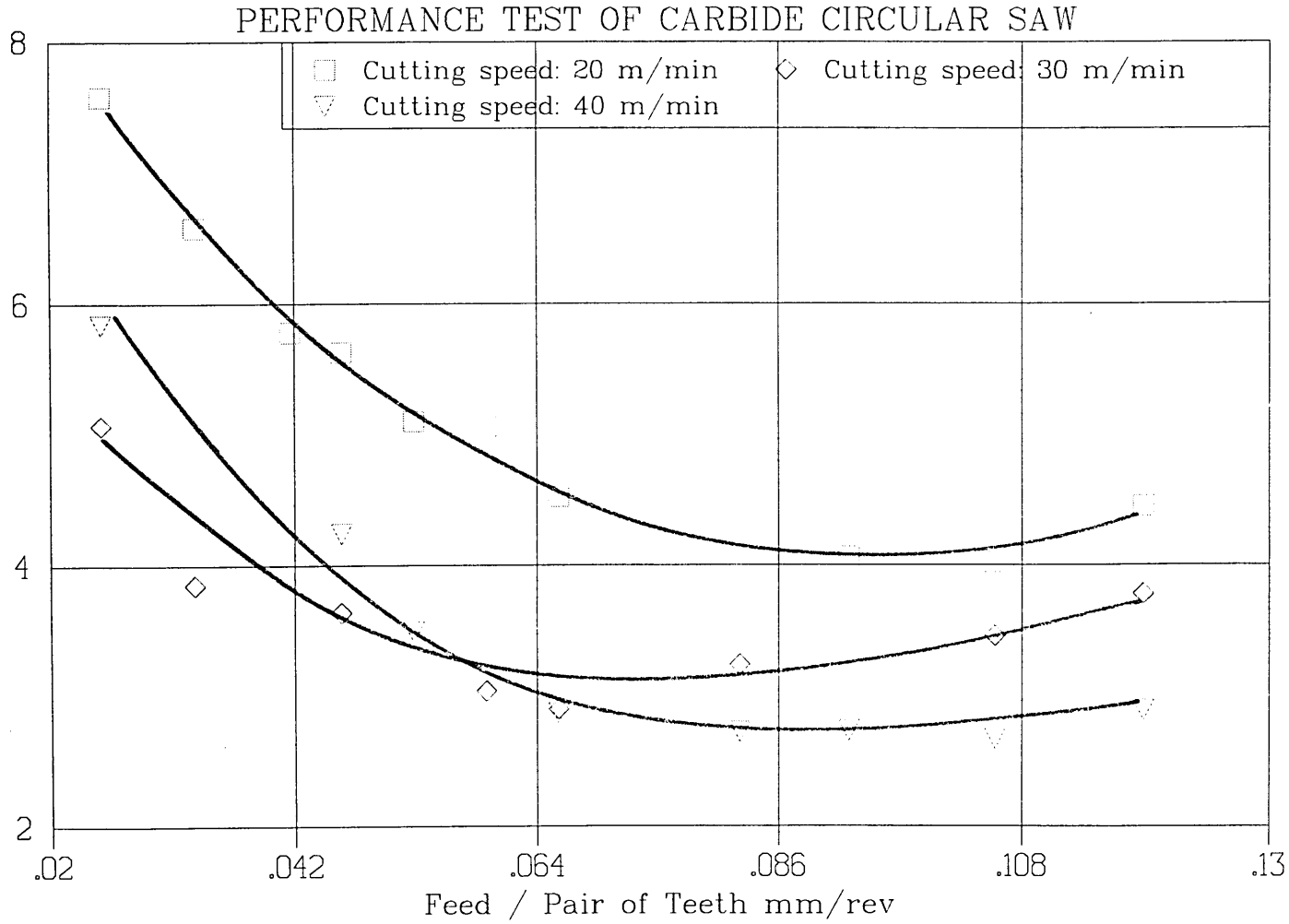

Figure 4.17 Performance curve of B2 segment when sawing 302 S25 stainless steel

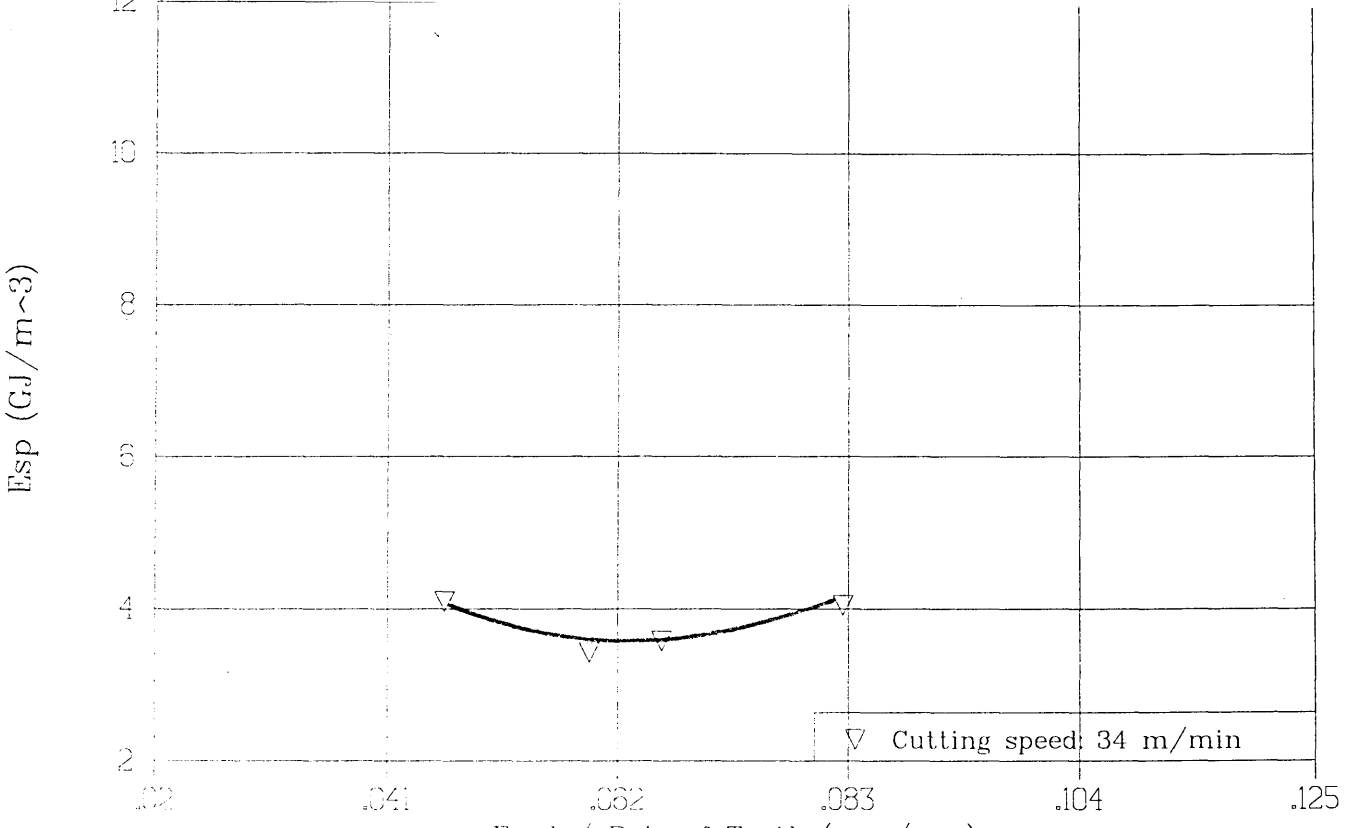

Figure 4.18 Optimised performance curve of A1 segment when sawing 302S25 stainless steel

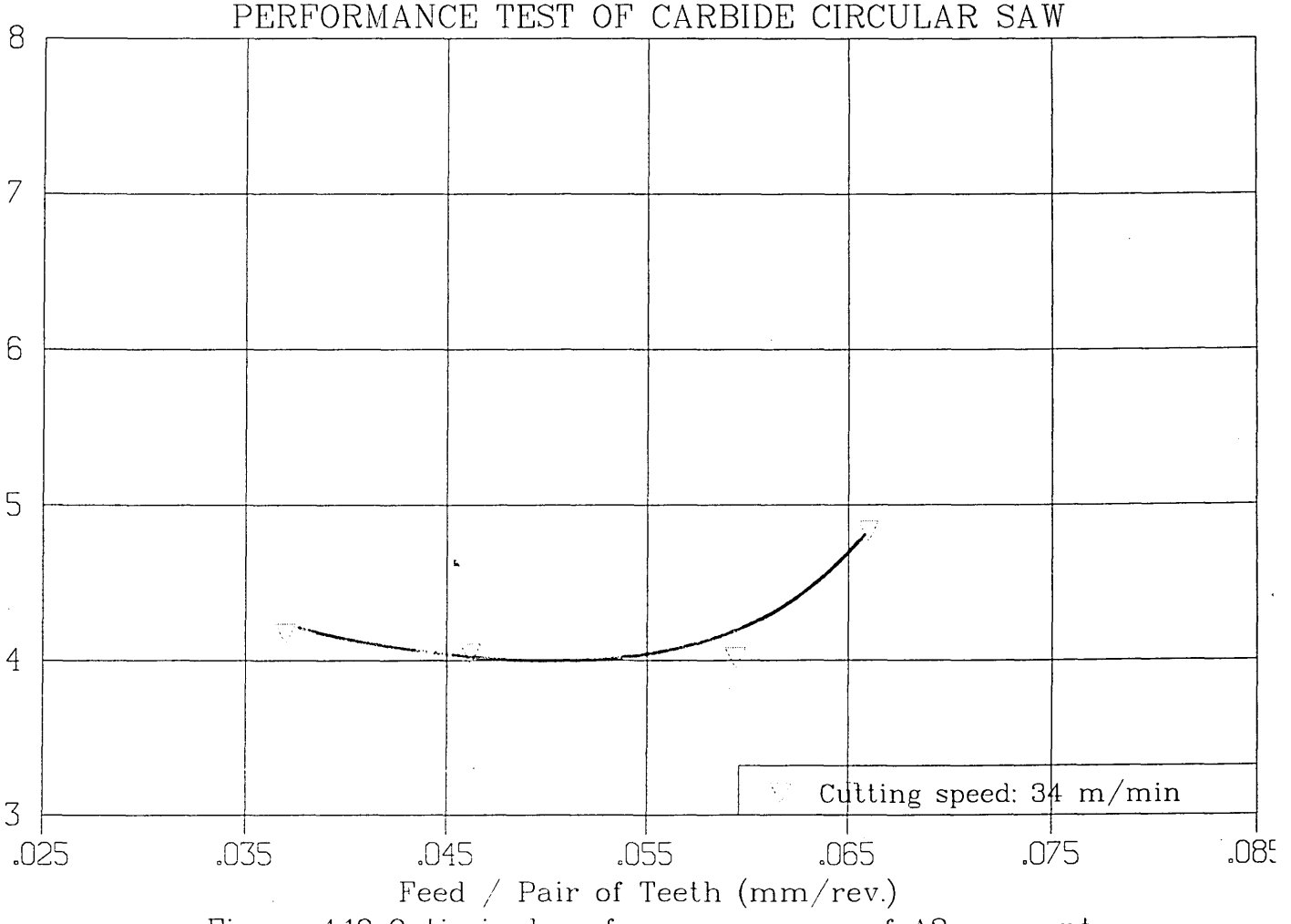

Figure 4.19 Optimised performance curve of A2 segment when sawing 302S25 stainless steel

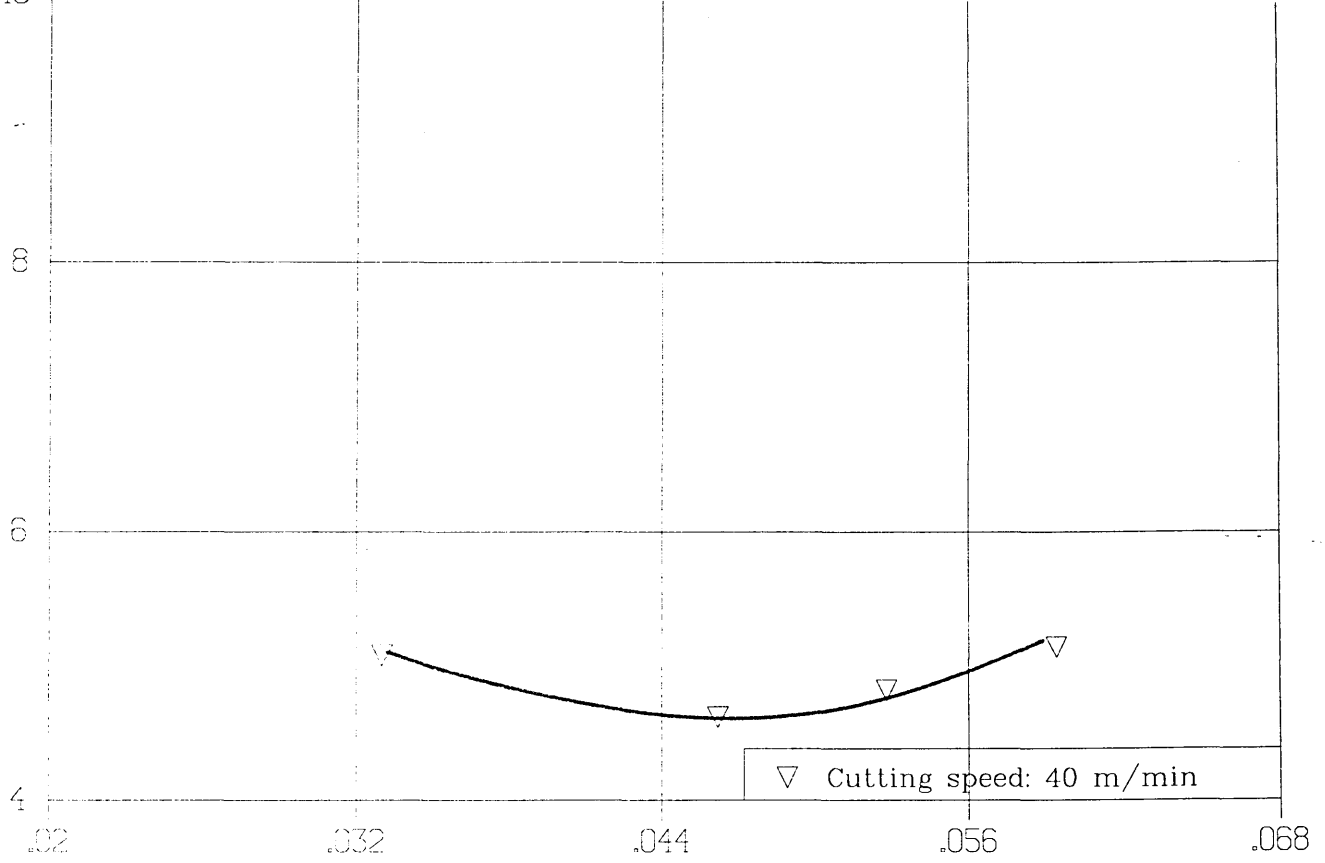

Feed / Pair of Teeth mm/rev

Figure 4.20 Optimised performance curve of B1 segment when sawing 302 S25 stainless steel

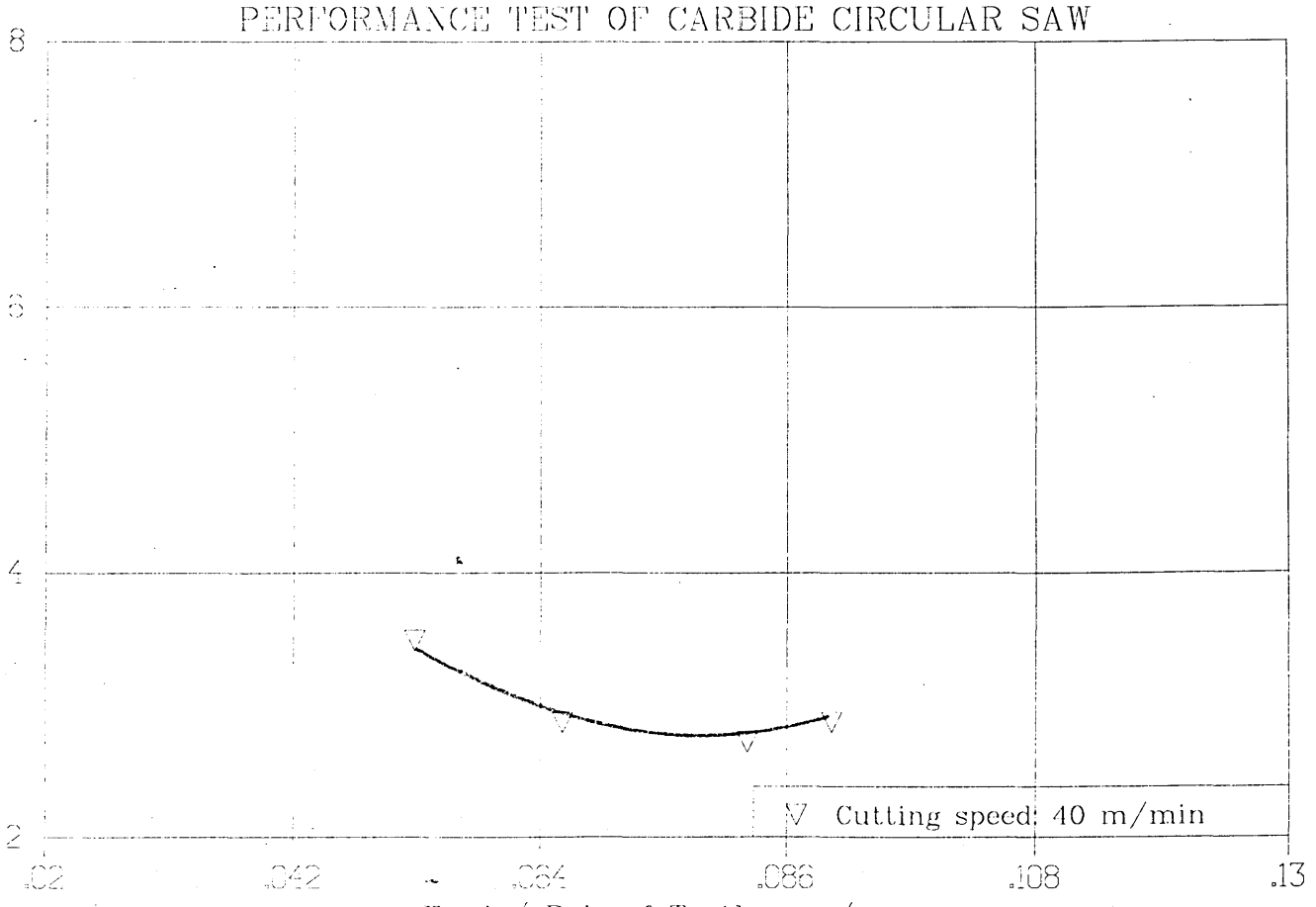

Feed / Pair of Teeth mm/rev

Figure 4.21 Optimised performance curve of B2 segment when sawing 302 S25 stainless steel

Cutting speed: 1400 m/min; Feed of pair of teeth: 0.033 mm/rev.

Figure 4.22 The long chip clogged in flute or space between the teeth of the circular saw blade when sawing aluminium with C1 segment

Cutting speed: 1400 m/min; Feed of pair of teeth: 0.033 mm/rev.

Figure 4.23 The long chip clogged in flute or space between the teeth of the circular saw blade when sawing aluminium with C2 segment

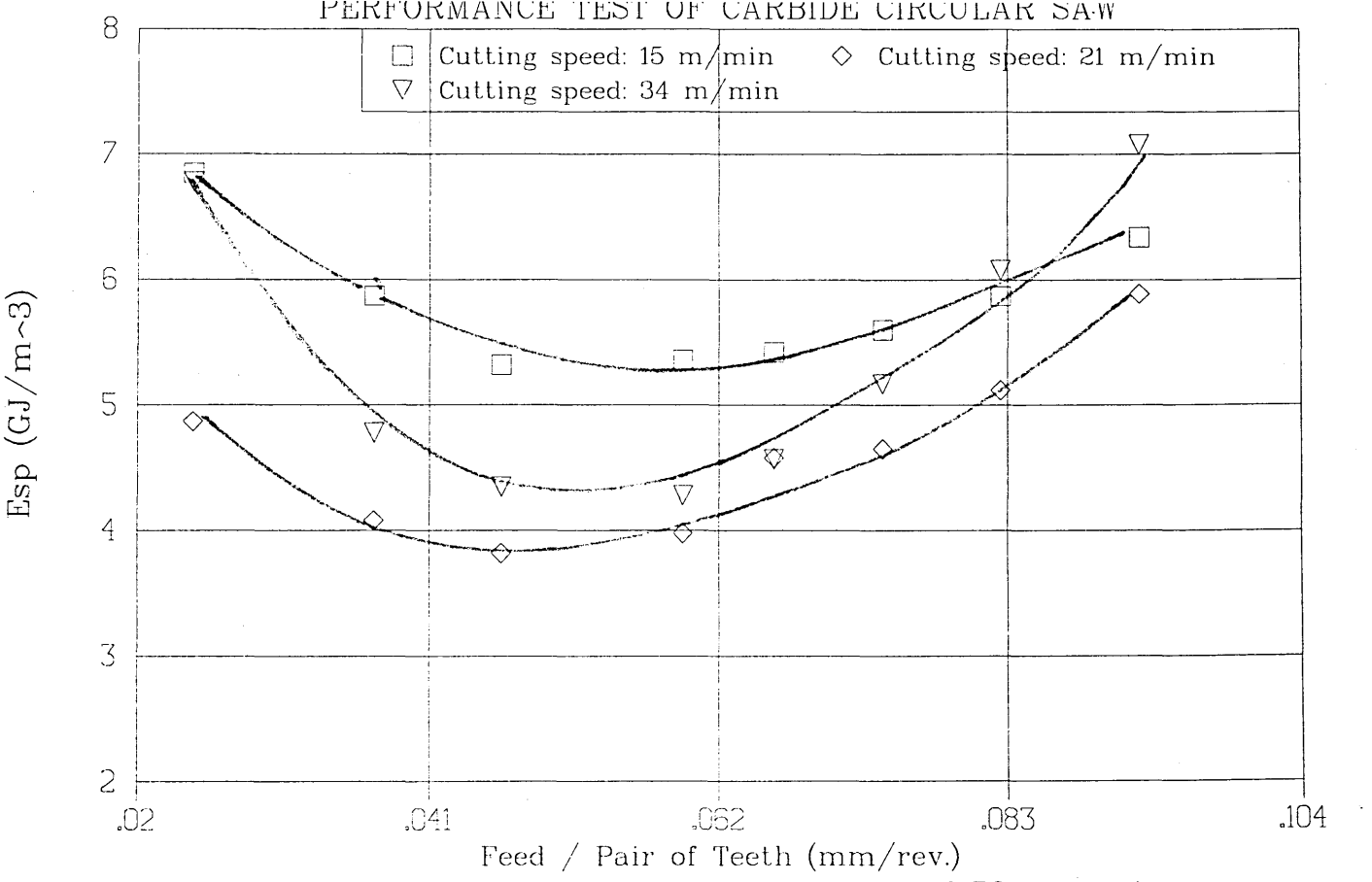

Figure 4.24 Performance curve of uncoated B2 segment when sawing C25 nimonic alloy

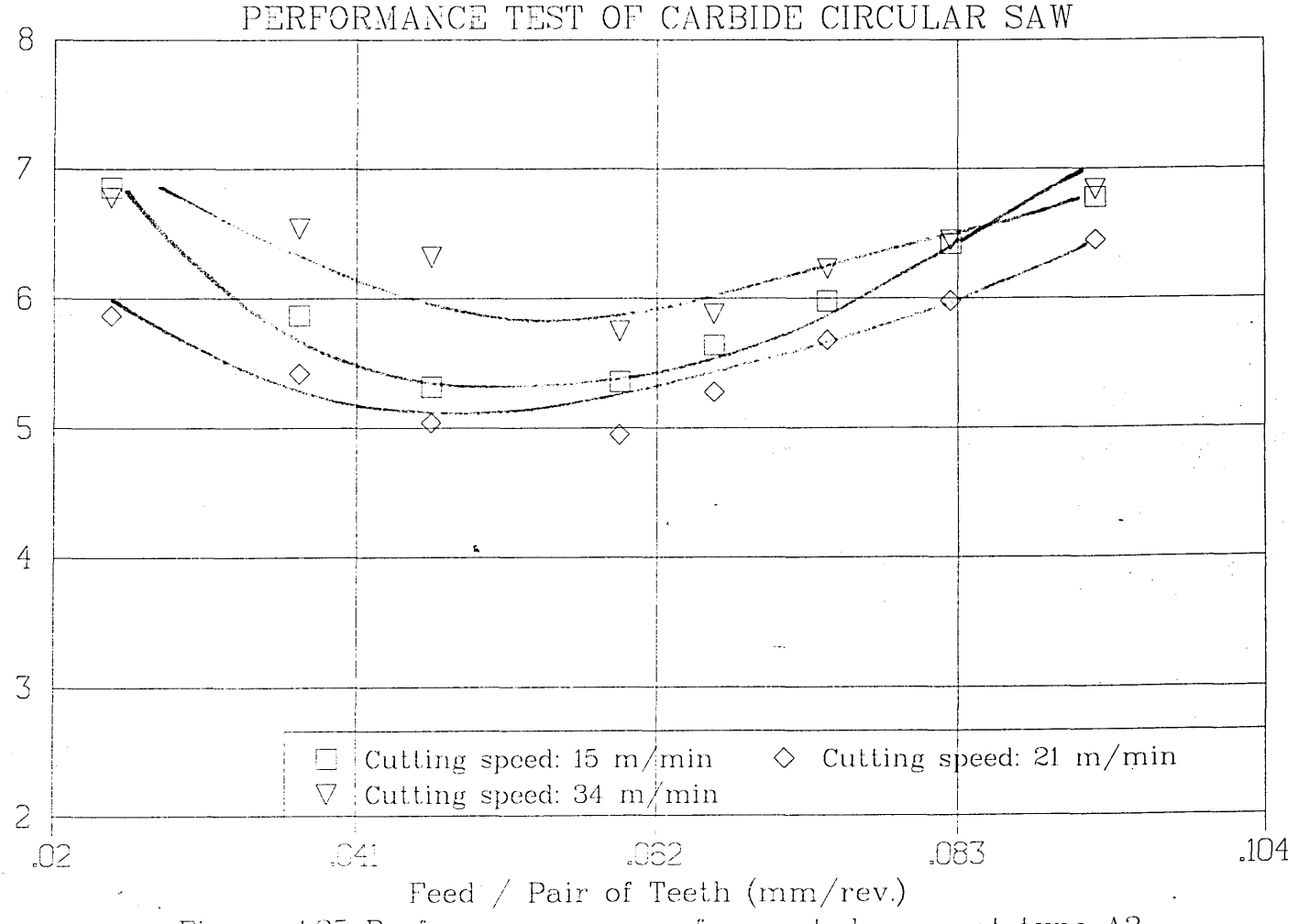

Figure 4.25 Performance curve of uncoated segment type A2 when sawing C25 nimonic alloy

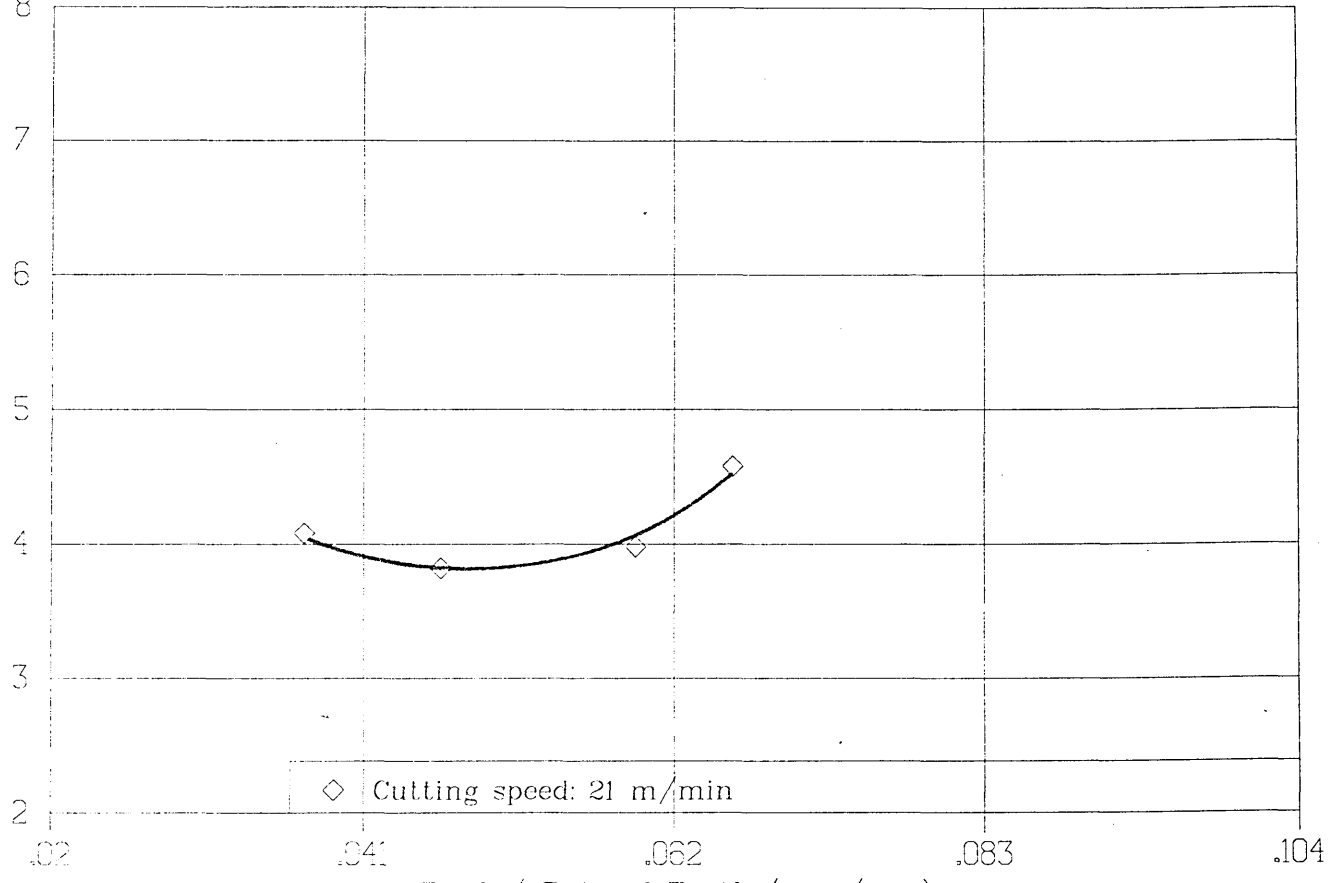

Figure 4.26 Optimised performance curve of uncoated segment type B2 when sawing C25 nimonic alloy

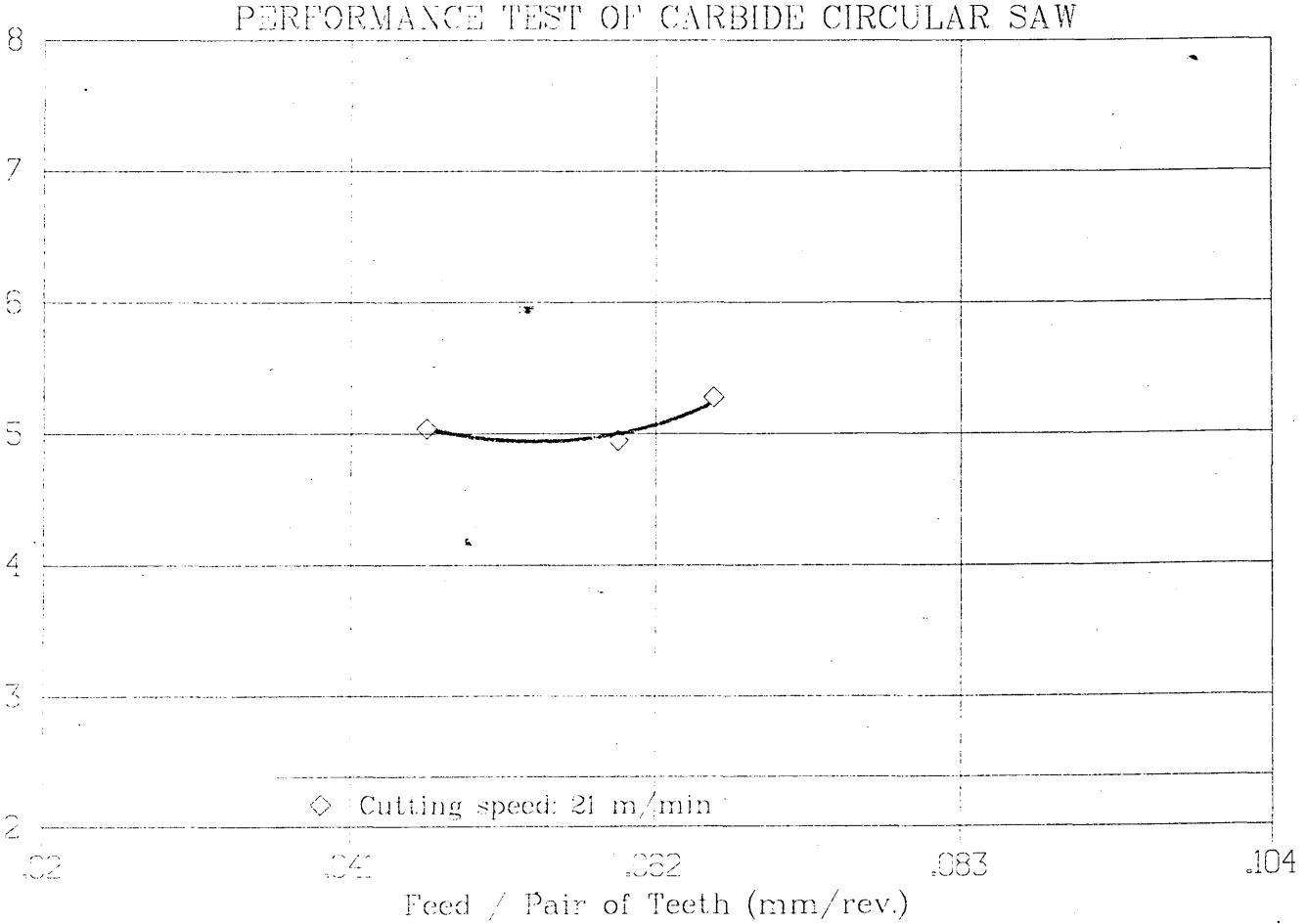

Figure 4.27 Optimised performance curve of uncoated segment type A2 when sawing C25 nimonic alloy

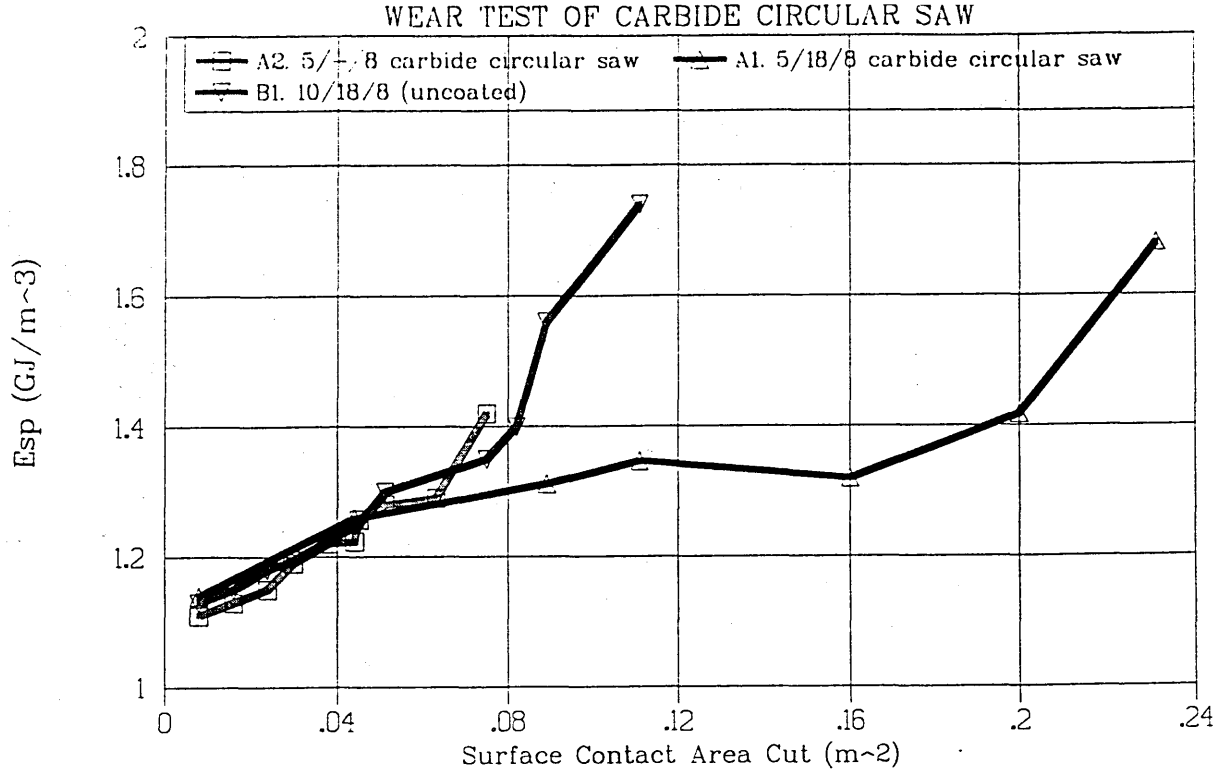

Cutting speed: 203 m/min; Feed / pair of teeth: 0.355 mm/rev.; Ctting condition: Dry

Figure 4.28 Comparison of tool life of A1, A2 and B1 segments when cutting mild steel

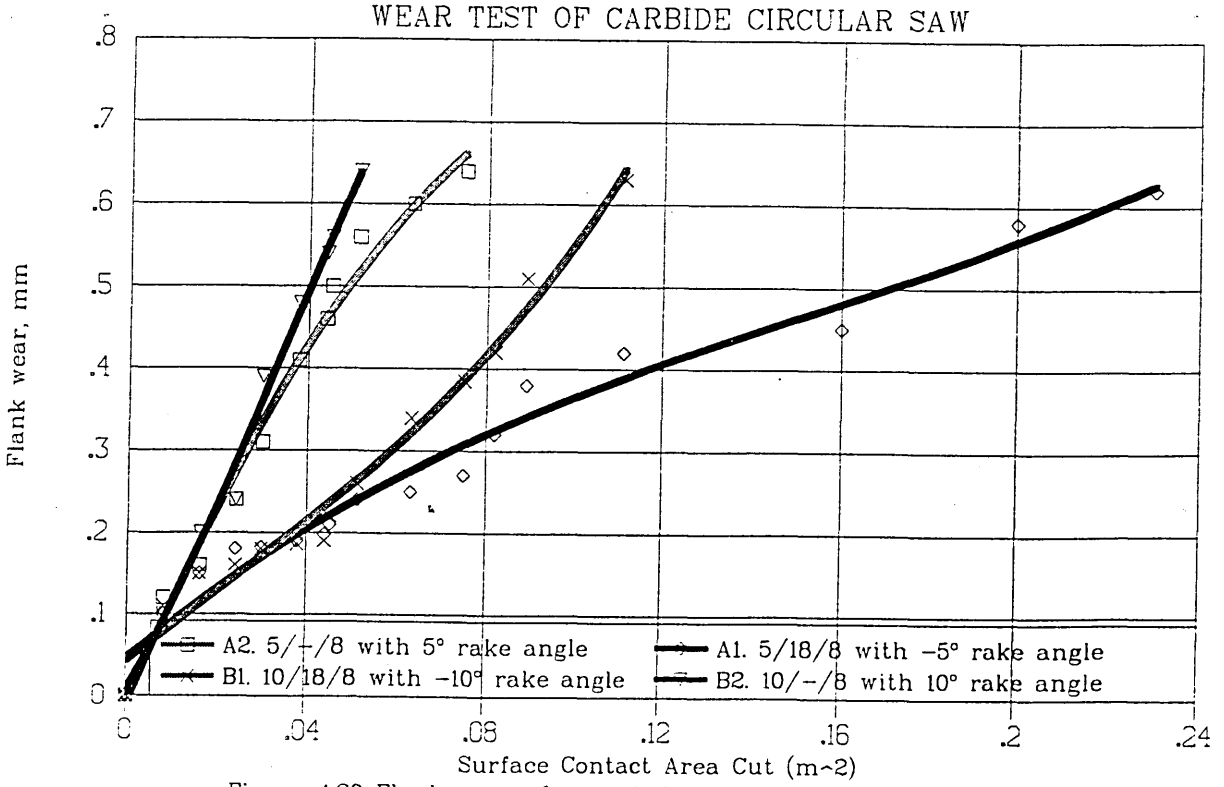

Figure 4.29 Flank wear of uncoated segment types A1, A2, B1 and B2
Cutting Speed : 203 m/min, Cutting condition: Dry
Feed/ Pair of teeth: 0.355 mm/rev., Work Material : MS

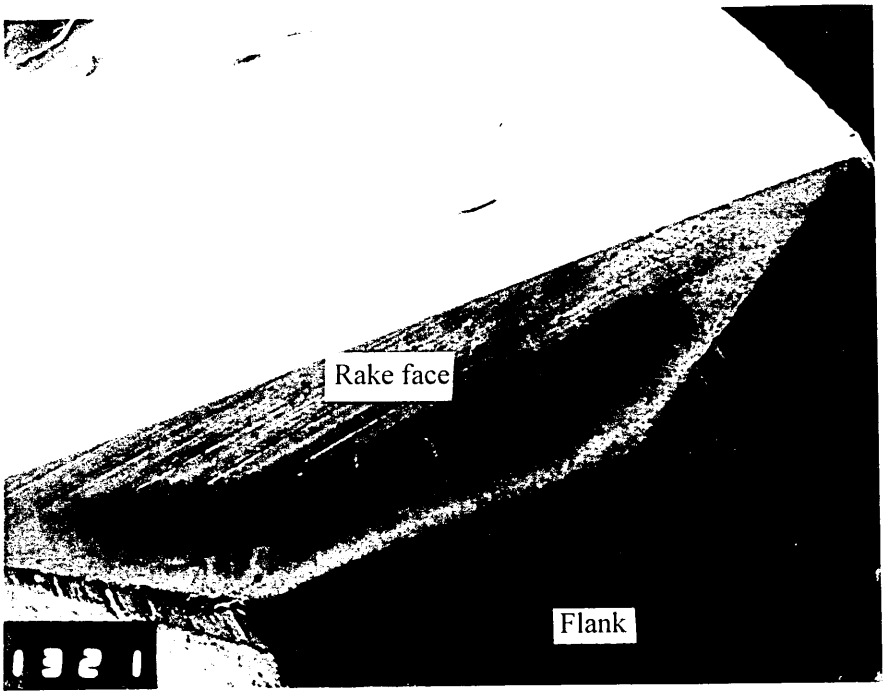

Figure 4.30 Crater wear and flank wear produced when sawing mild steel with segment type A1

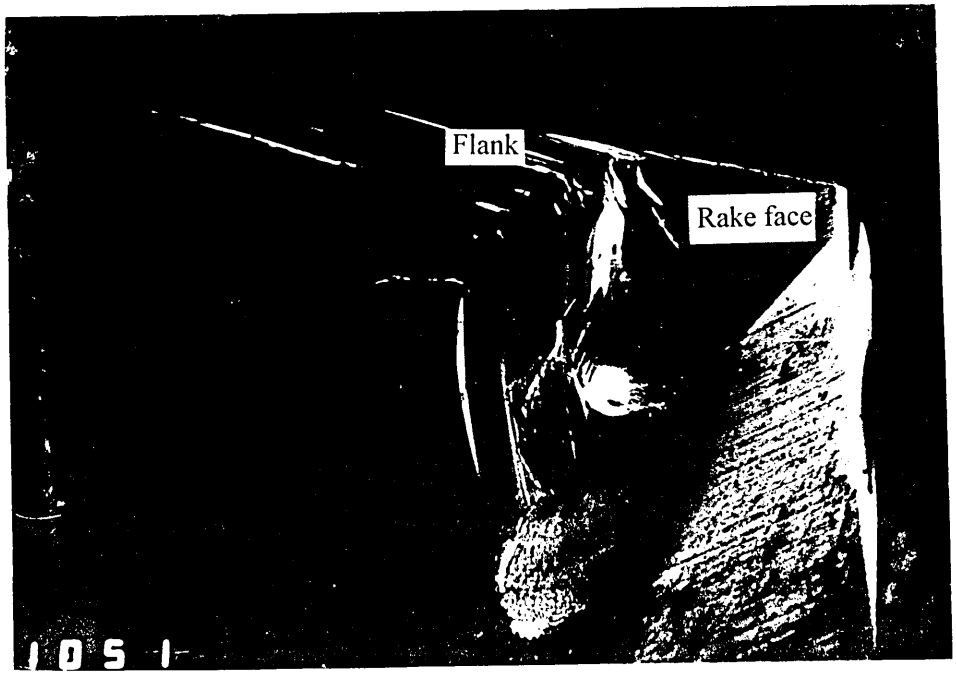

Figure 4.31 The breakage produced on the top of finishing tooth when sawing mild steel with segment type A1

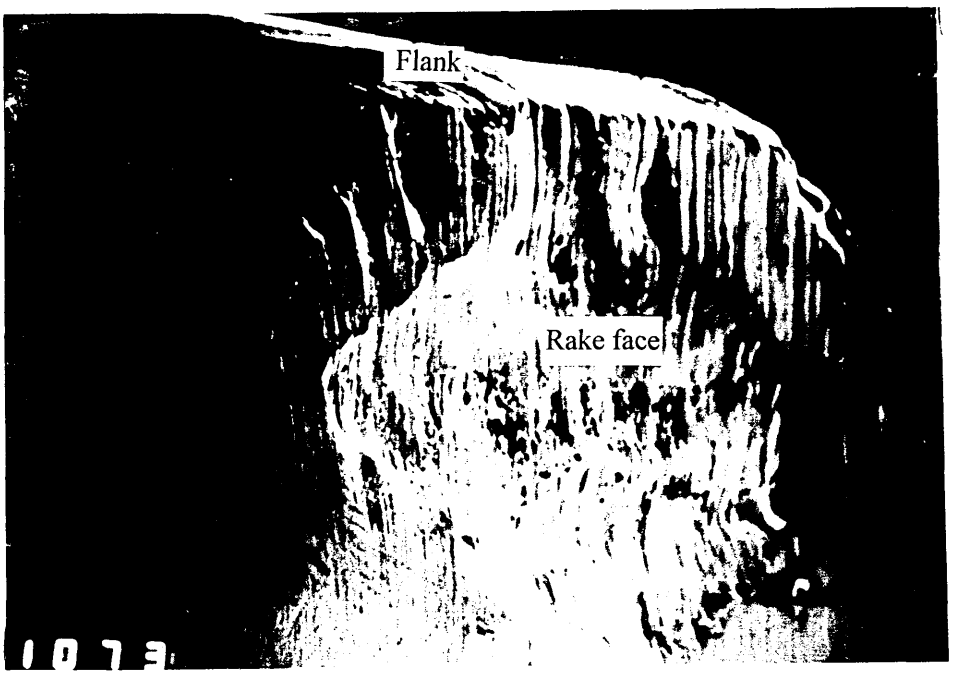

Figure 4.32(a) The crater wear and edge chipping produced on the rake face of roughing tooth when sawing mild steel with segment type A2

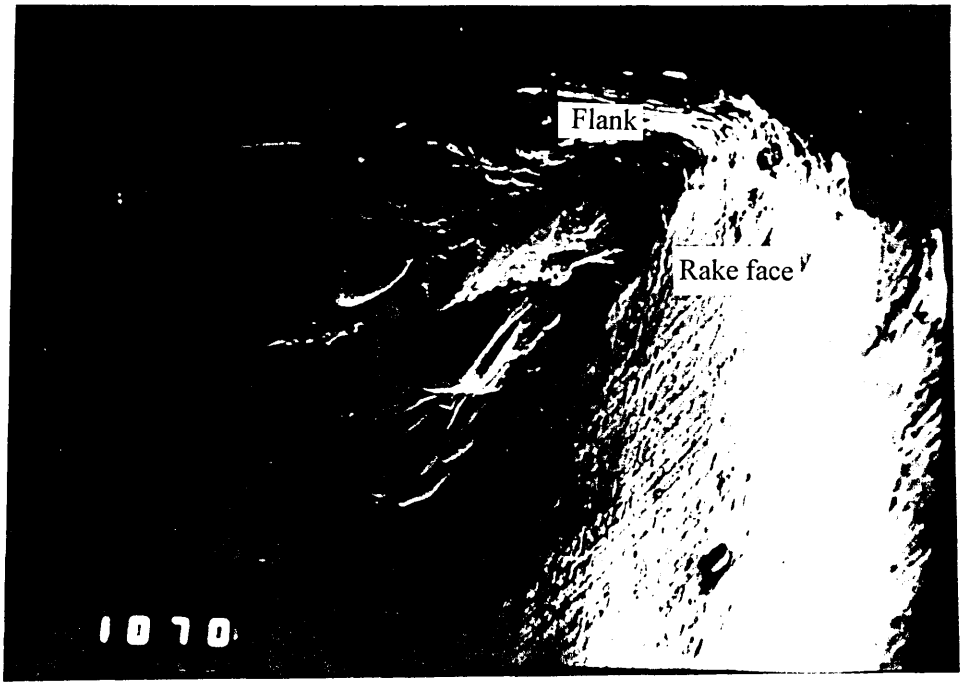

Figure 4.32(b) The large edge chipping occurred on the roughing tooth of segment B1

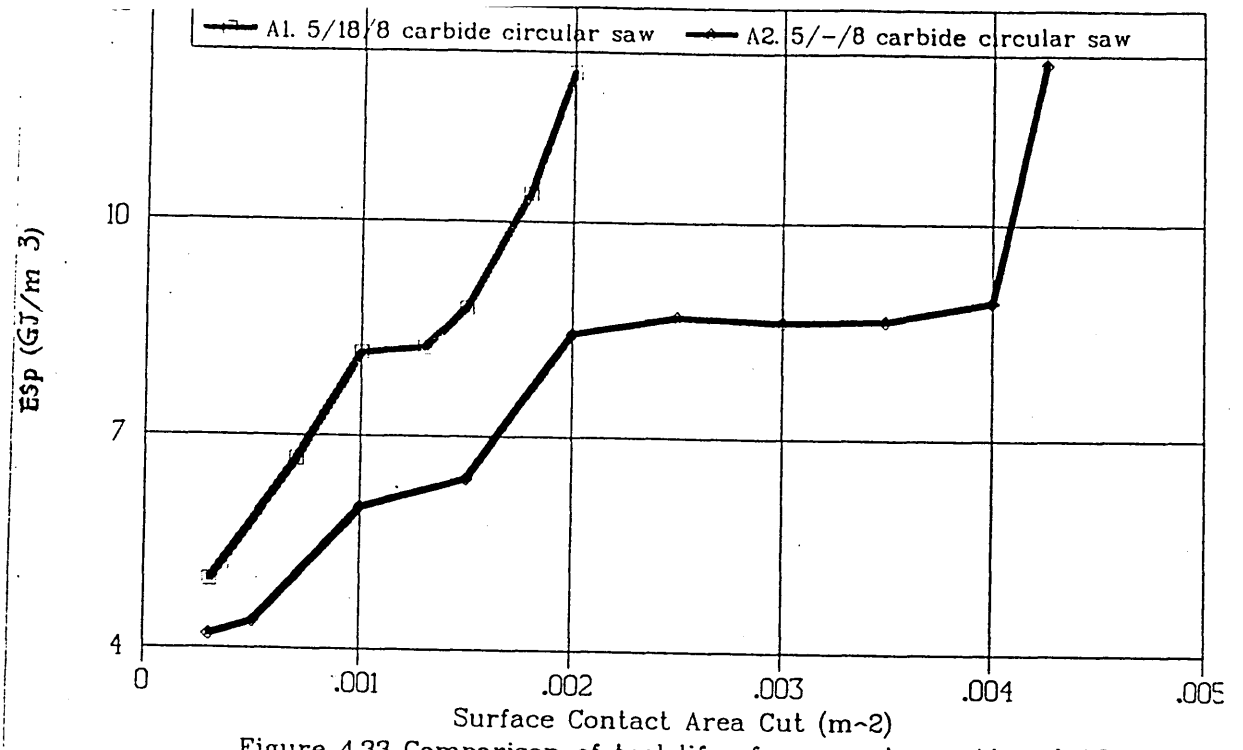

Figure 4.33 Comparison of tool life of segmen types A1 and A2
Cutting Speed : 34 m/min, Cutting condition: Dry
Feed/ Pair of teeth: 0.046 mm/rev., Work Material : 302S25

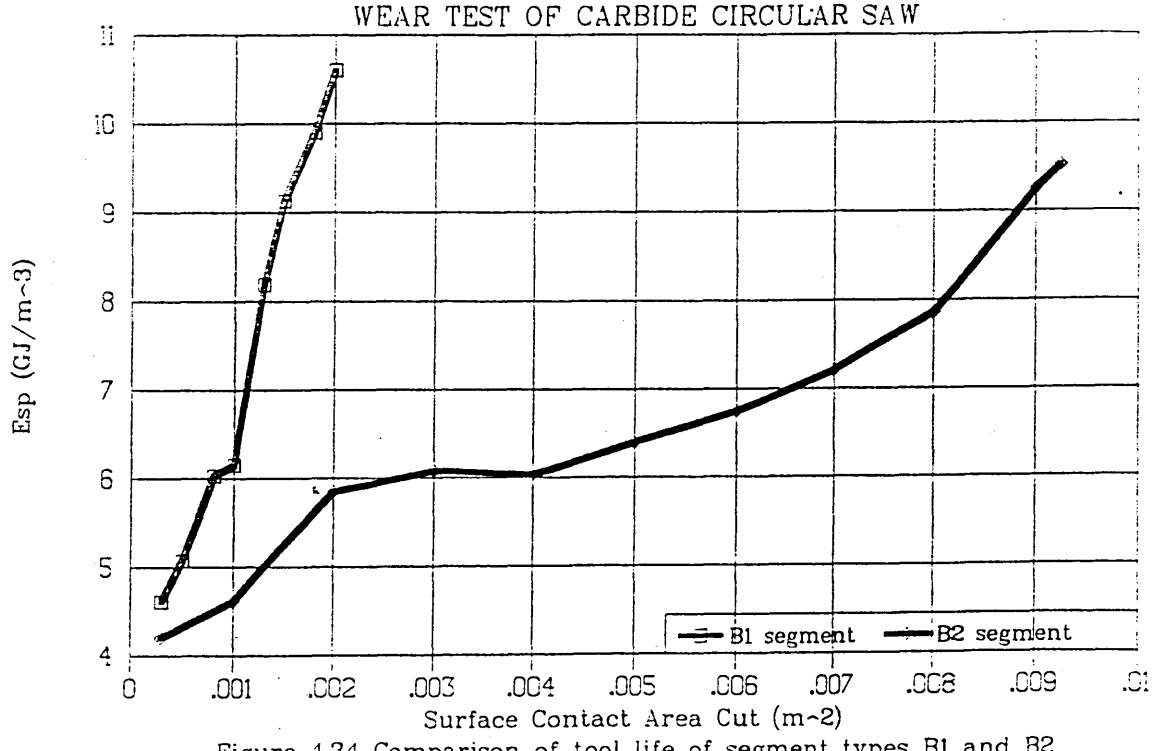

Figure 4.34 Comparison of tool life of segment types B1 and B2
Cutting Speed: 34 m/min, Cutting condition: Dry
Feed/ Pair of teeth: 0.046 mm/rev., Work Material : 302S25

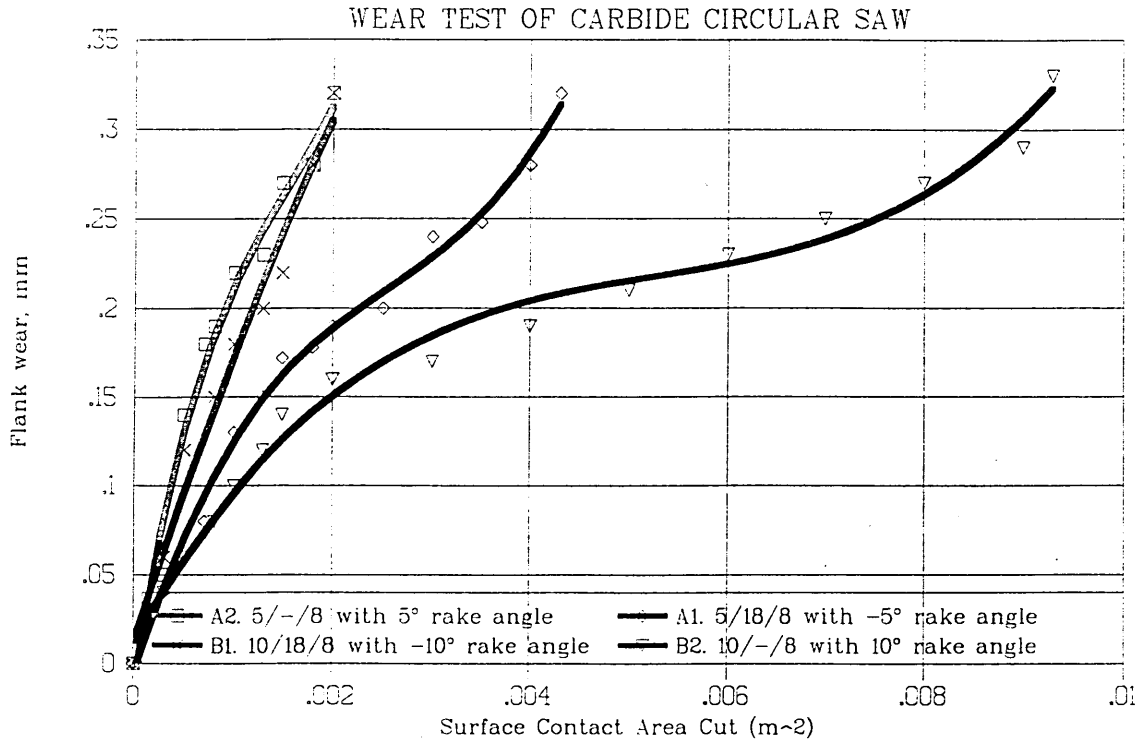

Figure 4.35 Flank wear of uncoated segment types A1, A2, B1 and B2
Cutting Speed : 34 m/min, Cutting condition: Dry
Feed/ Pair of teeth: 0.046 mm/rev., Work Material : 302S25

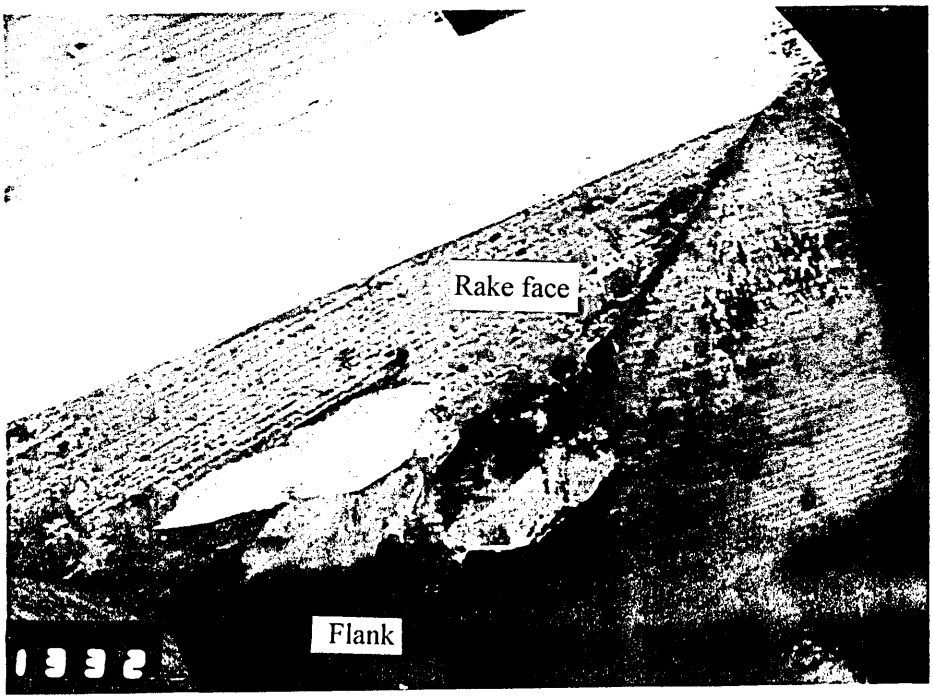

Figure 4.36 The edge chipping on roughing tooth produced when sawing 302S25 stainless steel with segment type A1

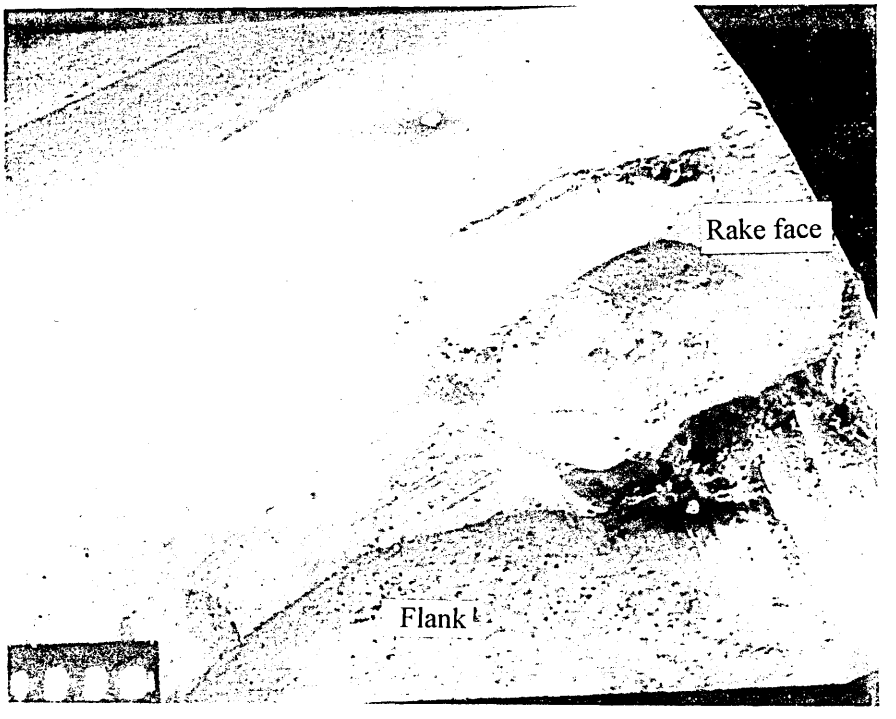

Figure 4.37 The bevel and edge chipping produced on finishing tooth when sawing 302S25 stainless steel with segment type A2

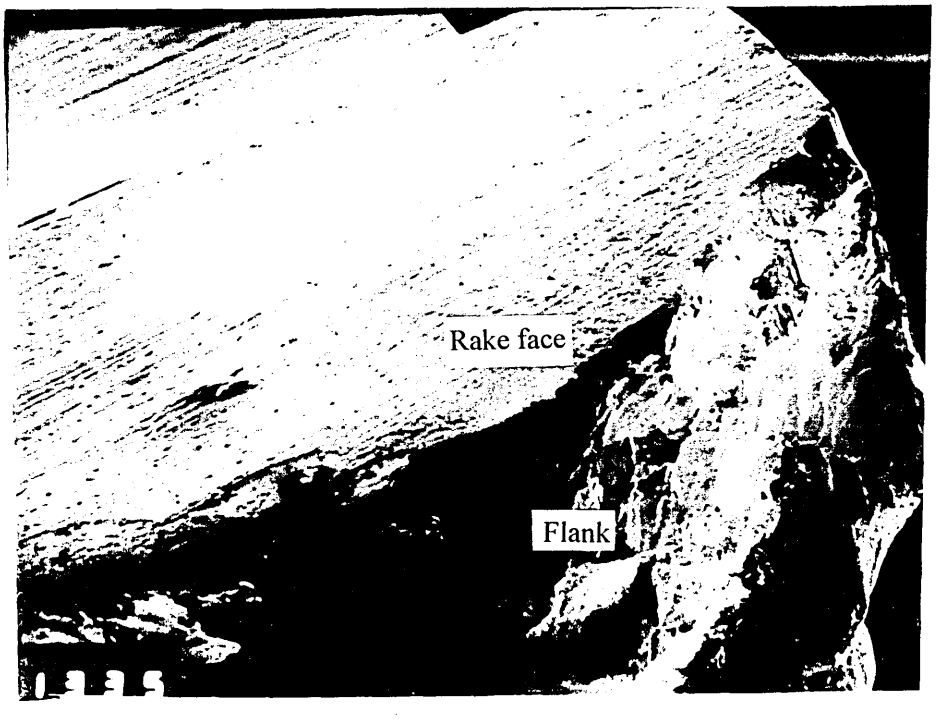

Figure 4.38 The large chipping on roughing tooth produced when sawing 302S25 stainless steel with segment type B1

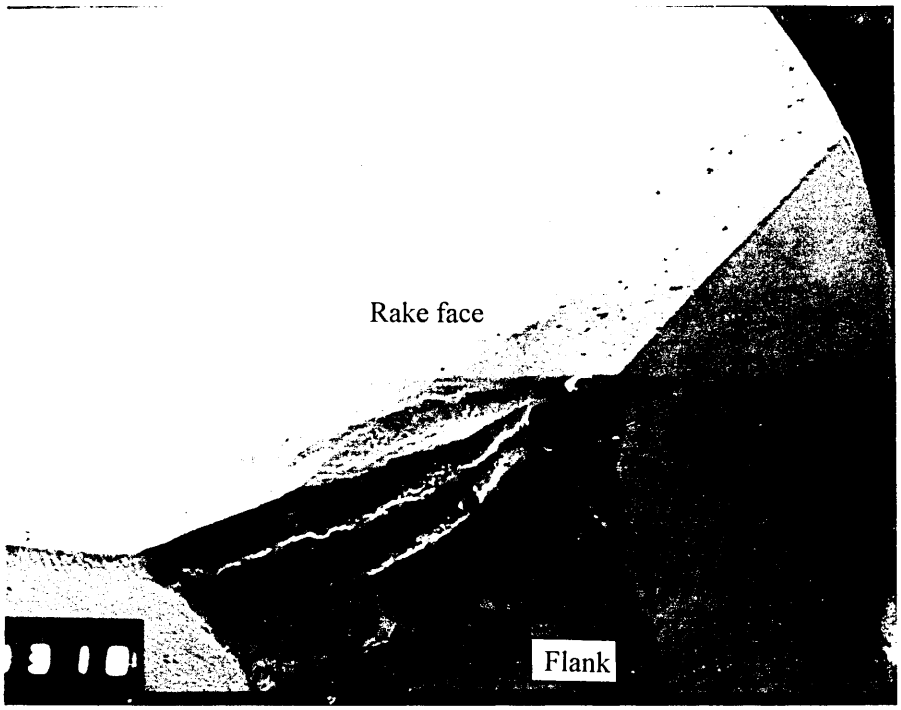

Figure 4.39 The cutting edge chipping on roughing tooth produced when sawing 302S25 stainless steel with segment type B2

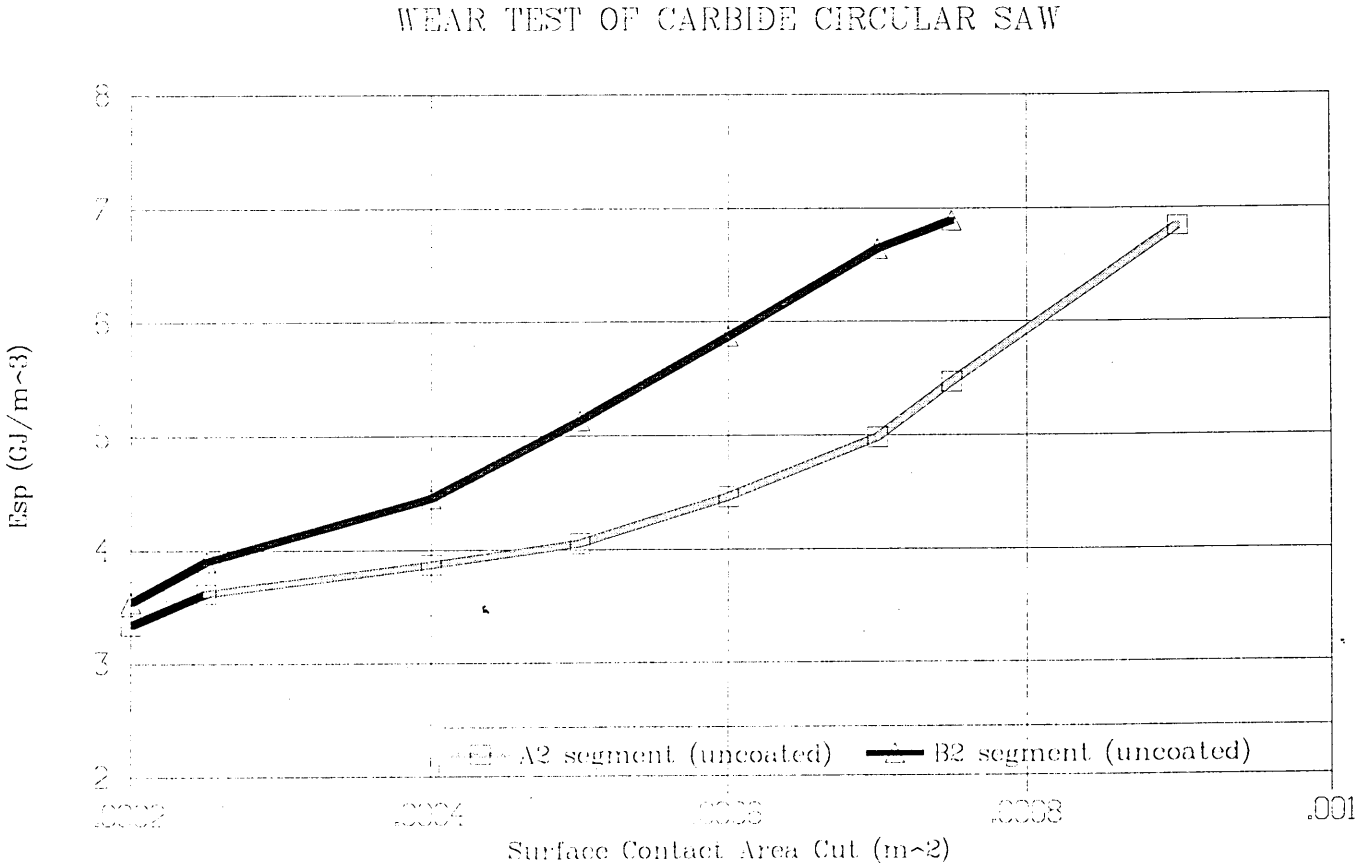

Figure 4.40 Comparison of tool life of uncoated segments
Cutting Speed : 29 m/min. Cutting condition: Dry
Feed / Pair of teeth: 0.045 mm/rev., Work Material : C25 Nimonic Alloy

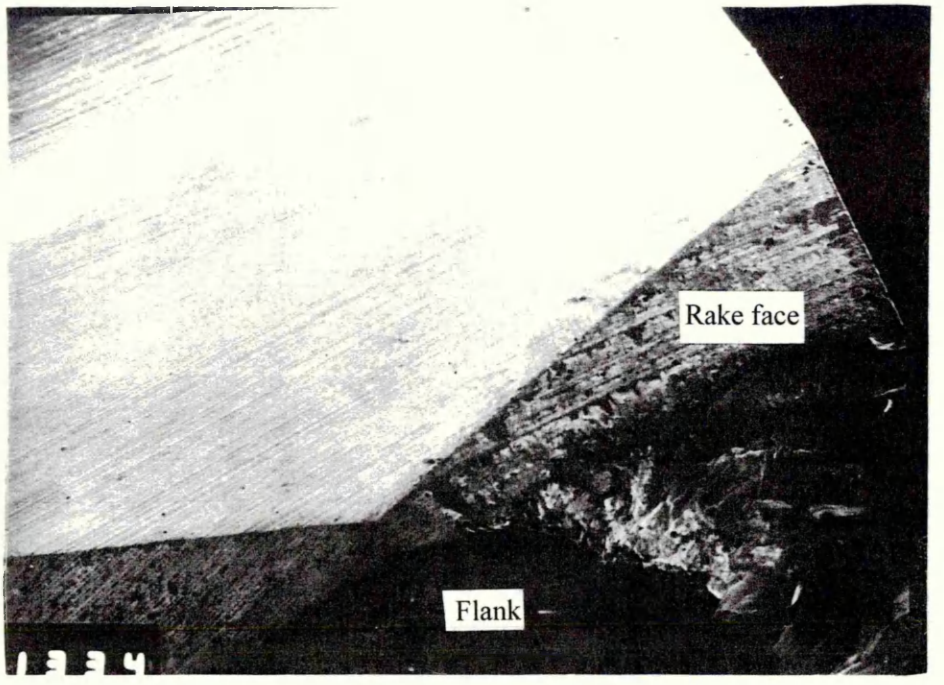

Figure 4.41 Edge chipping on the finishing tooth when sawing C25 nimonic alloy with segment type A2

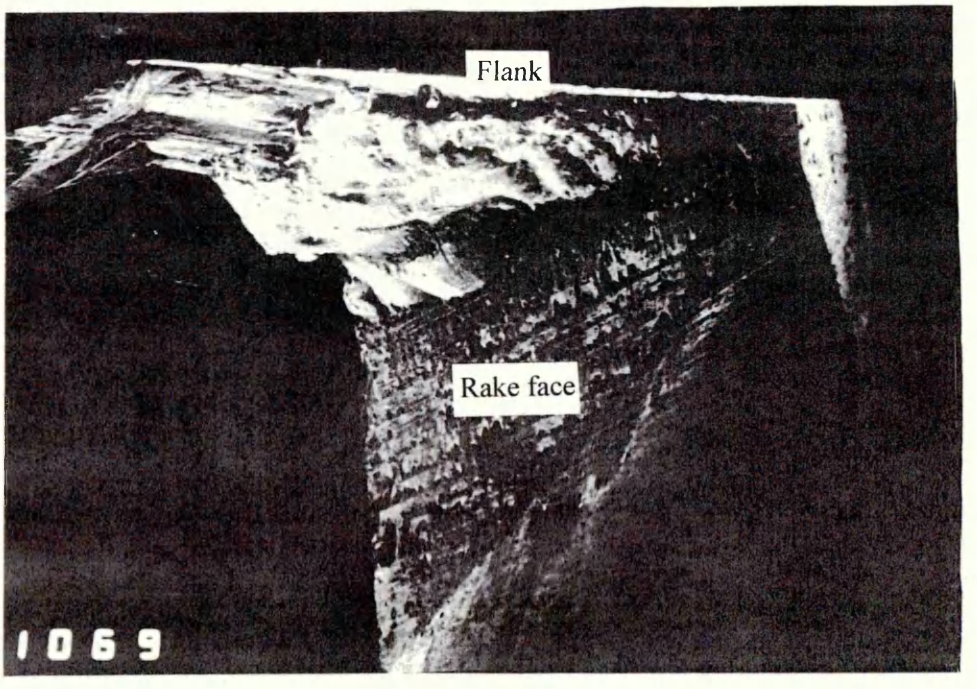

Figure 4.42 Edge chipping on the finishing tooth when sawing C25 nimonic alloy with segment type B2

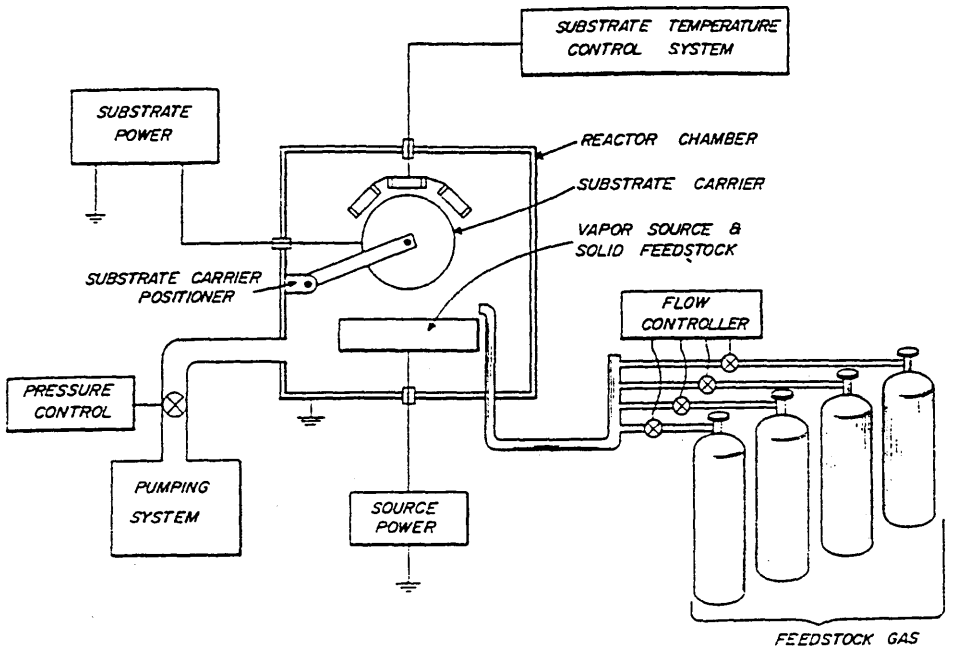

Figure 5.1 The typical schematic PVD system

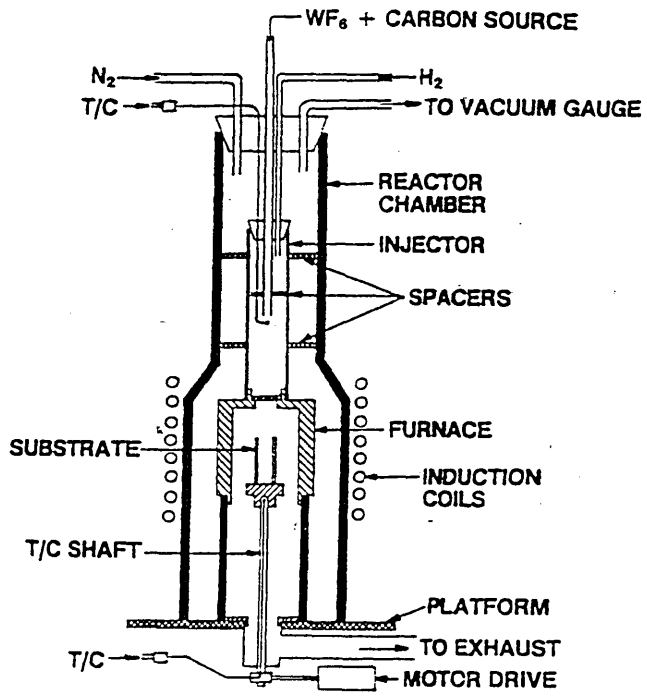

Figure 5.2 The typical schematic CVD system

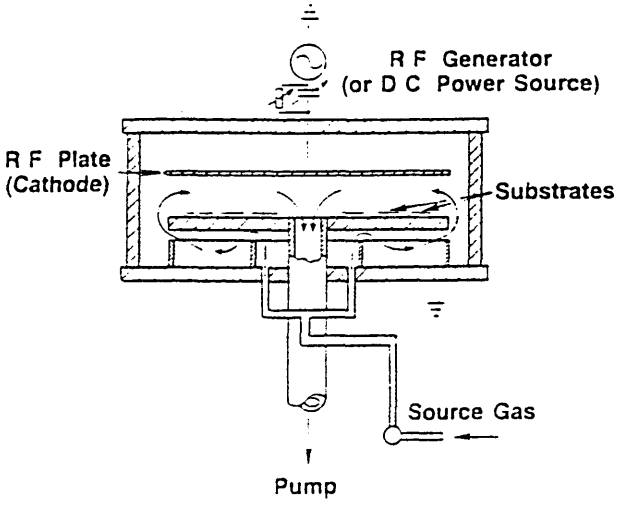

Figure 5.3 The typical schematic PCVD system

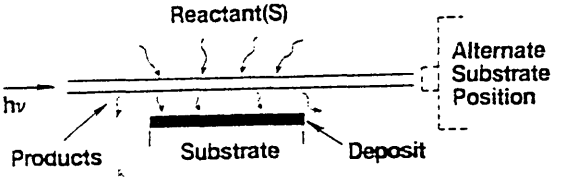

Figure 5.4 The typical schematic LCVD system

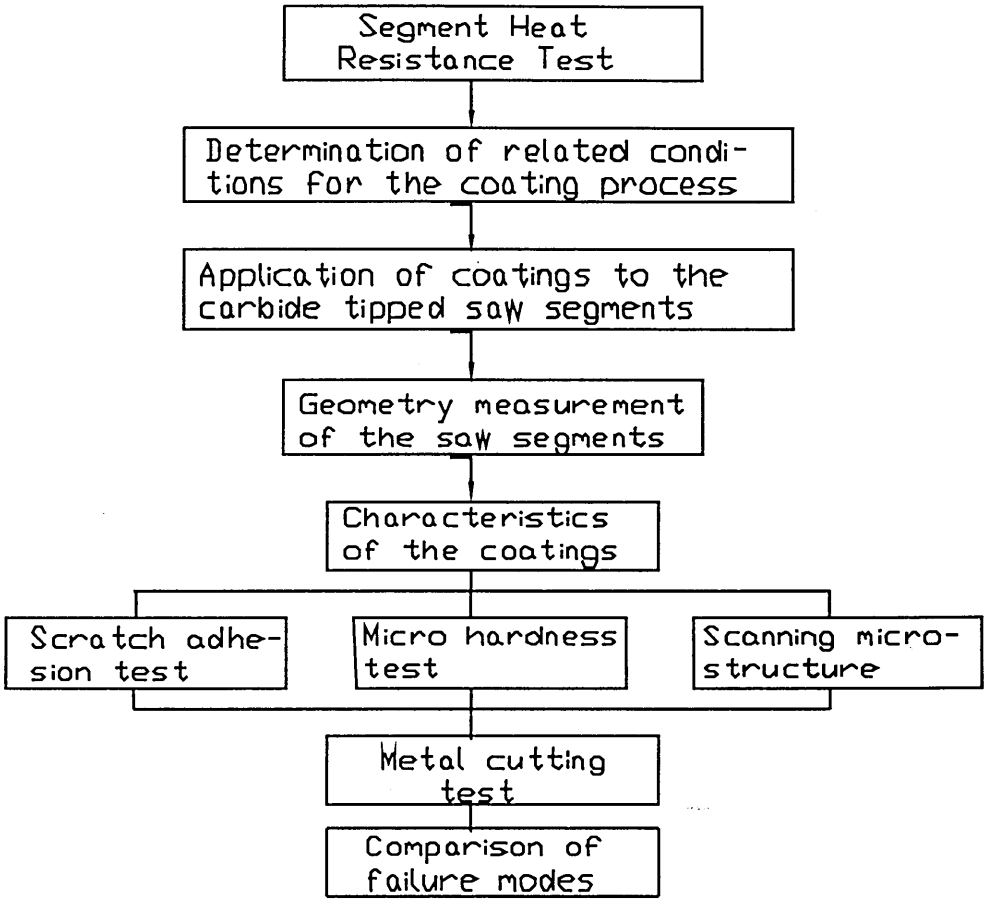

Figure 5.5 Experimental procedure for the application of coatings to the carbide substrates

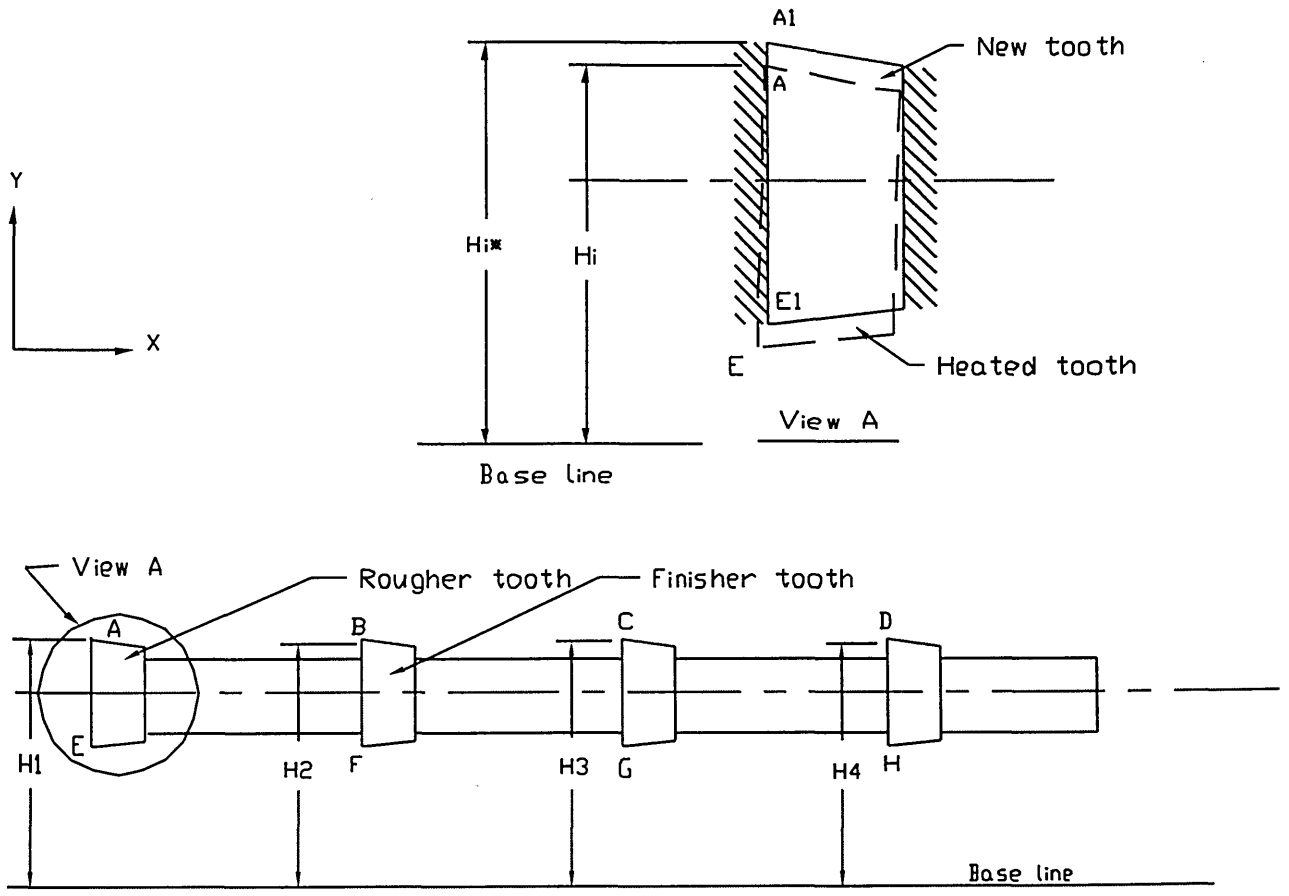

5.6

Figure 5.6 Top view of carbide tipped circular saw segment

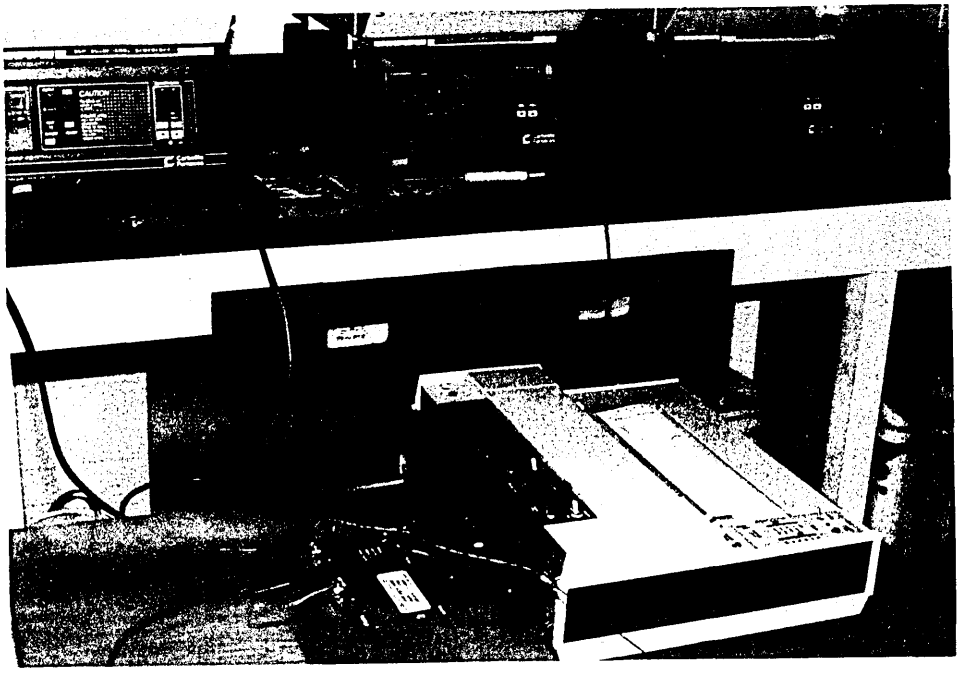

Figure 5.7 Carbolet furnace SW2 and the related temperature equipments

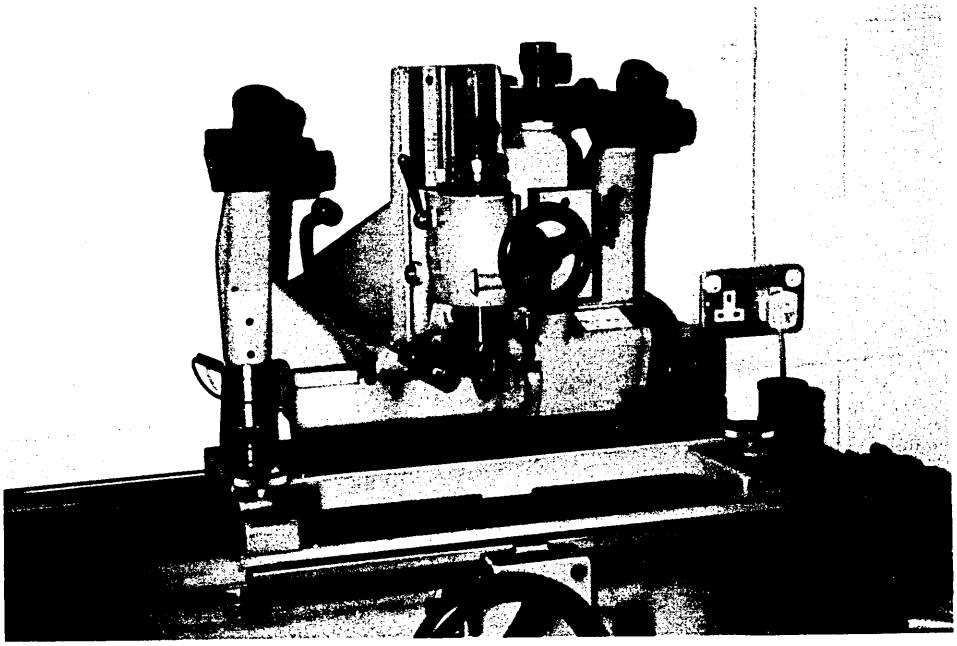

Figure 5.8 MU-214B Societe Genevoise used for measurement of saw segment geometry

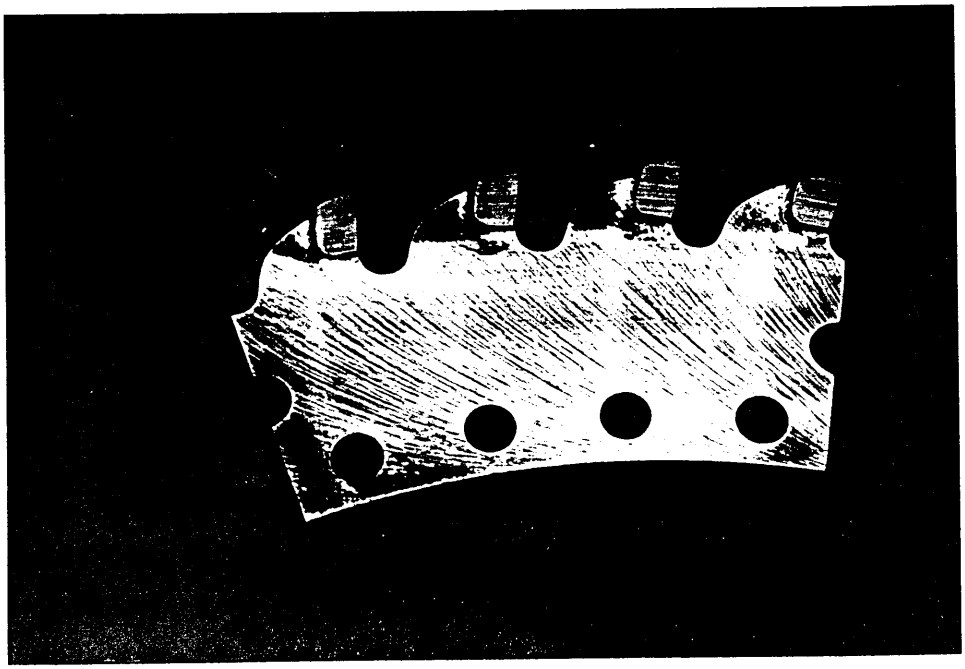

Figure 5.9 The segment after heat treatment at 450°C for two and half hours

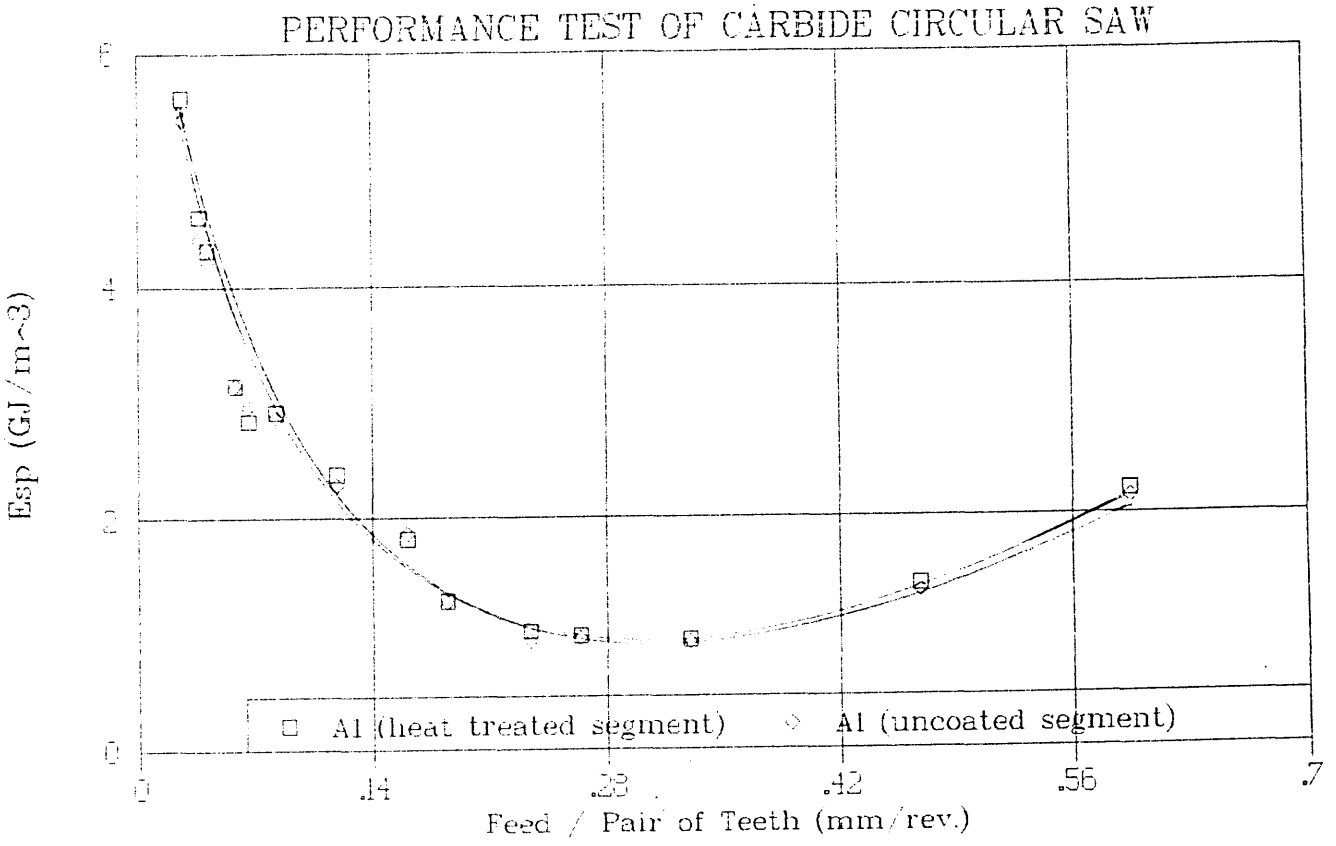

Figure 5.10 Comparison of performance of heated and unheated segments when cutting mild steel, Cutting speed: 203 m/min, Cutting condition: Dry

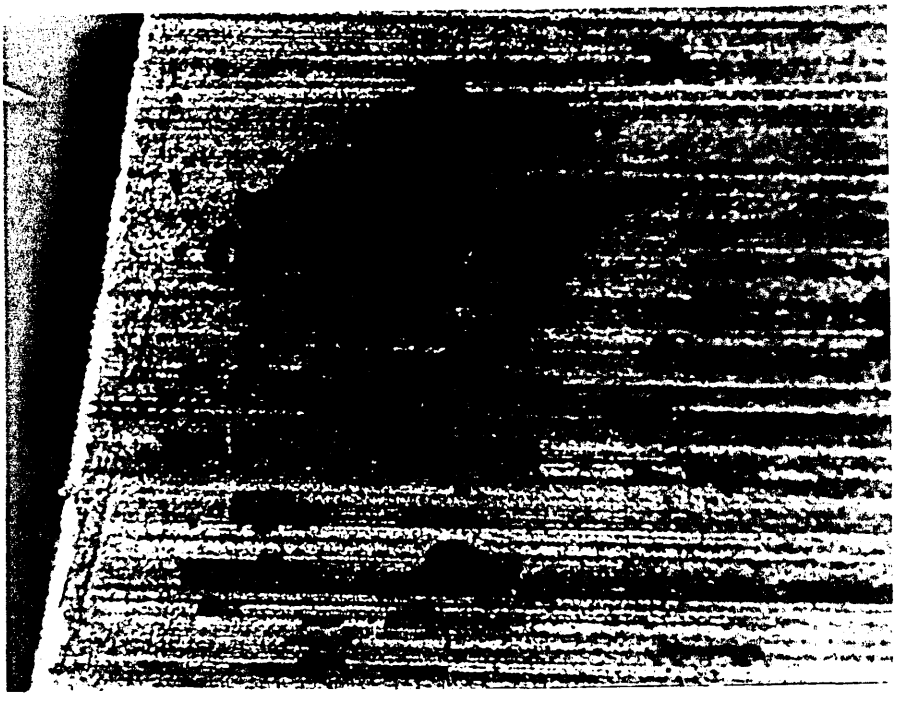

Figure 5.11(a) The coating produced at the working temperature of 300°C

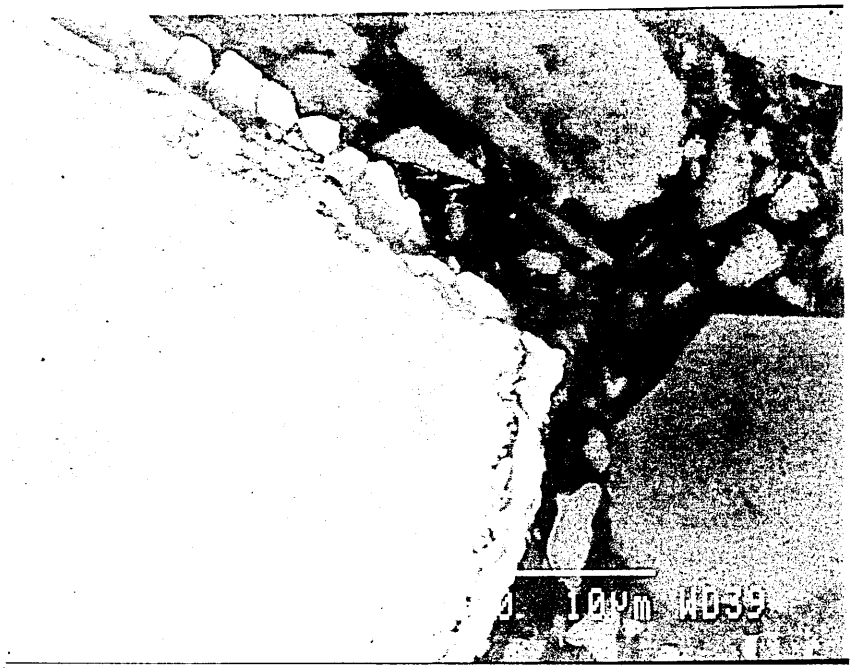

Figure 5.11(b) The cross section of the coating poorly bonded on the carbide substrate

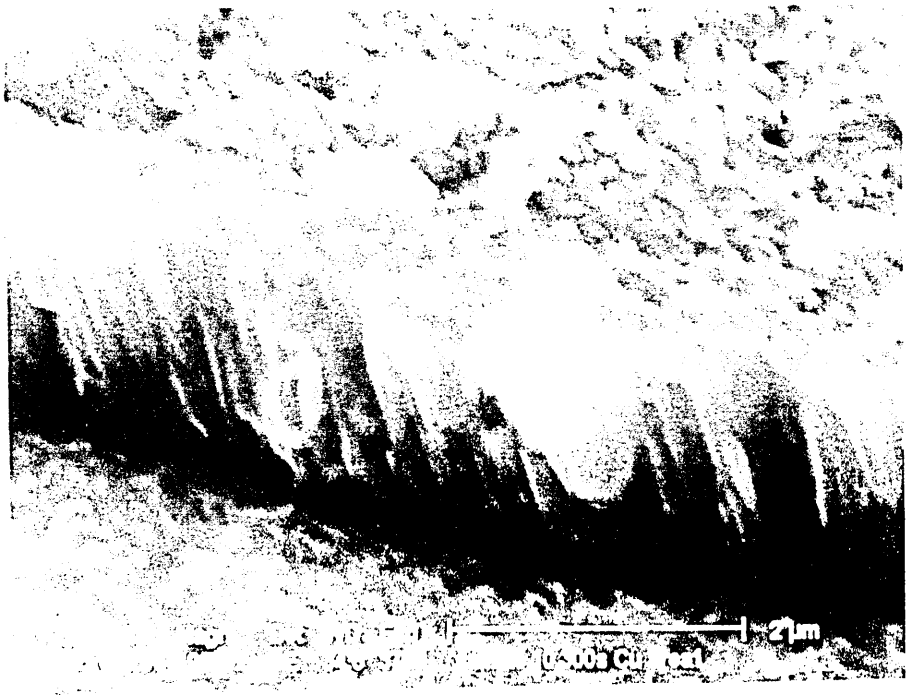

Figure 5.11(c) The poor bonding condition between the coating and the substrate

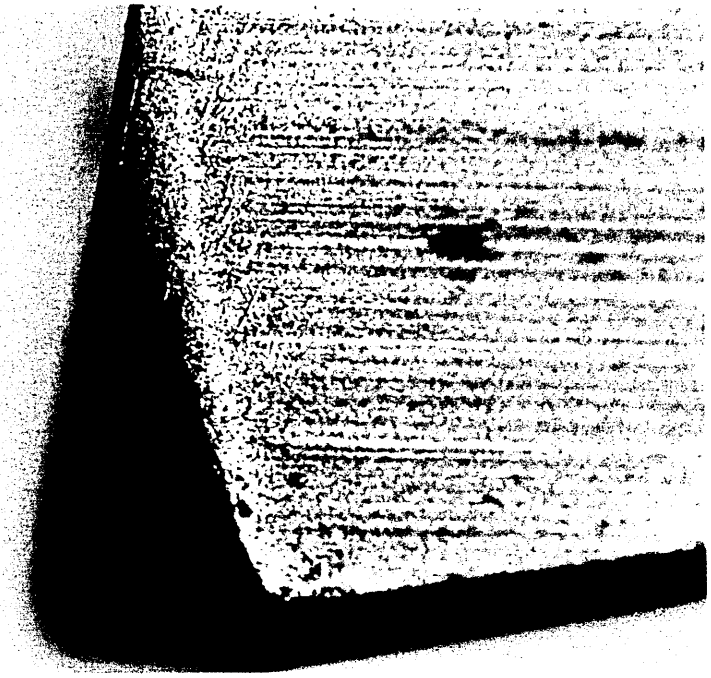

Figure 5.12(a) The coating produced at the working temperature of 400°C

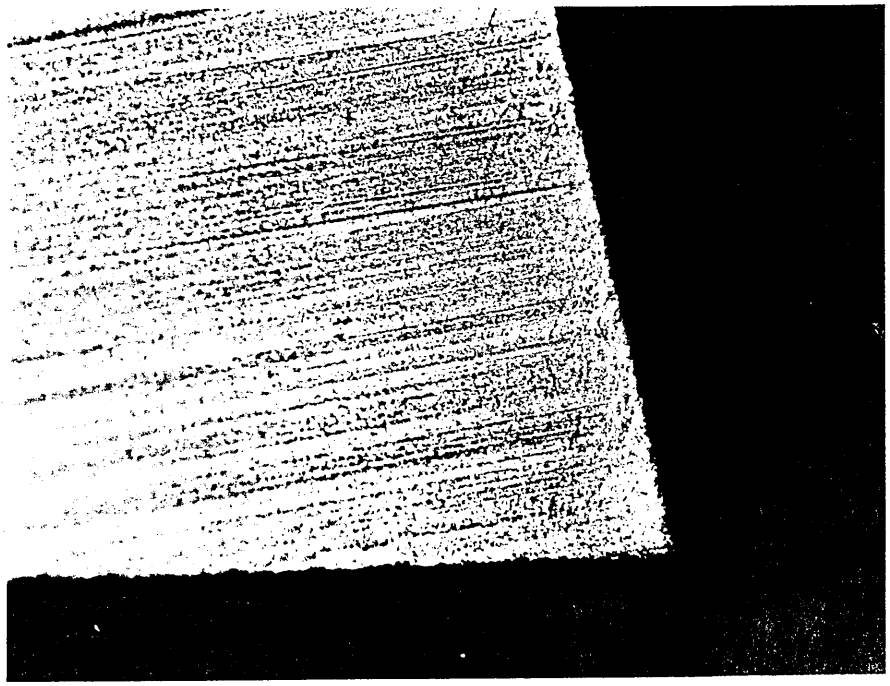

Figure 5.12(b) The coating produced at the working temperature of 450°C

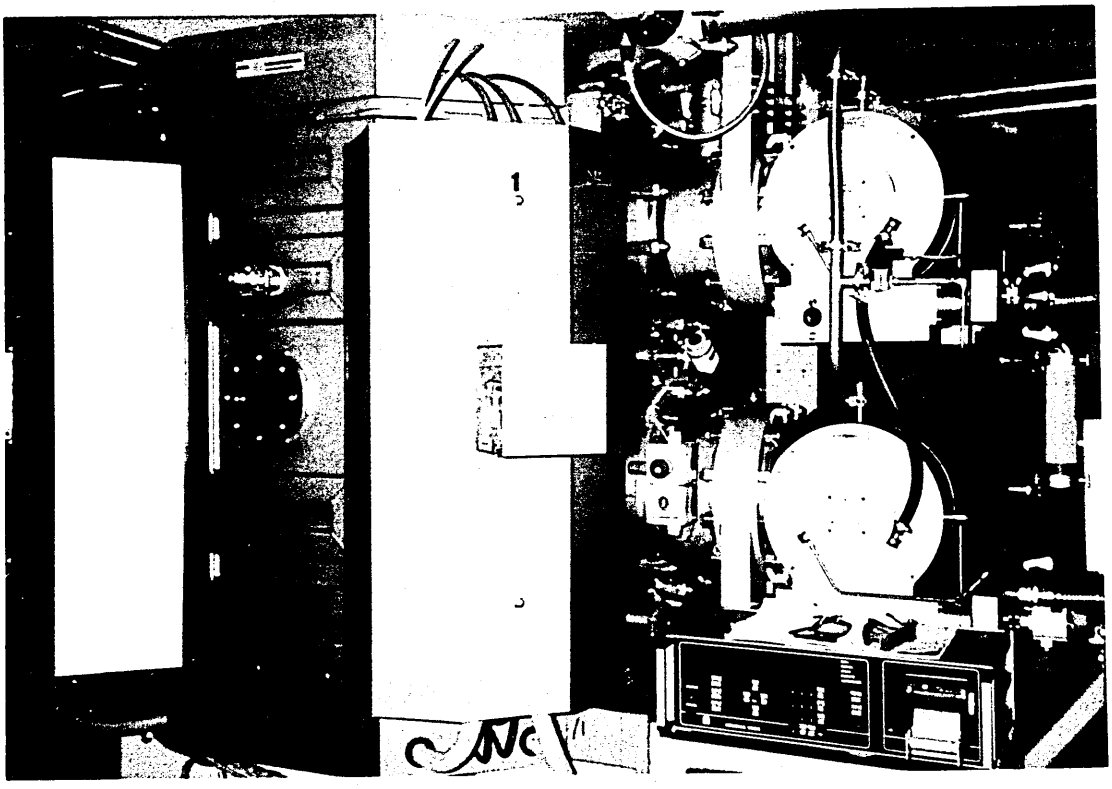

Figure 5.13 HTC 1000-4 ABS system which has four targets and was used for coating cutting tools

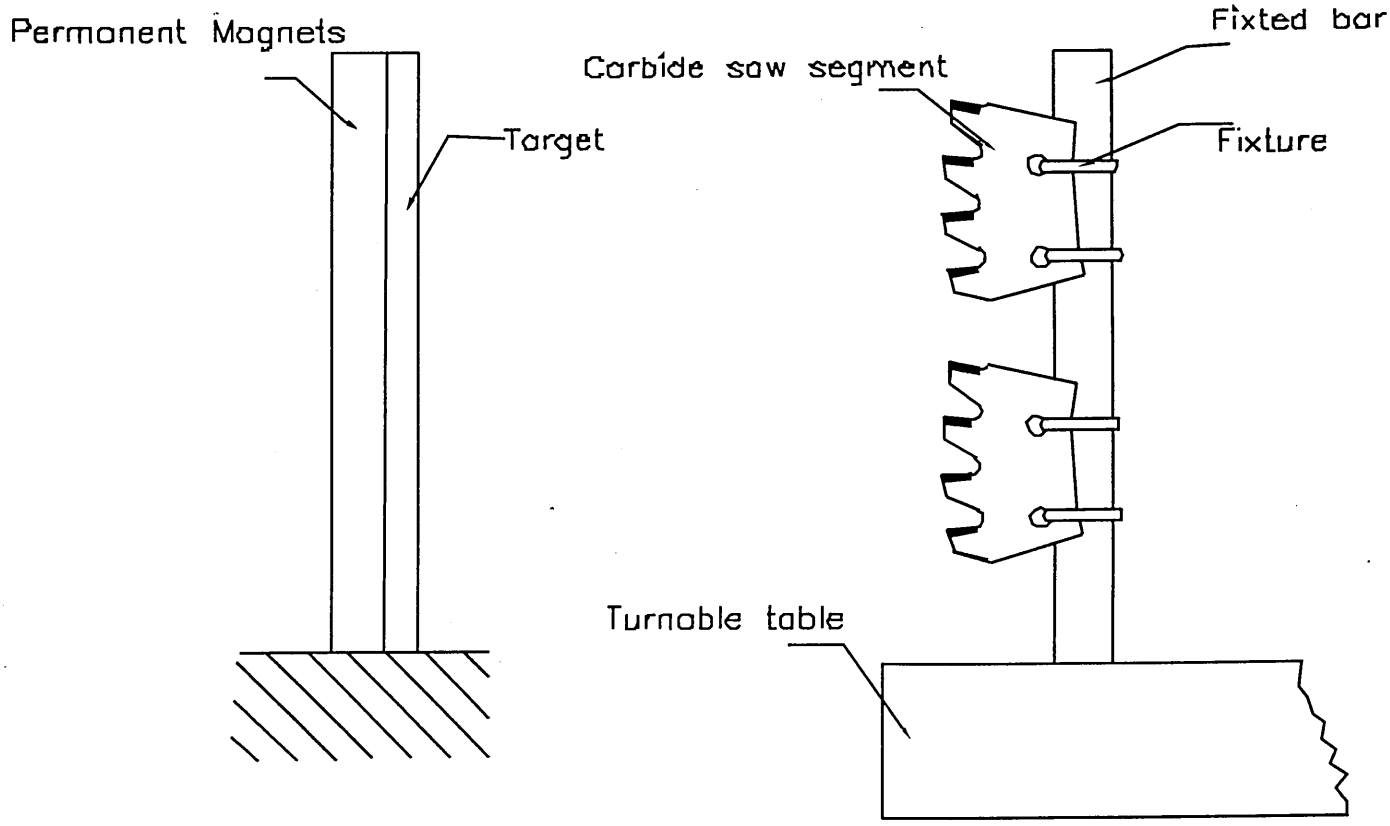

Figure 5.14 Substrate holder fixed on the turnable table

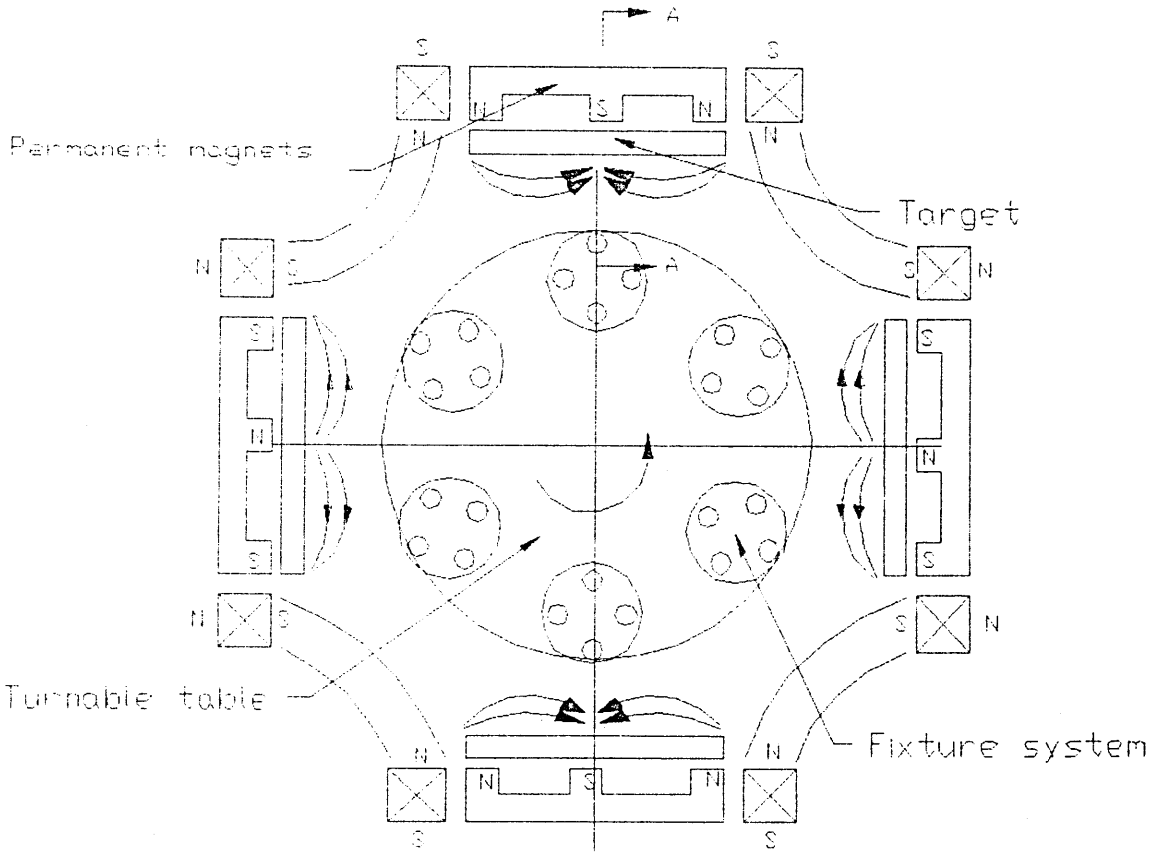

Figure 5.15 Multipolar magnet and rotate table arrangement

** For the A - A view see figure 5.14

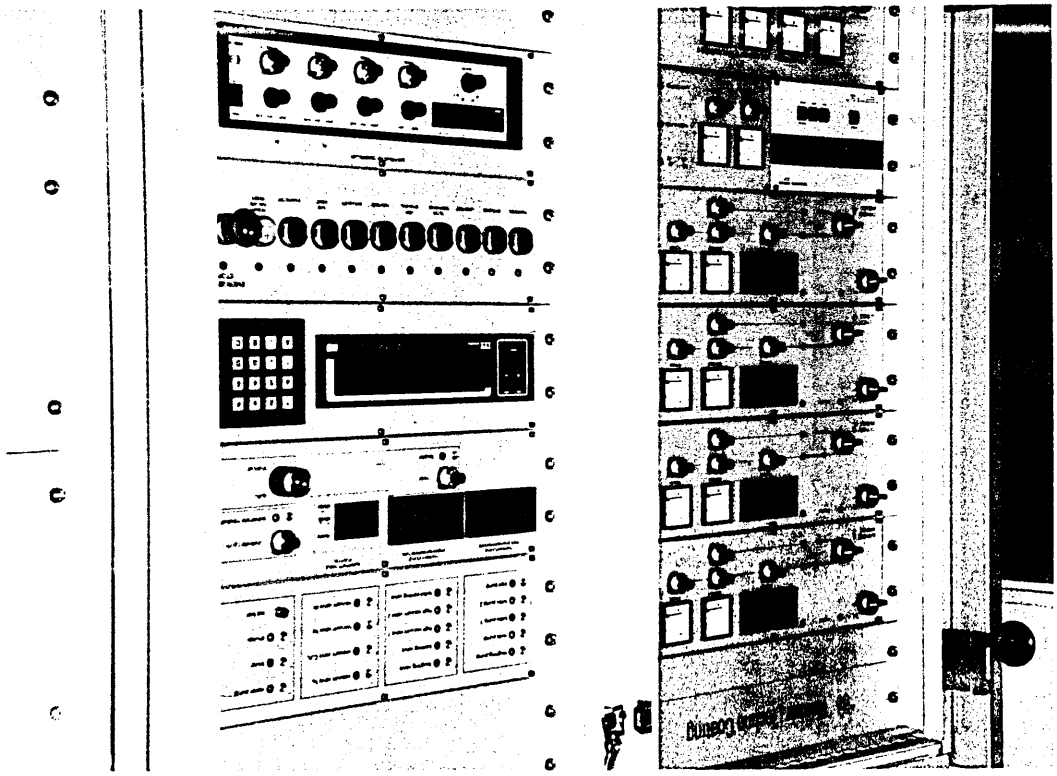

Figure 5.16 Mitsubishi SPS control system

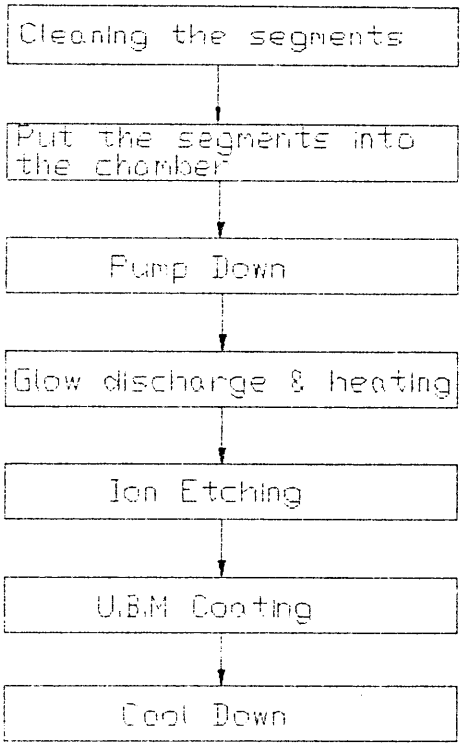

Figure 5.17 The coating process sequence

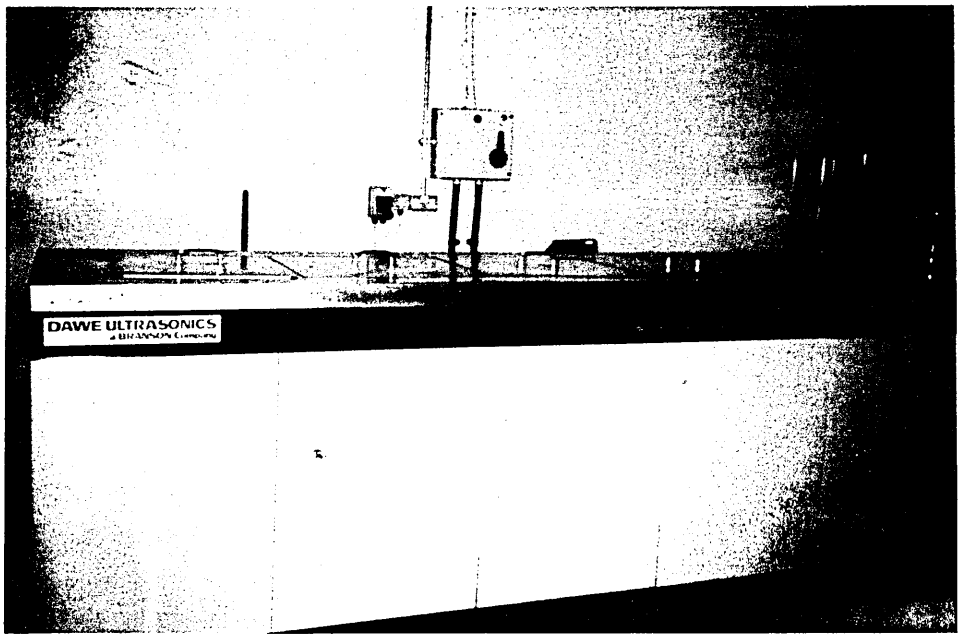

Figure 5.18 The vapour cleaning container for the substrate

Figure 5.19 The titanium nitride (TIN) coated segment produce by PVD technique

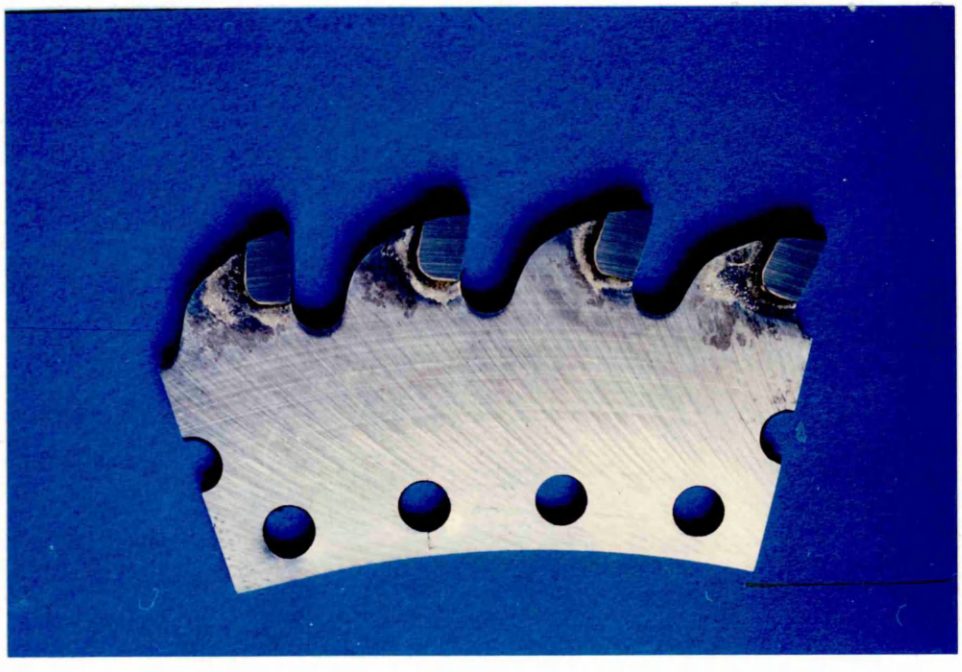

Figure 5.20 The titanium aluminium nitride (TiAlN) coated segment produce by PVD technique

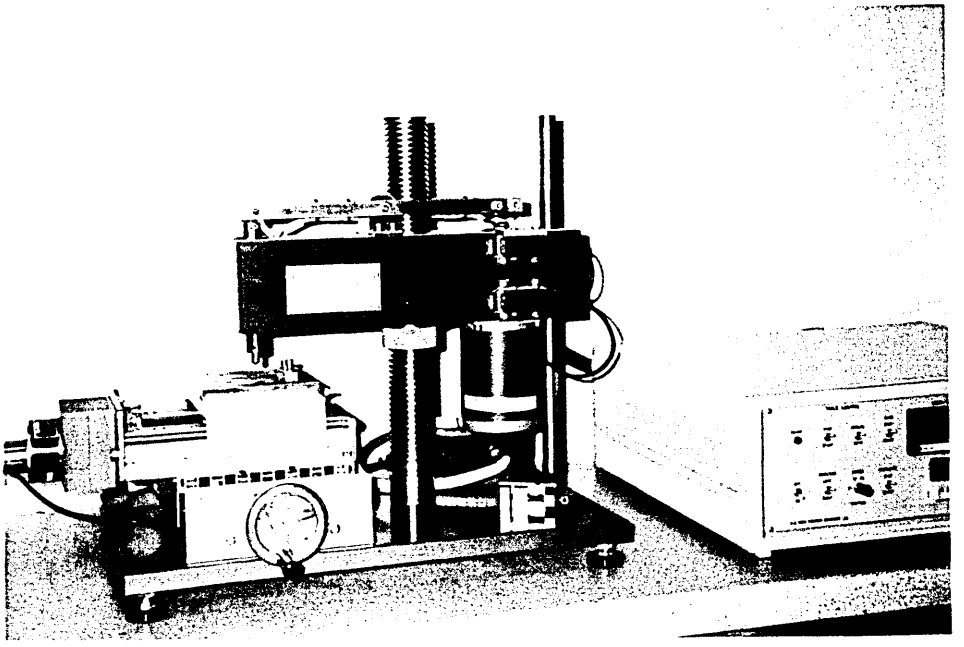

Figure 5.21 MEGATECH ST-200 Scratch Adhesion Tester

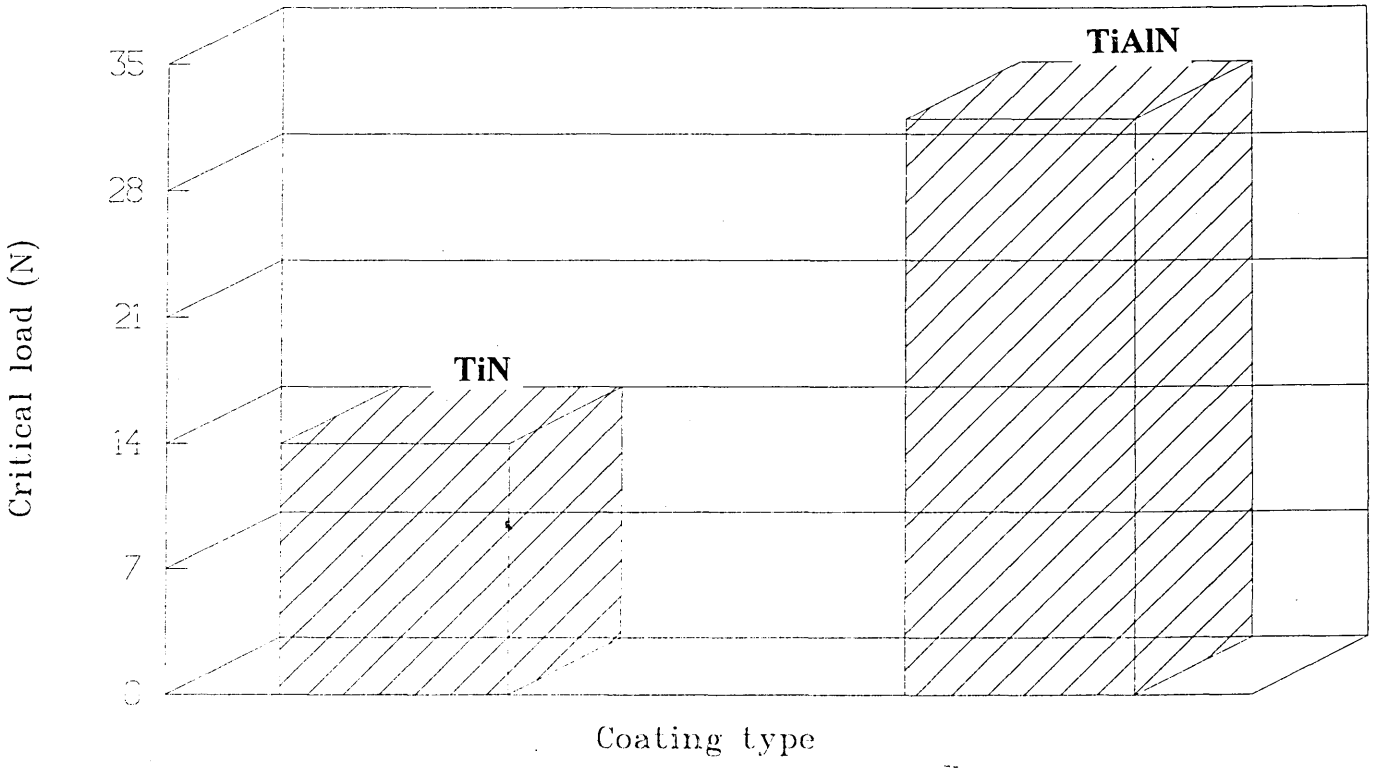

Figure 5.22 The critical load for the coating failure

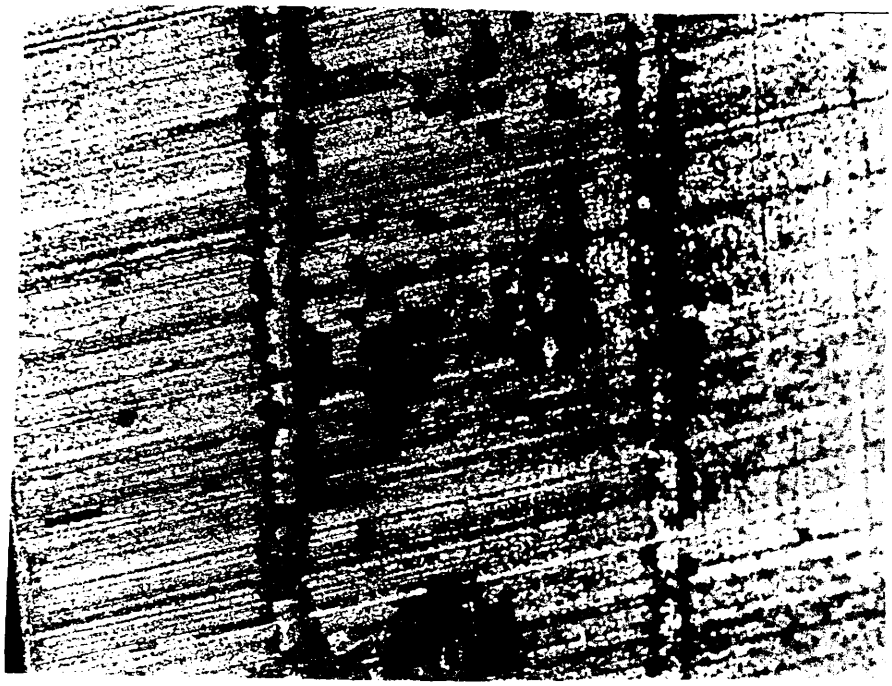

Figure 5.23 For TiN coating, the extensive cracking and spallation of the coating produced outside the scratch channel.

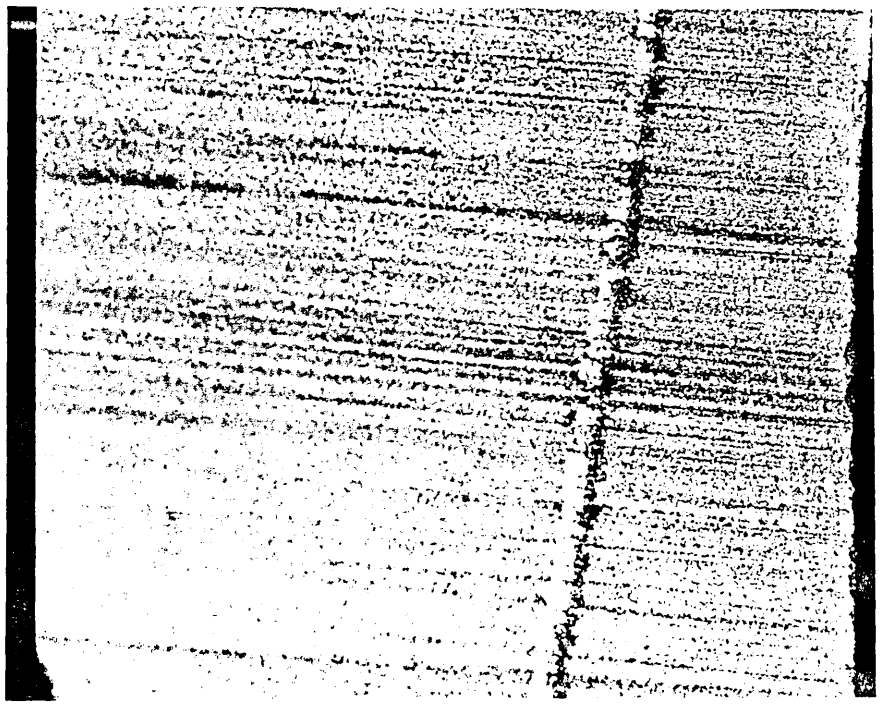

Figure 5.24 The scratch channel for the TiAlN coating showing no signs of coating spallation along the its scratch length.

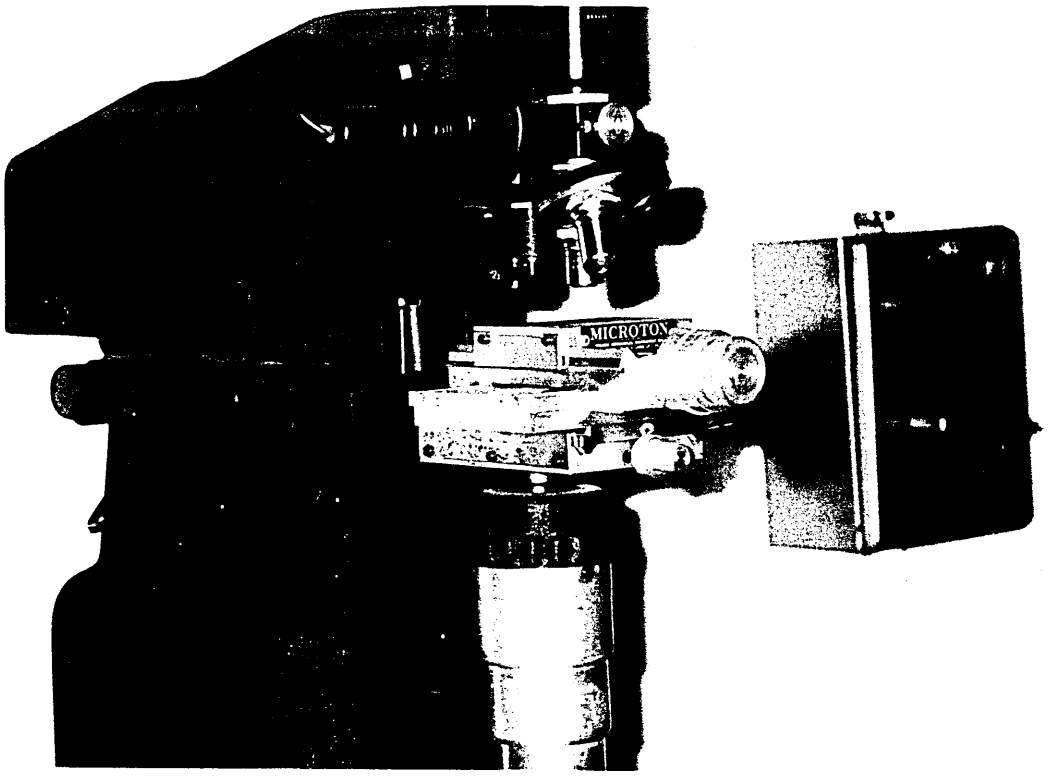

Figure 5.25 Microhardness Tester

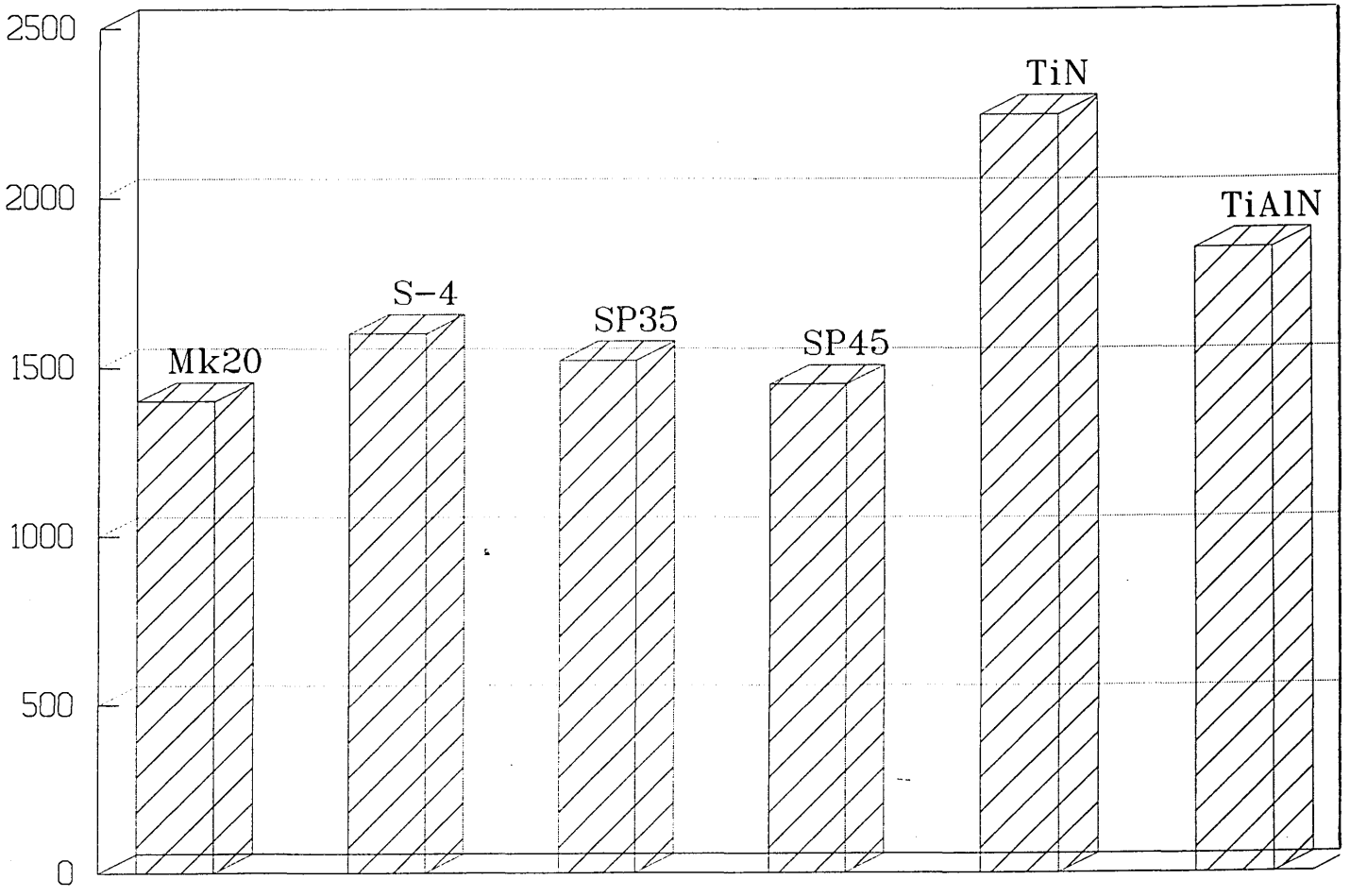

Figure 5.26 Comparison of hardness of the coatings and substrates (20 Kg load for substrate, 15 g load for coatings)

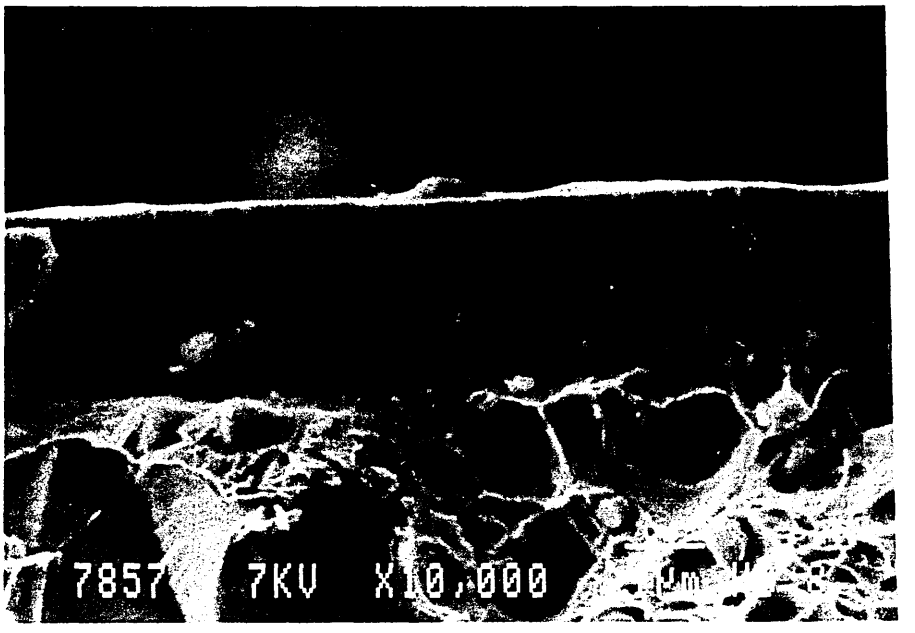

Figure 5.27 The cross structure of the TiN coating

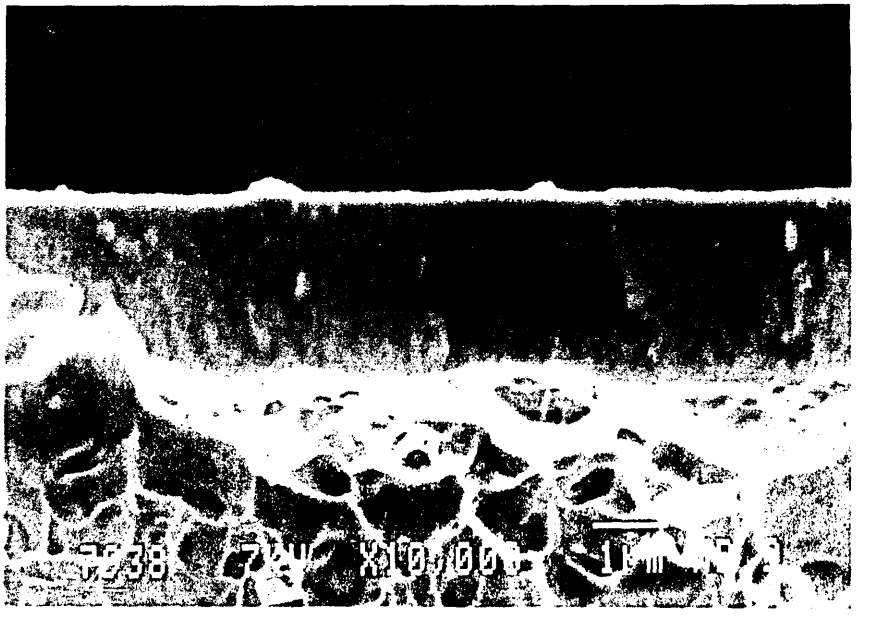

Figure 5.28 The cross structure of the TiAlN coating

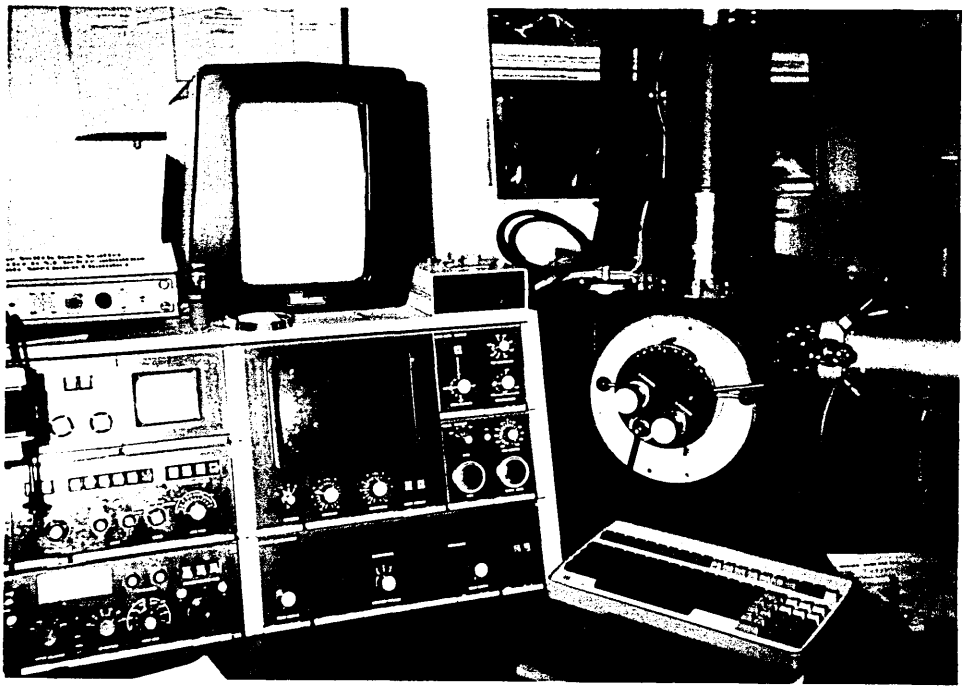

Figure 5.29 SEM 500 Scanning Electron Microscope used for the general view of the segments

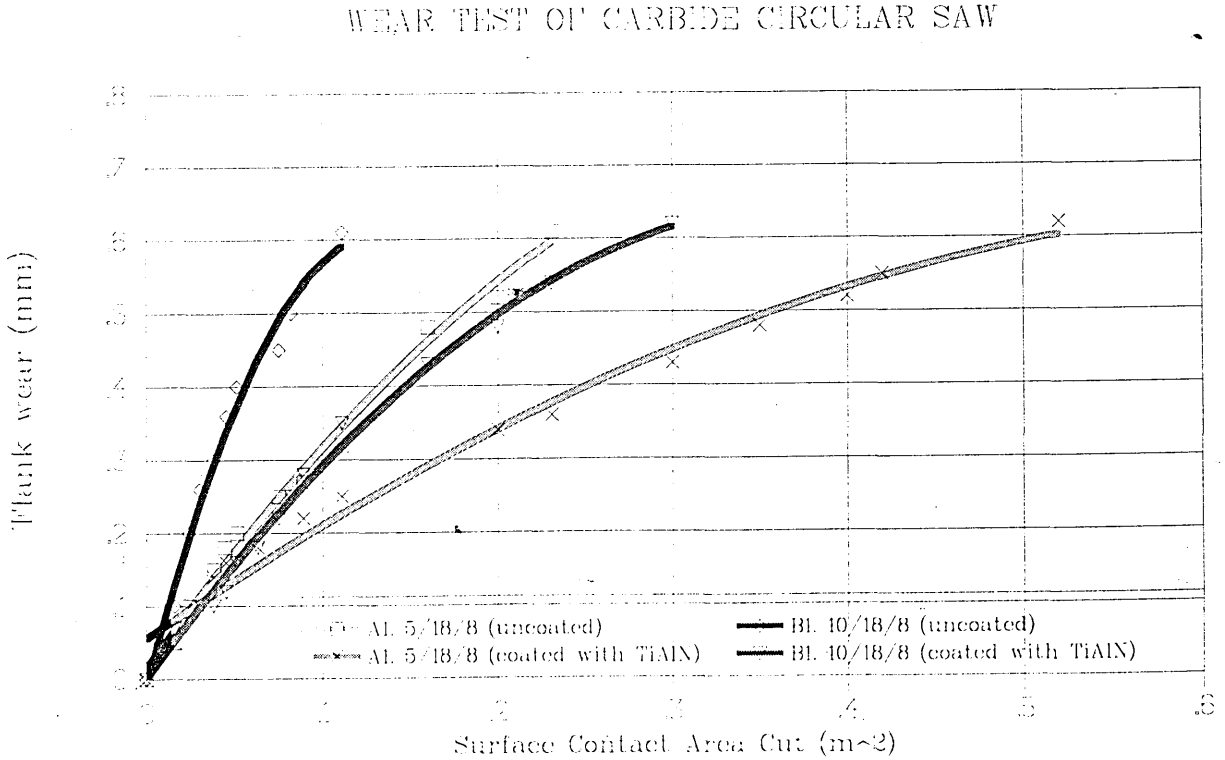

Figure 5.30 Comparison of flank wear when cutting mild steel
Cutting Speed : 203 m/min, Cutting condition: Dry
Feed/ Pair of teeth: 0.355 mm/rev., Work Material : MS

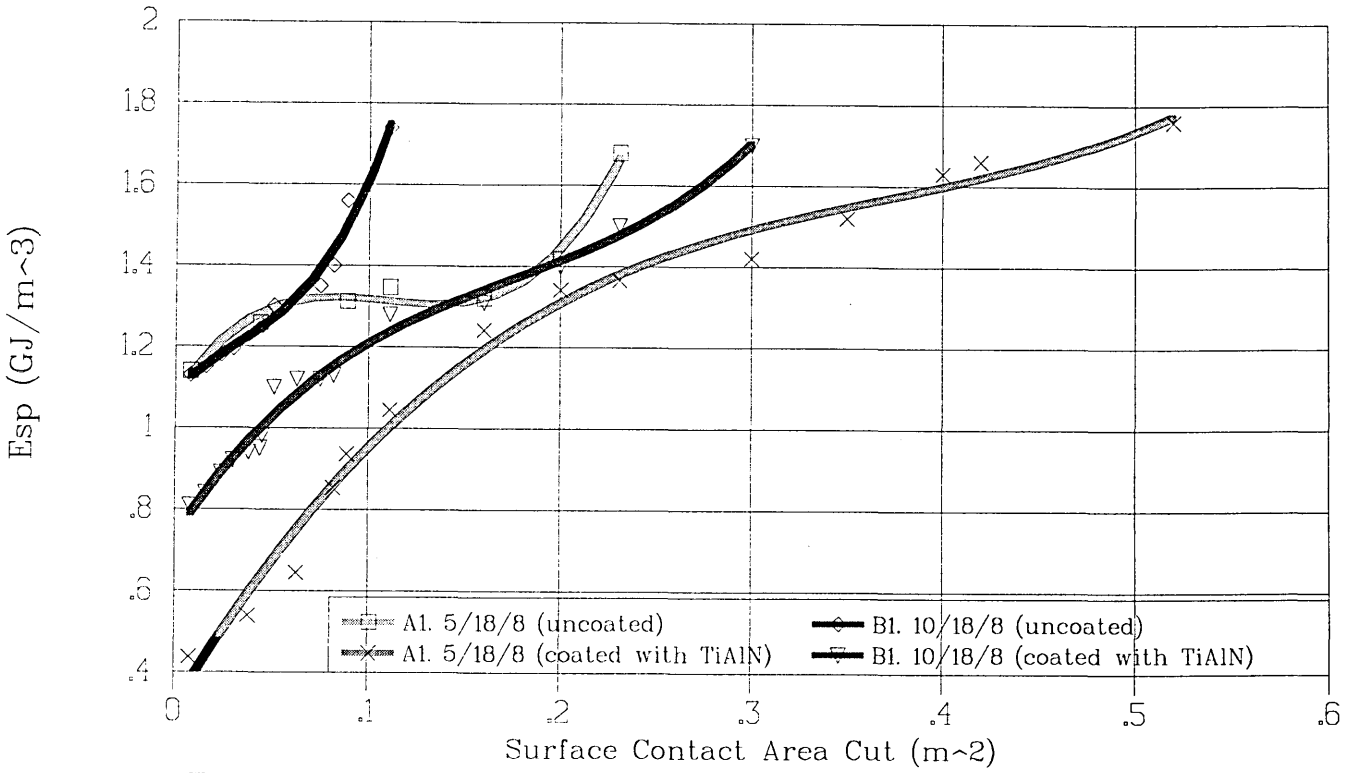

Figure 5.31 Comparison of performance when cutting mild steel
Cutting Speed : 203 m/min, Cutting condition: Dry
Feed/ Pair of teeth: 0.355 mm/rev., Work Material : MS

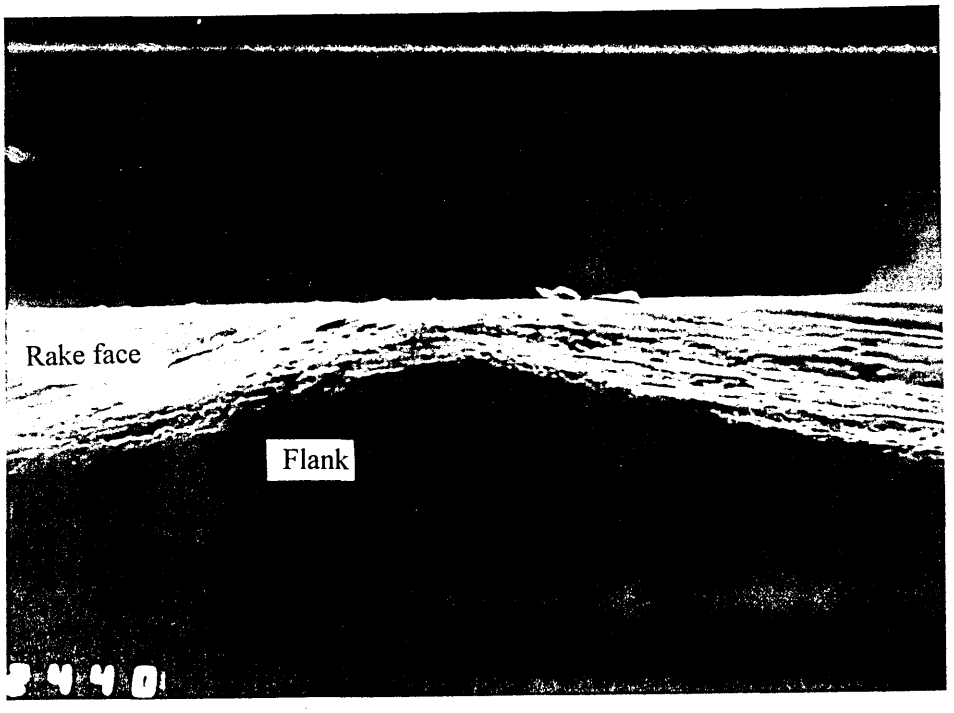

Figure 5.32(a) The cutting edge of the finishing tooth of the TiAlN coated A1 segment after 0.3 m^2 area cut in the case of cutting mild steel

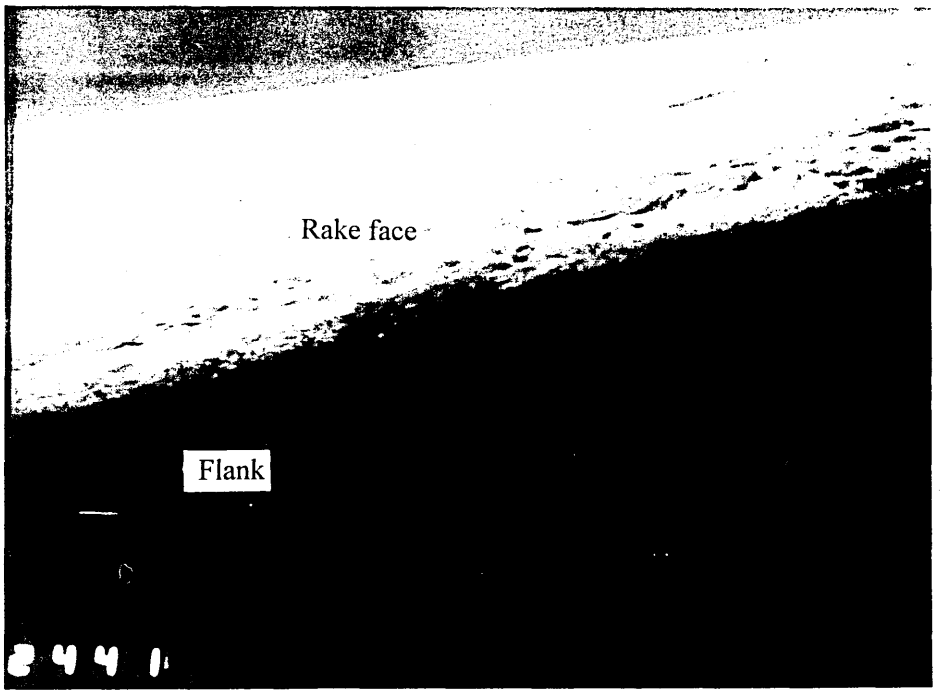

Figure 5.32(b) The cutting edge of the roughing tooth of the TiAlN coated A1 segment after 0.3 m^2 area cut in the case of cutting mild steel.

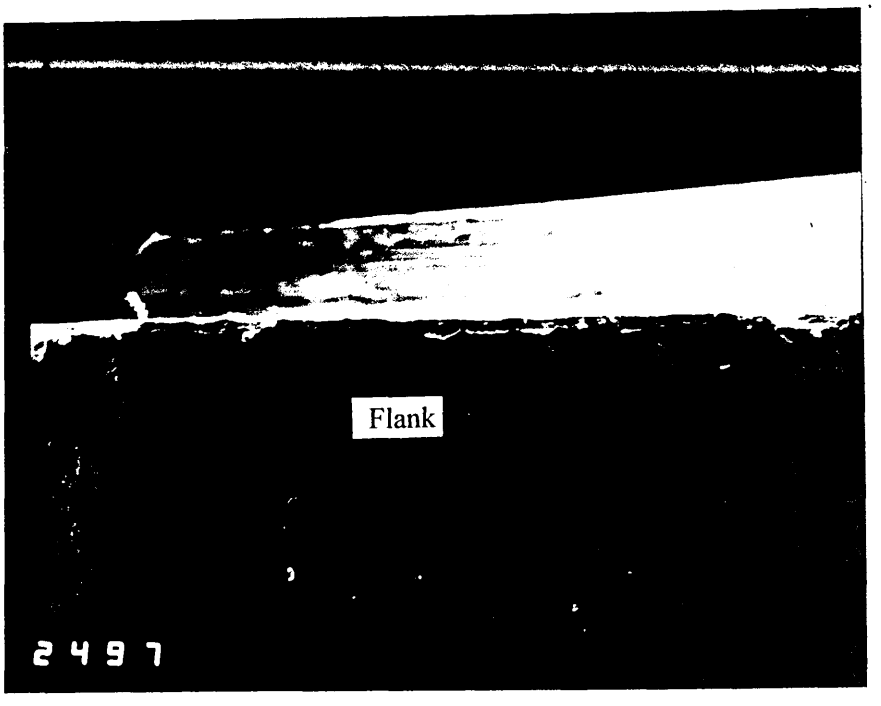

Figure 5.32(c) The flank wear on the TiAlN coated A1 when cutting mild steel.

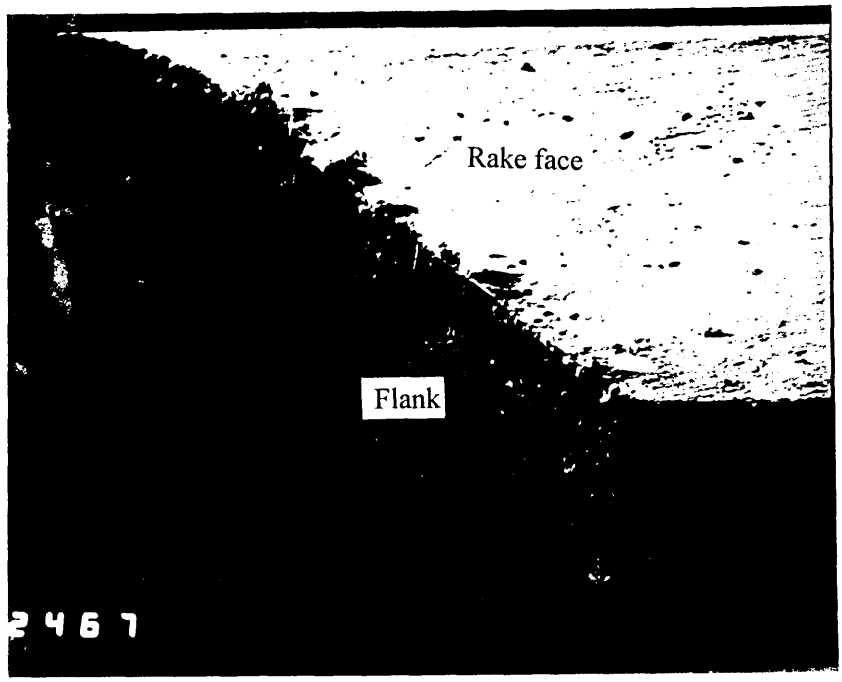

Figure 5.32(d) The cutting edge of the roughing tooth of the TiAlN coated B1 segment after 0.3 m^2 area cut in the case of cutting mild steel.

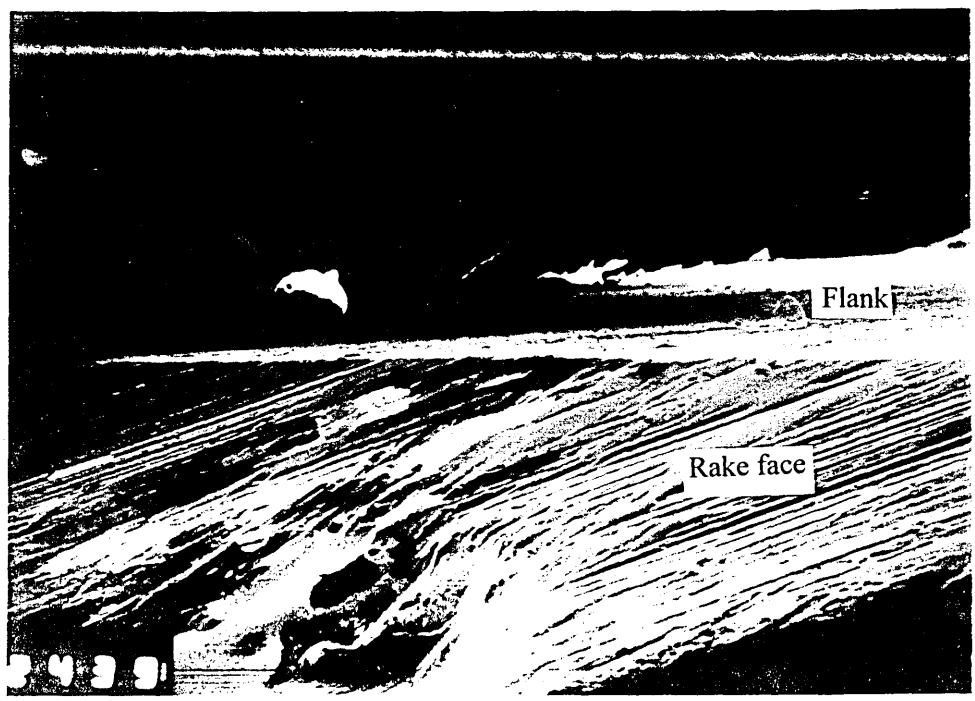

Figure 5.32(e) The chipping occurred on the bevelling of the finishing tooth of the TiAlN coated B1 segment when cutting mild steel

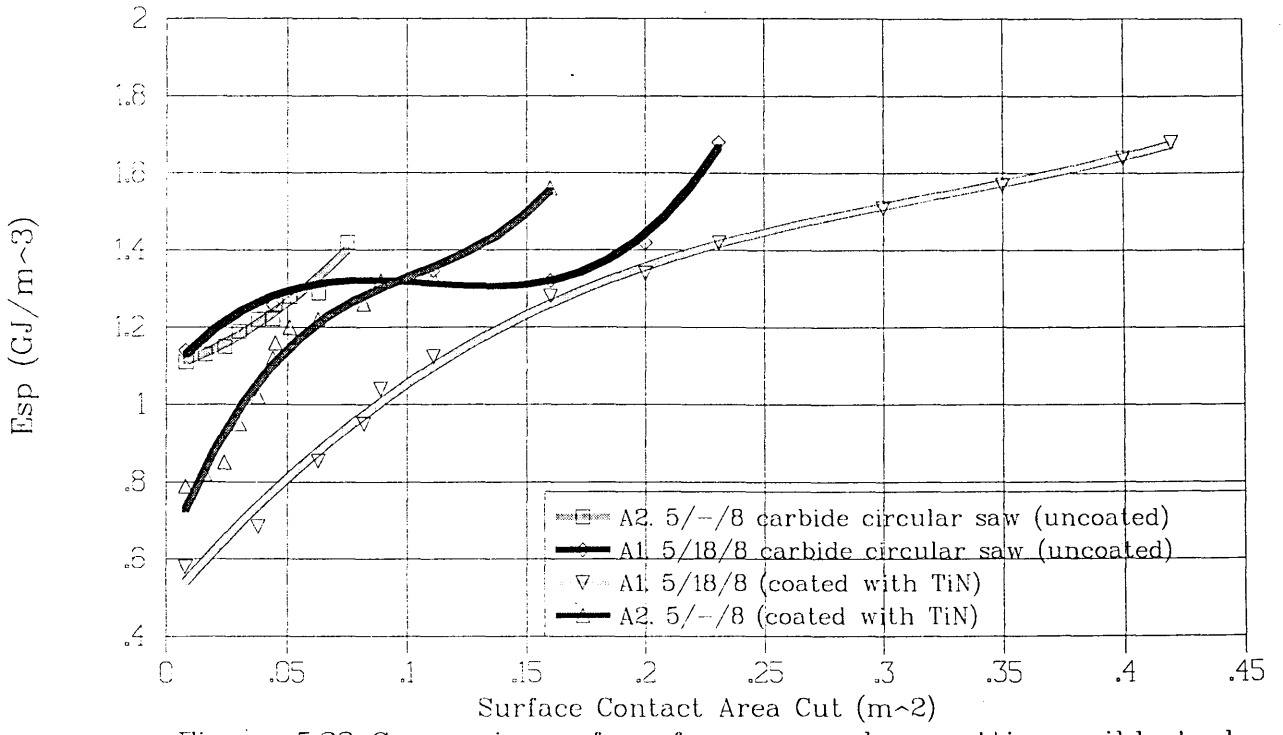

Figure 5.33 Comparison of performance when cutting mild steel
Cutting Speed : 203 m/min, Cutting condition: Dry
Feed/ Pair of teeth: 0.355 mm/rev., Work Material : MS

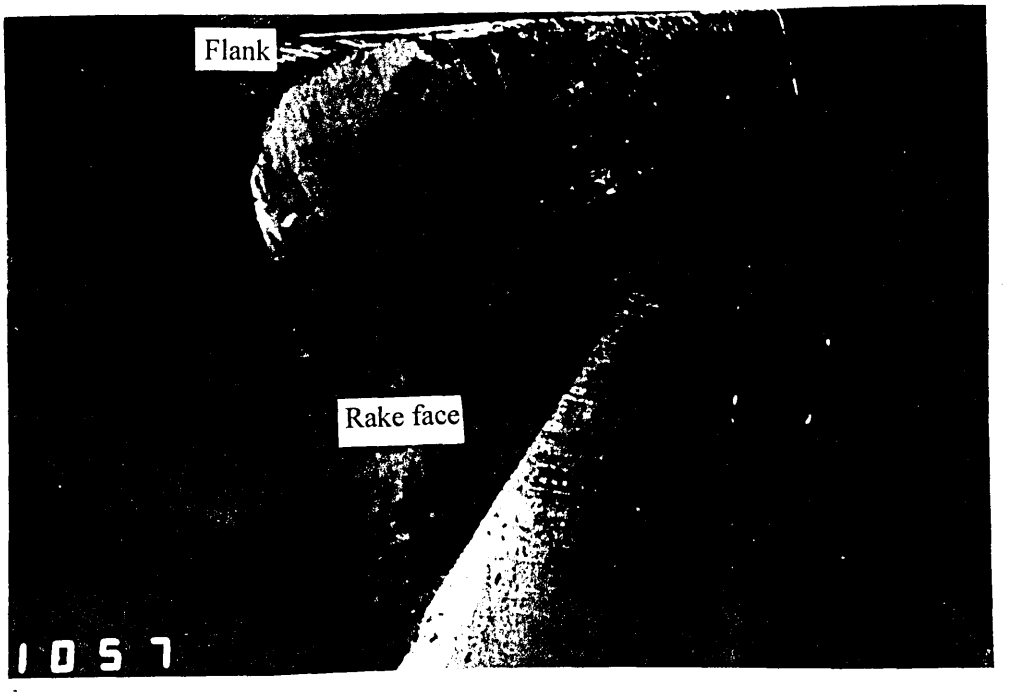

Figure 5.34(a) The cutting edge on the finishing tooth of the TiN coated A1 segment when cutting mild steel

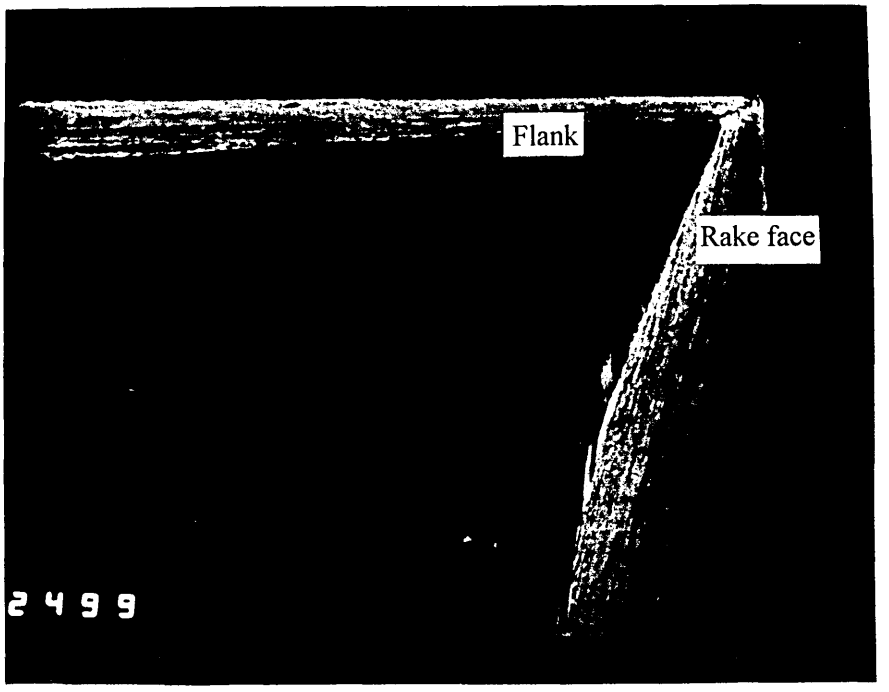

Figure 5.34(b) Flank wear produced on the cutting edge of the roughing tooth of the TiN coated A1 segment when cutting mild steel

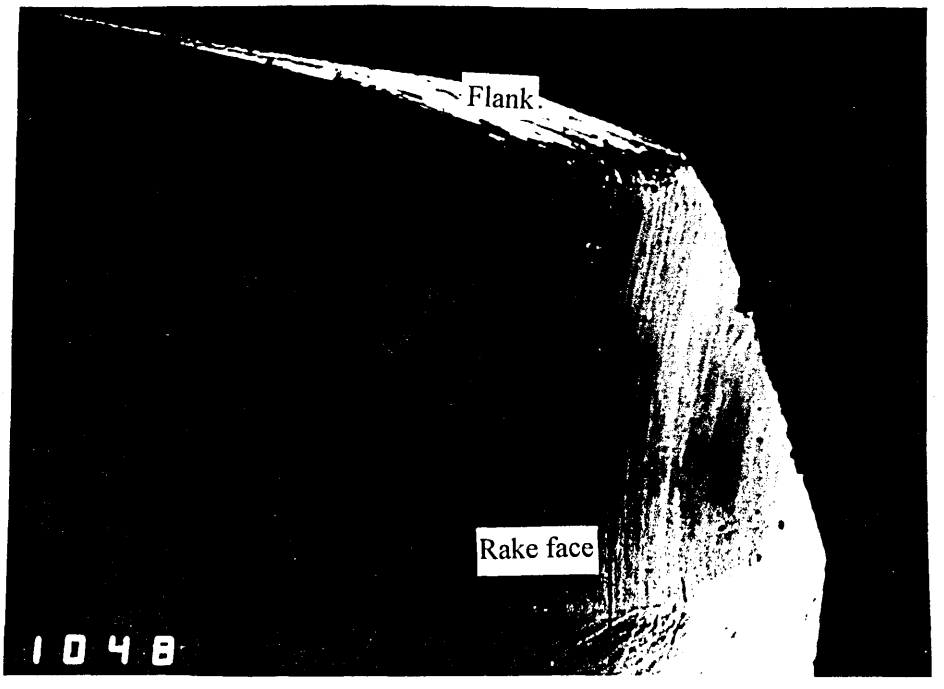

Figure 5.34(c) Crater wear produced on the cutting edge of the roughing tooth of the TiN coated A2 segments when cutting mild steel

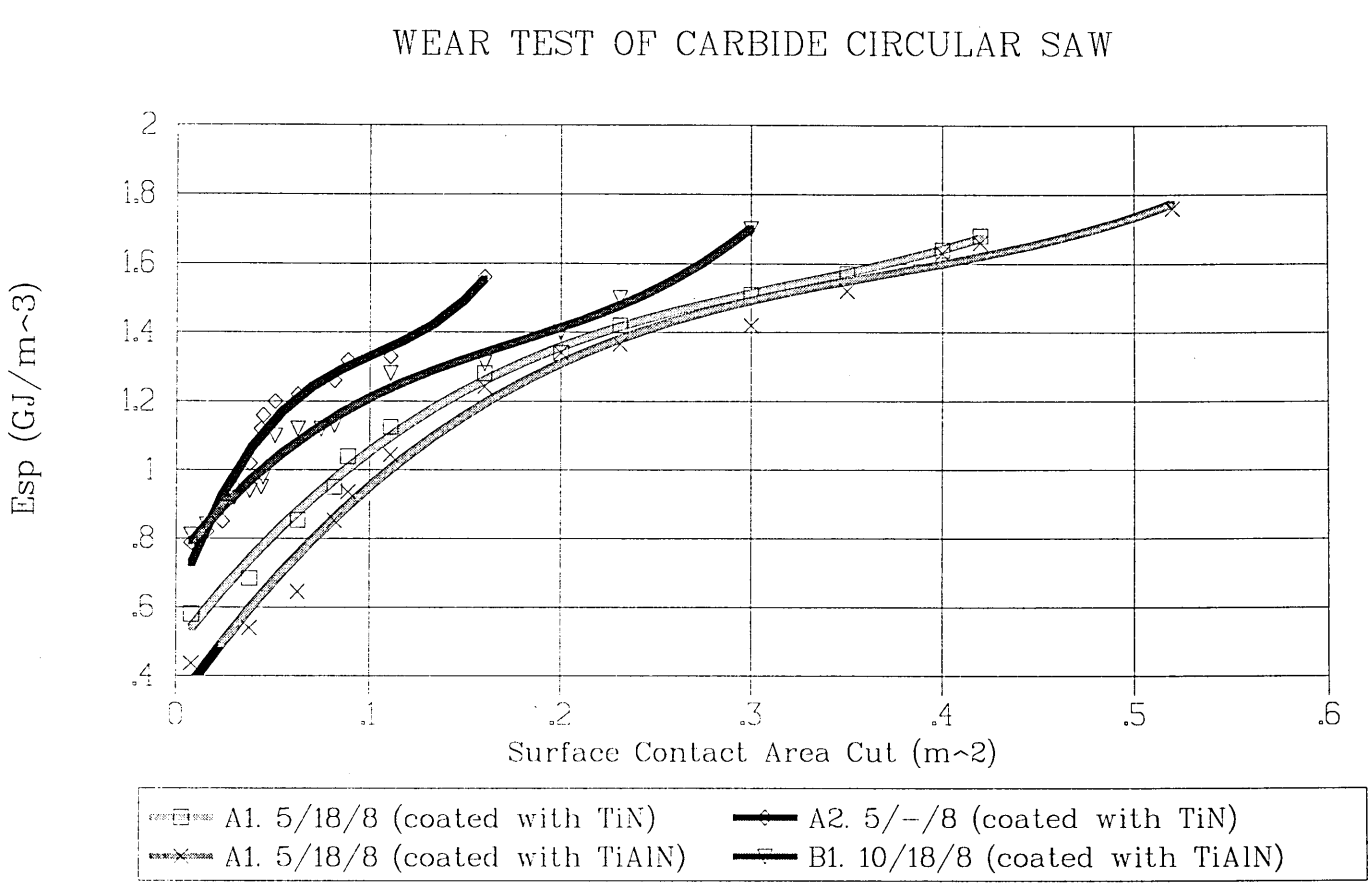

Figure 5.35 Comparison of performance with TiN and TiAlN coated segments
Cutting Speed : 203 m/min, Cutting condition: Dry
Feed/ Pair of teeth: 0.355 mm/rev., Work Material : MS

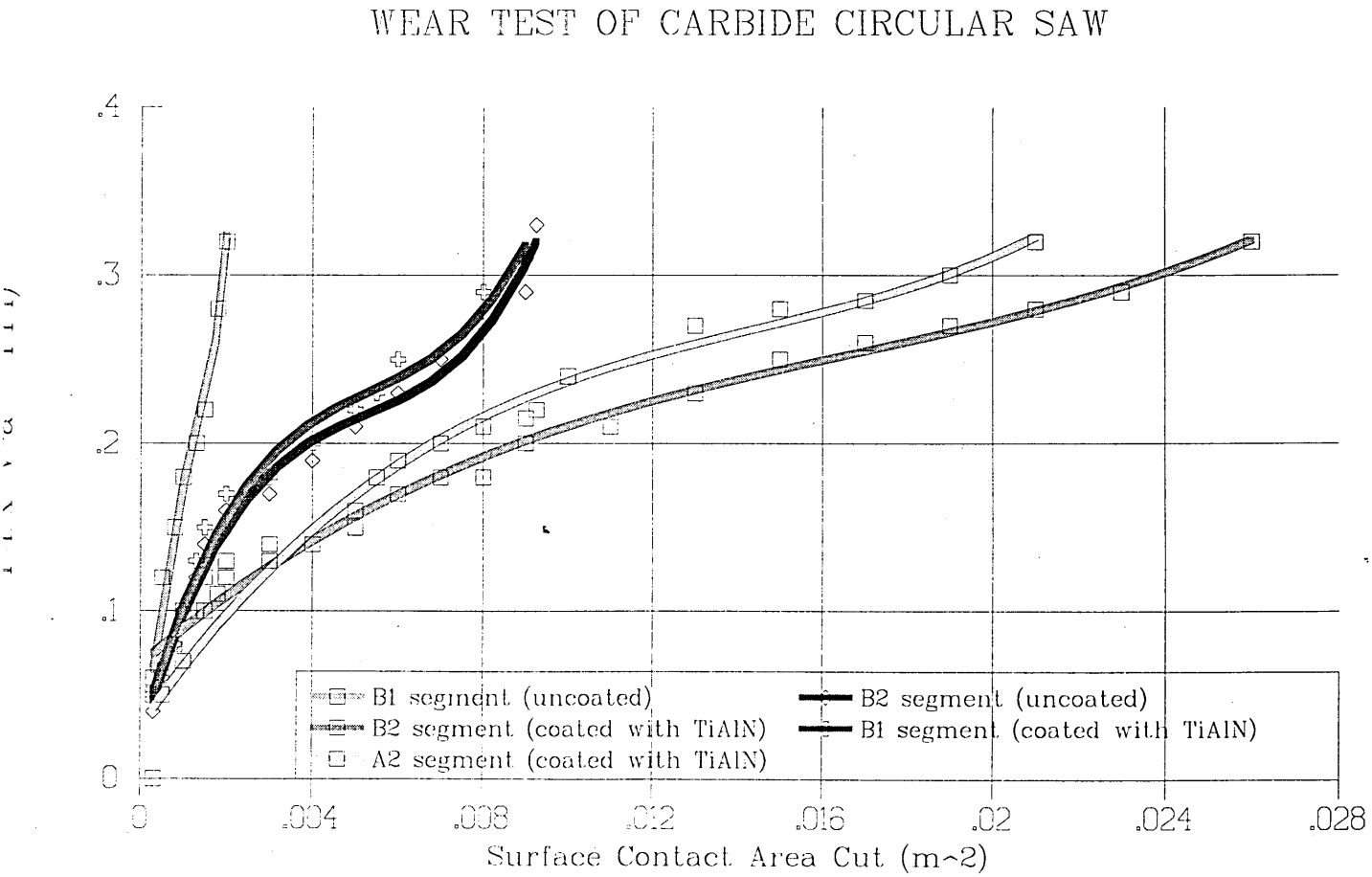

Figure 5.36 Comparison of flank wear with coated and uncoated segments
Cutting Speed : 34 m/min, Cutting condition: Dry
Feed/ Pair of teeth: 0.046 mm/rev., Work Material : 302 S25

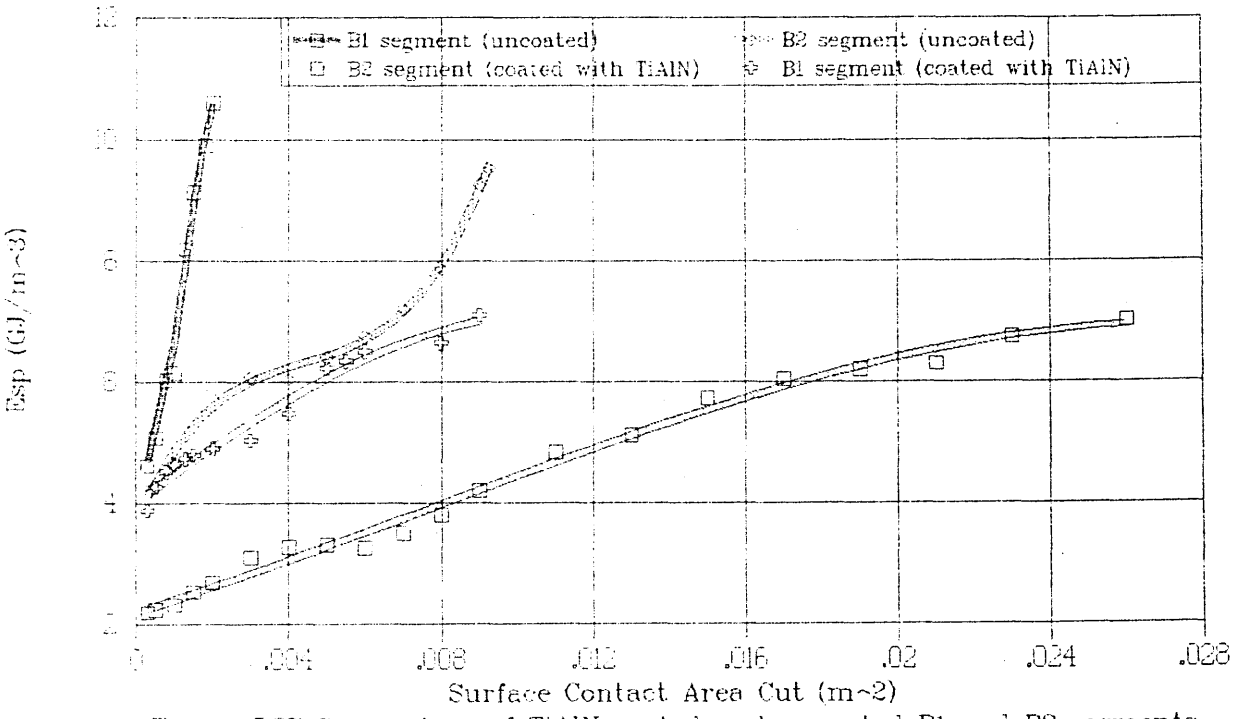

Figure 5.37 Comparison of TiAlN coated and uncoated B1 and B2 segments
Cutting Speed : 34 m/min, Cutting condition: Dry
Feed/ Pair of teeth: 0.046 mm/rev., Work Material : 302 S25

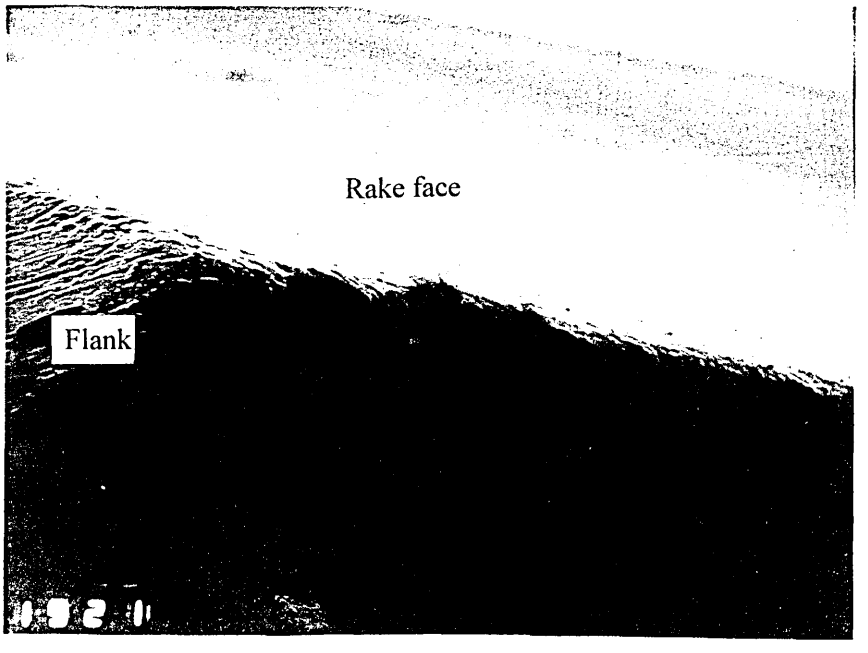

Figure 5.38(a) The cutting edge of the TiAlN coated B2 segment when cutting 302S25 stainless steel.

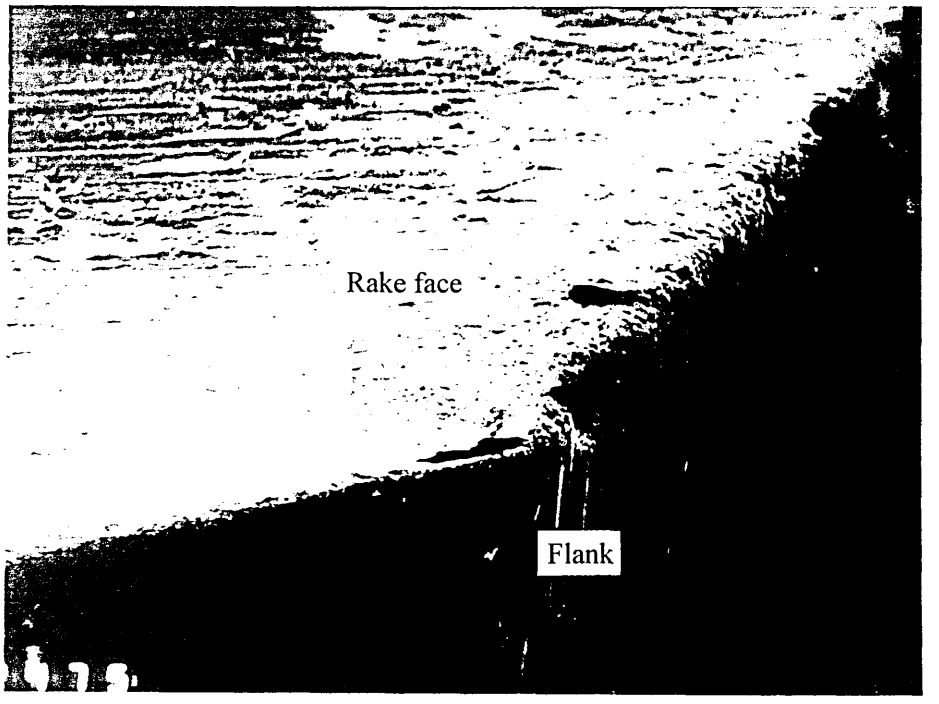

Figure 5.38(b) The chipping on the roughing tooth of the TiAlN coated B2 segment when cutting 302S25 stainless steel.

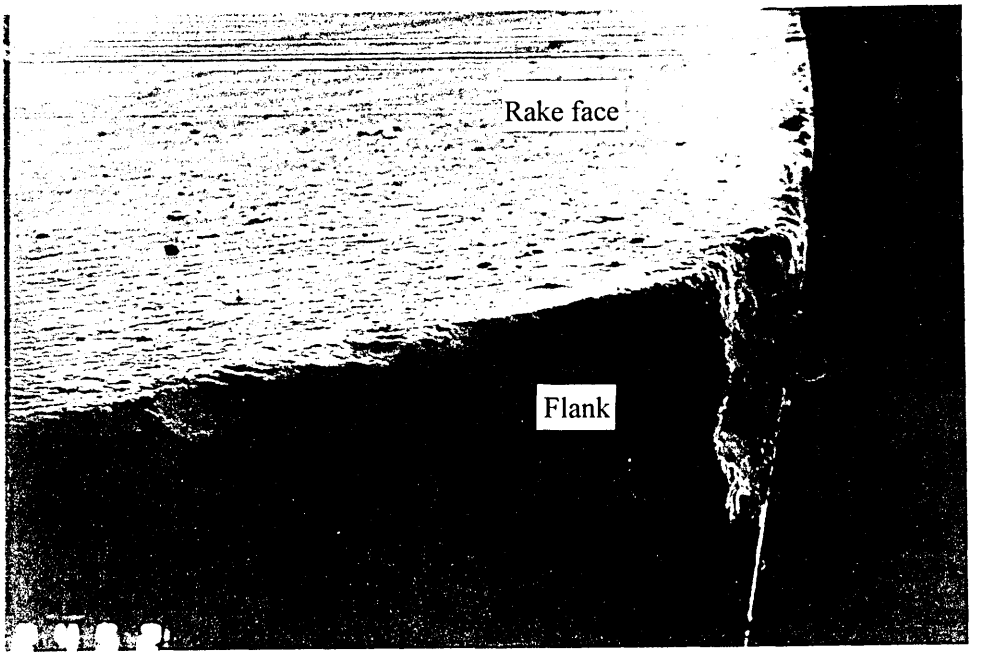

Figure 5.38(c) The cutting edge of the TiAlN coated B1 segment when cutting 302S25 stainless steel.

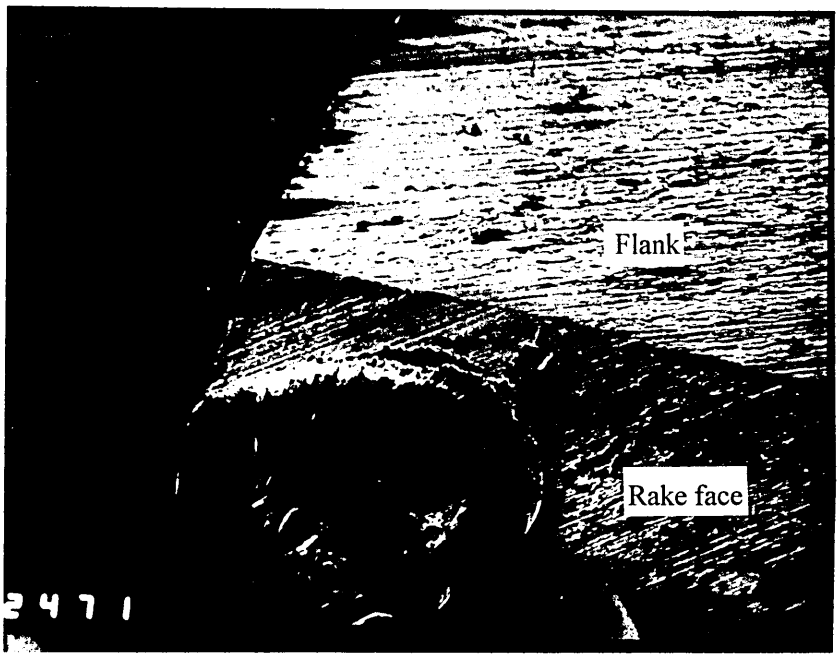

Figure 5.38(d) The chipping on the bevelling of the TiAlN coated B1 segment when cutting 302S25 stainless steel.

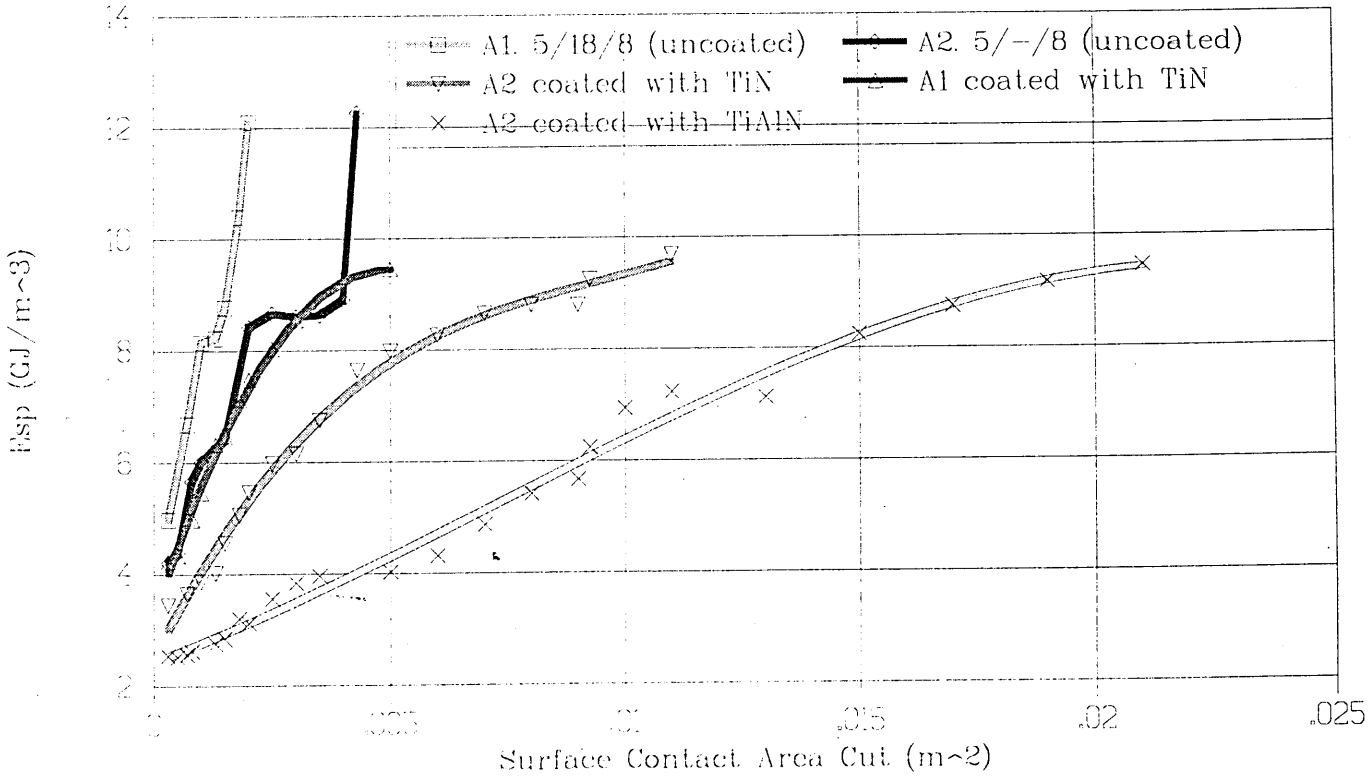

Figure 5.39 Comparison of performance of coated and uncoated A1 A2 segments when cutting stainless steel

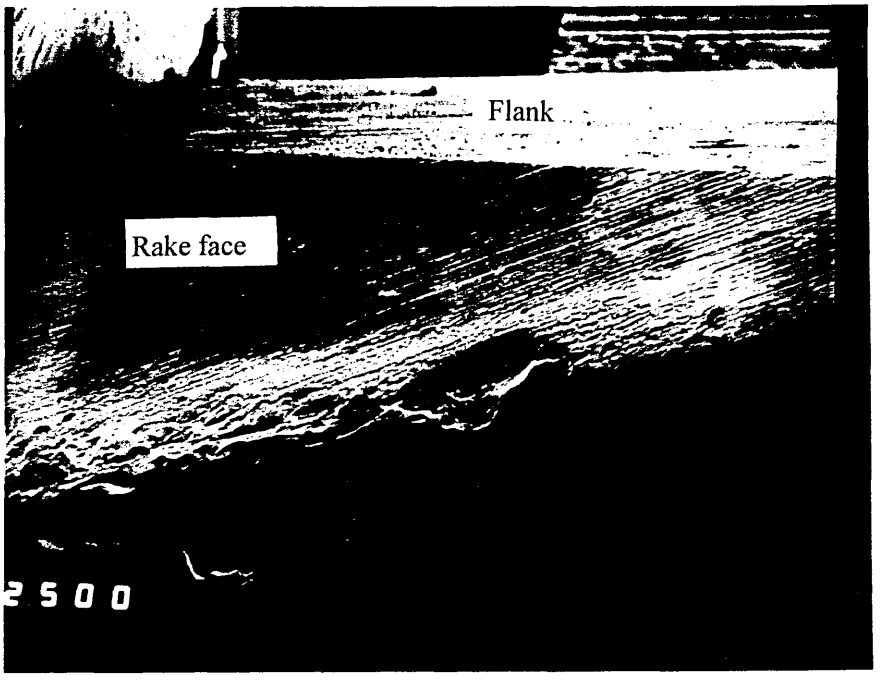

Figure 5.40(a) The chipping produced on the bevelling of the TiAlN coated A2 in case of cutting 302S25 stainless steel.

Figure 5.40(b) The cutting edge of the roughing tooth of the TiAlN coated A2 in case of cutting 302S25 stainless steel.

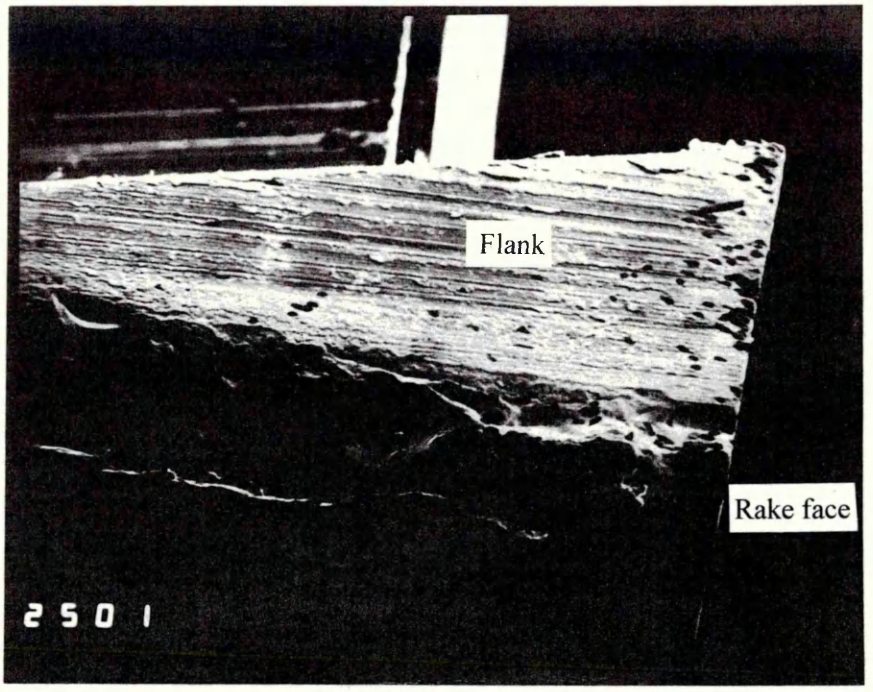

Figure 5.40(c) The chipping produced on the cutting edge of the TiN coated A1 in case of cutting 302S25 stainless steel.

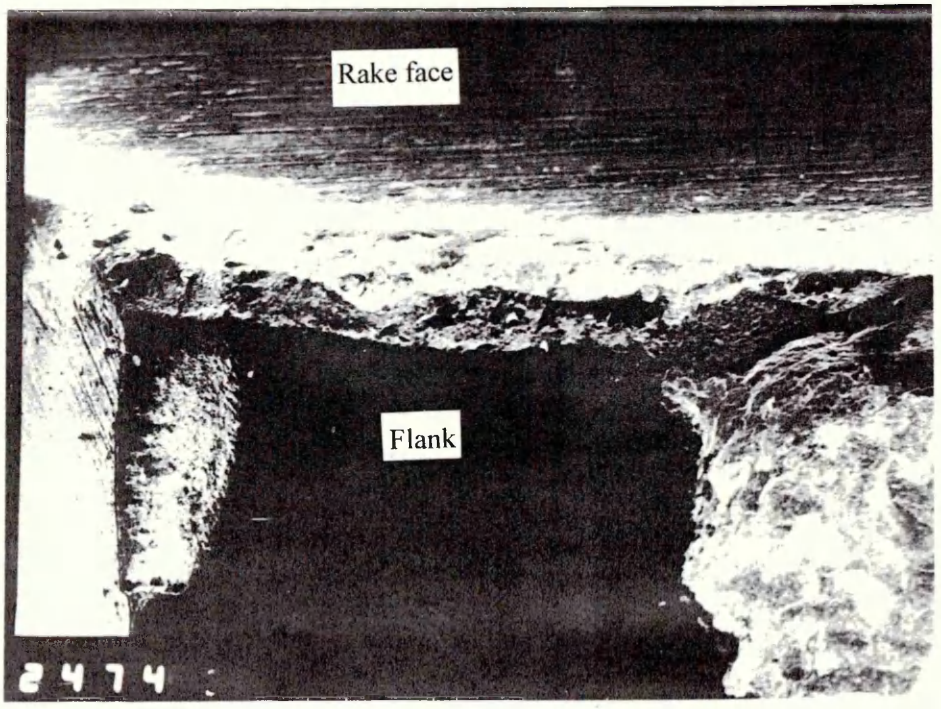

Figure 5.40(d) The large chipping and breakage produced on the cutting edge of the TiAlN coated A1 in case of cutting 302S25 stainless steel.

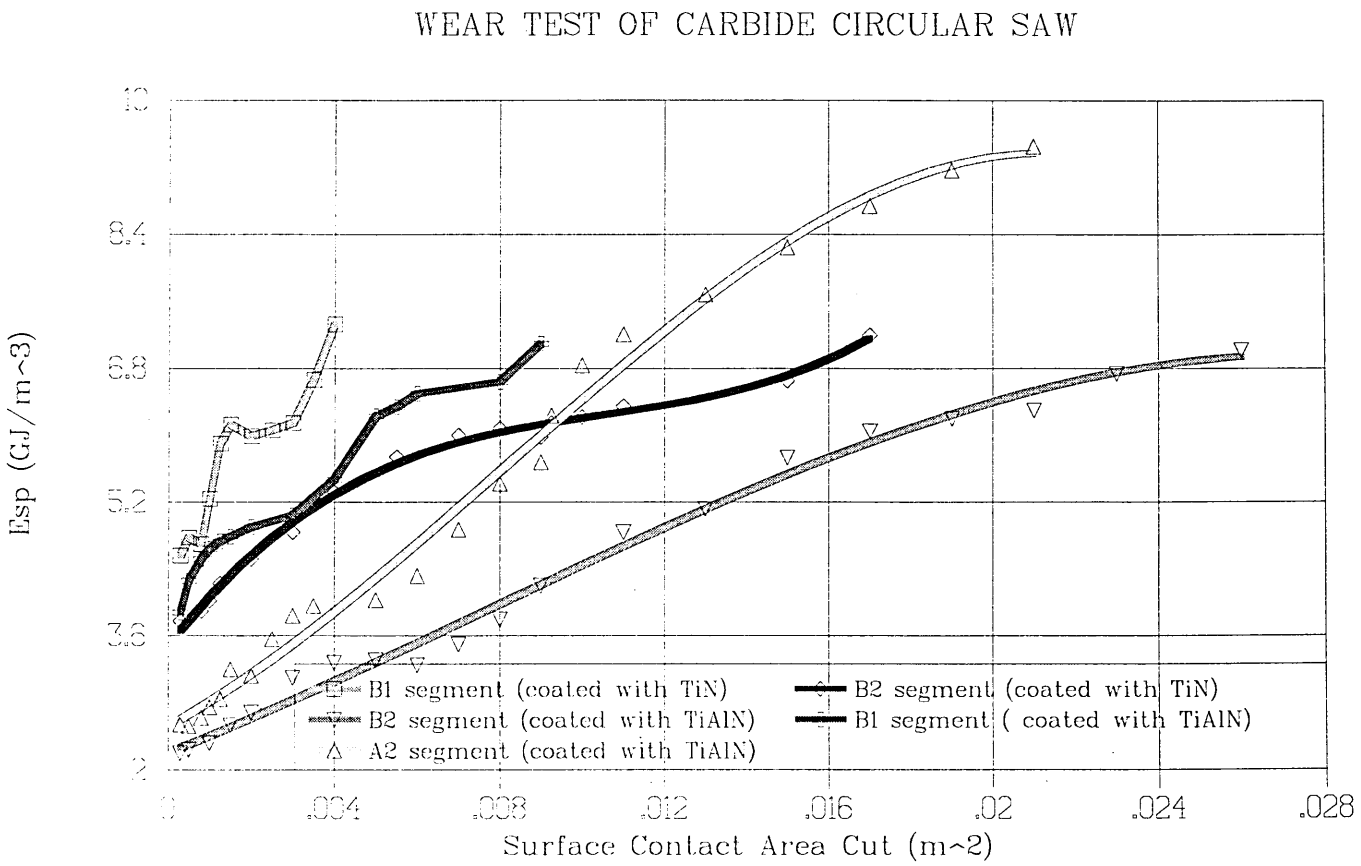

Figure 5.41 Comparison of performance with TiAlN and TiN coated segments
Cutting Speed : 34 m/min, Cutting condition: Dry
Feed/ Pair of teeth: 0.046 mm/rev., Work Material : 302S25

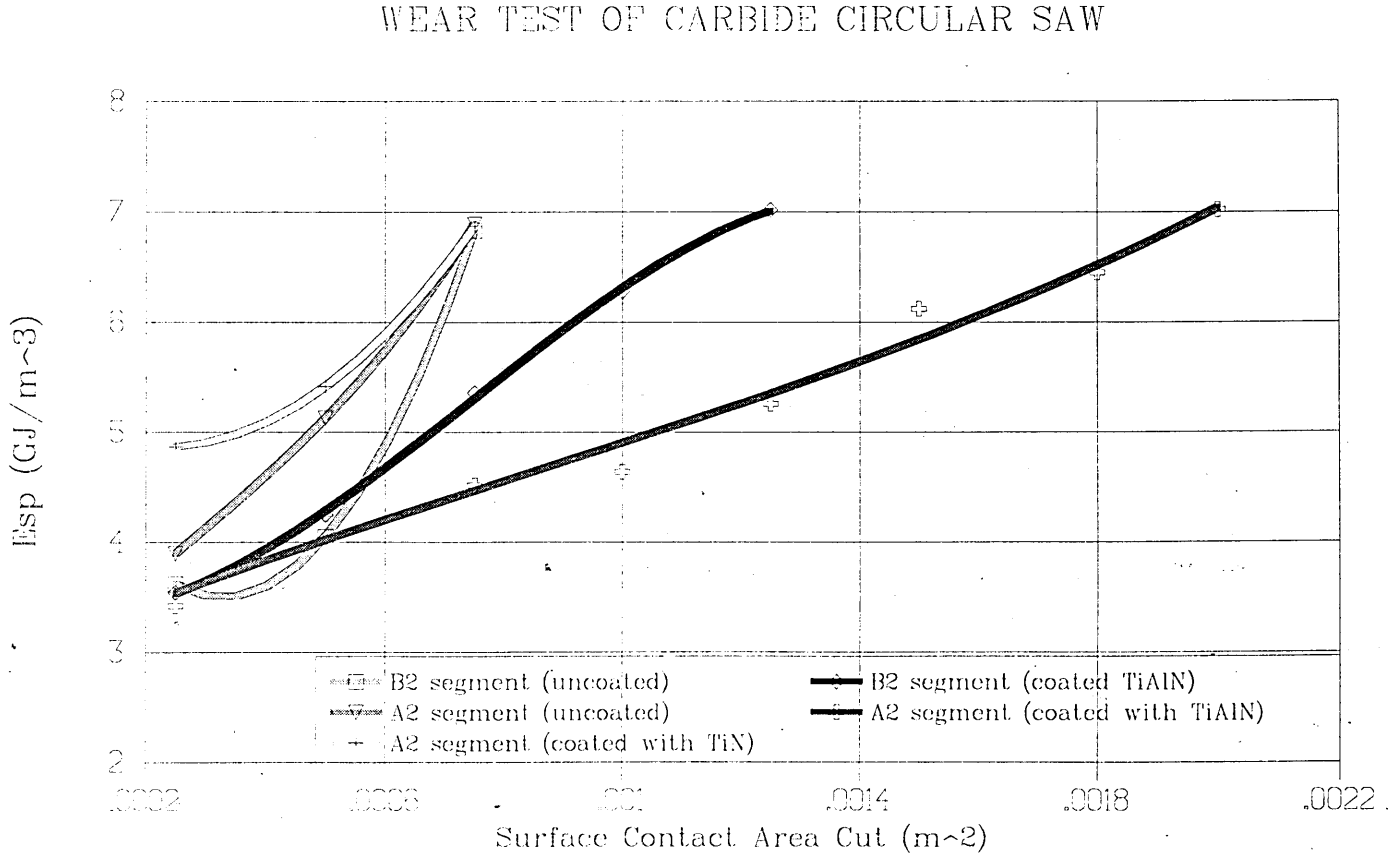

Figure 5.42 Comparison of performance of TiAlN and TiN coated segments
Cutting Speed : 29 m/min, Cutting condition: Dry
Feed/ Pair of teeth: 0.045 mm/rev., Work Material : C25 Nimonic Alloy

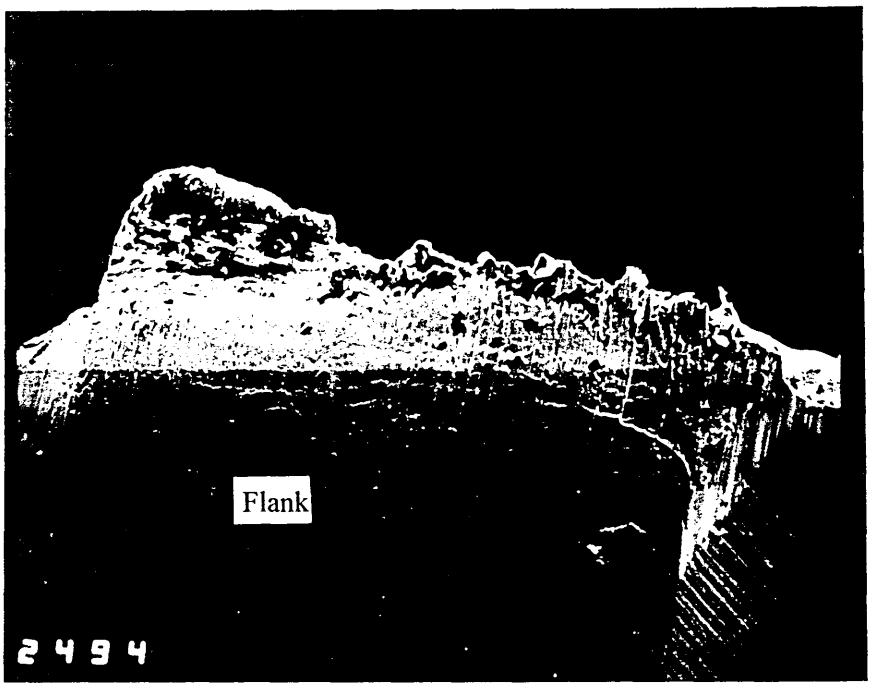

Figure 5.43(a) The built-up edge produced on the roughing tooth of the TiAlN coated B2 segment when cutting C25 nimonic alloy.

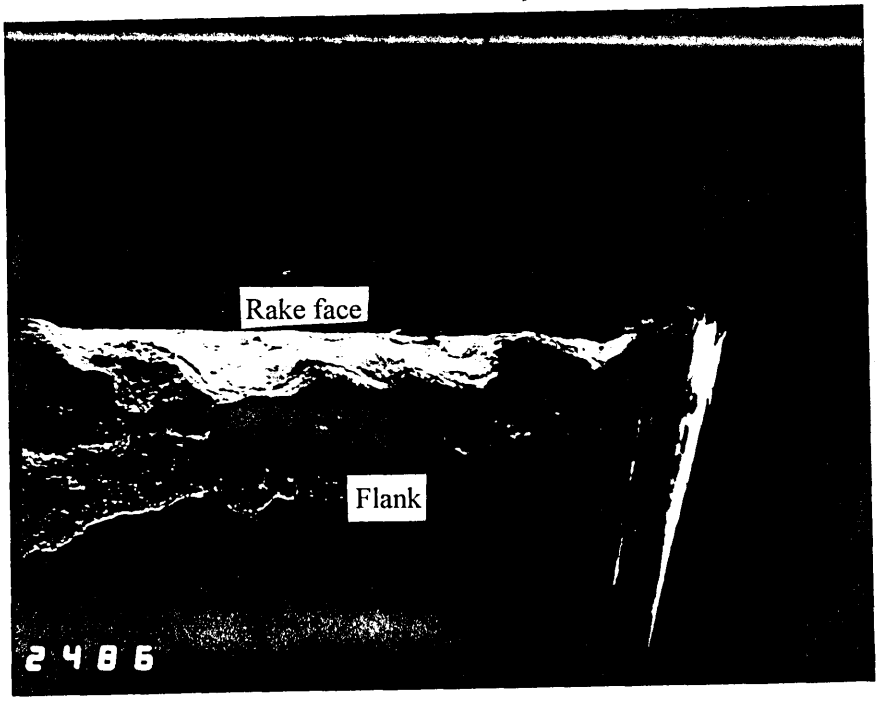

Figure 5.43(b) The large chipping produced on the roughing tooth of the TiAlN coated A2 segment when cutting C25 nimonic alloy.

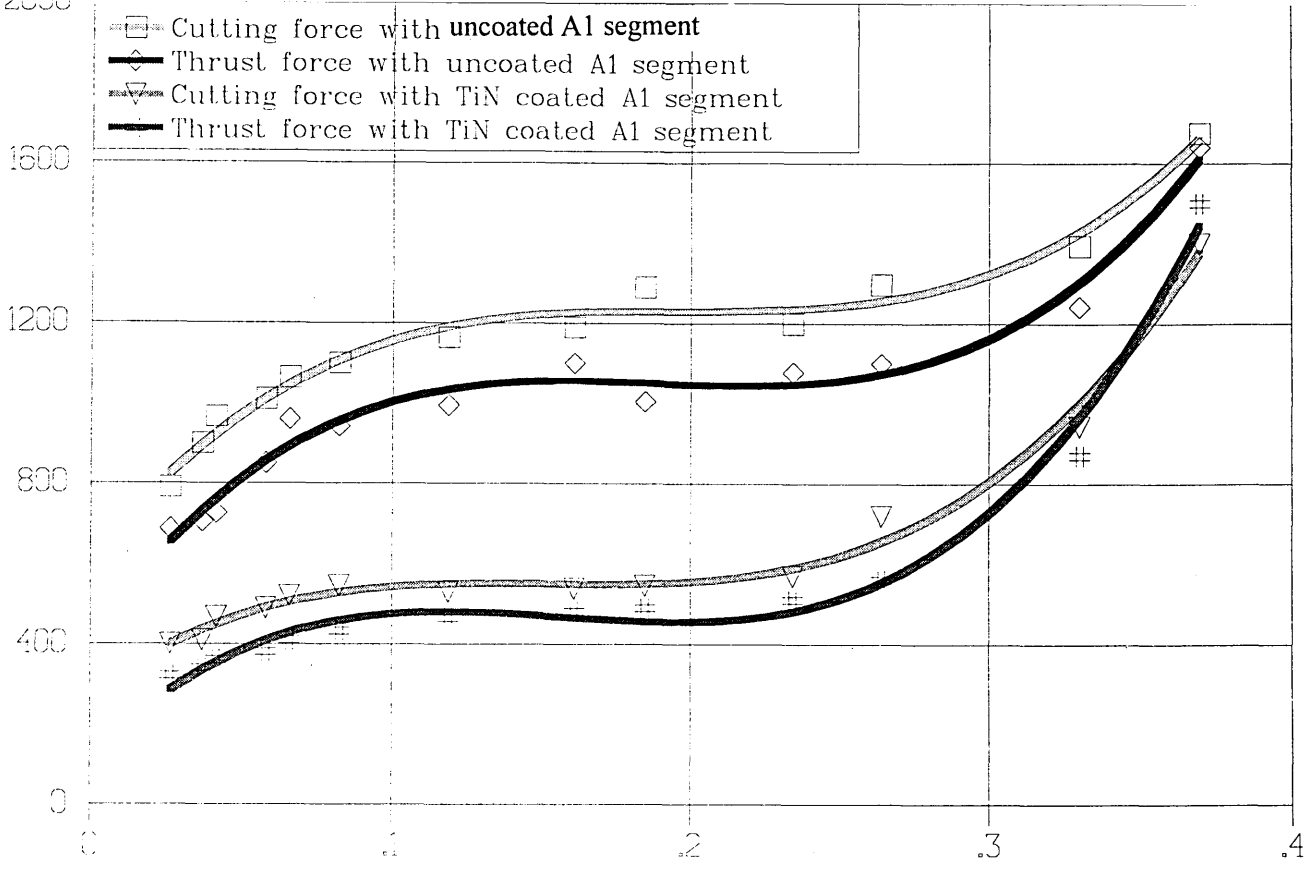

Cutting speed: 203 m/min; Workpiece material: mild steel

Figure 5.44 Comparison of forces when cutting with coated and uncoated segmer

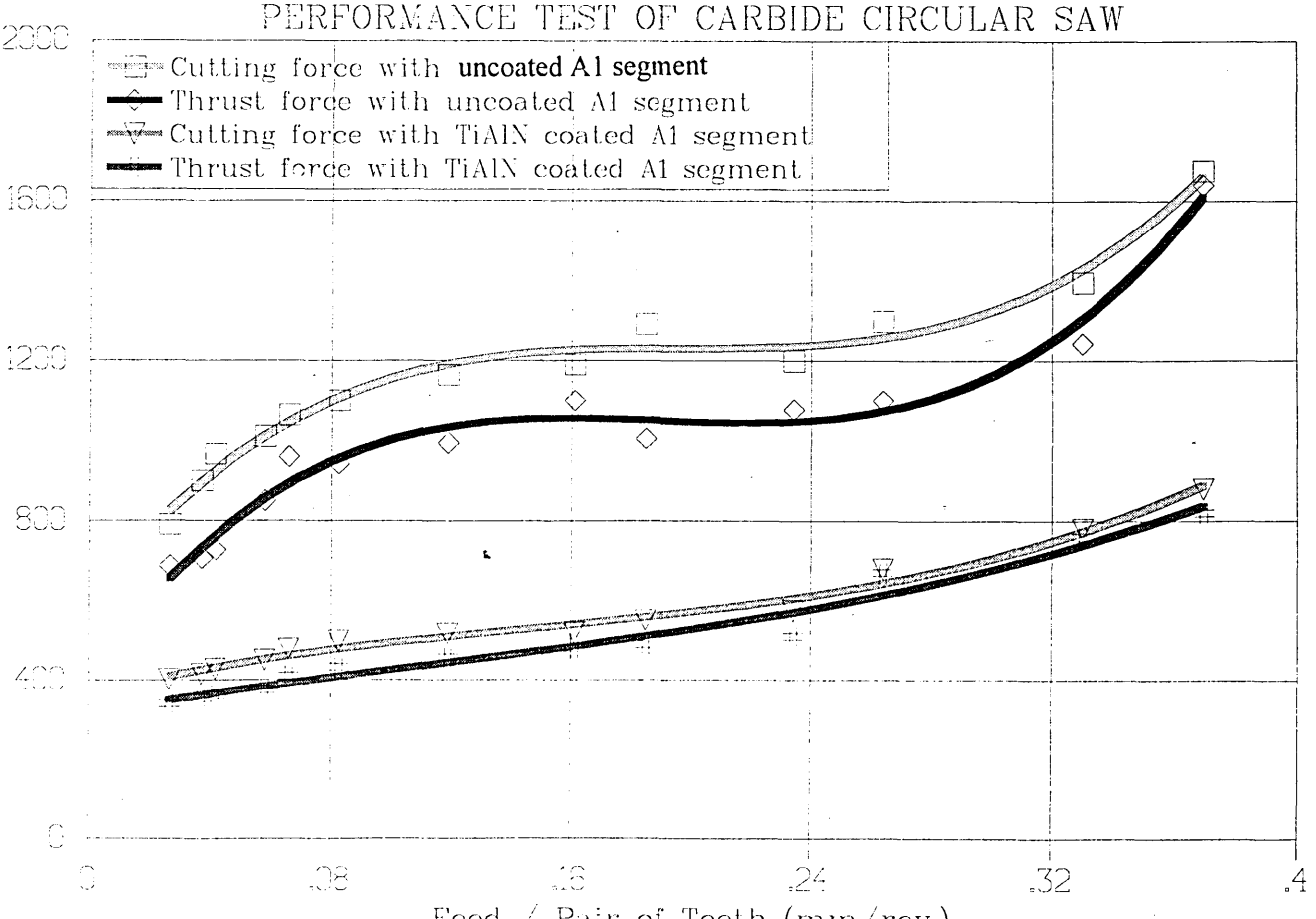

Cutting speed: 203 m/min; Workpiece material: mild steel

Figure 5.45 Comparison of forces when cutting with coated and uncoated segmer

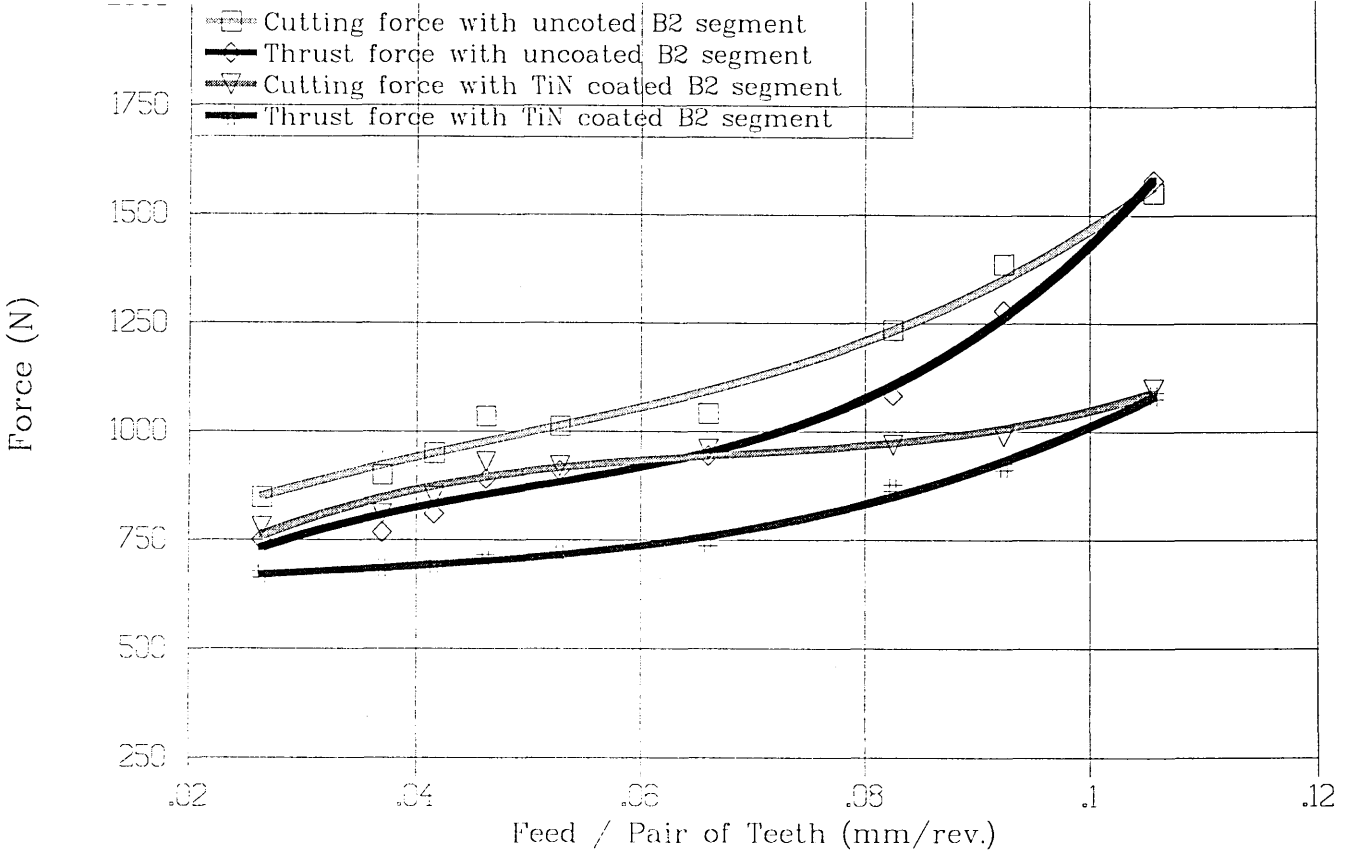

Cutting speed: 34 m/min; Workpiece material: EN58 stainless steel

Figure 5.46 Comparison of forces when cutting with coated and uncoated segments

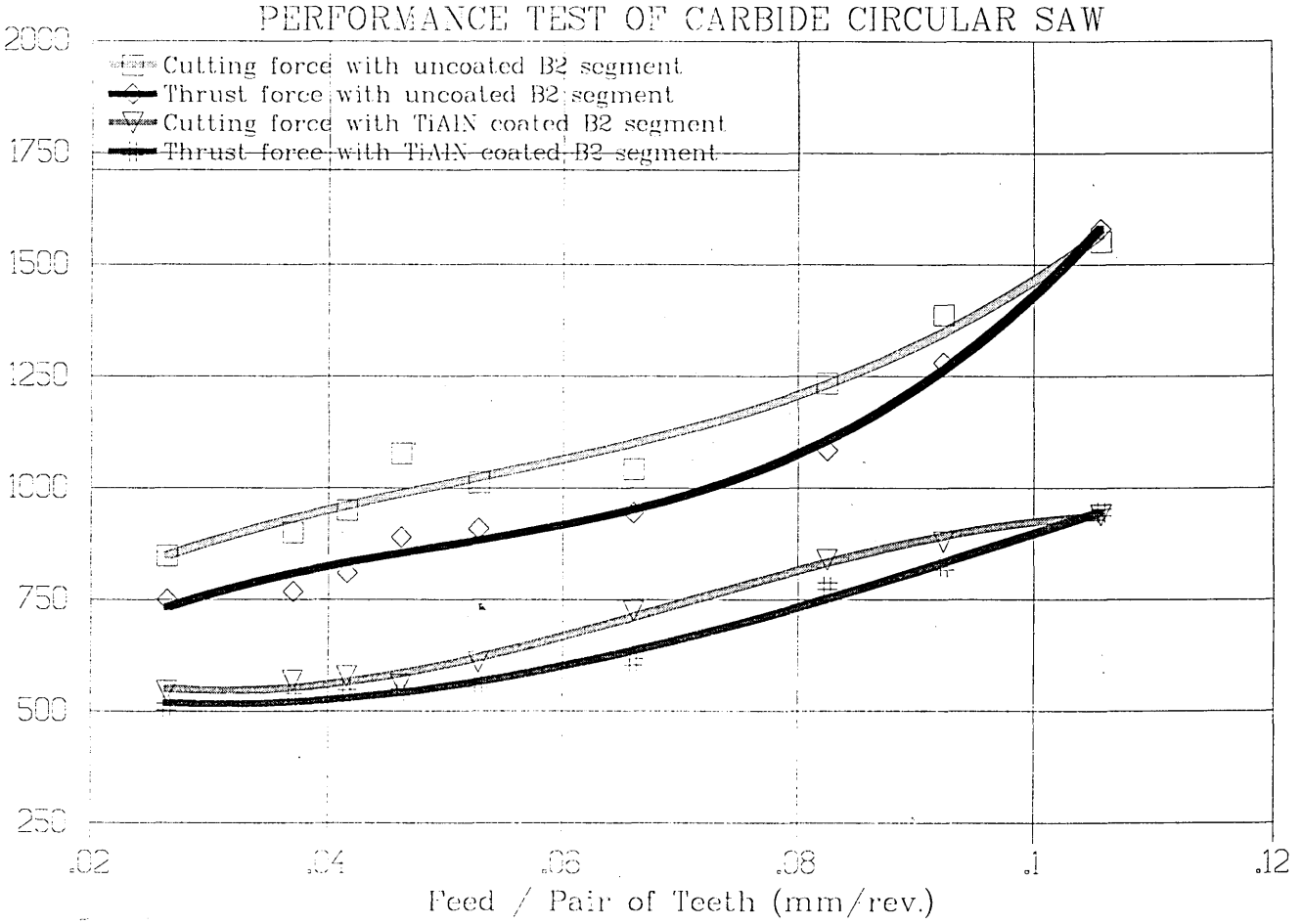

Cutting speed: 34 m/min; Workpiece material: EN58 stainless steel

Figure 5.47 Comparison of forces when cutting with coated and uncoated segmer

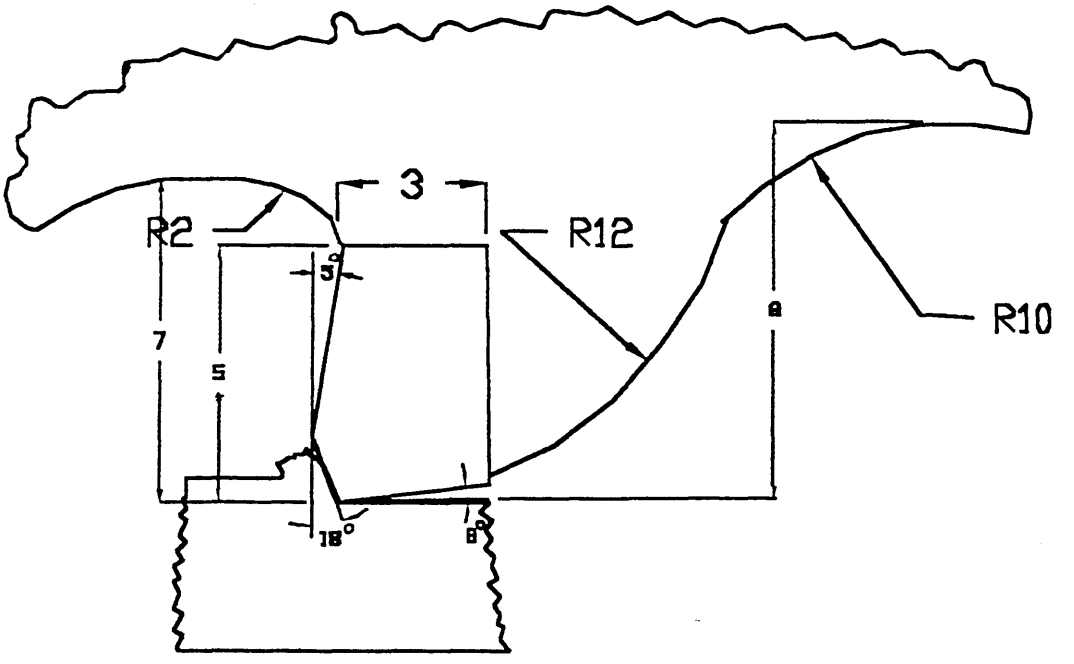

Figure 6.1 Geometry and dimension of one tooth model

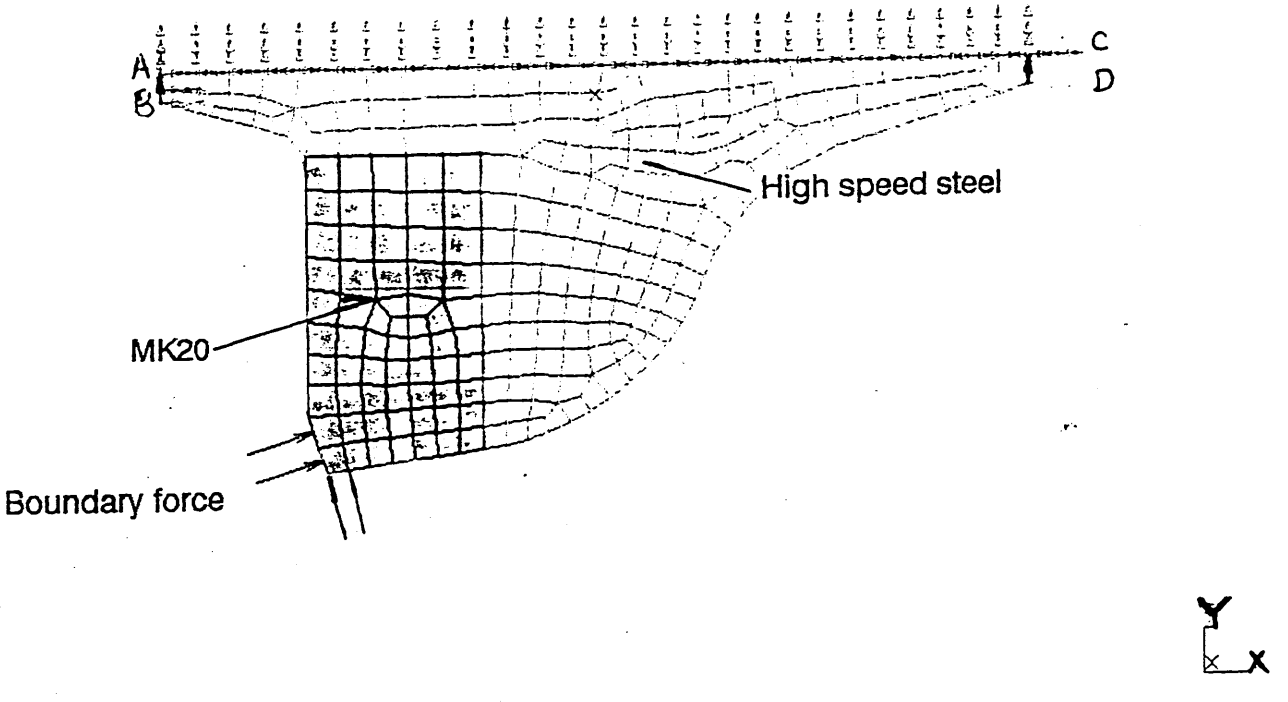

Figure 6.2 Finite element meshes and boundary conditions of two dimension single tooth model

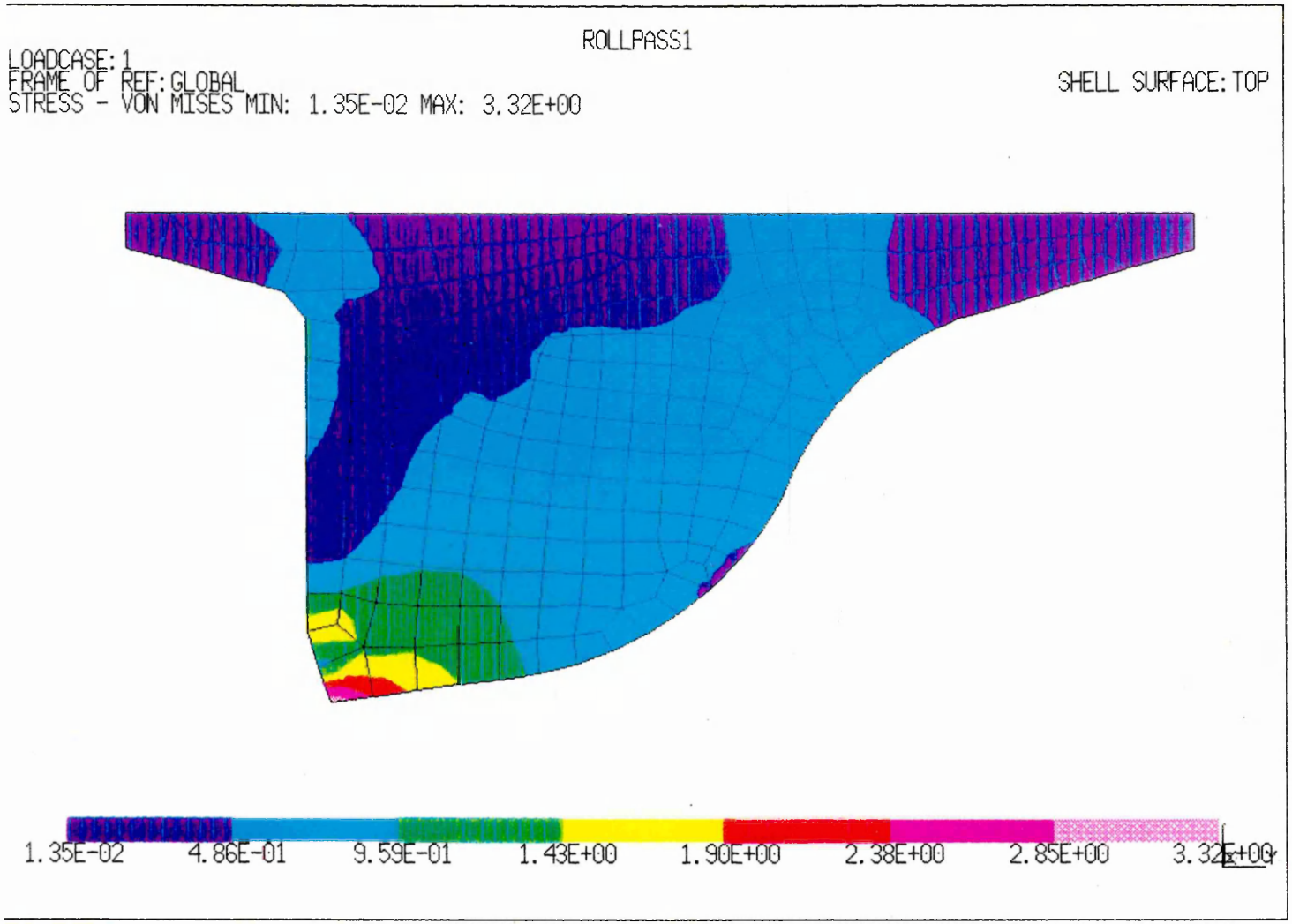

Figure 6.3 Distributions of σ_{eq} equivalent stress of 2D single tooth model

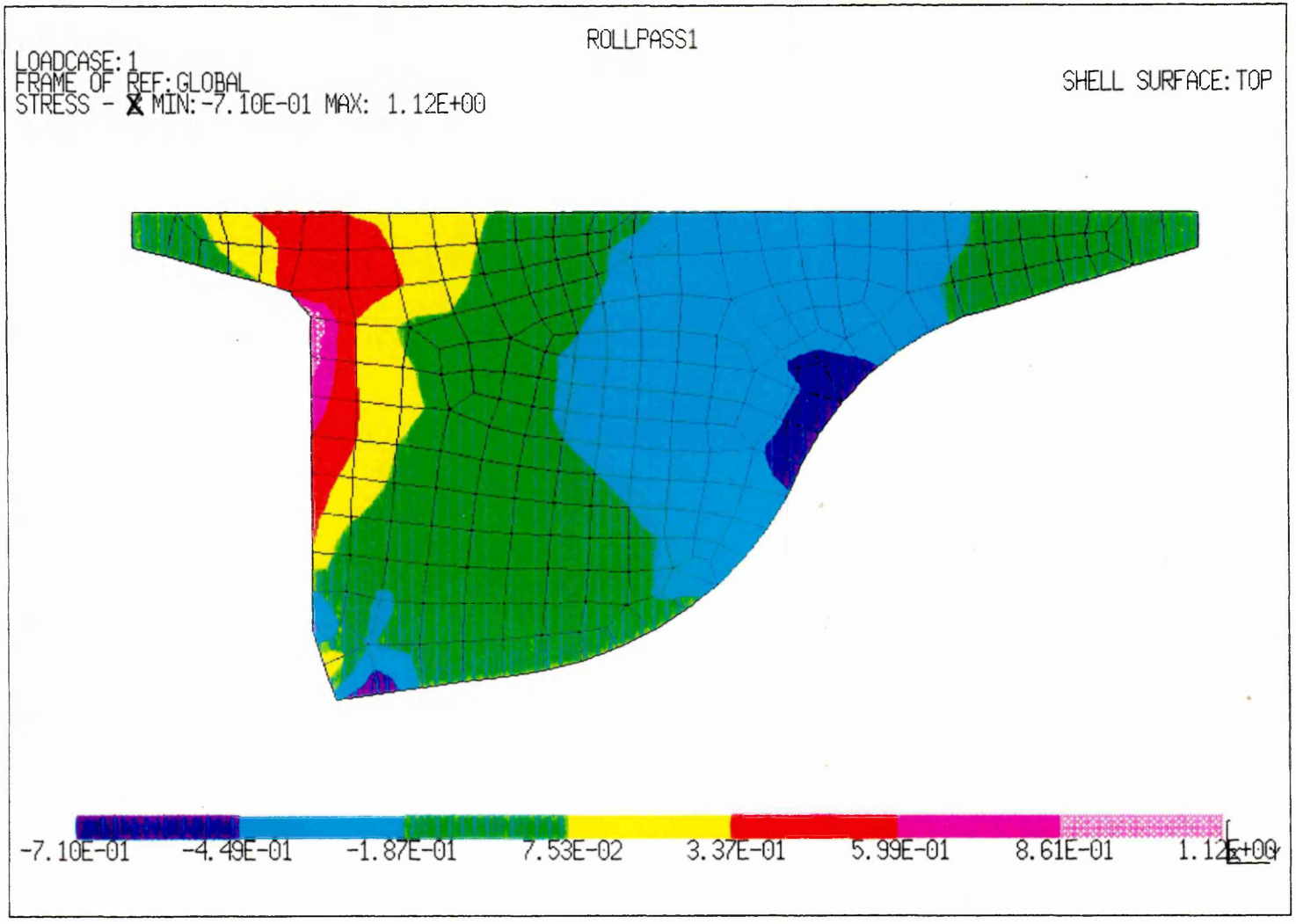

Figure 6.4 Distributions of σ_{x-x} stress of 2D single tooth model

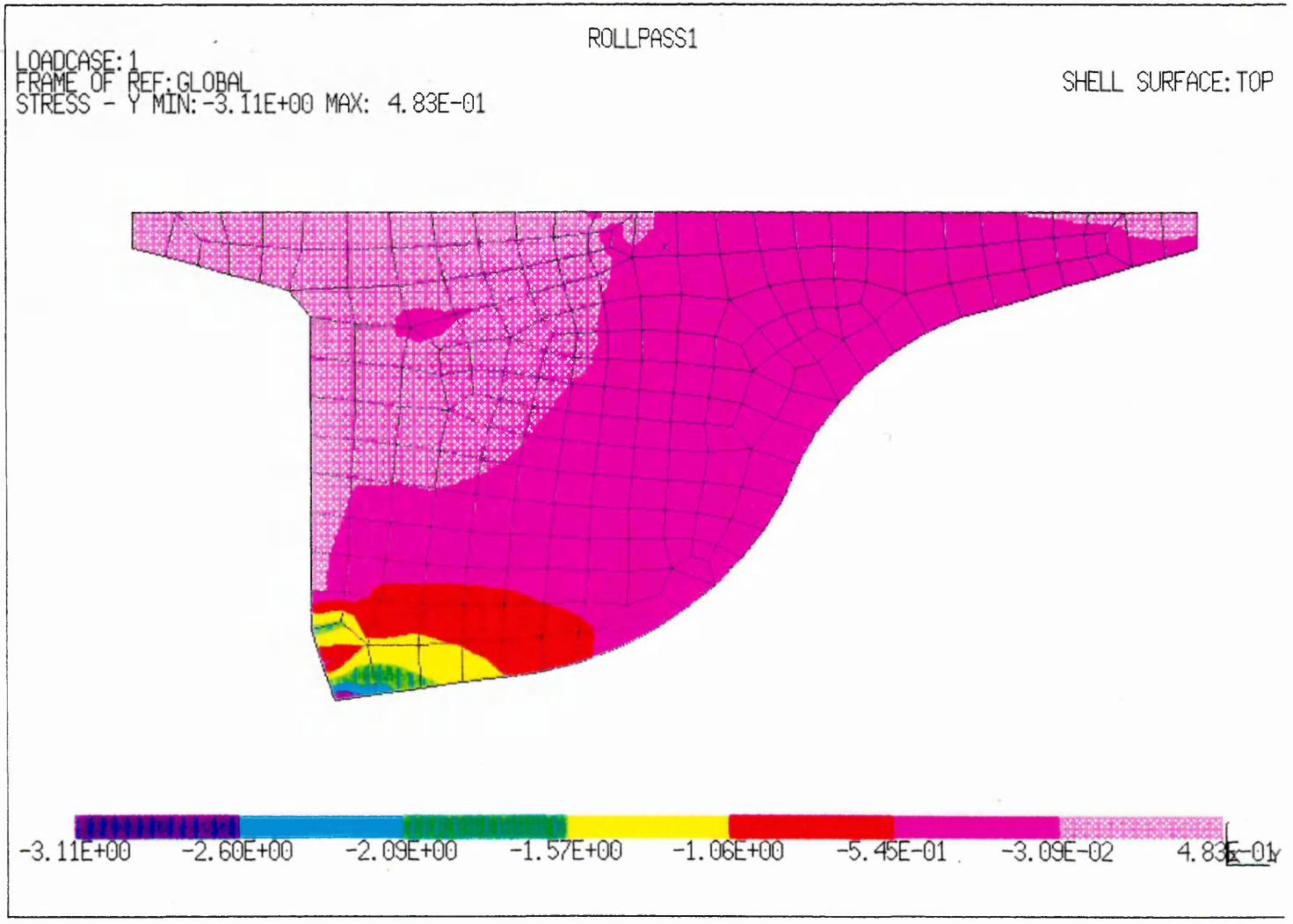

Figure 6.5 Distributions of σ_{y-y} stress of 2D single tooth model

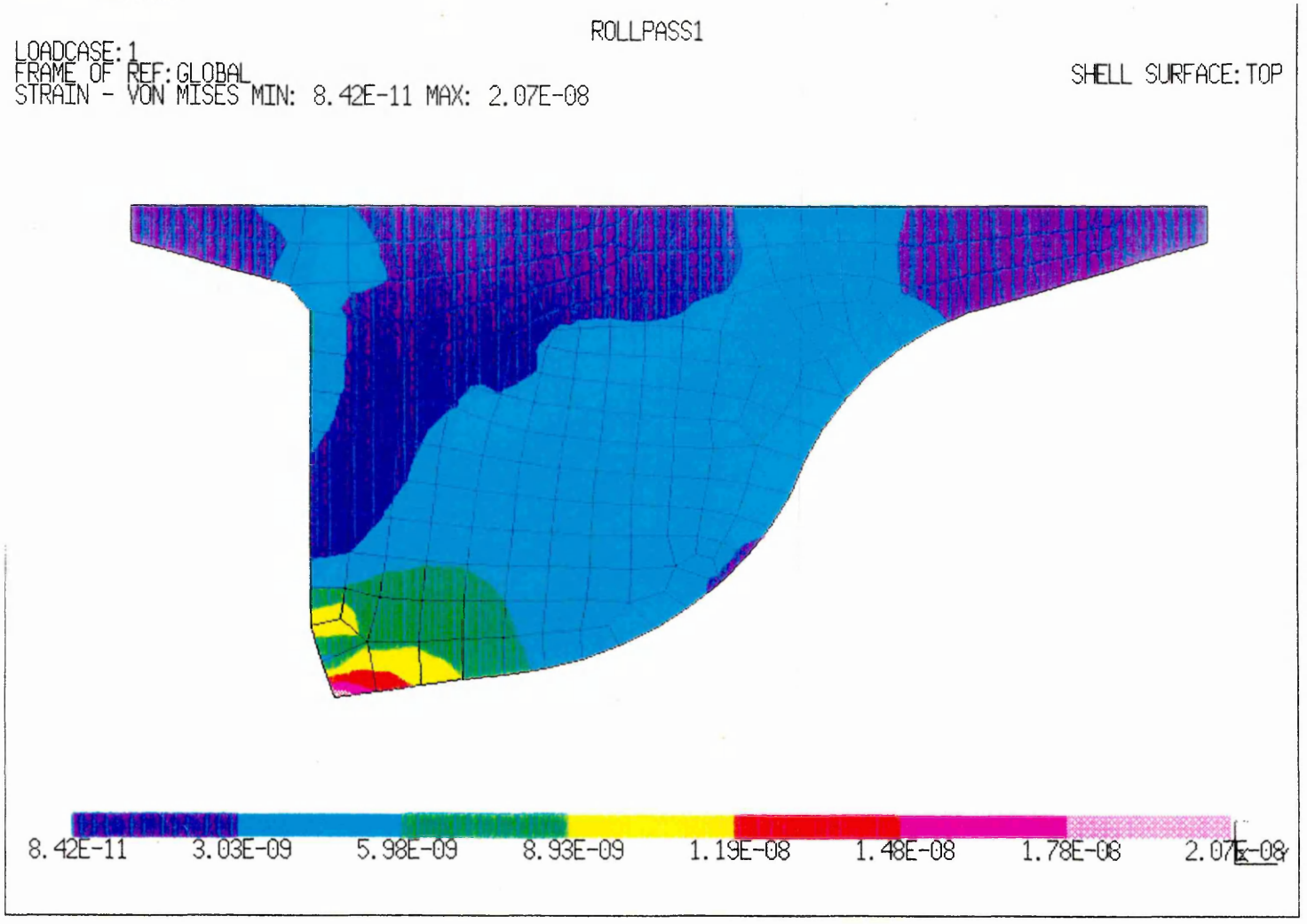

Figure 6.6 Distributions of ε_{eq} equivalent strain of 2D single tooth model

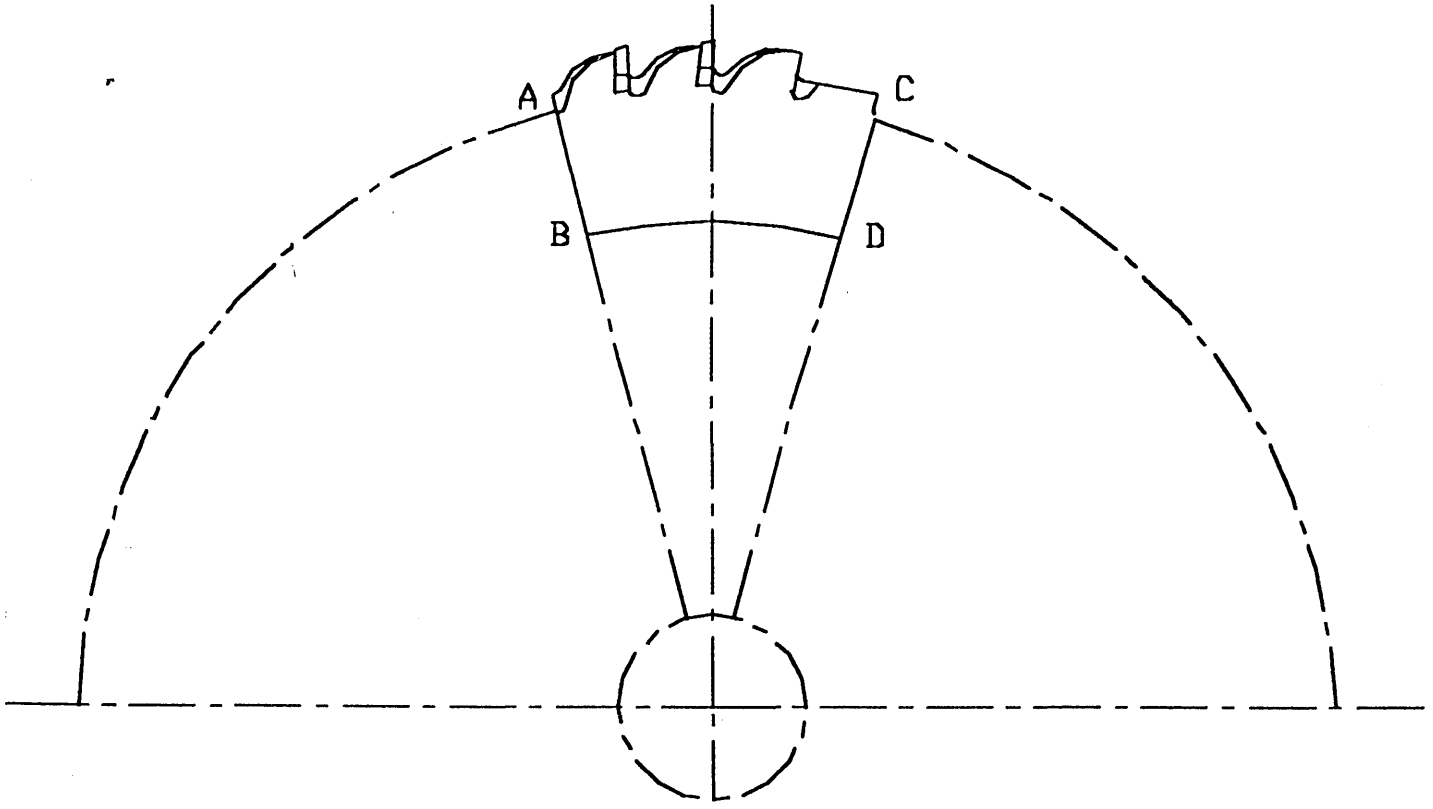

Figure 6.7 Geometric model with side boundaries (A-B, C-D) and bottom boundary (B-D) radially related to the centre of the saw

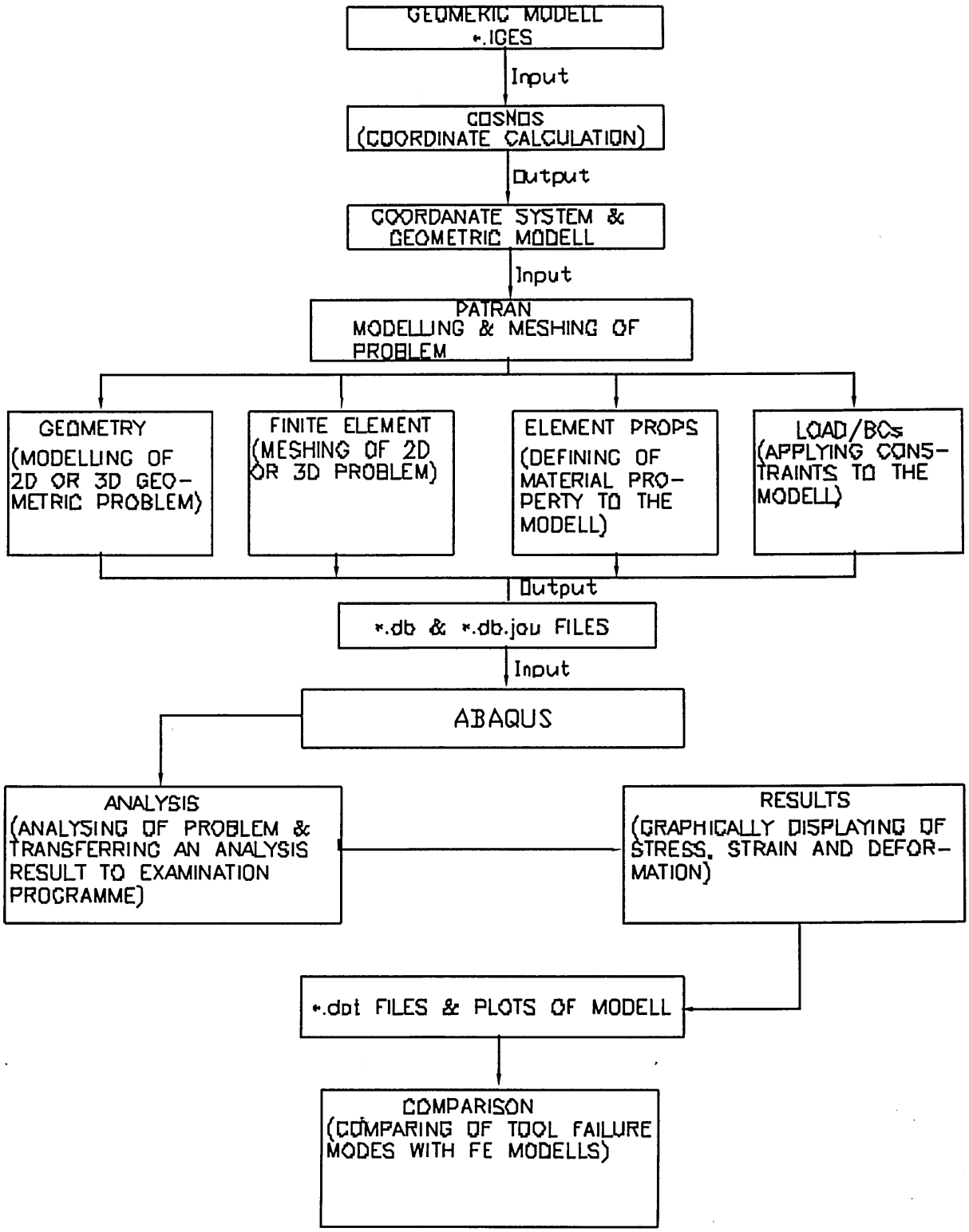

Figure 6.8 Modelling strategy of modification of the model

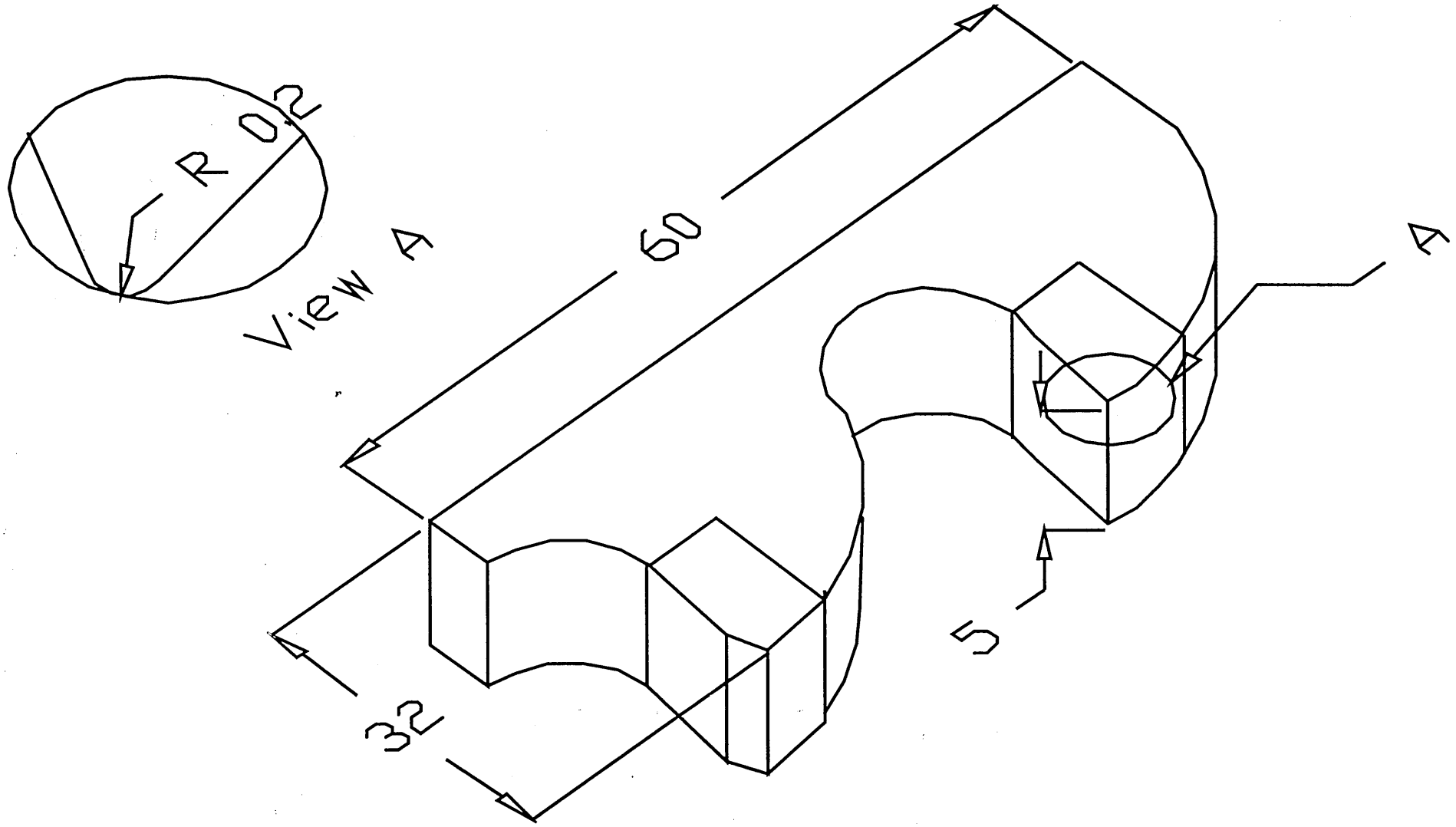

Figure 6.9 3D view of a carbide tipped circular saw segment with dimension of 60 x 32 x 5 mm, and a 0.2 mm nose radius

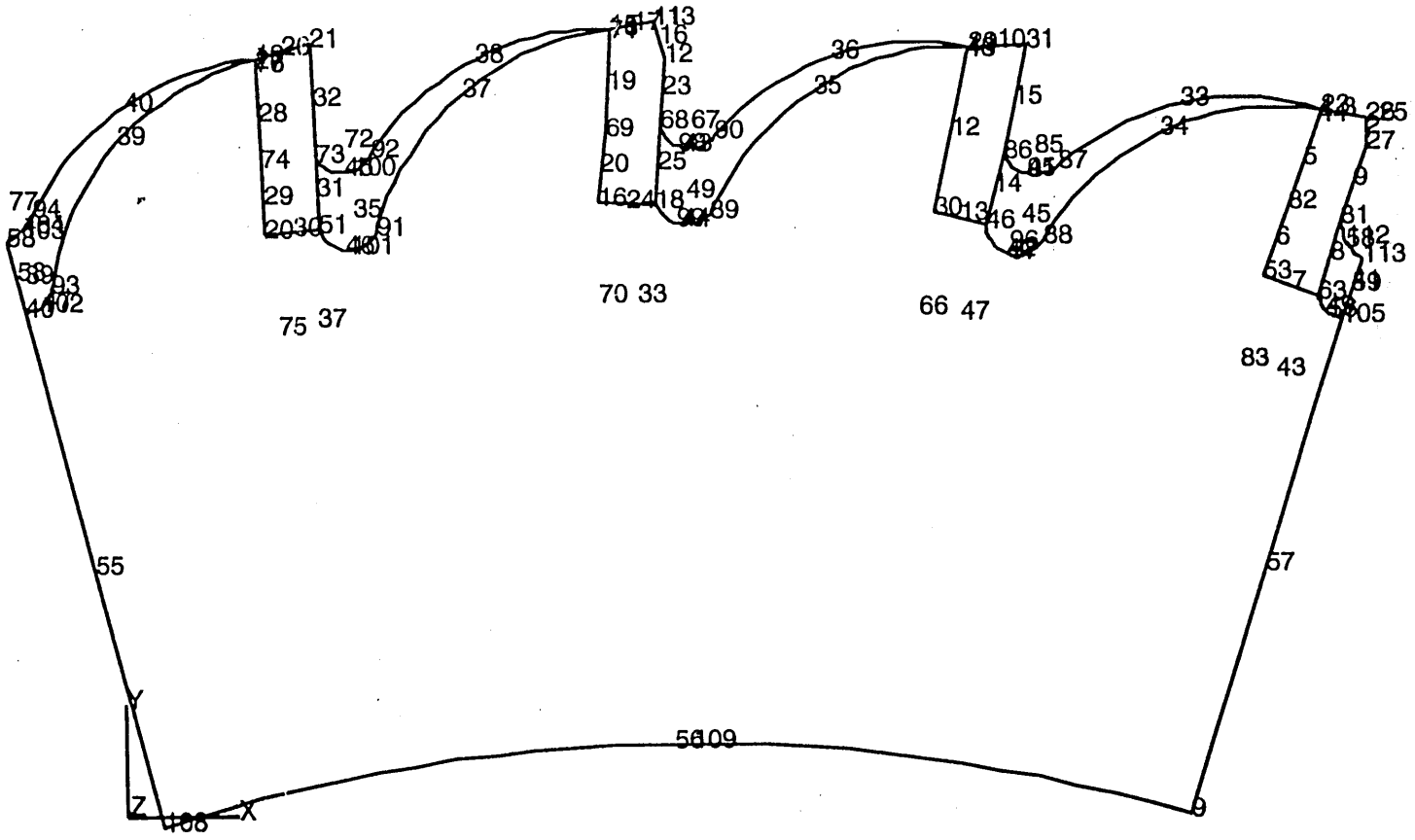

Figure 6.10 Geometric model input to the PATRAN programme

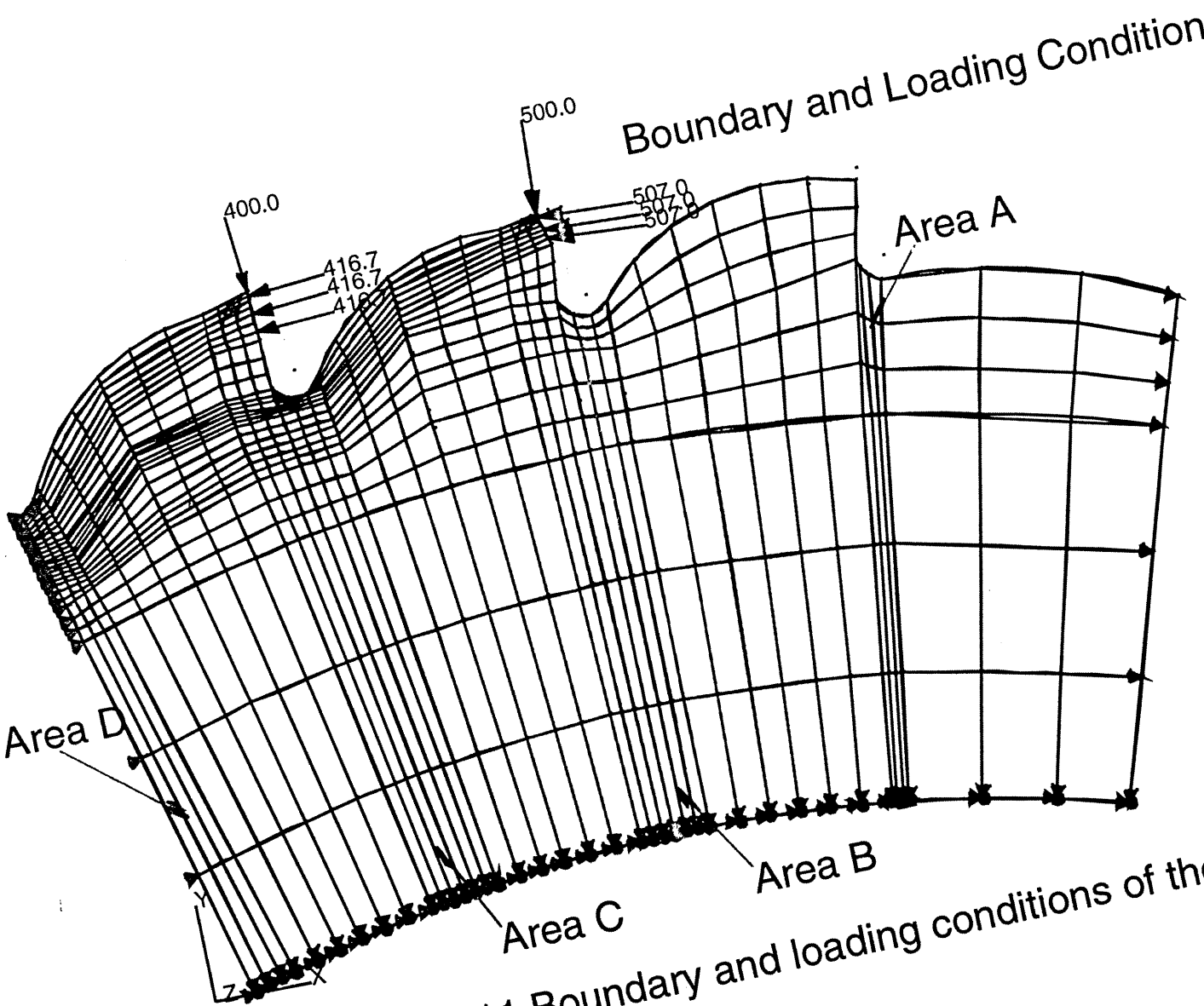

Figure 6.11 Boundary and loading conditions of the new model

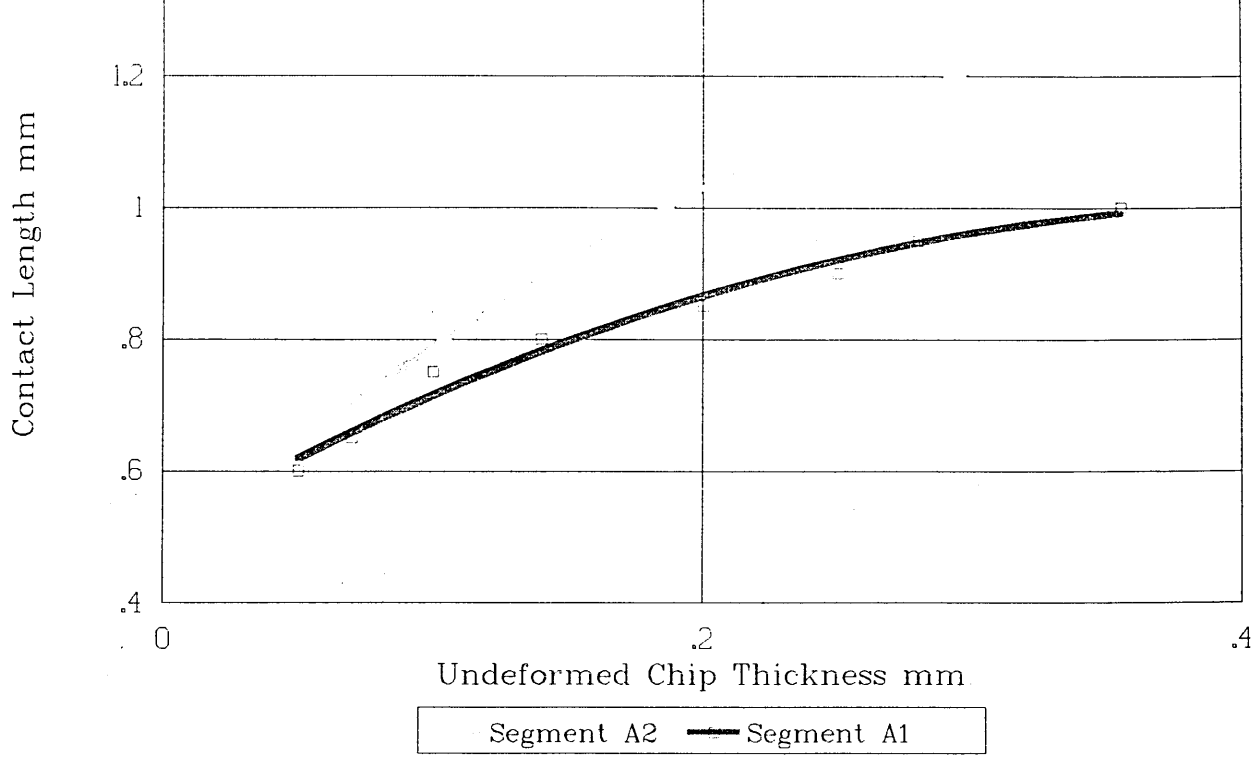

Figure 6.12 Tool-chip contact length when cutting mild steel used with A1 and A2 segments

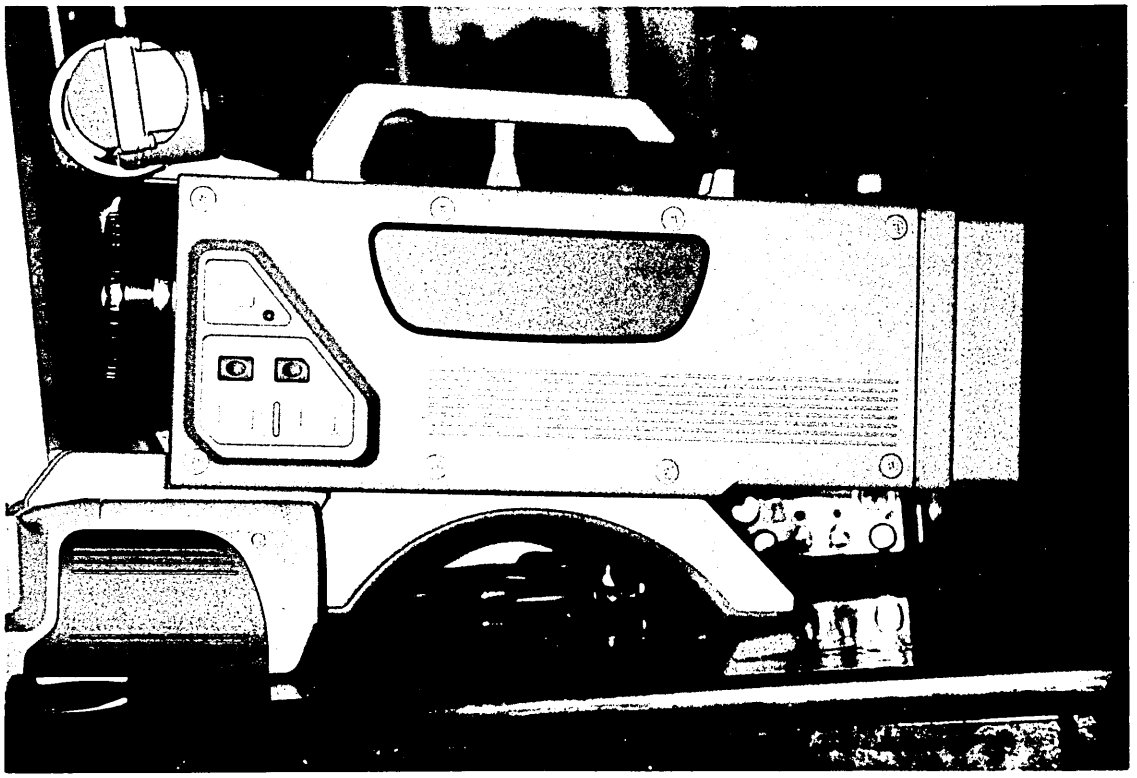

Figure 6.13 Scanner of Cyclops T135 sm Thermal Imager

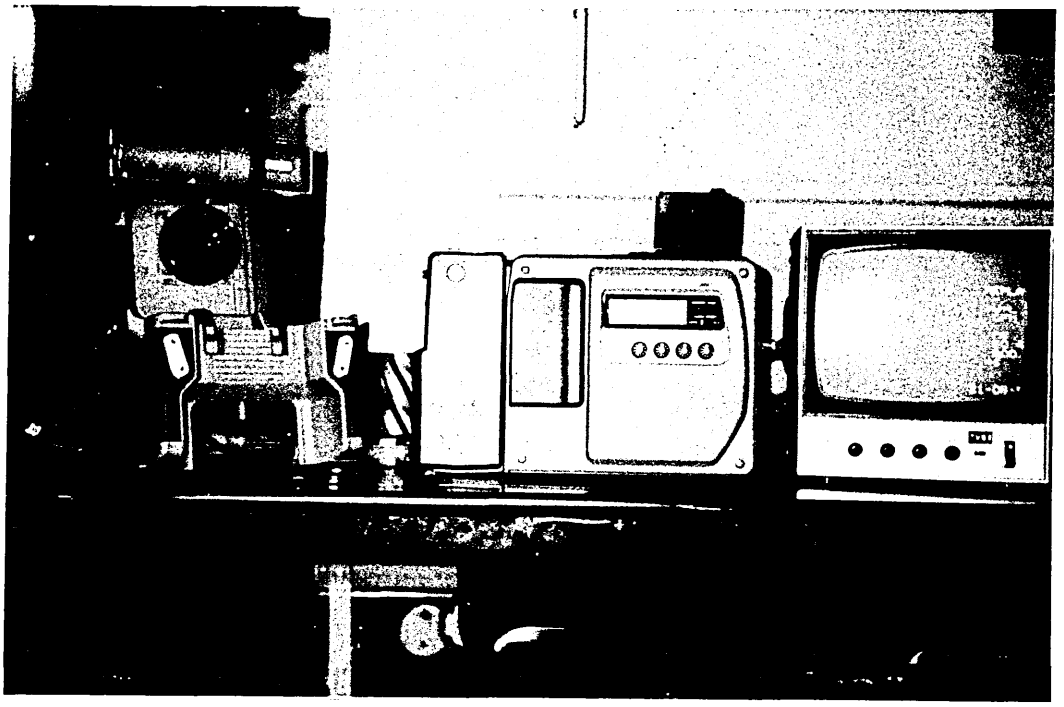

Figure 6.14 View of Cyclops T135 sm Thermal Imager and Monitor

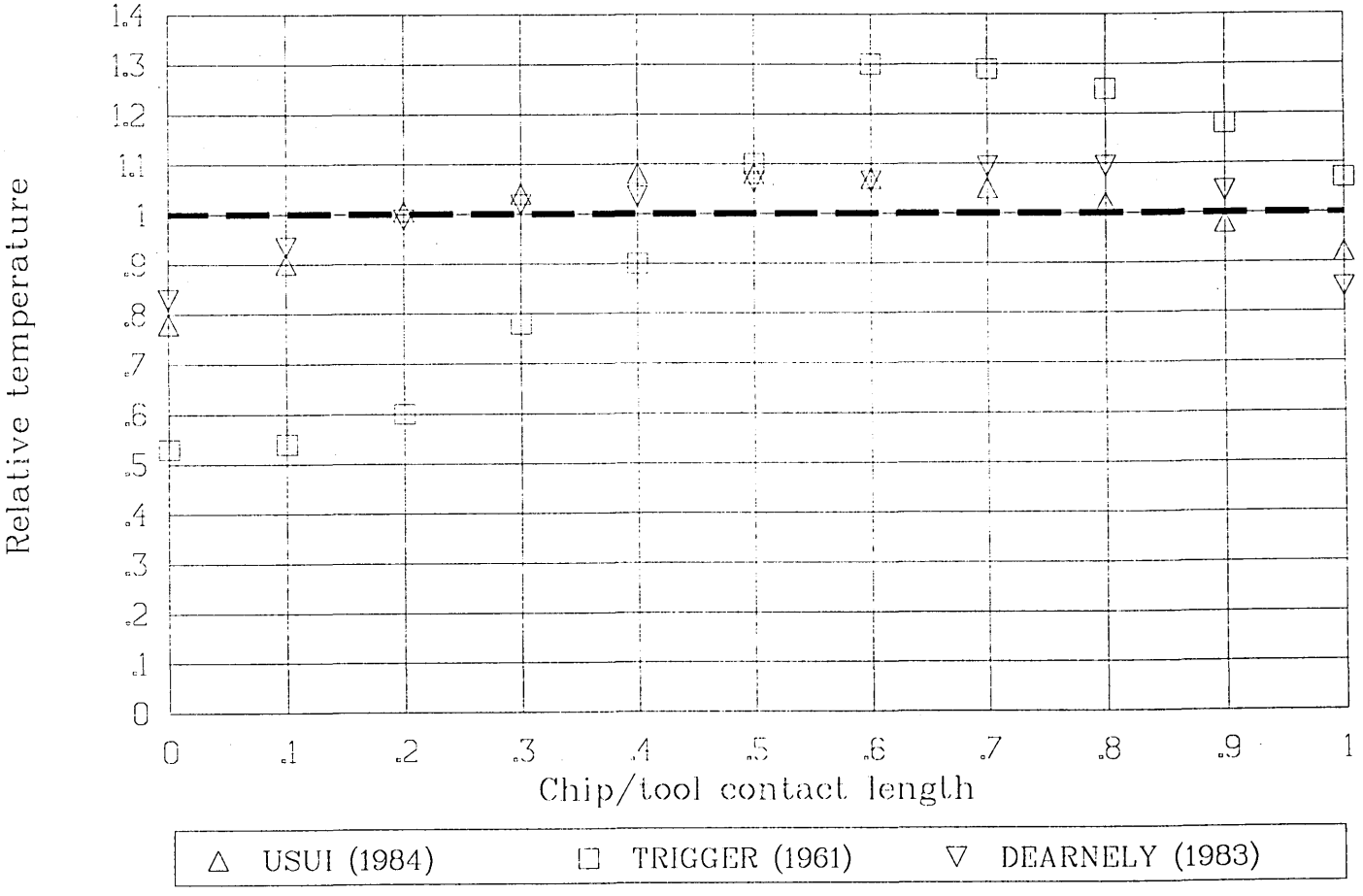

Figure 6.16 (a) Relative tool/chip temperature distributions

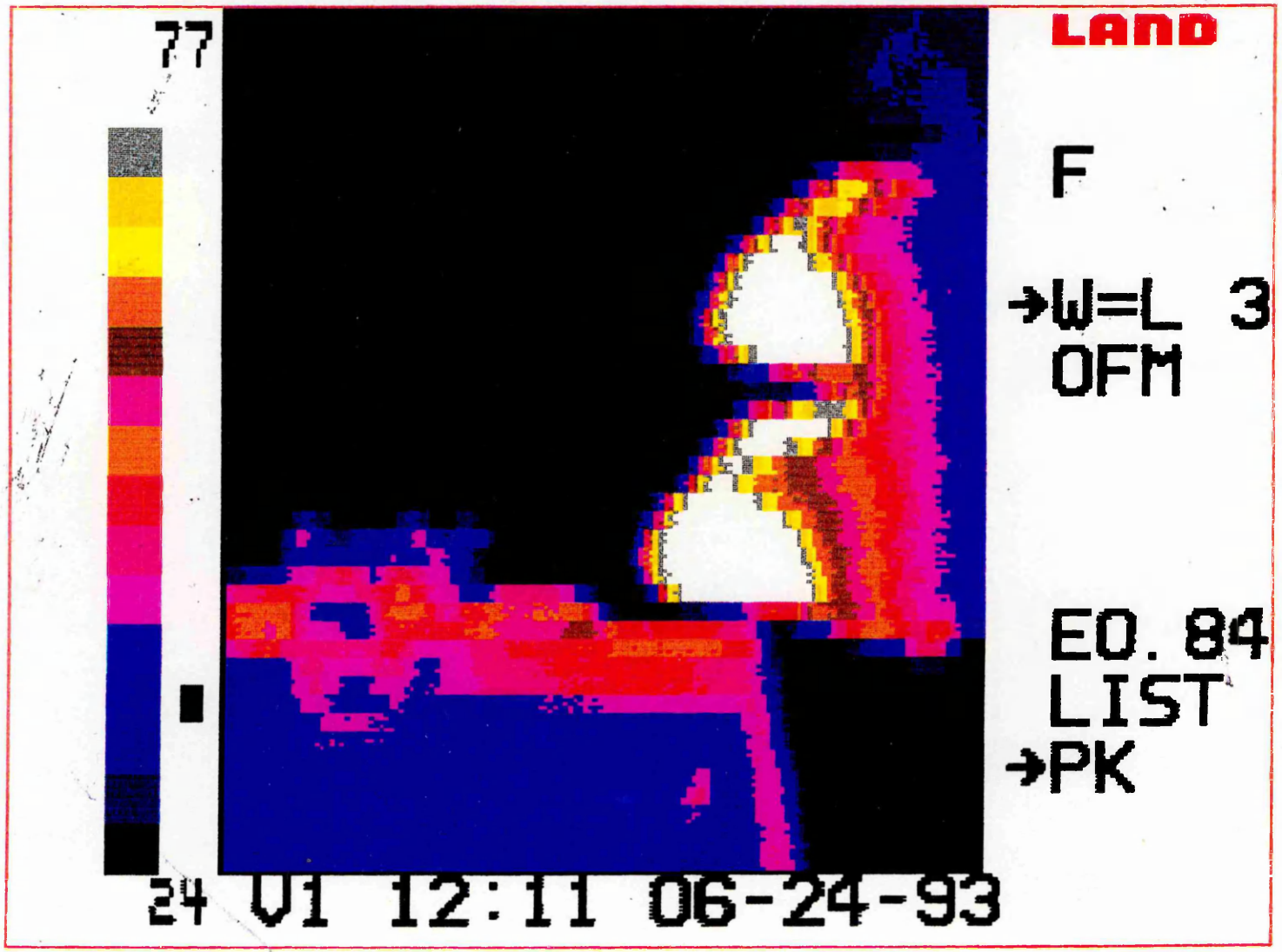

Figure 6.15 Image of the temperature obtained at cutting speed of 203 m/min when cutting mild steel

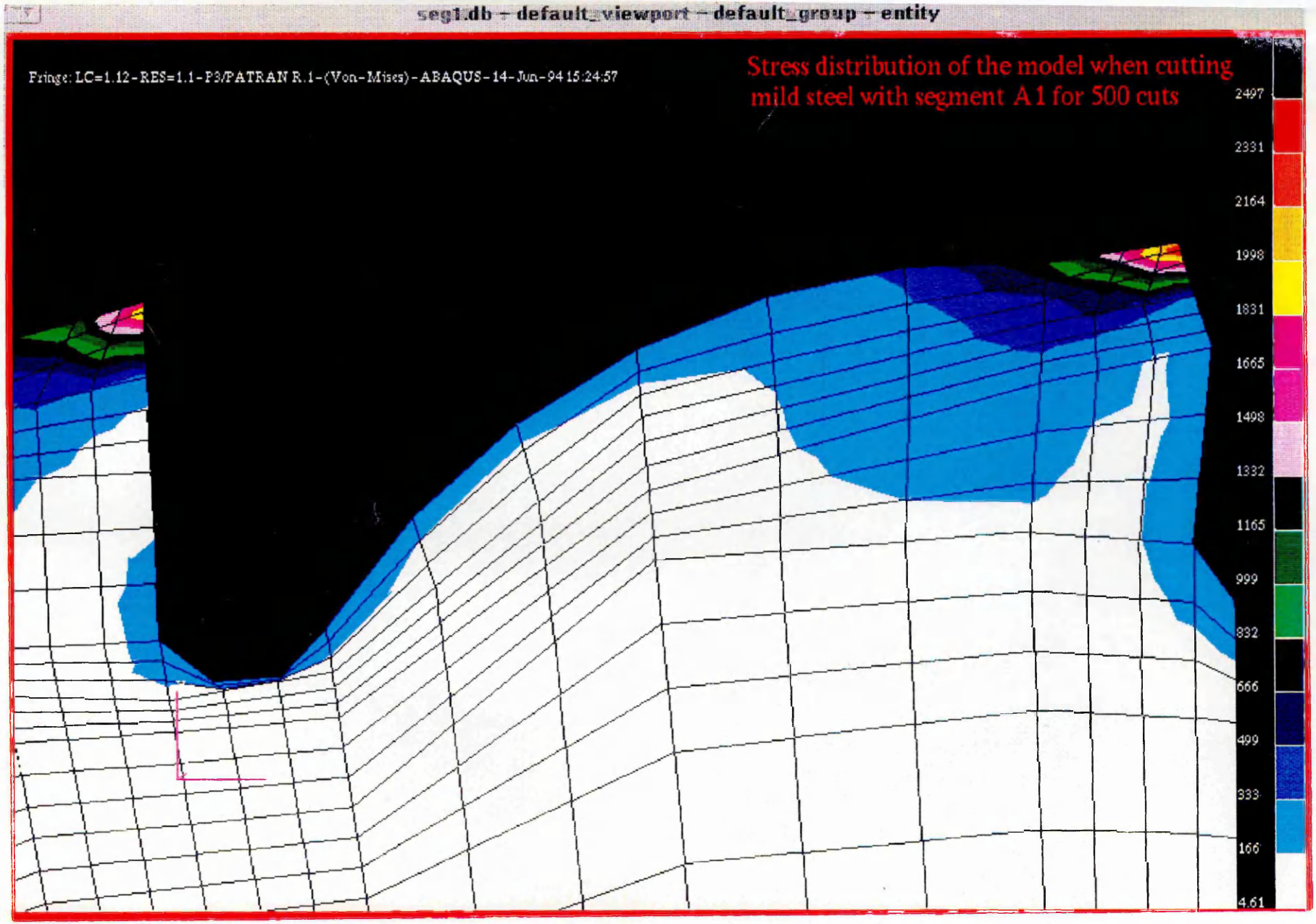

Figure 6.17 The equivalent stress σ_{eq} distribution of the new model

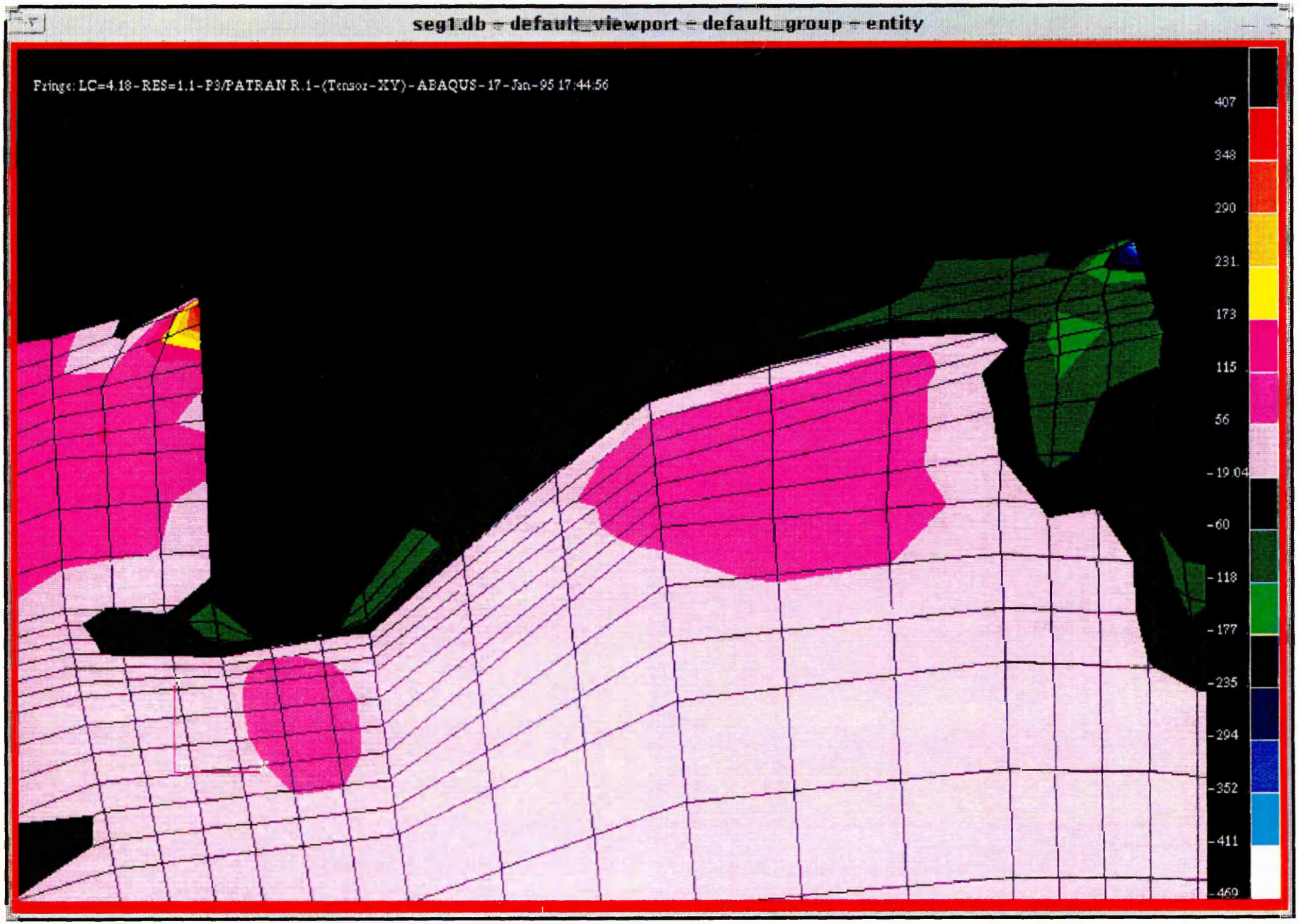

Figure 6.18 The shear stress σ_{xy} distribution of the new model

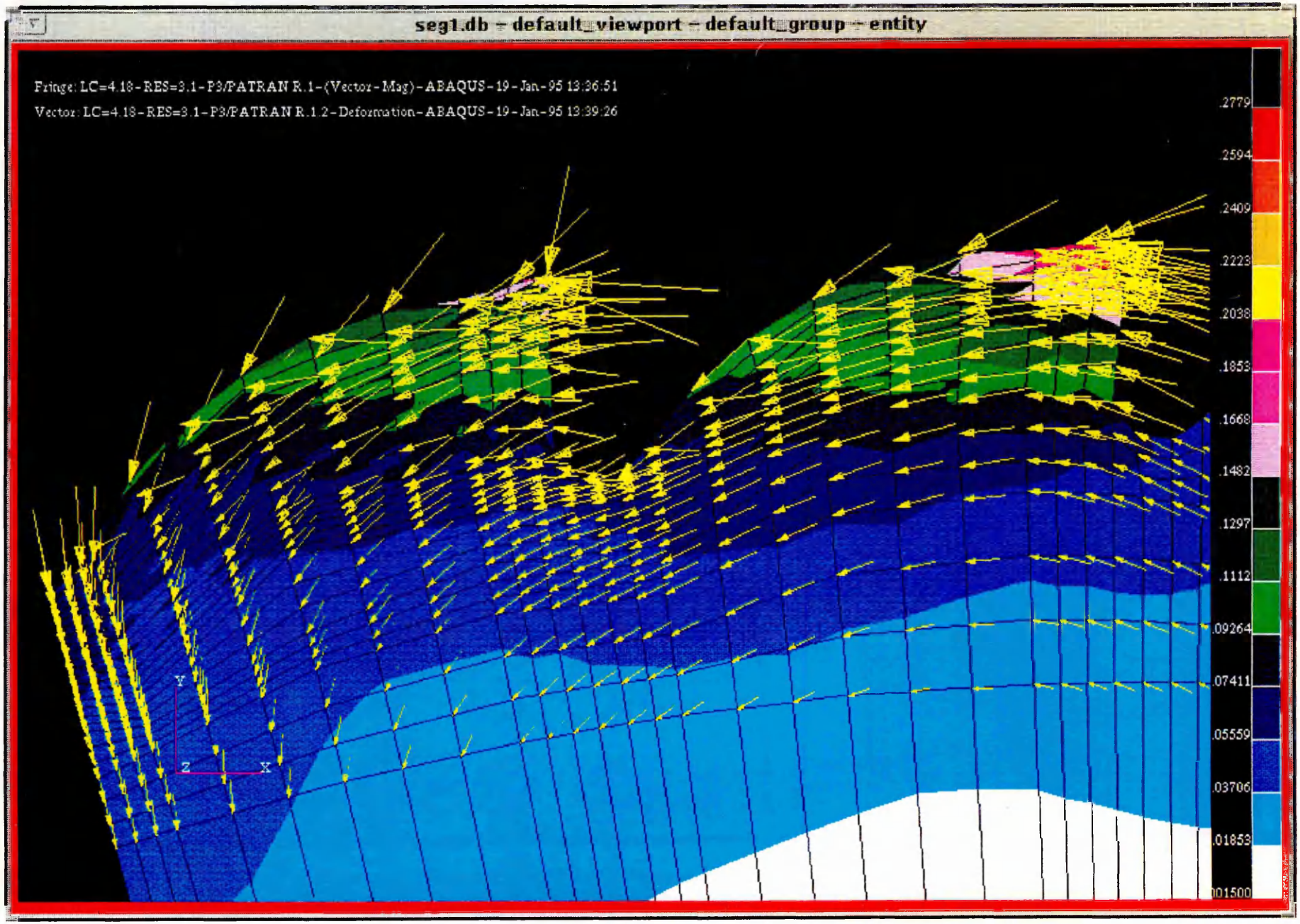

Figure 6.21 The distribution of displacement and equivalent strain ε_{eq} of the new model

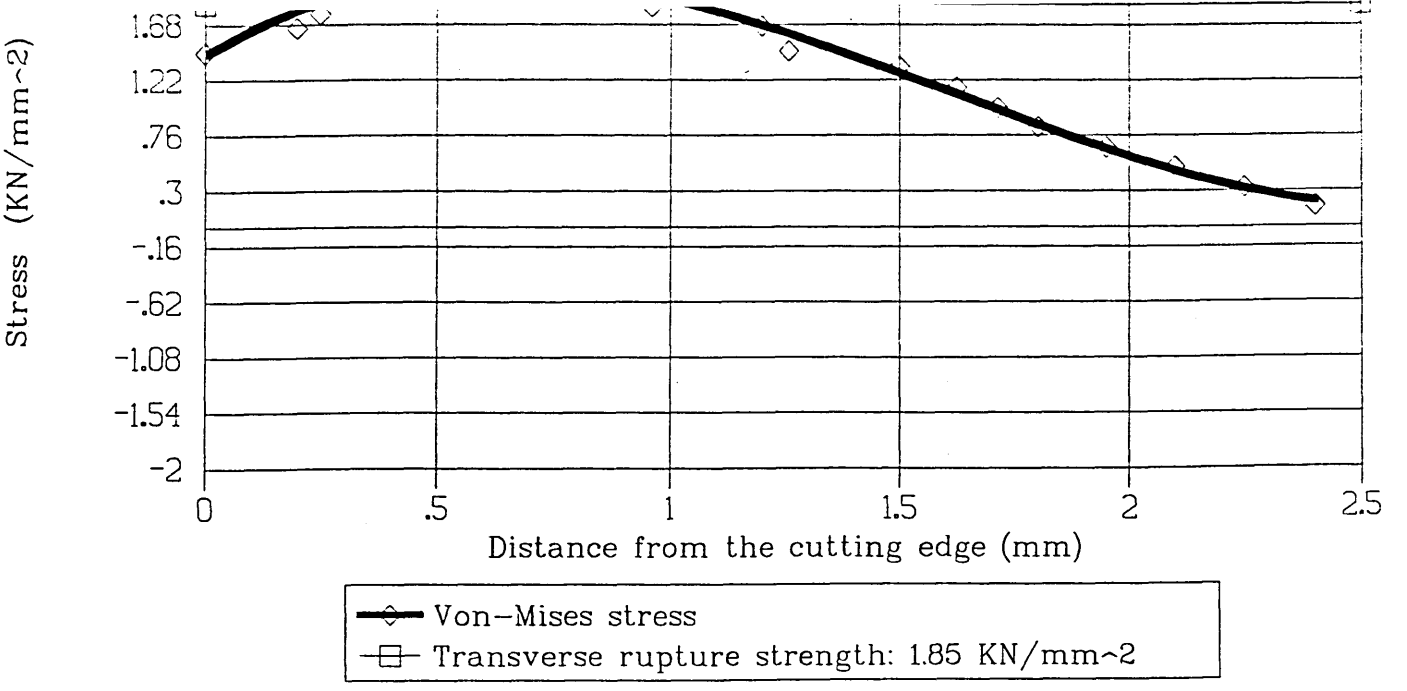

Figure 6.23 Equivalent stress σ_{eq} vs the distance from the cutting edge on the rake face of the roughing tooth

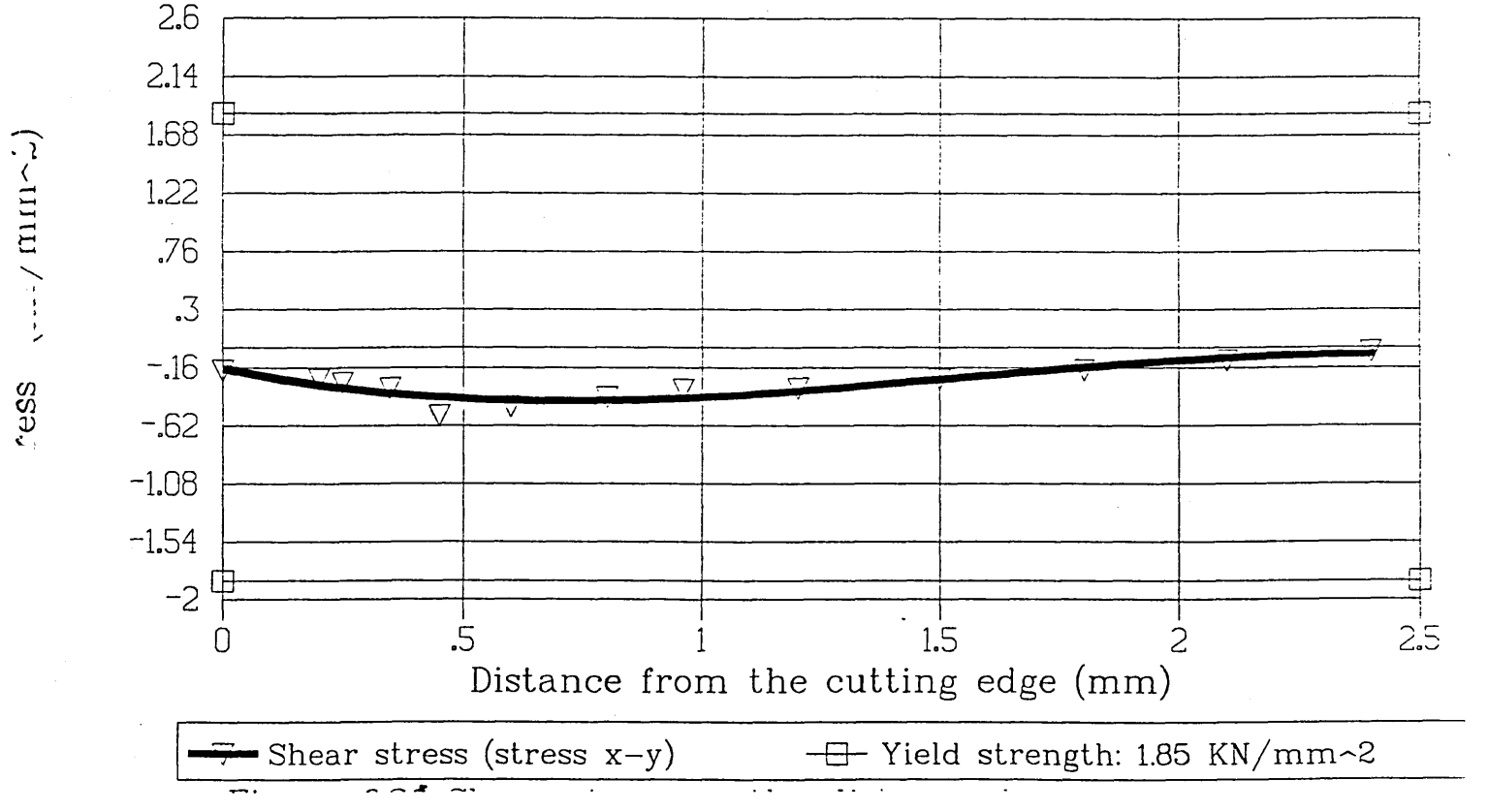

Figure 6.24 Shear stress σ_{xy} vs the distance from the cutting edge on the rake face of the roughing tooth

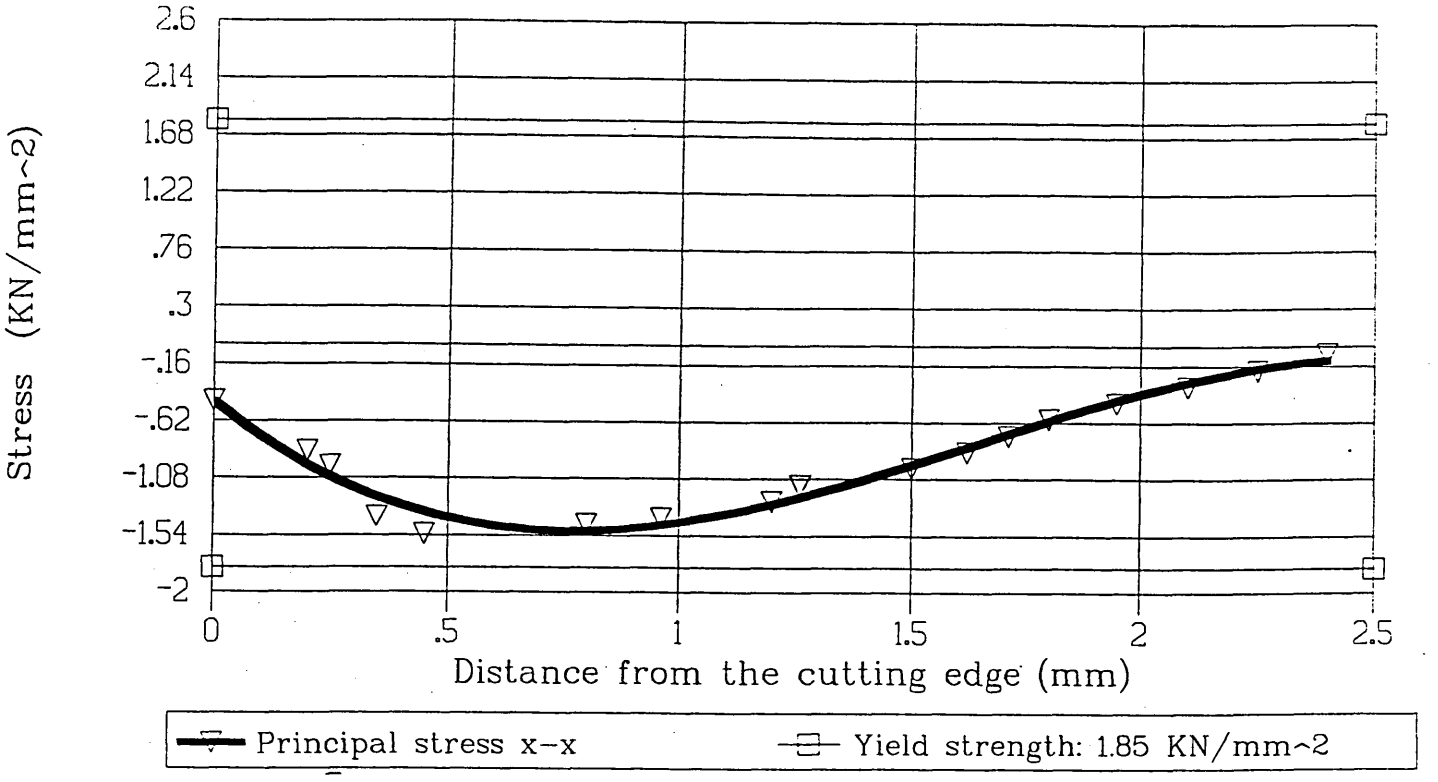

Figure 6.25 Stress σ_{xx} vs the distance from the cutting edge on the rake face of the roughing tooth

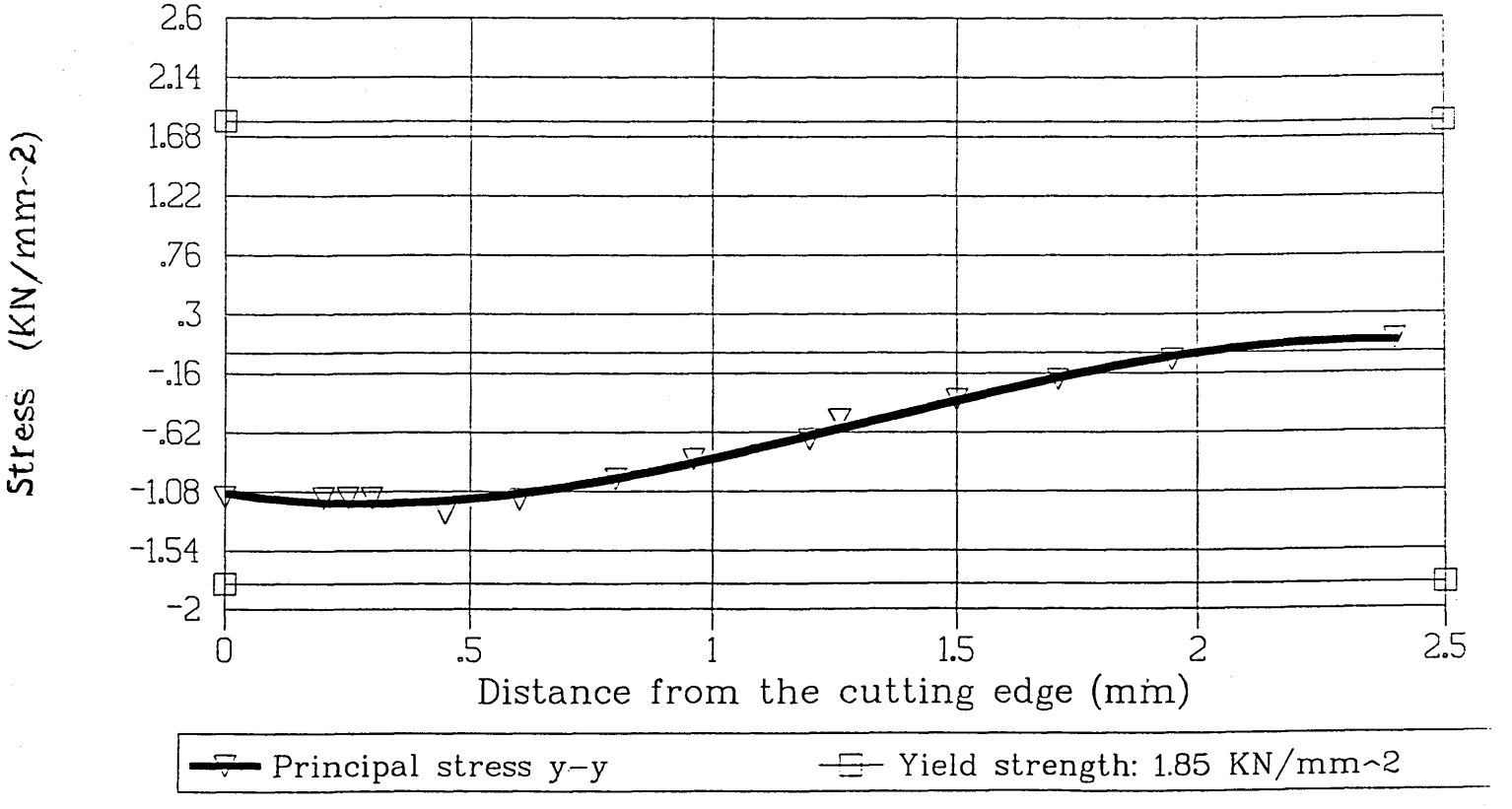

Figure 6.26 Stress σ_{yy} vs the distance from the cutting edge on the rake face of the roughing tooth

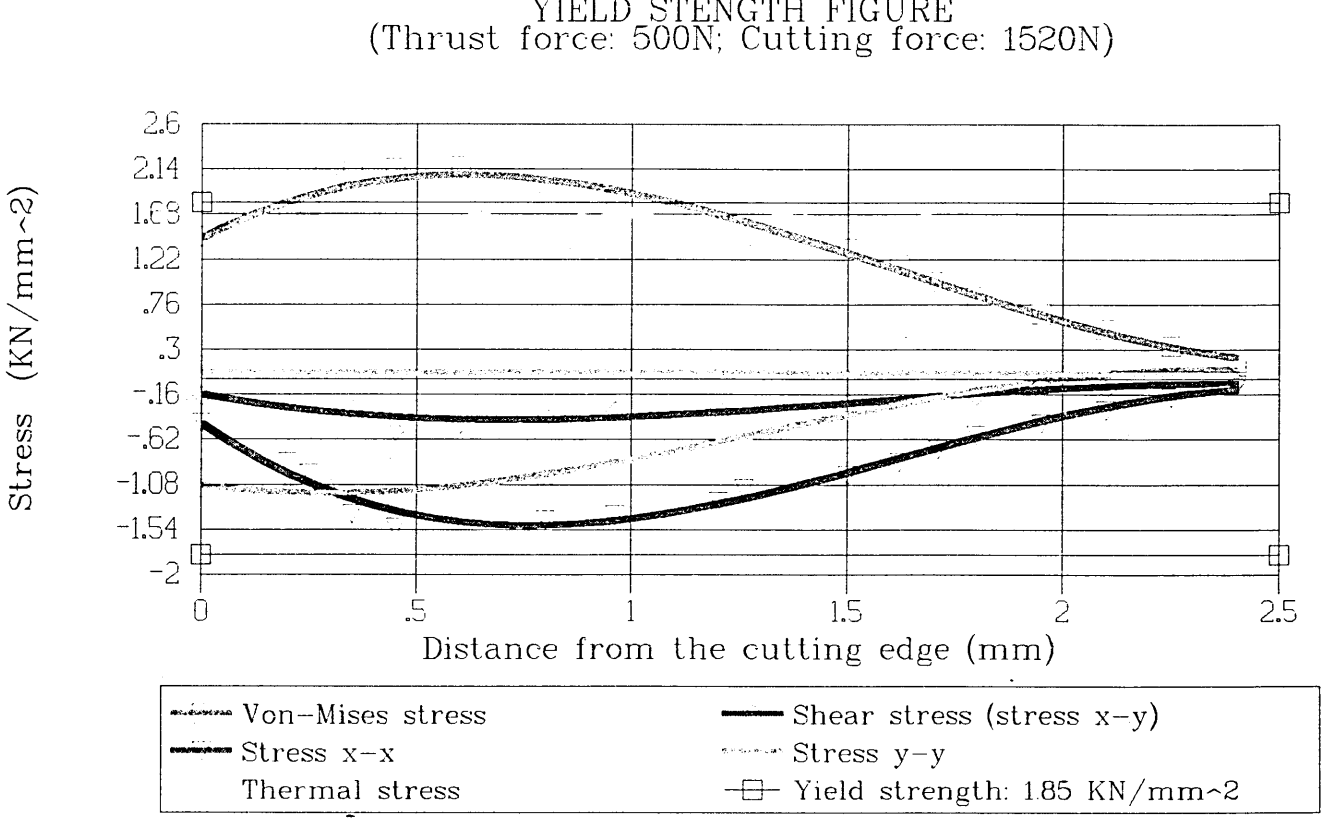

Figure 6.27 Stresses vs the distance from the cutting edge on the rake face of the roughing tooth

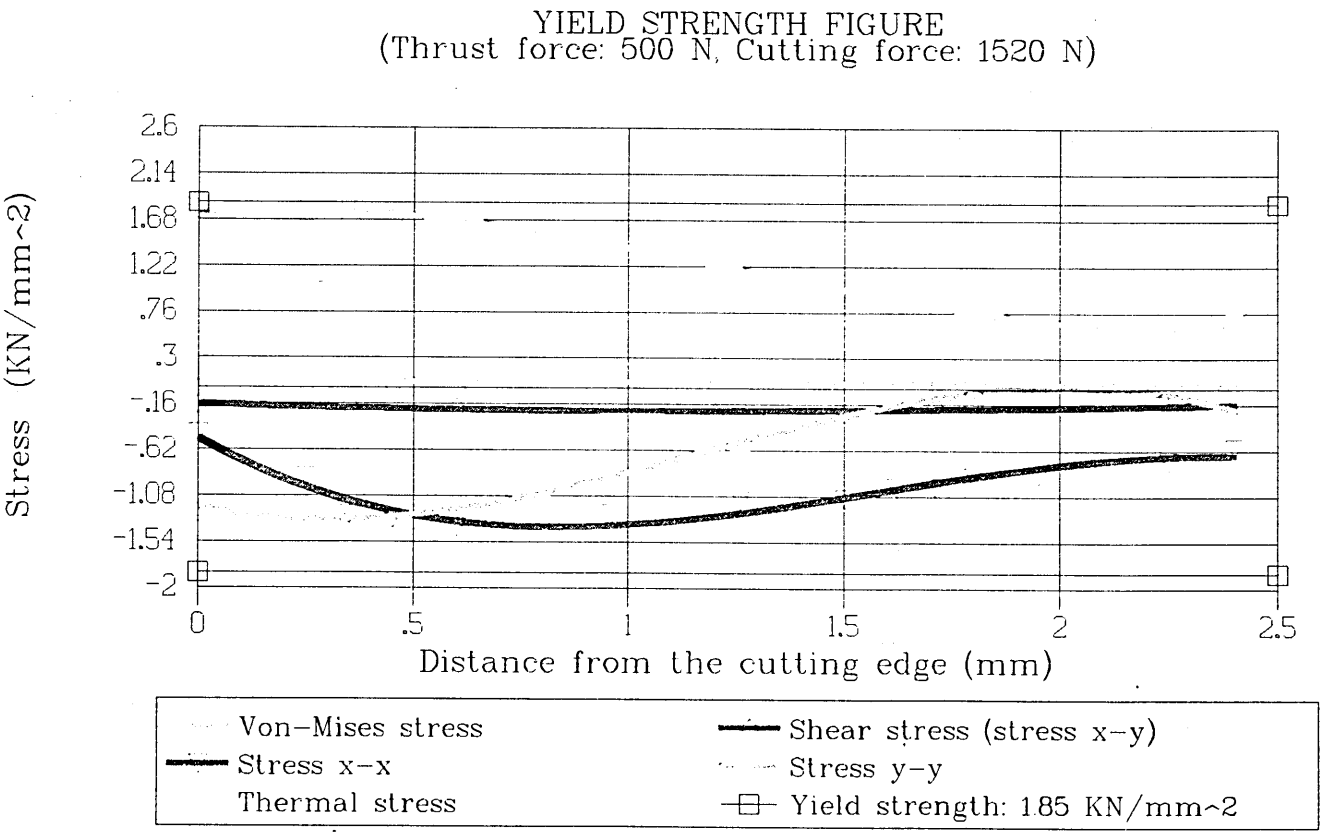

Figure 6.28 Stresses vs the distance from the cutting edge on the flank face of the roughing tooth

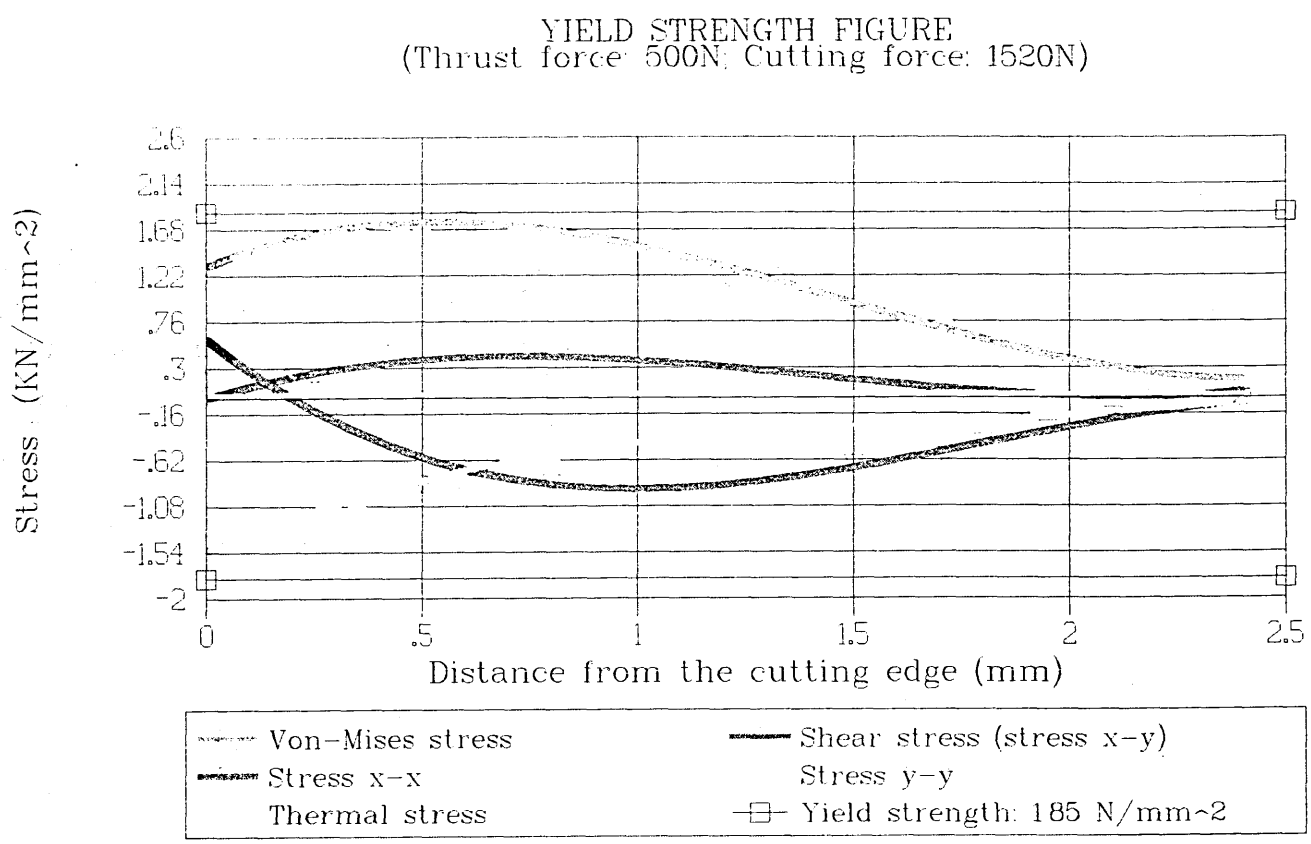

Figure 6.29 Stresses vs the distance from the cutting edge on the rake face of the finishing tooth

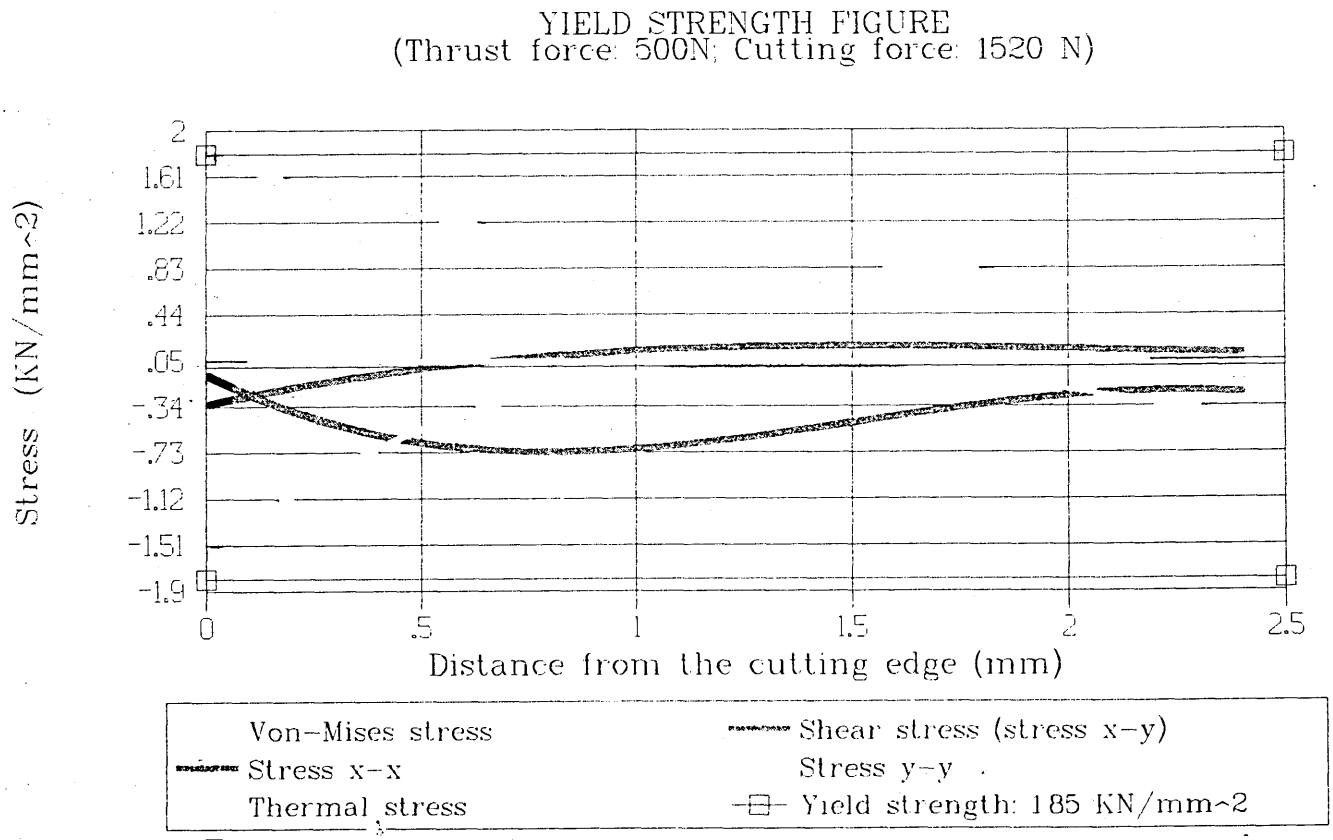

Figure 6.30 Stresses vs the distance from the cutting edge on the flank face of the finishing tooth

YIELD STRENGTH FIGURE

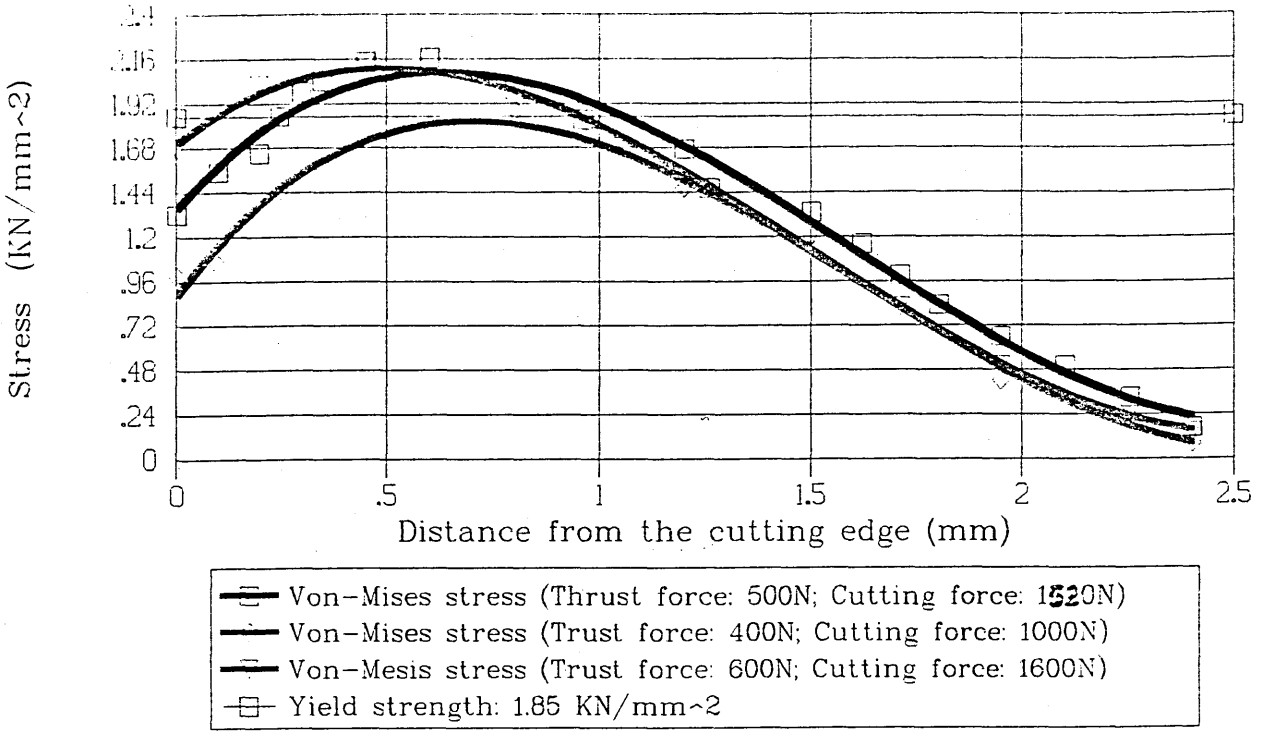

Figure 6.31 The equivalent stresses vs the distance from the cutting edge on the rake face of the roughing tooth under three loading conditions

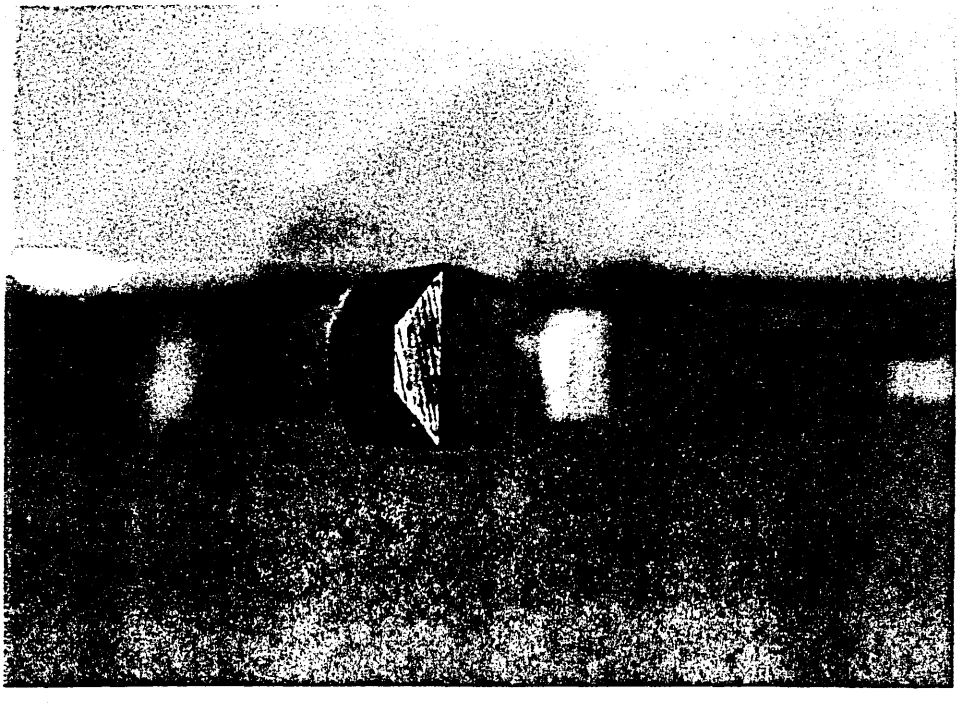

Figure 6.32(a) The crater wear occurred at a low loading condition

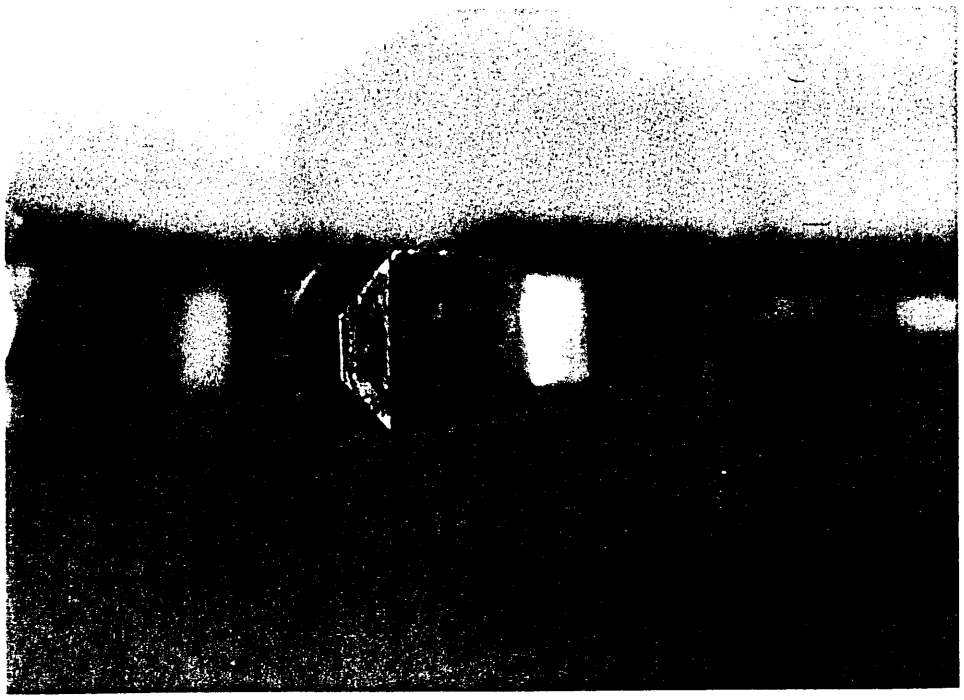

Figure 6.32(b) The crater wear occurred at a medium loading condition

Figure 6.32(c) The crater wear occurred at a high loading condition

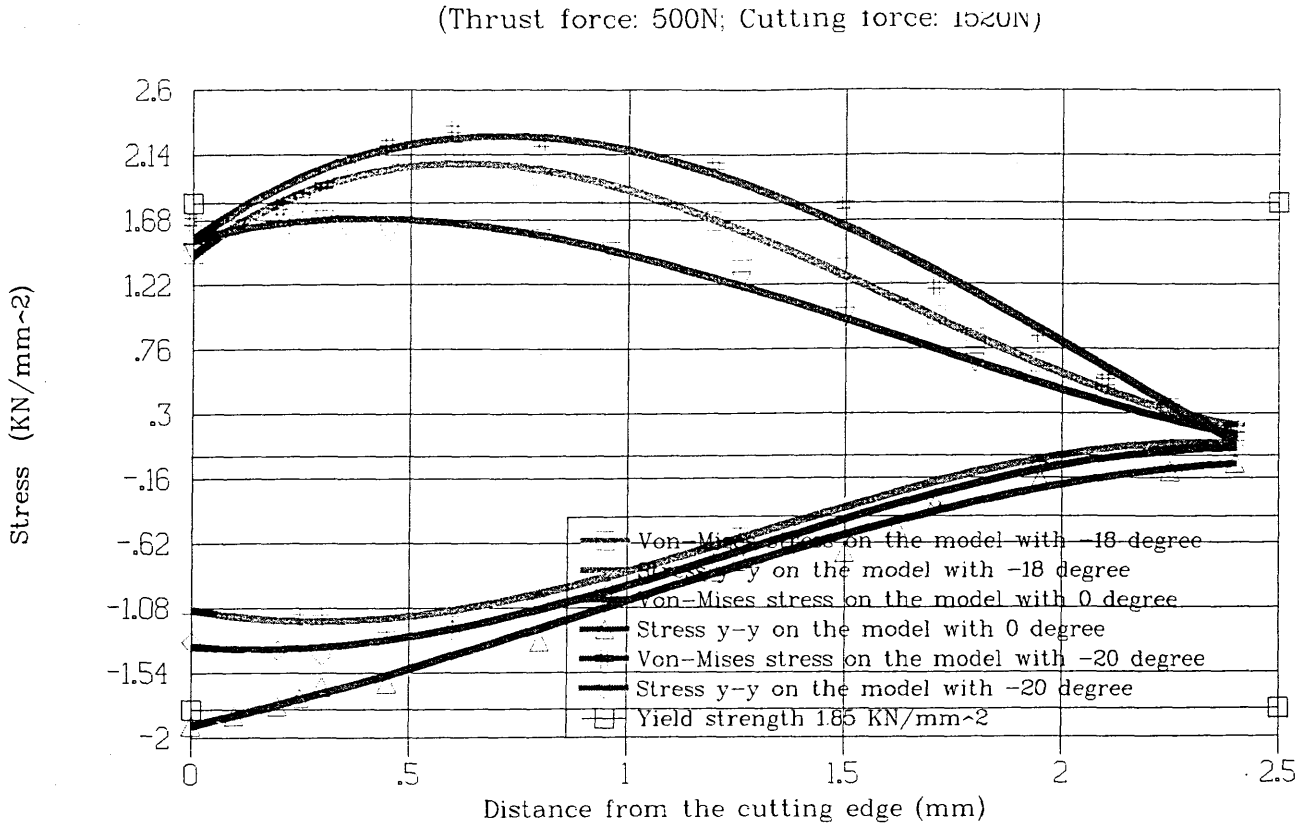

Figure 6.33 Stresses vs the distance from the cutting edge on the rake face of the roughing tooth with three different rake angles

TYPE OF BLADE	LIMITATIONS	ADVANTAGES	APPLICATION
High Speed Steel Solid Saw Blades	Generally used to cut smaller diameters not exceeding 14 to 16 inches, where it is impractical to use a larger solid blade. Not suitable for applying coating technology owing to restriction in chamber capacity not being able to accommodate full blades. When cutting temperature is above 600 °C, the hardness of the HSS blade sharply decreases, hence, not suitable for cutting "difficult" to cut materials.	Smoother surface finish and narrow kerf.	Ferrous,nonferrous materials, some alloy steels such as chromium based alloys.
High Speed Steel Segmental Saw Blades	Segmental blades generally have to be thicker than solid blades, and the surface finish produced is not usually as smooth as that produced with HSS solid blades. Since the hardness of HSS will be lost above 600 degree C, it is still not ideal for cutting "difficult" to cut materials.	More widely used than solid blades because of their greater ability to absorb shock. Teeth on the segments can be designed to suit specific requirements, also, when individual segments are worn or broken, they can be removed , resharpened, and replaced a number of times thus reducing blade costs. It is suitable for applying advanced coating techniques to relatively small segment size.	Ferrous, nonferrous materials, and some alloy steels.
Carbide Tipped Saw Blades	More expensive, lower thermal conductivity and more brittle than HSS sawblades.	Because of its high red hardness, it is suitable for cutting some difficult to cut materials under certain cutting conditions. Higher cutting rates can be obtained when sawing plastics, wooden materials and some difficult to cut materials. High surface finish produced when sawing difficult to cut materials. When teeth are broken or worn, they can be removed, resharpened or replaced for a number of times.	Ferrous, nonferrous materials,plastics, wooden materials and some "difficult" to cut materials.

Table 1.1 Comparison of three types of saw blades

Carbide grade	W	Co	Ta	Ti
	weight %	weight %	weight %	weight %
SP35	64.23	9.34	5.64	9.65
SP45	73.69	12.8	3.56	4.07
MK20	86.74	6.61	0.02	0.01
S4	64.32	9.69	5.71	9.49

Table 3.1 Chemical composition of the carbide grades

Carbide grades	Volume of sample (mm^3)	Weight of the sample (g)	Gravity (g/mm^3)
S4	58.6	0.674	0.0115
SP35	403.07	4.54	0.01126
SP45	370.558	4.374	0.0118
MK20	750.76	10.9	0.0145

Table 3.2 Comparison of speci fic gravity of the carbides

Carbide grade	Mean linear intercept ($d=\frac{l}{n}$) μm	True mean diameter ($D=1.75d$) μm
S4	1.23	2.15
SP45	0.72	1.26
SP35	1.082	1.89
MK20	0.848	1.48

Table 3.3 Comparison of the carbide grain sizes

Workpiece material	Cutting speed m/min	Feed mm/rev. per pair of teeth	Cutting condition
Mild steel	100, 151, 203	0..264 - 0.66	Dry
302S25 stainless steel	15, 23, 34	0.0264 - 0.046	Dry
LM4 aluminium	750, 1000, 1400	0.0264 - 0.0594	Dry
C25 nimonic alloy	15, 21, 34	0.0264 - 0.096	Dry

Table 4.1 The cutting conditions for performance cutting tests

Segment	Carbide grade	Rake angle (Degree)	Clearance angle (Degree)	Nose radius (mm)	Application
A1	S4	-18	+8	0.2	Cutting mild steel & 302S25 stainless steel
A2	S4	0	+8	0.3	Cutting mild steel & 302S25 stainless steel
B1	MK20	-18	+8	0.2	Cutting 302S25 stainless steel
B2	MK20	0	+8	0.3	Cutting 302S25 stainless steel
C1	K20	+10	+15	0.2	Cutting LM4 Aluminium
C2	K20	+15	+10	0.2	Cutting LM4 Aluminium

Table 4.2 Geometries of the segments and their applications

Name	C	Si	Mn	P	S	Cr	Ni	Mo	Ti	Hardness HV
Mild steel	0.17	0.2	0.8	0.026	0.039	-	-	-	-	123.9
EN 58 stainless steel	0.06	0.8	1.8	0.035	0.026	18	9	-	-	164.8

Table 4.3 Chemical compositions and hardness of mild steel and EN58 stainless steel

Name	Al	Mn	Cu	Si	Tensile strength N/mm^2	Hardness HV
LM4 aluminium	98.8	0.2	2.0	4.0	140	66

Table 4.4 Chemical composition and hardness of LM4 aluminium

C	Co	Cr	Fe	Mn	Mo	Ni	P	S	Si	V	W	Hardness HV
0.002	0.67	21.4	4.1	0.27	13.3	BAL	0.007	0.003	<0.02	0.17	2.9	164

Table 4.5 Chemical composition and hardness of C25 nimonic alloy

Workpiece materials	Cutting speed m/min	Feed mm/rev. per pair of teeth
Mild steel	203	0.355
302S25 stainless steel	34	0.046
C25 nimonic alloy	29	0.045

Table 4.6 The optimised cutting conditions for wear cutting tests, cutting dry.

Workpiece materials cut	The saw segments used	The main failure modes of the segments used for wear cutting test	The segments having the best cutting performance	Geometric feature, tool material, failure modes and tool life of the segment having the best cutting performance				
				Rake angle (degree)	Clearance angle (degree)	Tool materials (carbide grade)	Comparison of tool life	Main failure modes
Mild steel	A1, A2, B1 and B2	Crater wear and edge chipping for A1, Crater wear for A2, Edge chipping for both B1 and B2	A1	-18	+8	S4	A1>B1>A2>B2	Edge chipping on the finisher tooth
302S25 stainless steel	A1, A2, B1 and B2	Edge chipping for A1, Bevel chipping for A2, Edge and corner chipping for B2, Crater wear and edge chipping for B1	B2	+5	+8	MK20	B2>A2>B1>A1	Edge chipping on the rougher tooth
C25 nimonic alloy	A2 and B2	Edge chipping for both A2 and B2	B2	+5	+8	MK20	B2>A2	Edge chipping on the finisher tooth

Table 4.7 Performance and normal feature of the uncoated segments

SEGMENT TYPE	GEOMETRIC FEATURES											
	DISTANCE mm		E ** %	DISTANCE mm		E ** %	DISTANCE mm		E ** %	DISTANCE mm		E ** %
NEW A1	H1*	51.07	0.137	H2*	51.08	0.1078	H3*	51.03	0.157	H4*	51.07	0.157
HEATED A1	H1	51.		H2	51.15		H3	51.11		H4	51.15	
NEW A2	H1*	51.07	0.12	H2*	51.07	0.0196	H3*	51.07	0.039	H4*	51.07	0.1174
HEATED A2	H1	51.13		H2	51.06		H3	51.05		H4	51.13	
NEW B1	H1*	51.07	0.1175	H2*	51.07	0.098	H3*	51.07	0.059	H4*	51.08	0.0196
HEATED B1	H1	51.01		H2	51.12		H3	51.1		H4	51.19	
NEW B2	H1*	51.07	0.098	H2*	51.08	0.059	H3*	51.07	0.039	H4*	51.08	0.078
HEATED B2	H1	51.12		H2	51.05		H3	51.05		H4	51.12	

*** * E-- Absolute value of cross deviation error.**

Table 5.1 Comparison of cross deviation error for the heated segments

SEGMENT TYPE	GEOMETRIC FEATURES											
	DISTANCE mm		E ** %	DISTANCE mm		E ** %	DISTANCE mm		E ** %	DISTANCE mm		E ** %
NEW A1	H1*	51.07	0.039	H2*	51.08	0.078	H3*	51.08	0.039	H4*	51.07	0.098
COATED A1	H1	51.09		H2	51.12		H3	51.1		H4	51.12	
NEW A2	H1*	51.07	0.0196	H2*	51.07	0.0196	H3*	51.07	0.039	H4*	51.07	0.059
COATED A2	H1	51.06		H2	51.08		H3	51.09		H4	51.1	
NEW B1	H1*	51.07	0.0196	H2*	51.07	0.039	H3*	51.07	0.0196	H4*	51.08	0.059
COATED B1	H1	51.06		H2	51.09		H3	51.08		H4	51.11	
NEW B2	H1*	51.07	0.039	H2*	51.08	0.078	H3*	51.07	0.039	H4*	51.08	0.059
COATED B2	H1	51.09		H2	51.12		H3	51.09		H4	51.05	

*** * E-- Absolute value of cross deviation error.**

Table 5.2 Comparison of cross deviation error for coated segments

SEGMENT TYPE	COATING TYPE	COATING THICKNESS μm	WORKPIECE MATERIAL TO BE CUT
A1	TiN	5	Mild steel, 302S25
A2	TiN	5	Mild steel, 302S25, C25
A1	TiAlN	5	Mild steel,
A2	TiAlN	5	Mild steel, 302S25, C25
B1	TiN	5	302S25,
B1	TiAlN	5	Mild steel, 302S25,
B2	TiN	5	302S25,
B2	TiAlN	5	302S25, C25

Table 5.3 The coated segments and their applications

Name	Tool material	Young's modulus E KN/mm^2	Poisson ratio ν	Yield strength σ_s N/mm^2
Carbide Tip	MK20	553.7	0.25	1200
Backing material	HSS	210	0.3	2400

Table 6.1 Material properties imposed to the single tooth model

Material	Young's modulus E KN/mm^2	Poisson ratio μ	Density kg/mm^2	Thermal conductivity Cal / (cm s °C)	Application
Carbide K20	550 (78.57E **Psi)	0.25	0.000012	0.065	Tips for segment types A1 and A2
Carbide P35	610 (87.14E6 Psi)	0.25	0.00001	0.12	Tips for segments types B1 and B2
High speed steel	210 (30E6 Psi)	0.3	0.0000078	0.085	Backing material for every type of segment

** Psi= 0.07 kg/cm^2 = 0.007 N/mm^2

Table 6.2 Related material properties imposed to the modified models

Type of segment	Cutting force (Rougher tooth) N	Thrust force (Rougher tooth) N	Workpiece material	Cutting speed (m/min) & feed (mm/rev.)
A1	1000	400	Mild steel	203 & 0.355
	1520	500		
	1600	600		

Table 6.3 The loding conditions for the model

APPENDIX 1

Data For The Geometric Modell

Coordinate system 0 (Cartesian)

Keypoint	X-Coordinate	Y-Coordinate	Z-Coordinate
1	-1.257211e+02	4.619711e+00	0.000000e+00
2	1.382054e+01	4.619711e+00	0.000000e+00
3	1.394028e+02	4.619711e+00	0.000000e+00
4	7.077556e+00	4.619711e+00	0.000000e+00
5	7.077556e+00	8.988008e+00	0.000000e+00
6	7.077556e+00	1.369301e+02	0.000000e+00
7	7.077556e+00	-1.281938e+02	0.000000e+00
8	6.632354e+00	4.368115e+00	0.000000e+00
9	3.114610e+01	9.304211e+01	0.000000e+00
10	1.261169e-44	5.135571e-21	4.203895e-45
11	7.077556e+00	1.296197e+02	0.000000e+00
12	7.510180e+00	1.282882e+02	0.000000e+00
13	7.633504e+00	1.296978e+02	0.000000e+00
14	6.900089e+00	1.213149e+02	0.000000e+00
15	5.097020e+00	1.293414e+02	0.000000e+00
16	4.403421e+00	1.213586e+02	0.000000e+00
17	7.086167e+00	1.212904e+02	0.000000e+00
18	7.030277e+00	1.212904e+02	0.000000e+00
19	-1.116548e+01	1.280158e+02	0.000000e+00
20	-1.081357e+01	1.200647e+02	0.000000e+00

Hit <Esc> to abort or any other key to continue Page 1

Coordinate system 0 (Cartesian)

Keypoint	X-Coordinate	Y-Coordinate	Z-Coordinate
21	-8.697224e+00	1.287003e+02	0.000000e+00
22	-8.330167e+00	1.202934e+02	0.000000e+00
23	3.744484e+01	1.256042e+02	0.000000e+00
24	3.470879e+01	1.180729e+02	0.000000e+00
25	3.998716e+01	1.252920e+02	0.000000e+00
26	3.942994e+01	1.253604e+02	0.000000e+00
27	3.950321e+01	1.239624e+02	0.000000e+00
28	3.710907e+01	1.173845e+02	0.000000e+00
29	2.139341e+01	1.285329e+02	0.000000e+00
30	1.972102e+01	1.209679e+02	0.000000e+00
31	2.395472e+01	1.285552e+02	0.000000e+00
32	2.213338e+01	1.203397e+02	0.000000e+00
33	6.201434e+00	1.170620e+02	0.000000e+00
34	5.087183e+00	1.290101e+02	0.000000e+00
35	-6.842103e+00	1.209867e+02	0.000000e+00
36	-8.367843e+00	1.203326e+02	0.000000e+00
37	-8.467730e+00	1.159856e+02	0.000000e+00
38	-1.113200e+01	1.276861e+02	0.000000e+00
39	-2.191195e+01	1.181743e+02	0.000000e+00
40	-2.185811e+01	1.165151e+02	0.000000e+00

Coordinate system 0 (Cartesian)

Keypoint	X-Coordinate	Y-Coordinate	Z-Coordinate
41	3.874918e+01	1.174556e+02	0.000000e+00
42	3.708929e+01	1.174352e+02	0.000000e+00
43	3.533348e+01	1.134573e+02	0.000000e+00
44	3.734961e+01	1.252868e+02	0.000000e+00
45	2.375018e+01	1.206242e+02	0.000000e+00
46	2.210716e+01	1.203874e+02	0.000000e+00
47	2.088559e+01	1.162144e+02	0.000000e+00
48	2.132125e+01	1.282065e+02	0.000000e+00
49	8.465918e+00	1.218080e+02	0.000000e+00
50	6.867864e+00	1.213587e+02	0.000000e+00
51	-8.357342e+00	1.203646e+02	0.000000e+00
52	2.219124e+01	1.203646e+02	0.000000e+00
53	3.471822e+01	1.181084e+02	0.000000e+00
54	3.714462e+01	1.170301e+02	0.000000e+00
55	2.457756e+01	4.619711e+00	0.000000e+00
56	3.767278e+01	1.161919e+02	0.000000e+00
57	1.102367e+01	2.166900e+01	0.000000e+00
58	-2.267673e+01	1.197373e+02	0.000000e+00
59	2.293589e+00	2.145312e+01	0.000000e+00
60	5.889997e+00	2.552198e+00	0.000000e+00

Hit <Esc> to abort or any other key to continue Page 3

Coordinate system 0 (Cartesian)

Keypoint	X-Coordinate	Y-Coordinate	Z-Coordinate
61	-2.189861e+01	1.166745e+02	0.000000e+00
62	3.714323e+01	1.170354e+02	0.000000e+00
63	3.726352e+01	1.171044e+02	0.000000e+00
64	-2.033351e+01	1.176603e+02	0.000000e+00
65	-2.034154e+01	1.177213e+02	0.000000e+00
66	1.908760e+01	1.164162e+02	0.000000e+00
67	8.659092e+00	1.250730e+02	0.000000e+00
68	7.185357e+00	1.245755e+02	0.000000e+00
69	4.682129e+00	1.245663e+02	0.000000e+00
70	4.362207e+00	1.169861e+02	0.000000e+00
71	5.037805e+00	1.289671e+02	0.000000e+00
72	-7.107021e+00	1.242077e+02	0.000000e+00
73	-8.503214e+00	1.235221e+02	0.000000e+00
74	-1.098383e+01	1.231862e+02	0.000000e+00
75	-1.031160e+01	1.156291e+02	0.000000e+00
76	-1.120561e+01	1.275958e+02	0.000000e+00
77	-2.262531e+01	1.212919e+02	0.000000e+00
78	-2.510187e+01	-1.118920e+02	0.000000e+00
79	-2.354959e+01	-1.117929e+02	0.000000e+00
80	-2.112929e+01	-1.124319e+02	0.000000e+00

Hit <Esc> to abort or any other key to continue Page 4

Coordinate system 0 (Cartesian)

Keypoint	X-Coordinate	Y-Coordinate	Z-Coordinate
81	3.830385e+01	1.205292e+02	0.000000e+00
82	3.588354e+01	1.211682e+02	0.000000e+00
83	3.361262e+01	1.139290e+02	0.000000e+00
84	3.736610e+01	1.253269e+02	0.000000e+00
85	2.440327e+01	1.238730e+02	0.000000e+00
86	2.287721e+01	1.235721e+02	0.000000e+00
87	2.039420e+01	1.238898e+02	0.000000e+00

APPENDIX 2

Conferences Attended and Publications

(1) "35th International conference on advances in coatings and surface engineering" May, 1992, Newcastle Polytechnic.

(2) "International conference on advances in materials and processing technologies (AMPT'93)", 24-27 Aug.,1993, Dublin City University, Republic of Ireland.

(3) Xi-yang Zhang, M Sarwar "Characteristics of carbide circular saws", Proceedings of the AMPT'93, Vol. 3, P1897, Aug.,1993.

Abstract:

High speed steel M2 circular saws have traditionally been used for cutting a variety of metals. However high speed steel saws is not suitable cutting the difficult-to-cut material eg, nickel based alloys, stainless steel etc. Furthermore present-day machines do not have the power to provide the high speeds required for carbide tipped circular saws.

The paper reviews the limitations of high speed steel circular saws and the need to develop carbide tipped circular saws in order to meet further manufacturing requirements.

(4) Xi-yang Zhang, M Sarwar "The influence of hot hardness on life of carbide tipped circular saws when sawing MS and stainless steel", Proceedings of the AMPT'93, Vol. 3, P1945, Aug.,1993.

Abstract:

This paper presents results from an investigation into the influence of hot hardness on the life of carbide-tipped circular saws, with special reference to the composition and microstructure of the saw tip materials.

The cutting tests were carried out to assess the performance of the saw materials in case of cutting mild steel and stainless steel. The results indicates that hot hardness has different effect on the life of carbide tipped circular saws when sawing mild steel and stainless steel.

(5) Xi-yang Zhang, D Gillibrand, M Sarwar, "Performance of titanium nitride coated carbide tipped circular saws when cutting stainless steel and mild steel", School of Engineering, Sheffield University, Feb., 1995.

Abstract:

The use of TiN coatings on cutting tools for general ferrous machining applications to enhance tool life and increase productivity has been for many years. However, application of coatings to the carbide TIPPED cutting tools is still a new research area in the use of coatings on cutting tools.

In this investigation a new experimental approach was used, in which TiN coatings were applied to four different types of carbide tipped circular saw segments. The four cathodes PVD technique was used for coating deposition at a low coating temperature. This results in a fine grain thin, hard film with excellent adherence to the substrates. When deposited on the tools, coating acts as a chemical and thermal barrier between the tool and workpiece. Applications including machining mild steel and stainless steel benefit from the coating. Also comparison between coated carbide tipped circular saw and uncoated carbide circular saw was given. The cutting test results have shown that TiN coated carbide tipped circular saws presented much better performance and longer tool life than uncoated saws. This information will be useful in the development of a coating system applied to the carbide tipped circular saws.

(6) Xi-yang Zhang, D Gillibrand, M Sarwar, "Performance of titanium aluminium nitride coated carbide tipped circular saws", School of Engineering, Sheffield University, Feb., 1995.

Abstract:

Industrial practice shows that the single compound film TiN cannot be the only choice for the tremendous variety of machined material in cutting tool applications. TiN with all the advantages it provides, has given less than satisfactory results when used to machine difficult to machine materials such as stainless steel and nickel-based alloys. In the case of these materials cut, it is apparently the lack of resistance to oxidation that does not allow TiN films to perform adequately. In consequence, the basis for the introduction of aluminium into the deposited film was to improve the oxidation behaviour of the coating.

In the investigation, four alloyed cathodes were used to produce TiAlN film on the carbide tipped circular saw segments. The programme focus was on the use of this new TiAlN coating on carbide tipped circular saw to arrest the acceptable failure modes such as edge chipping, crater wear, flank wear produced when machining stainless steel and mild steel.

(7) Xi-yang Zhang, T Campbell, G Cockerham, M Sarwar, " Prediction of failure of carbide tipped circular saws by FE model", School of Engineering, Sheffield University, Feb., 1995.

Abstract

The development and application of mathematical models to simulate and control the metal cutting process has occurred over a number of decades. However, the basic finite element technology originated only in the early 1960s. With the availability of inexpensive computational power, the number of numerical investigations of cutting has been increasing rapidly for a variety of tasks, including: off-line model and process design, prediction of tool failure modes and tool geometry design etc. With in creased demands from customers, a better understanding of the wear behaviour of the related carbide tipped circular saws has been given much attention by the saw producers. This is now considered to be a key point towards the improvement of the saw quality. In this project a completely new FE model was established to predict the failure behaviour of carbide tipped circular saws; evaluate and compare the stress distributions with the carbide circular saw failure configurations.